NASA Conference Publication 2266

Structural Dynamics and Control of Large Space Structures - 1982

Proceedings of a workshop held at
NASA Langley Research Center
Hampton, Virginia
January 21-22, 1982

NASA

NASA Conference Publication 2266

Structural Dynamics and Control of Large Space Structures - 1982

Compiled by
M. Larry Brumfield
Langley Research Center

Proceedings of a workshop held at
NASA Langley Research Center
Hampton, Virginia
January 21-22, 1982

National Aeronautics
and Space Administration

**Scientific and Technical
Information Branch**

1983

PREFACE

This publication contains the proceedings of a workshop held at NASA Langley Research Center, January 21-23, 1982, on technology for controlling large structures currently being conceived for space applications. This workshop was a follow-up to a workshop held at Langley in October 1980. (NASA CP-2187, Structural Dynamics and Control of Large Space Structures (1981) contains the proceedings of that workshop.)

The workshop focused on progress in NASA Langley's basic research program in control of large space structures and heard reports on in-house efforts, university grants, and industry contracts, as well as on some efforts not directly supported by the NASA Langley Research Center program. This document contains copies of most of the visual material presented by each participant, together with as much descriptive material as was provided to the compiler.

Use of trade names or names of manufacturers in this report does not constitute an official endorsement of such products or manufacturers, either expressed or implied, by the National Aeronautics and Space Administration.

M. Larry Brumfield
Langley Research Center

CONTENTS

ACTIVE DAMPING OF A FLEXIBLE BEAM

Garnett C. Horner
NASA Langley Research Center
Hampton, Virginia

One objective in the flexible-beam research program is to develop an algorithm that will determine actuator and sensor locations. This is necessary because large space structures will have many locations where actuators can be placed. This research seeks to determine the "best" or optimum locations. In addition, the "best" locations are determined while certain constraints are satisfied which guarantee that mission performance requirements are achieved.

The approach adopted in this research is to consider actuators and sensors to be collocated so as to produce an equivalent viscous damper. Ultimately, the experimental results of measuring the log decrement during free decay will correlate with the analytical predictions. (See fig. 1.)

OBJECTIVE: TO DEMONSTRATE ACTIVE VISCOUS DAMPING ON A FLEXIBLE BEAM

APPROACH:

- o TO USE COLLOCATED ACTUATOR/SENSOR TO PRODUCE VISCOUS FORCE
- o MEASURE DAMPING DURING FREE-DECAY

Figure 1.- Active damping of a flexible beam.

Figures 2 and 3 show the flexible-beam facility.

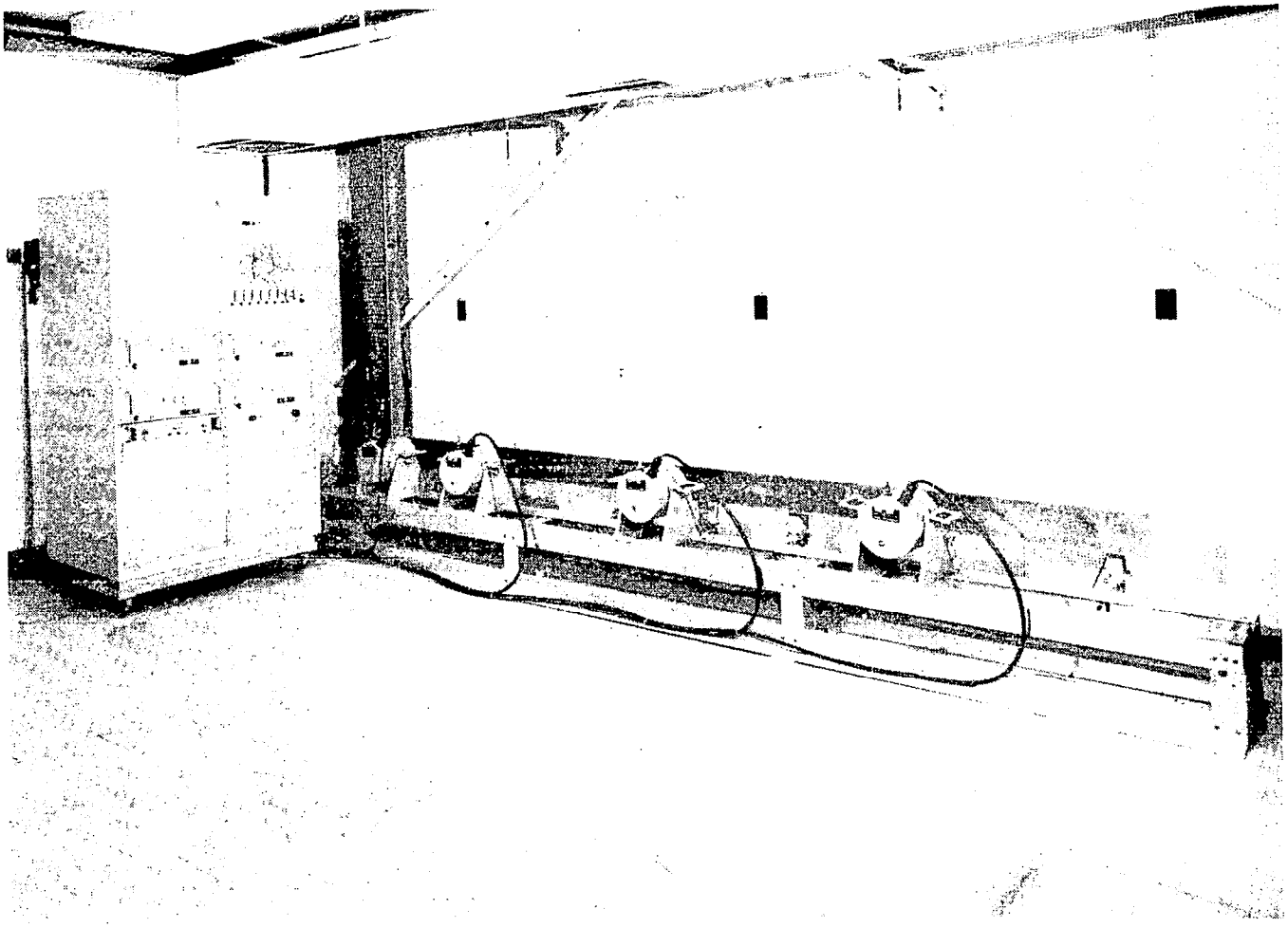

Figure 2.- Side view of flexible-beam facility.

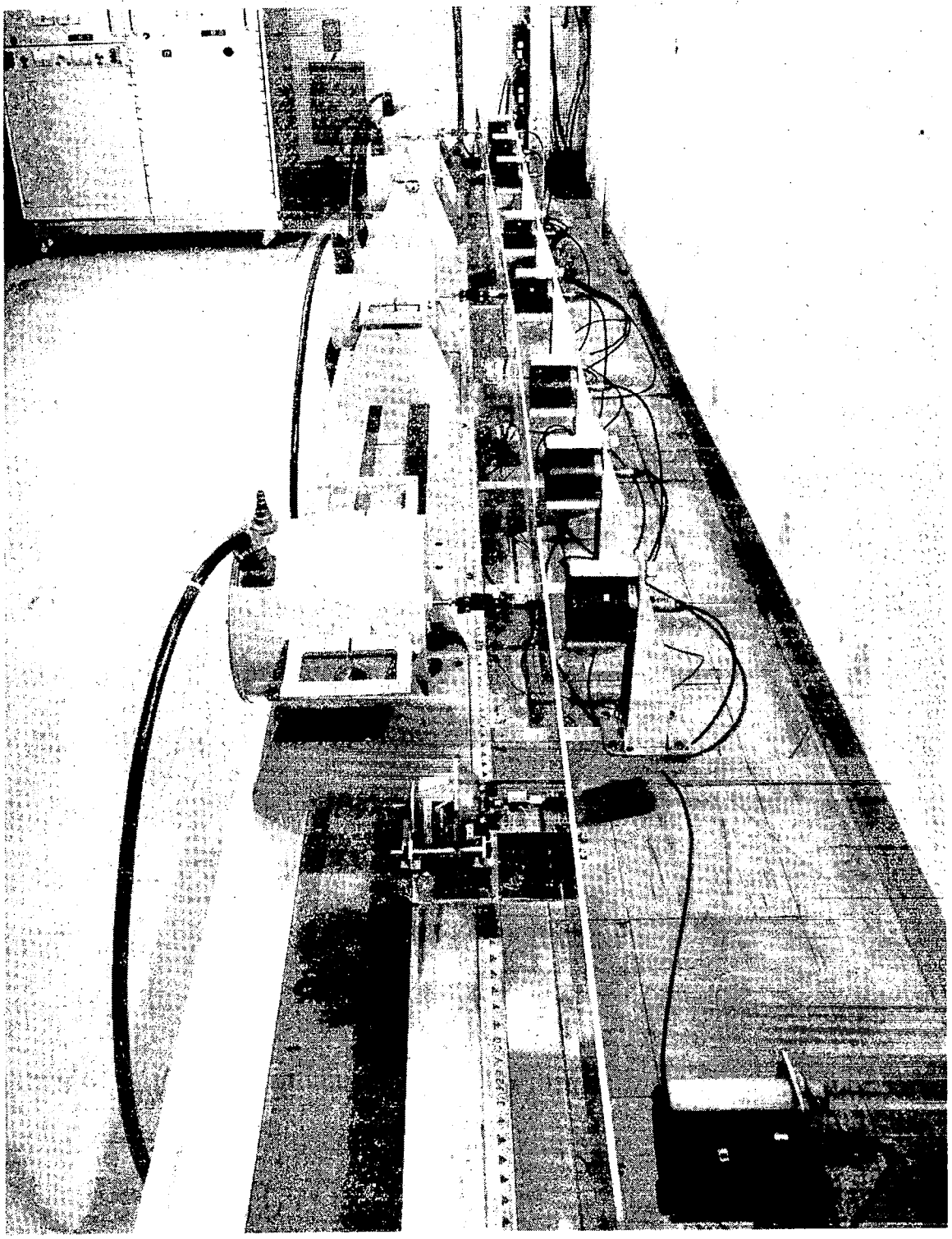

Figure 3.- Flexible-beam facility.

Figure 4 shows the locations of the actuators and sensors along the beam axis. These locations were determined by the optimization algorithm so that the first five bending modes are controlled.

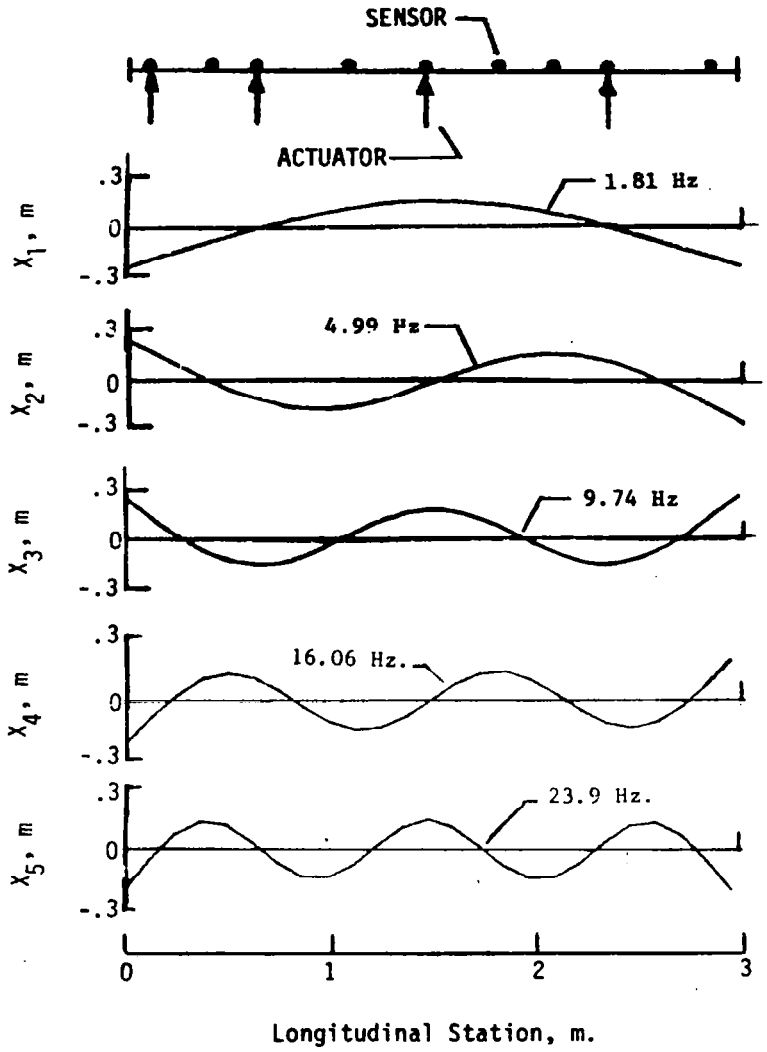

Figure 4.- Actuator and sensor locations on flexible beam.

Figure 5 shows the results of active damping as applied to the flexible beam. Four different sets of damper gains are shown in the right-hand column. The vertical bar is proportional to the damping rate of the damper at the location shown on the beam. The experimental plots at the left of the figure were obtained from the first bending mode of the beam. With the damping rate of each damper set to zero, the beam was vibrated in the first mode. At the time that free decay starts, the damping rate of each damper is set to the desired value. The comparison of the percent of modal damping is made using two experimentally based methods. These values should be compared to the analytically determined value. The column entitled "graph" used a graphical technique to measure the amplitude of adjacent peaks. This data is used to calculate the log decrement, which in turn is used to calculate percent of modal damping. The column entitled "ITD" contains the results of using the Ibrahim time domain method. There seems to be reasonable agreement between the two experimental methods until large modal damping is achieved. In this region small measurement errors can cause large modal damping errors.

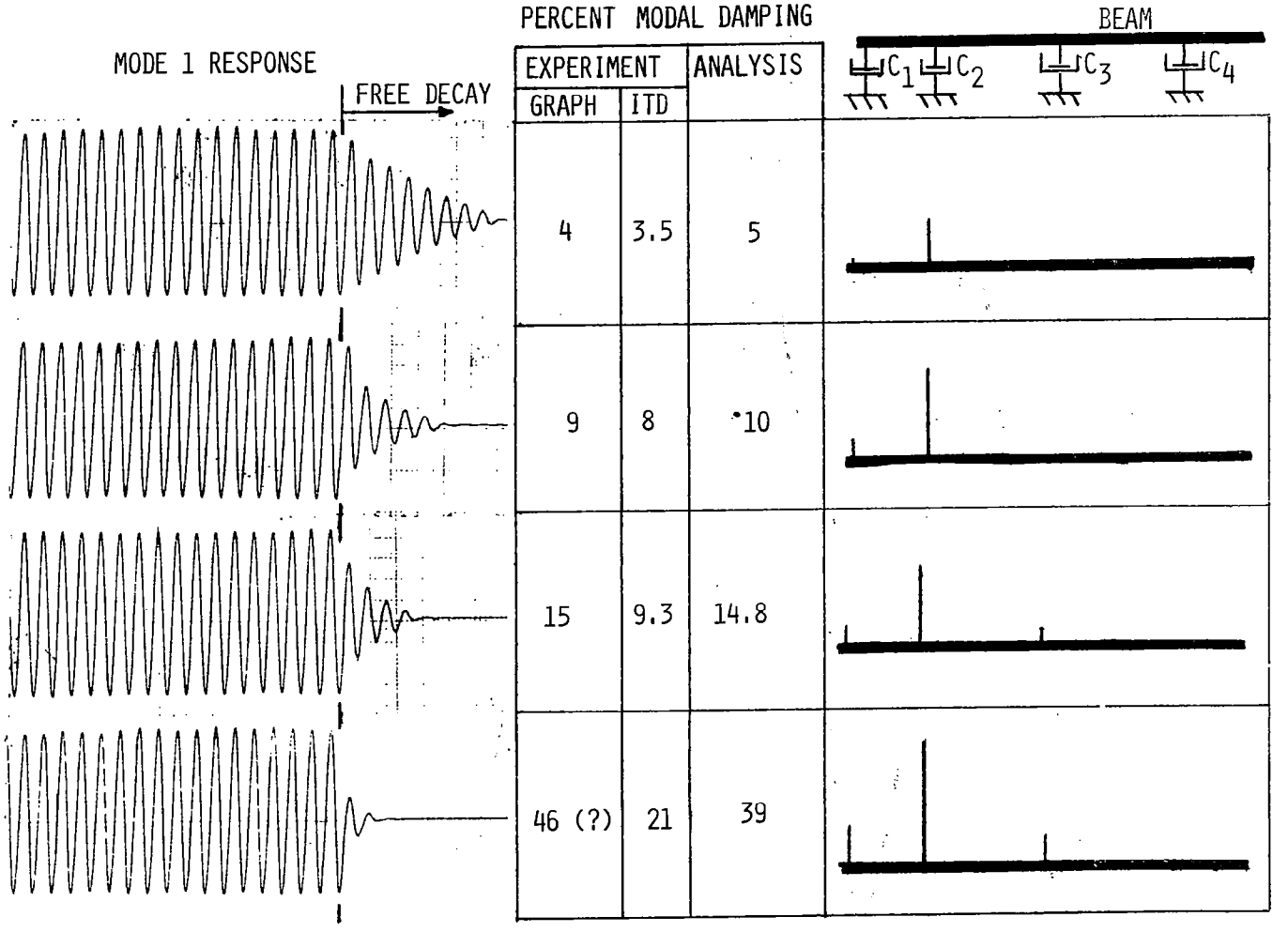

Figure 5.- Active damping results.

Figure 6 and 7 are expanded amplitude and time scale plots that show better the response detail during free decay when the dampers are turned on.

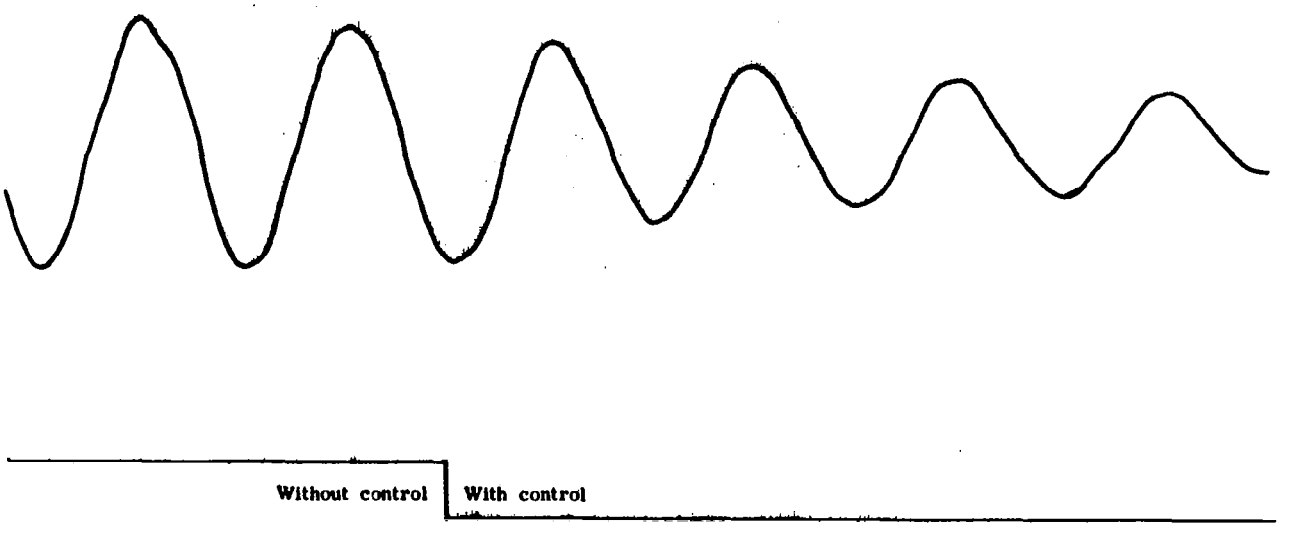

Figure 6.- Mode 1 response with a design modal damping = 0.05.

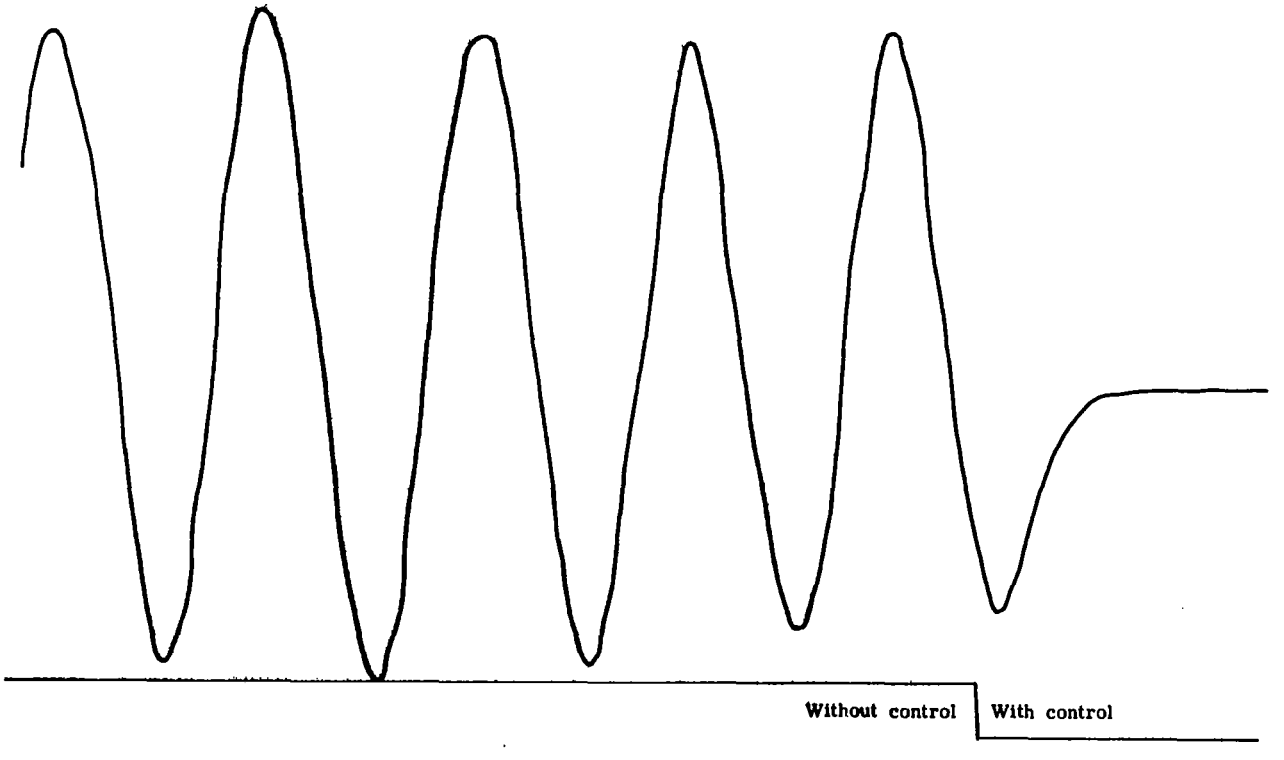

Figure 7.- Mode 1 response with a design modal damping = 0.6.

Figure 8 summarizes the accomplishments and needs of this research.

- o ACTIVE VISCOUS DAMPING HAS BEEN DEMONSTRATED
- o DIFFICULT TO MEASURE HIGH MODAL DAMPING
- o ACTUATORS REQUIRE COMPENSATION
- o DIGITAL CONTROL (VERSUS ANALOG) MAY REQUIRE MORE ANALYSIS

Figure 8.- Summary.

DECOUPLING AND OBSERVATION THEORY APPLIED TO CONTROL OF A LONG FLEXIBLE BEAM IN ORBIT

Harold A. Hamer
NASA Langley Research Center
Hampton, Virginia

INTRODUCTION

Decoupling theory is a convenient tool for devising control laws for structures with a large number of state variables because it allows independent control of each state. Complete decoupled control requires that the number of control actuators equal the number of modes in the system, which is a basic limitation in applying decoupling theory to the control of large space structures. Complete decoupled control is usually not achievable in practical application because a large space structure may have an infinite number of flexible modes; hence, procedures must be developed which maintain control of the structure with a small number of control actuators. Reduced-order systems must be utilized wherein only a few modes are included in the math model of the structure when calculating the gains for the feedback control law. In addition, some of the modes in the math model itself may be exempt from the control law if the number of actuators selected is less then the number of modeled modes. In both cases the control system must be designed to avoid serious problems associated with observation and control spillover effects caused by residual modes, which could result in poor performance or an unstable system.

The present analysis presents techniques which use decoupling theory and state-variable feedback to control the pitch attitude and the flexible-mode amplitudes of a long, thin beam. An observer based on the steady state Kalman filter has been incorporated into the control-design procedure in order to estimate the values of the modal-state variables required for the feedback control law.

EQUATIONS OF MOTION

Figure 1 shows the linearized equations of motion used for the decoupled-control analysis of a 450-m long, thin, flexible beam in low Earth orbit. The equations are in modal form. The first equation represents the rigid-body (pitch) mode and includes the gravity-gradient effect, where ω_c is the orbital frequency. In the second equation n represents the number of flexible modes included in the math model, plus the residual modes. The damping term $2\zeta\omega\dot{A}$ is included inasmuch as the residual modes require a small amount of damping for stability. The objective is to design a control system which provides independent control for each of the decoupled variables.

$$\frac{d^2\theta}{dt^2} + 3\omega_c^2\theta = \frac{T_P}{J}$$

$$\frac{d^2A_n}{dt^2} + 2\zeta_n\omega_n\frac{dA_n}{dt} + \omega_n^2 A_n = \frac{E_m}{M_n}$$

$$n = 1, 2, 3, \ldots$$

Figure 1

BASIC EQUATIONS

Figure 2 shows the basic equations used in the decoupled-control design. The equations are in state-vector form where the states x are the modal amplitudes and rates and include the residual modes. In the decoupling control law, u, the quantity v is the input command vector. The matrices F and G are the feedback and feedforward gains, respectively, which are calculated by the decoupling procedure. The estimator equation calculates the estimates of the modeled states $\hat{x}$ which are required by the control law. (The primes indicate modeled modes only.) The estimator utilizes the observation equation y and Kalman gains K which are precomputed by the steady state Kalman filter. The observation matrix senses attitude at two locations on the beam, where the ϕ values are the corresponding slopes of the mode shapes.

SYSTEM:

$$\dot{x} = Ax + Bu + w$$

$$u = F\hat{x} + Gv$$

$$y = Cx + w$$

ESTIMATOR:

$$\dot{\hat{x}} = A'\hat{x} + B'u + K(y - C'\hat{x})$$

$$= (A' - KC')\hat{x} + KCx + B'u$$

OBSERVATION MATRIX:

$$C = \begin{bmatrix} 1 & \phi_1 & \phi_2 & \phi_3 & - - - - & \phi_n & 0 & 0 & 0 & 0 & - - - - & 0 \\ 1 & \phi_1'' & \phi_2'' & \phi_3'' & - - - - & \phi_n'' & 0 & 0 & 0 & 0 & - - - - & 0 \end{bmatrix}$$

Figure 2

COMPOSITE EQUATIONS

Figure 3 shows the basic equations in composite form as a 20th order system. These equations are used to produce simulated time histories of system responses for various control input commands. The upper set of equations represents the system equations and includes four modeled modes and two residual modes. The lower set represents the estimator equations, which incorporate estimates only of the modeled modes. It is apparent that the control and observation spillover effects are caused by the matrices B_{12x2} and C_{2x12}.

In the present analysis two torque actuators are used; each is one-sixth the distance from the end of the beam. One attitude sensor (e.g., star tracker) is at an actuator location, the other at one-third the distance from the end of the beam. Analyses were also performed by (1) replacing the latter sensor with a rate sensor, and (2) by moving this attitude sensor to the location of the other actuator; in both cases, however, overall performance was not as good as for the original setup.

2 Control Actuators
2 Attitude Sensors
4 Controlled Modes
2 Residual Modes

$$\begin{pmatrix} \dot{x} \\ \dot{\hat{x}} \end{pmatrix} = \left[\begin{array}{c|c} A_{12x12} & B_{12x2}\, F_{2x8} \\ \hline K_{8x2}C_{2x12} & A'_{8x8} - K_{8x2}C'_{2x8} + B'_{8x2}F_{2x8} \end{array}\right] \begin{pmatrix} x \\ \hat{x} \end{pmatrix} + \left[\begin{array}{c} B_{12x2}\, G_{2x2} \\ \hline B'_{8x2}\, G_{2x2} \end{array}\right] \begin{pmatrix} v \end{pmatrix}$$

Figure 3

DYNAMIC CHARACTERISTICS

The dynamics of the system are shown in figure 4. The natural (open loop) frequencies and damping ratios are given in the second column. The value of 0.001 for ω_θ is the orbital angular velocity (orbital frequency). Small values of damping were assumed for the flexible modes, starting at a low value of 0.005 and increasing each successive mode by 10 percent. The fourth and fifth modes are taken as the residual modes. Some damping is required in these modes to avoid producing a system with constant oscillatory responses.

The last two columns show values selected for the closed-loop dynamics for two decoupled control cases. In the FAST PITCH case the commanded pitch attitude is reached in about 40 seconds; in the SLOW PITCH case about 2 minutes are required. In the first case, the two actuators are used to decouple the pitch attitude and first flexible mode. The symmetric arrangement of the actuators produces an interaction between all four modeled modes such that a full-order F matrix is achieved; i.e., feedback control is available for all 4 modes in the math model. This condition exists only because the absolute values of the control-influence coefficients are the same in both columns of the B matrix. For other control arrangements, techniques have been developed in which the control-influence coefficients and/or the feedback gains are adjusted to produce simplified procedures for achieving overall control of the system. The current analysis also included model errors of up to ± 15 percent in the control-influence matrix, with no apparent detrimental effect on the overall system performance.

In the SLOW PITCH case, the same two actuator locations were employed; however, the control-influence coefficients were slightly changed so that the decoupling control law provided control for two modes only. In this case it was necessary to perform two separate decoupling calculations: (1) the pitch and first flexible modes were decoupled, and (2) the second and third flexible modes were decoupled. The feedback gains obtained from both calculations were then combined to provide control for all four modeled modes.

DYNAMIC CHARACTERISTICS

	NATURAL	DECOUPLED	
		FAST-PITCH RESPONSE	SLOW-PITCH RESPONSE
ω_θ, R/S	.001	.07677	.0302
ω_1	.4275	.70	1.1
ω_2	1.172	2.084	1.1635
ω_3	2.297	3.063	2.091
ω_4	3.797		
ω_5	5.6716		
ζ_θ	0	.736	.70
ζ_1	.005	.2185	.3354
ζ_2	.0055	.863	.2013
ζ_3	.00605	.225	.2344
ζ_4	.00665		
ζ_5	.00732		

Figure 4

CLOSED-LOOP EIGENVALUES

The symbols in figure 5 depict the eigenvalues of the closed-loop system, assuming perfect knowledge of the state variables. Also shown are the loci of closed-loop eigenvalues for the observer as the Kalman gains are increased. The observer (based on the steady-state Kalman filter) was designed to have a certain stability margin. This was attained by adding a positive scalar term to the diagonal elements of the system matrix A'. The gains were changed by varying this scalar. (The A matrix in the composite equations shown in figure 3, of course, is not altered.) In calculating the Kalman gains, the objective is to produce an observer whose response is faster than that of the closed-loop system with perfect knowledge of the state vector (eigenvalue real parts more negative than those of the closed-loop system). As shown in figure 5, there is no problem in meeting this condition for the filter eigenvalue corresponding to the pitch mode. (Hence, estimates of the pitch attitude should be very accurate.) However, for the flexible modes, large Kalman gains are required to drive the eigenvalues past the corresponding closed-loop values. In fact, it was found that Kalman gains which produced eigenvalues with real parts less than about -0.1 resulted in poor performance; i.e., excessive control forces and/or excessive overshoot in the flexible-mode response. An example of this is shown in a subsequent figure.

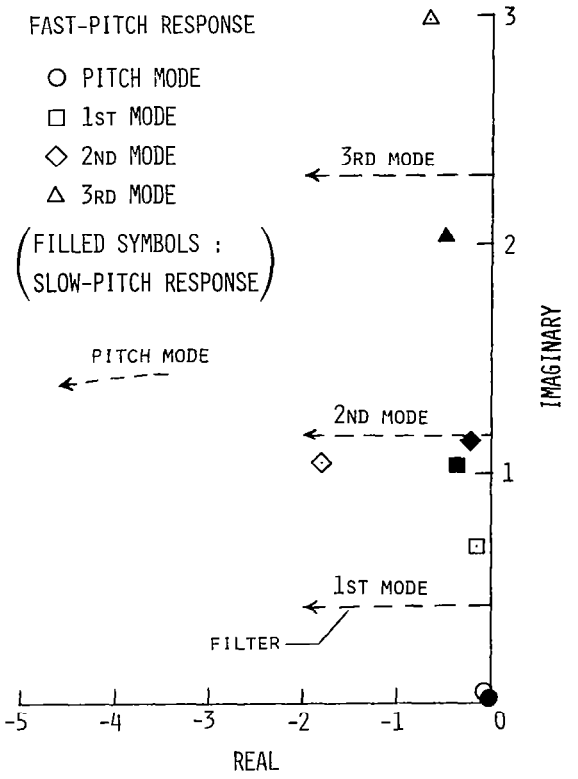

Figure 5

ZERO COMMAND-FAST PITCH

Figure 6 is an example of an instantaneous zero command (FAST PITCH case) to null arbitrary initial disturbances of -0.01 in pitch and 0.015, -0.005, and -0.02 in the first, second, and third flexible modes, respectively, and 0.01 in the residual modes (4th and 5th flexible modes). The Kalman gains used to determine the estimates of the modal variables (shown in 2nd column of time histories) correspond to real eigenvalues = -0.1, as previously discussed. It is assumed that instantaneous control torques T_1 and T_2 are available at time = 0, with initial estimates of 90 percent in pitch attitude and 80 percent in the three modeled flexible mode amplitudes; that is, the control actuators are not turned on until these estimates are established by the observer. Analysis has shown that without the effect of the controls, these estimates are achieved in about 100 seconds. The values of initial disturbances and initial estimates quoted here are used for all figures which follow, except where noted. All figures except figure 13 pertain to the FAST PITCH case.

As shown in figure 6, the four modeled mode responses (first column of time histories) are nulled after about 40 seconds. As for the residual modes, there is some effect on A_5 during the first few seconds; however, responses in both modes gradually die out due to natural damping. It should be noted that, with the controls operating, the observer obtains good estimates of the first three modes, but fails in estimating A_3 due to observation spillover caused by the residual modes. Attempts to improve this estimate by varying the Kalman filter gains are shown in the next two figures.

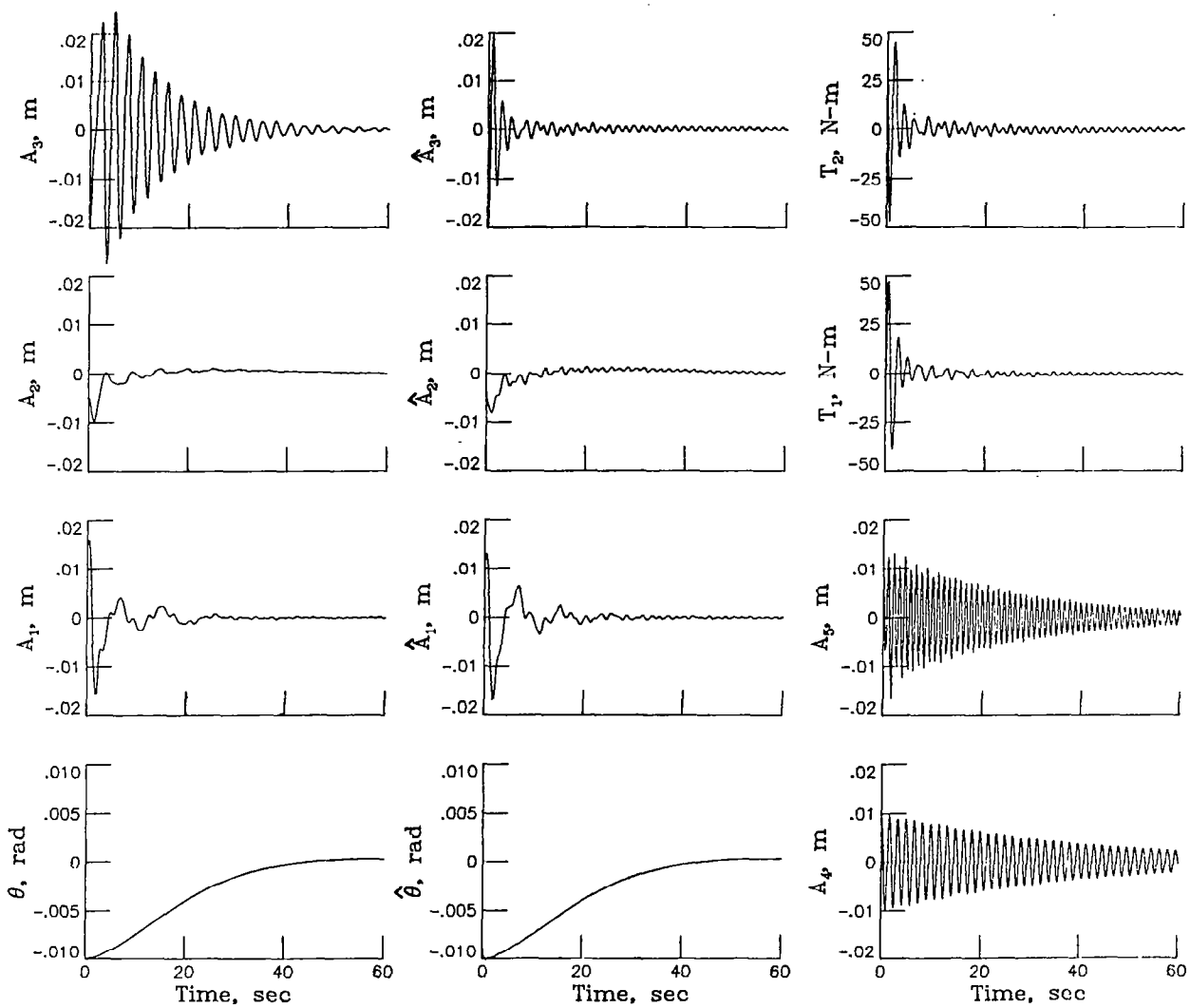
A_3, m
$\hat{A}_3$, m
T_2, N-m
A_2, m
$\hat{A}_2$, m
T_1, N-m
A_1, m
$\hat{A}_1$, m
A_5, m
θ, rad
$\hat{\theta}$, rad
A_4, m
Time, sec
Time, sec
Time, sec

Figure 6

FILTER GAINS REDUCED

For the zero command in figure 7 the Kalman gains were reduced so that the real eigenvalues, corresponding to the flexible modes, were close to zero. This resulted in slowly damped oscillations in the three modeled flexible modes due to poor estimates in all these modes.

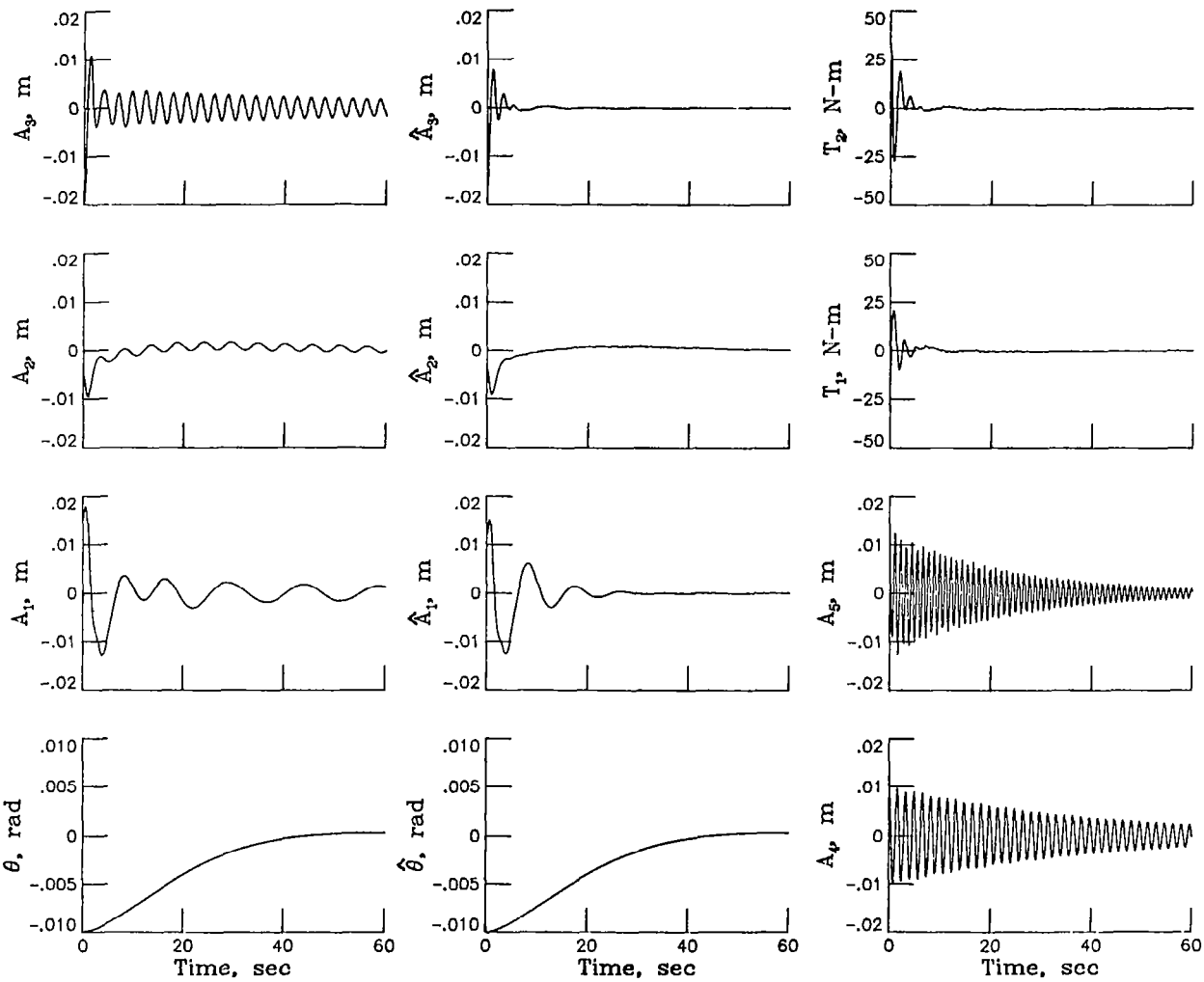

Figure 7

FILTER GAINS INCREASED

The Kalman gains were increased for the zero command case in figure 8 so that the real eigenvalues, corresponding to the flexible modes, were approximately -0.2. Here again, estimates were poor in A_2 and A_3. More notable is the poor performance as exemplified by the increased control torques and the peak overshoots in the flexible mode responses, which far exceeded the initial disturbances. Large control spillover effect is also evident in the residual A_5. Attempts were made to improve the performance for this case, as shown in the next two figures.

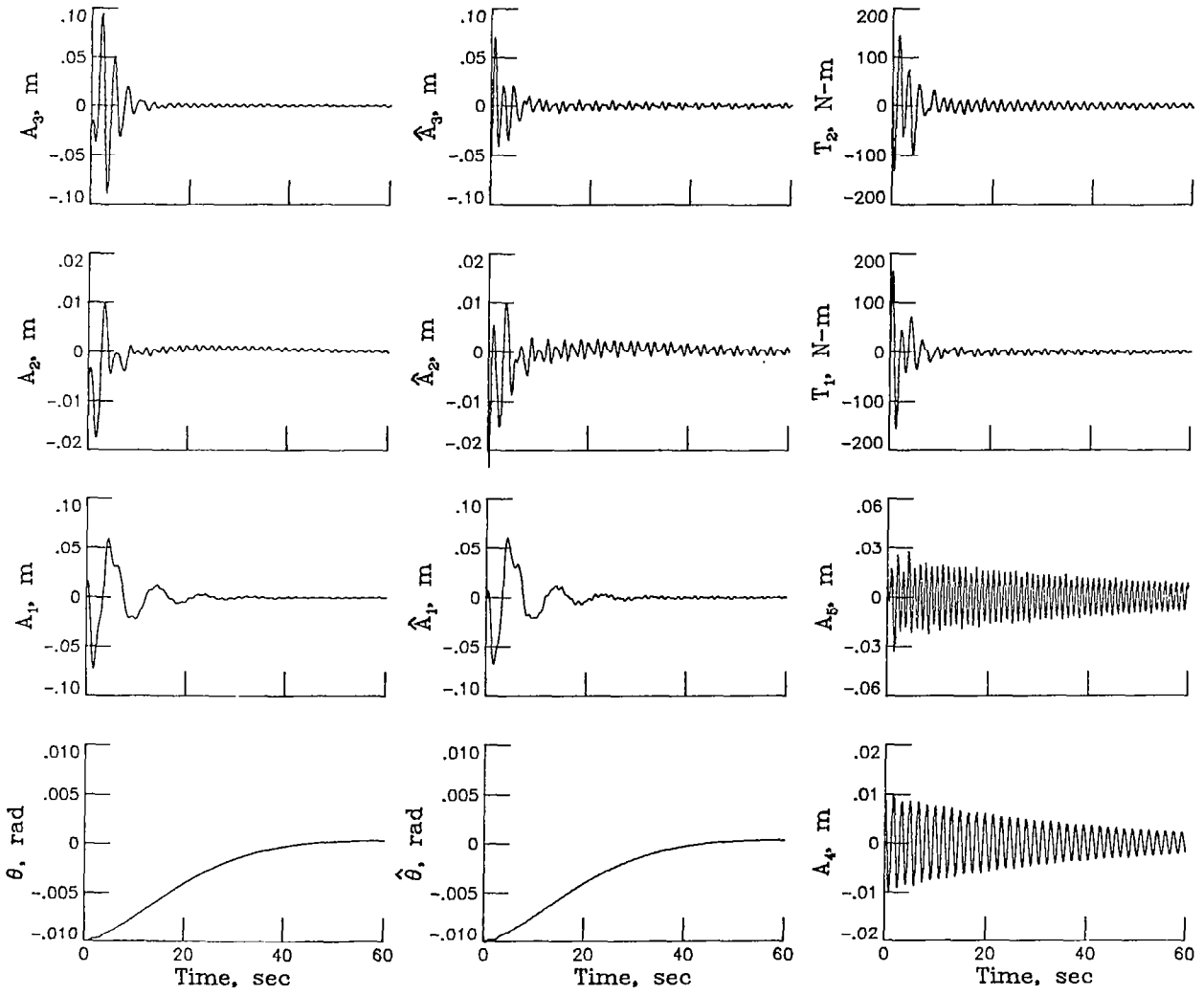

Figure 8

FEEDBACK GAINS ADJUSTED

Figure 9 is similar to figure 8, except the decoupling feedback gain matrix was changed by deleting the gains for the three flexible-mode amplitude displacements. Hence, the control system included feedback gains only for the pitch attitude and rate and the three flexible-mode amplitude rates. As shown by the lower control torques and peak responses, some improvement in performance was accomplished. Also, note the large reduction in the A_5 residual response. The system performance, however, is still unacceptable; the following figure shows a further attempt to improve this performance.

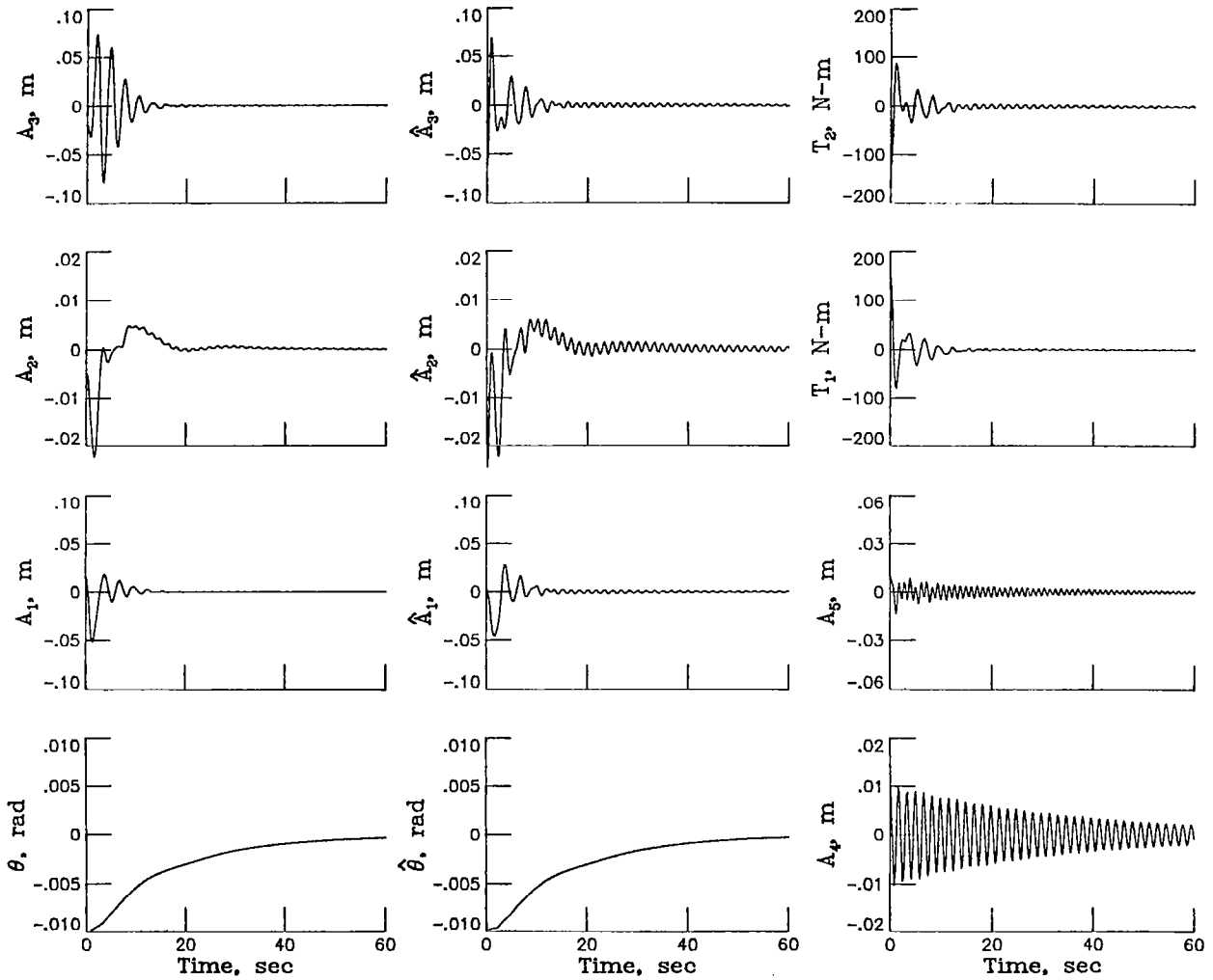

Figure 9

1st ORDER LAG: TAU = 5 SEC

For figure 10, in addition to the feedback gain adjustment, a first order lag (time constant = 5 sec) was included in the control system. This condition more closely resembles practical operational procedures because some lag will always be present in a control system. The results show further improvement in performance (especially in control requirements); however, it appears that the Kalman gains must be reduced for acceptable response in the flexible modes.

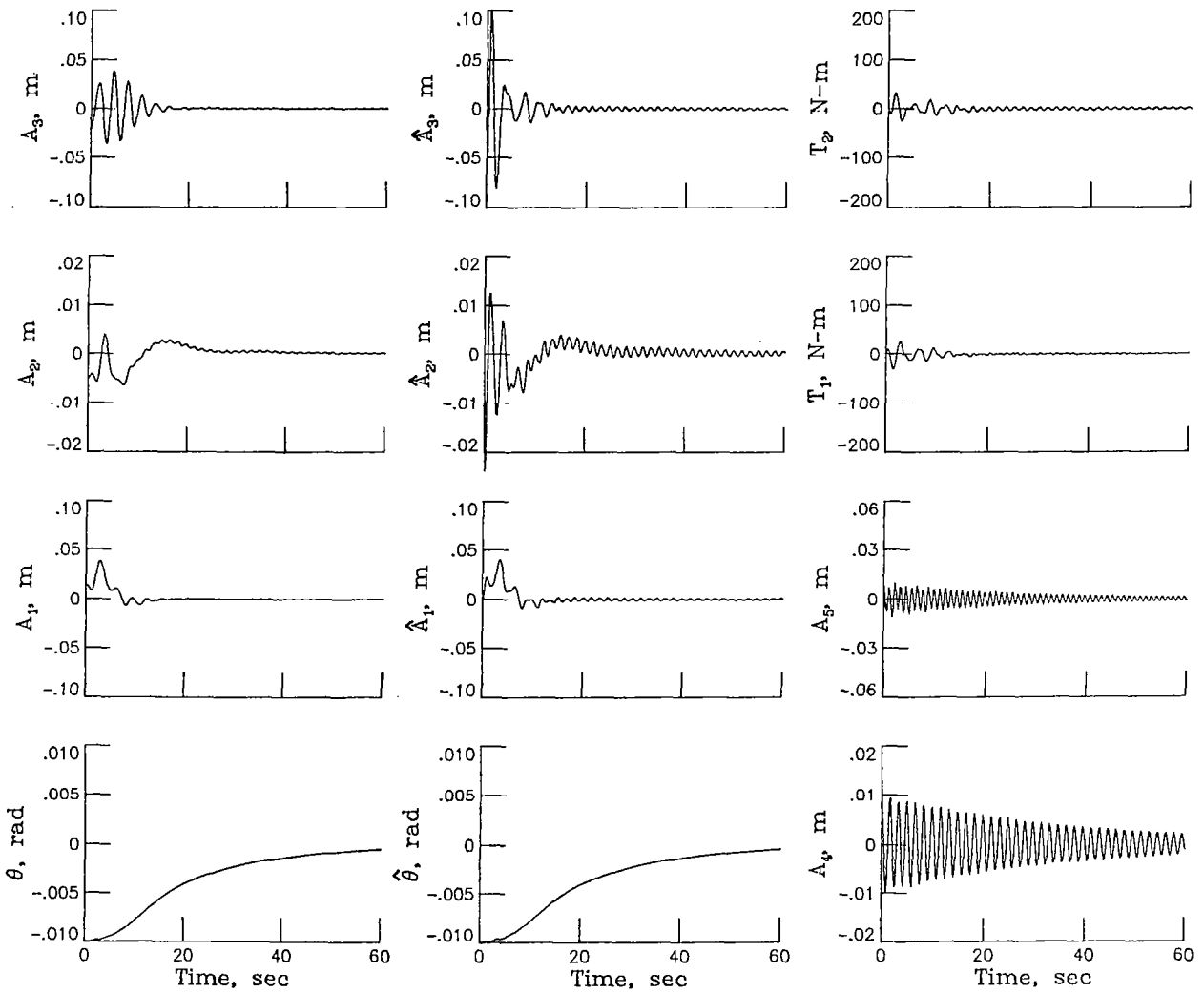

Figure 10

NO PITCH DISTURBANCE

Figure 11 shows a zero command case similar to that of figure 6, except with no initial pitch disturbance. Comparison of the two figures shows the large effect of pitch disturbance on nulling the system. With no pitch to consider (and consequently no error in the initial estimate in pitch), figure 11 shows considerably lower control torques and a much better response in the third flexible mode.

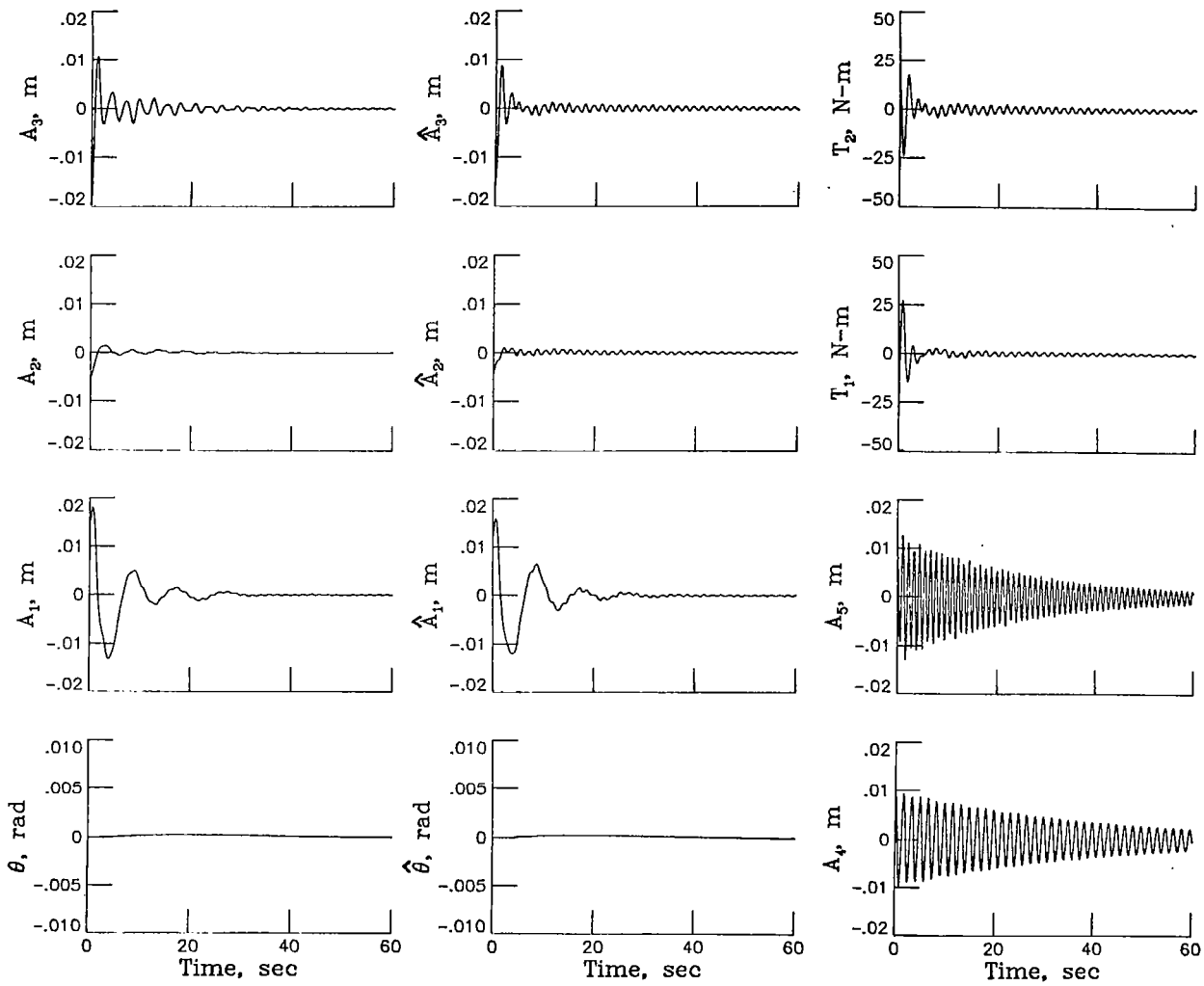

Figure 11

NO RESIDUAL DISTURBANCES

Figure 12 is similar to figure 6, except there are no initial disturbances in the residual modes. Comparison of the two figures shows that the responses in the modeled modes are not materially affected by the motions of the residual modes. Also, the control requirements are about the same in both cases, except for the small lingering oscillations in figure 6.

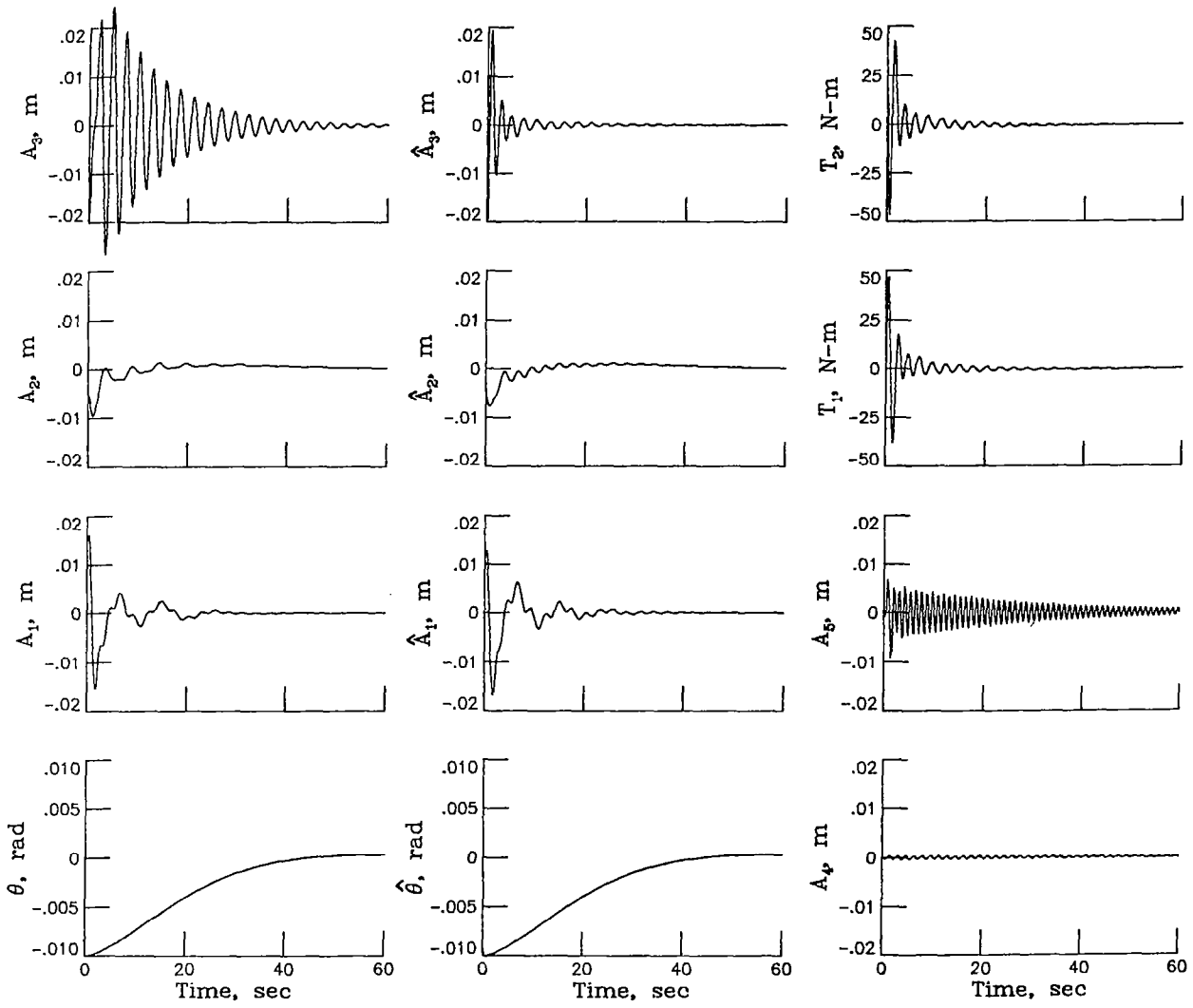

Figure 12

ZERO COMMAND-SLOW PITCH

Figure 13 is an example of a zero command for the SLOW PITCH case. The results are similar to the FAST PITCH case (figure 6). Although not shown, about two minutes are required to null the pitch attitude. Also, the maximum control torque is reduced by about one-half, as are the response amplitudes in the residual A_5.

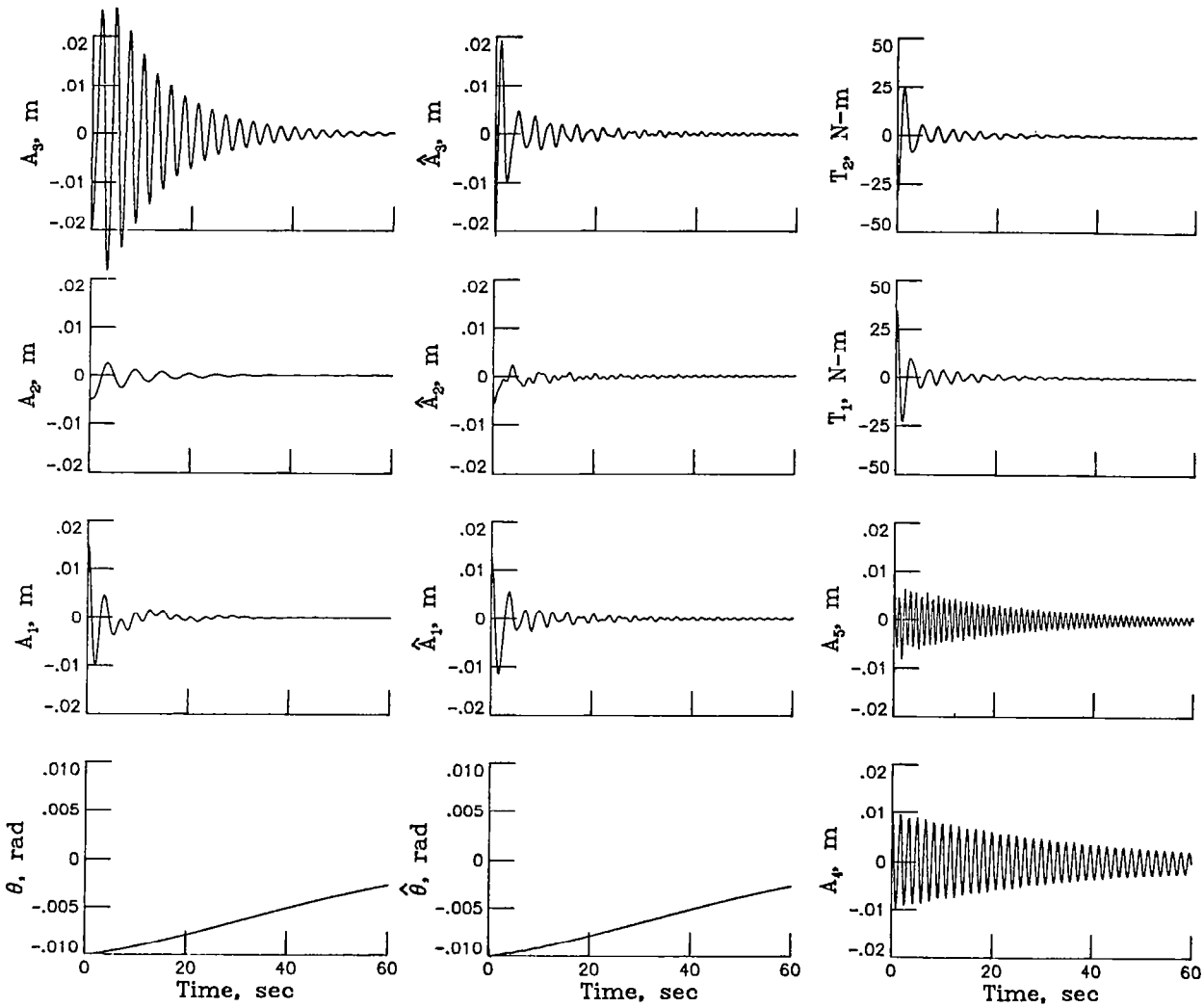

Figure 13

ONE CONTROL INOPERATIVE

Figure 14 is an example of a zero command (FAST PITCH case) where one of the control actuators is considered to be inoperative. The feedback gains for the remaining actuator were not altered. The time histories show adequate responses in nulling the system. In contrast to the two-actuator case (figure 6), θ and A_1 require about three times as much time to null (Note expanded time scale).

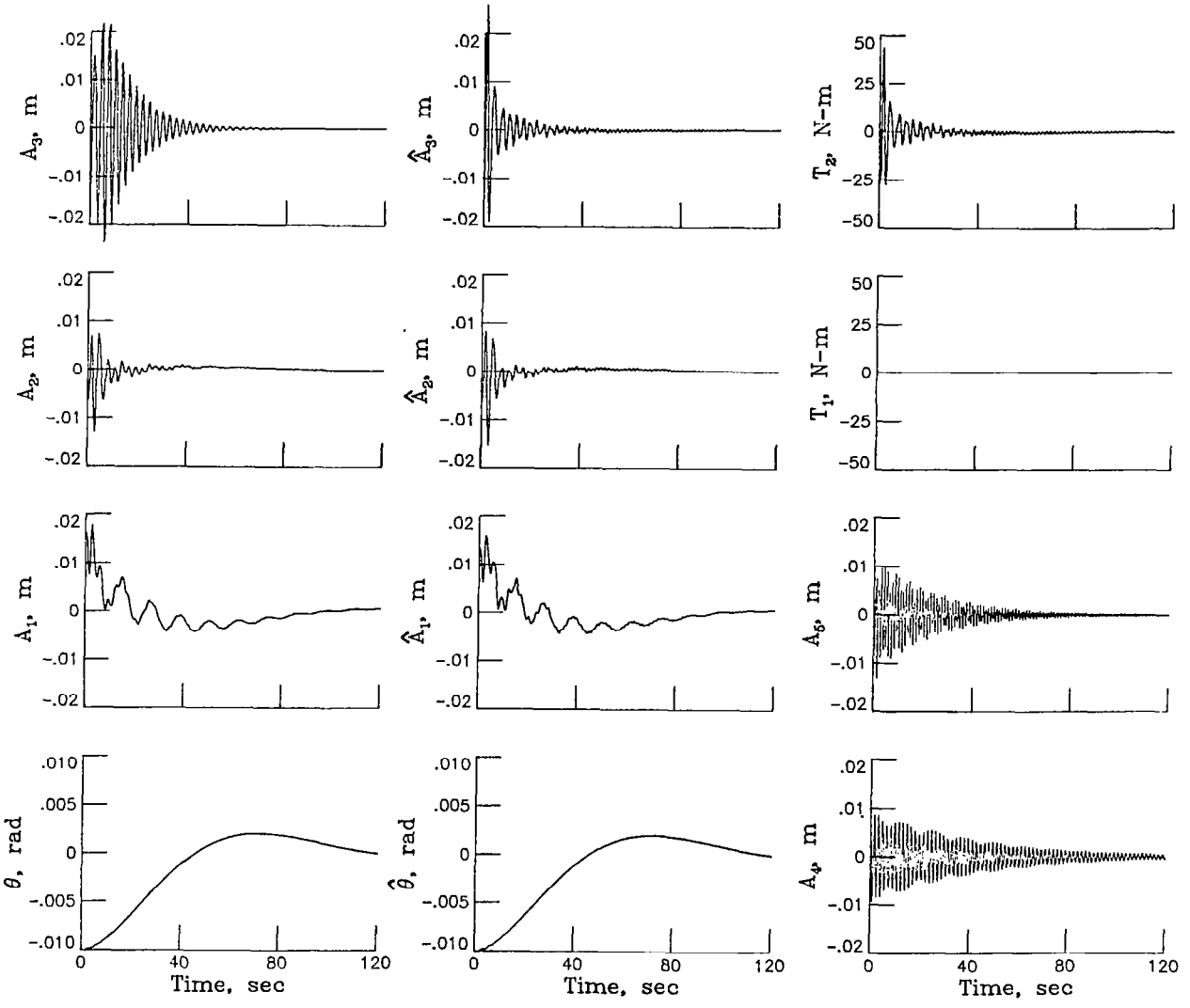

Figure 14

FEEDBACK GAINS ADJUSTED, LAG INCLUDED

Figure 15 illustrates the same case as the previous figure, except that the decoupling feedback gains were changed in the same manner as in the case of figure 9 and a first-order lag (tau = 5 sec) was included in the control system. Comparison with figure 14 shows better response characteristics for θ and A_1, as well as a large reduction in control requirements. Also, note that the observer obtains good estimates of A_3 after about 30 seconds.

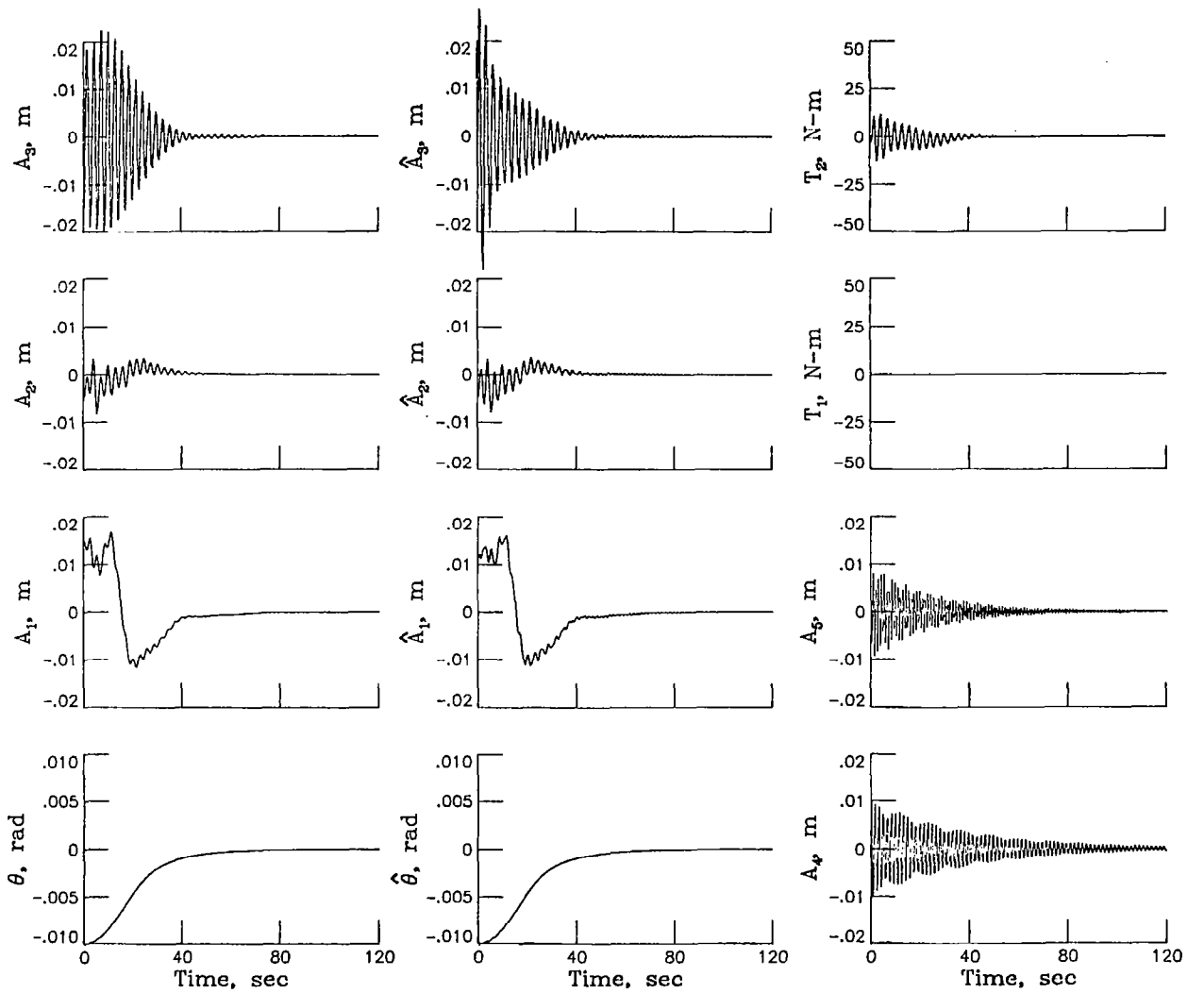

Figure 15

TWO ZERO-COMMAND PROCEDURE

The following four figures demonstrate a practical procedure for nulling initial disturbances with two separate zero-commands. Figure 16 represents the first zero-command and differs from the one in figure 6 in that actuator lag (tau = 5 sec) is included and the closed-loop pitch frequency has been doubled. Because of the increased pitch response, all disturbances are essentially nulled within 30 seconds. The control actuators are then turned off (observer remains on) at this time as shown in the next figure.

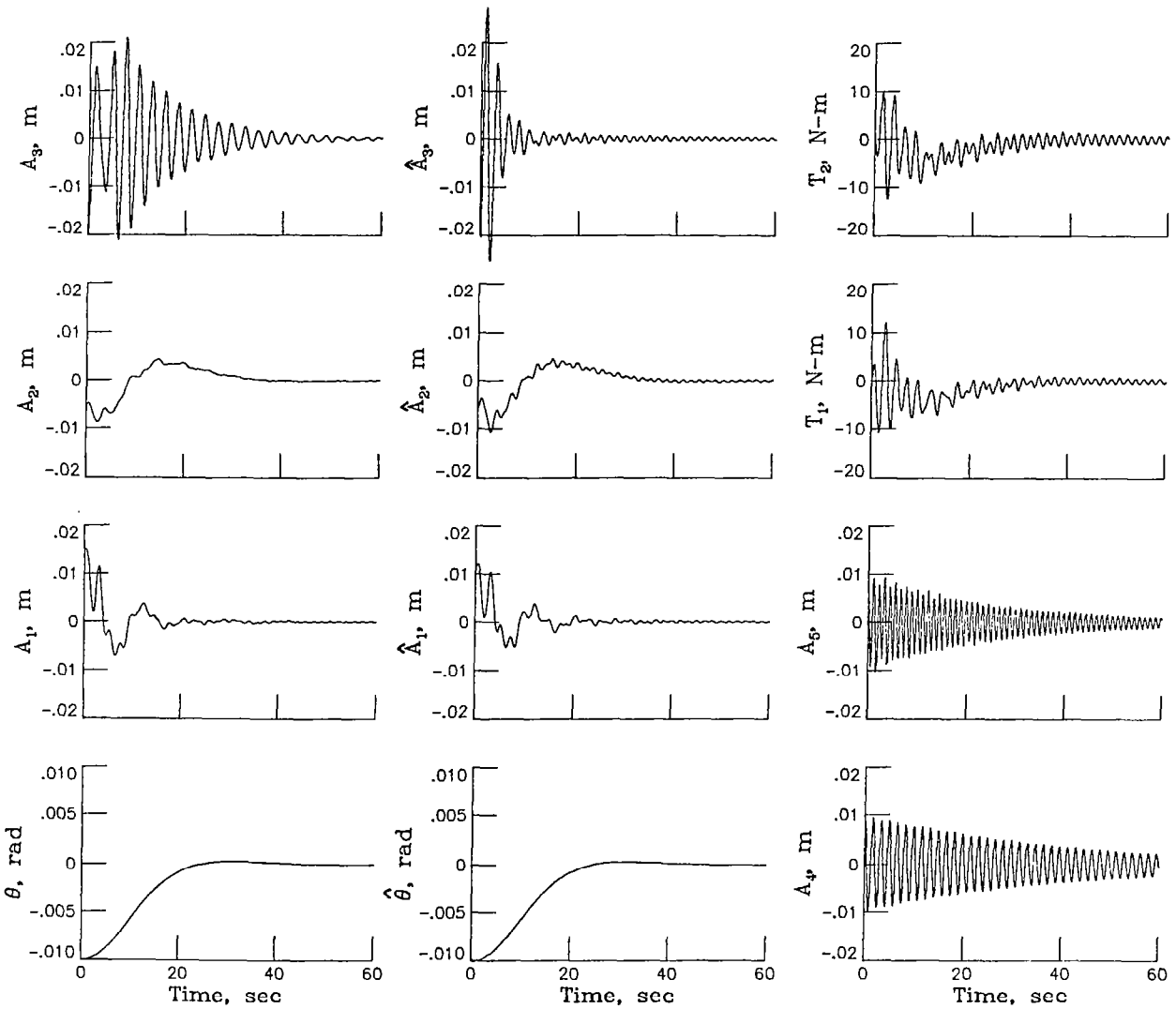

Figure 16

CONTROLS OFF - OBSERVER ON

The results of turning off the controls at time 30 seconds are shown in figure 17. The actuators were turned off in order to avoid the oscillating control torques which are shown to persist over a long time period in figure 16. As shown in figure 17, the disturbances have not been completely nulled, but fairly good estimates of these disturbances are obtained after 30 more seconds. (Note that without the controls operating the observer is able to obtain a good estimate of A_3.) The next step, then, is to apply the second zero command at this time. The resulting responses are shown in the next figure.

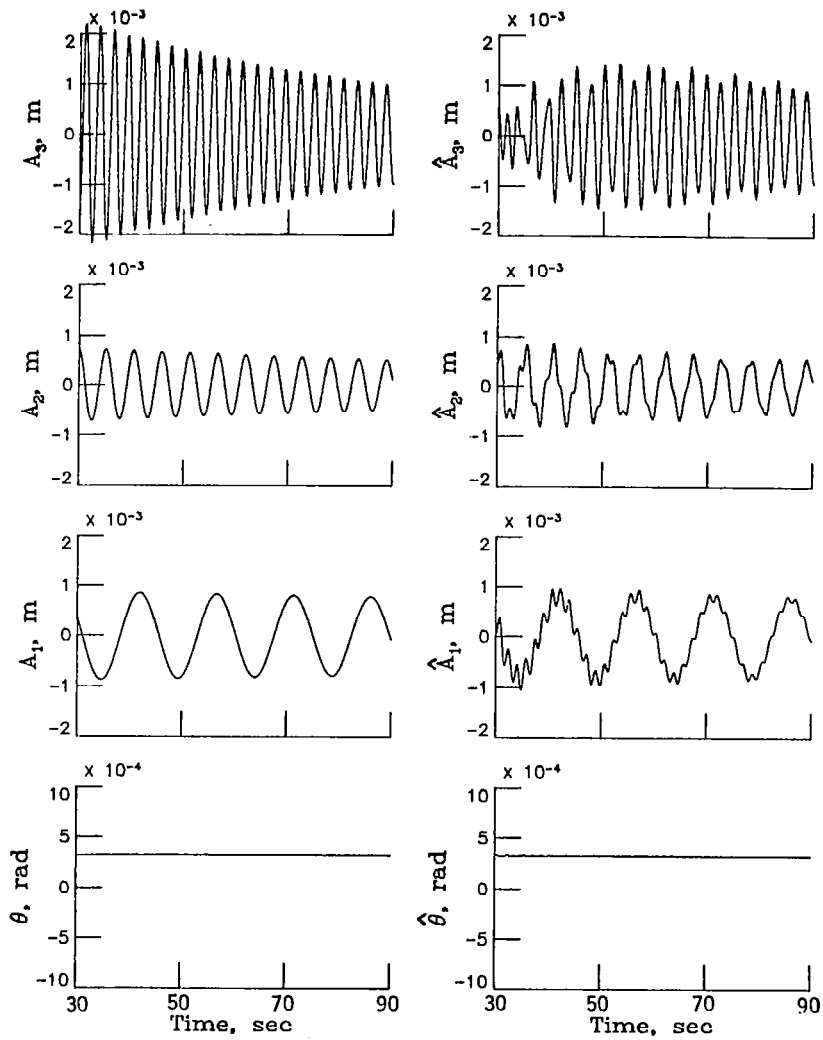

Figure 17

SECOND ZERO COMMAND AT 60 SEC

The modal responses in figure 18 are essentially nulled after 30 seconds. Here, the control actuators are turned off for the final time, again to avoid the oscillating control torques which would be required over a long time period. The final results of the two-zero command procedure are shown in the next figure.

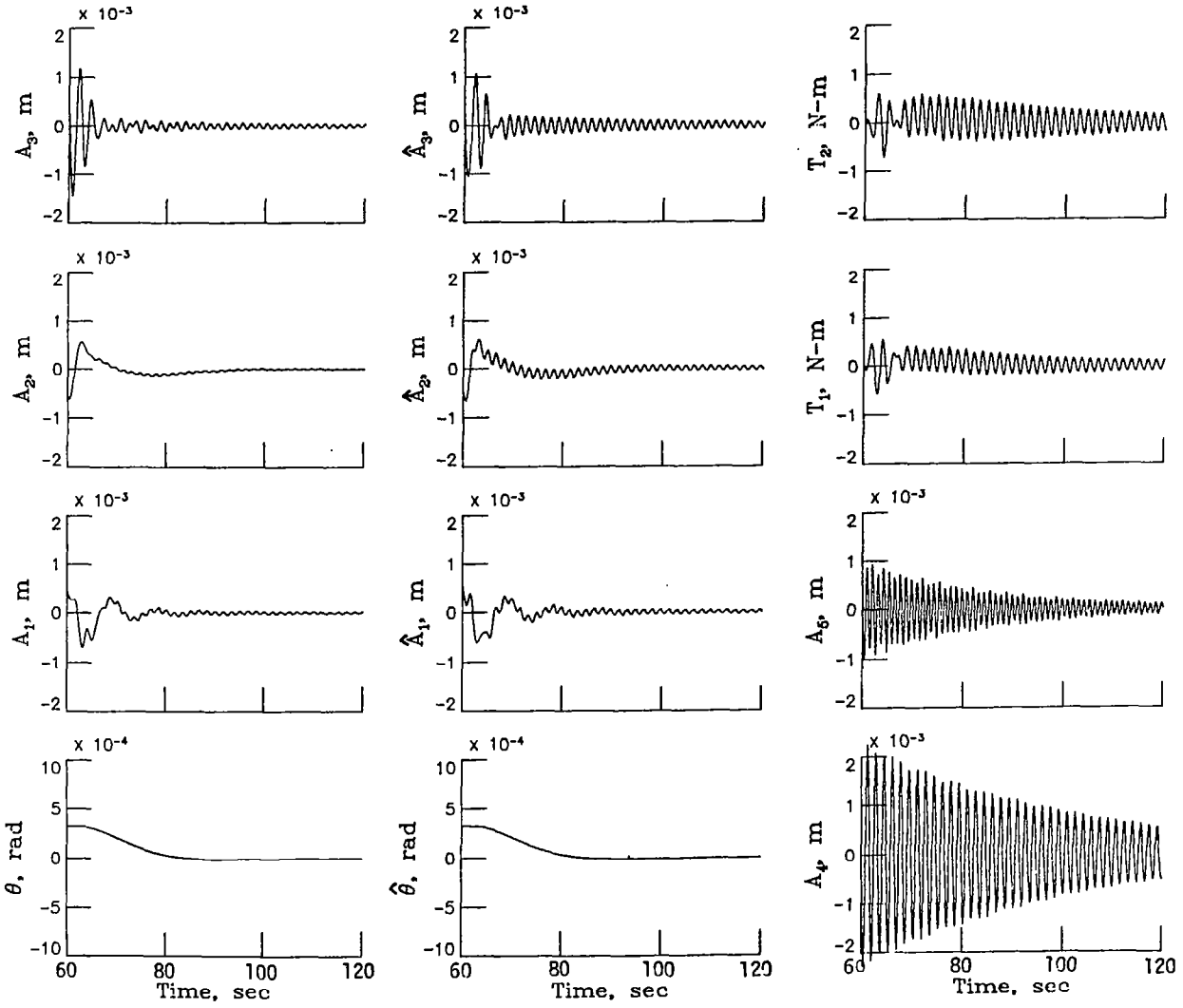

Figure 18

CONTROLS OFF AT 90 SEC

The results of turning off the actuators after the second zero command are shown in figure 19. The remaining disturbances are practically zero and will eventually die out through natural damping.

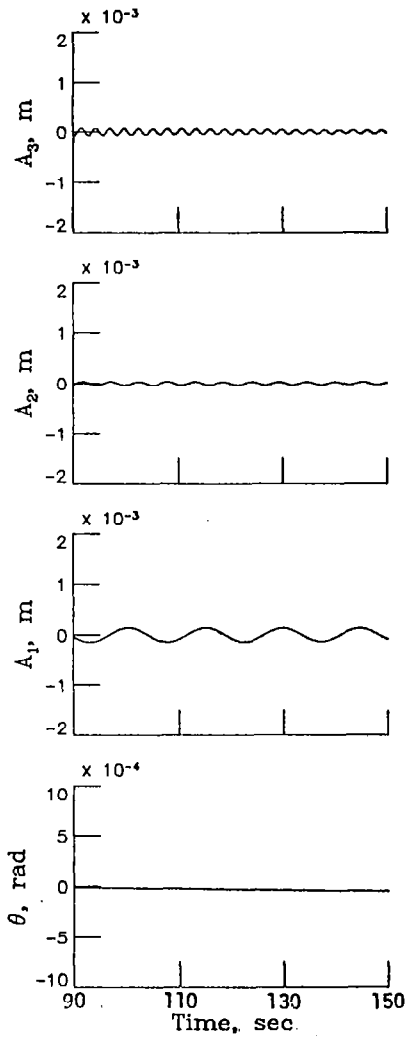

Figure 19

PITCH COMMAND - NO DISTURBANCES

The next two figures illustrate examples of pitch commands whereby a pitch attitude of 0.01 radian is commanded. For the case in figure 20, there are no initial dusturbances, and hence no errors in the initial estimates. The commanded pitch attitude is reached in about 40 seconds, with only a small coupling effect on the second flexible mode.

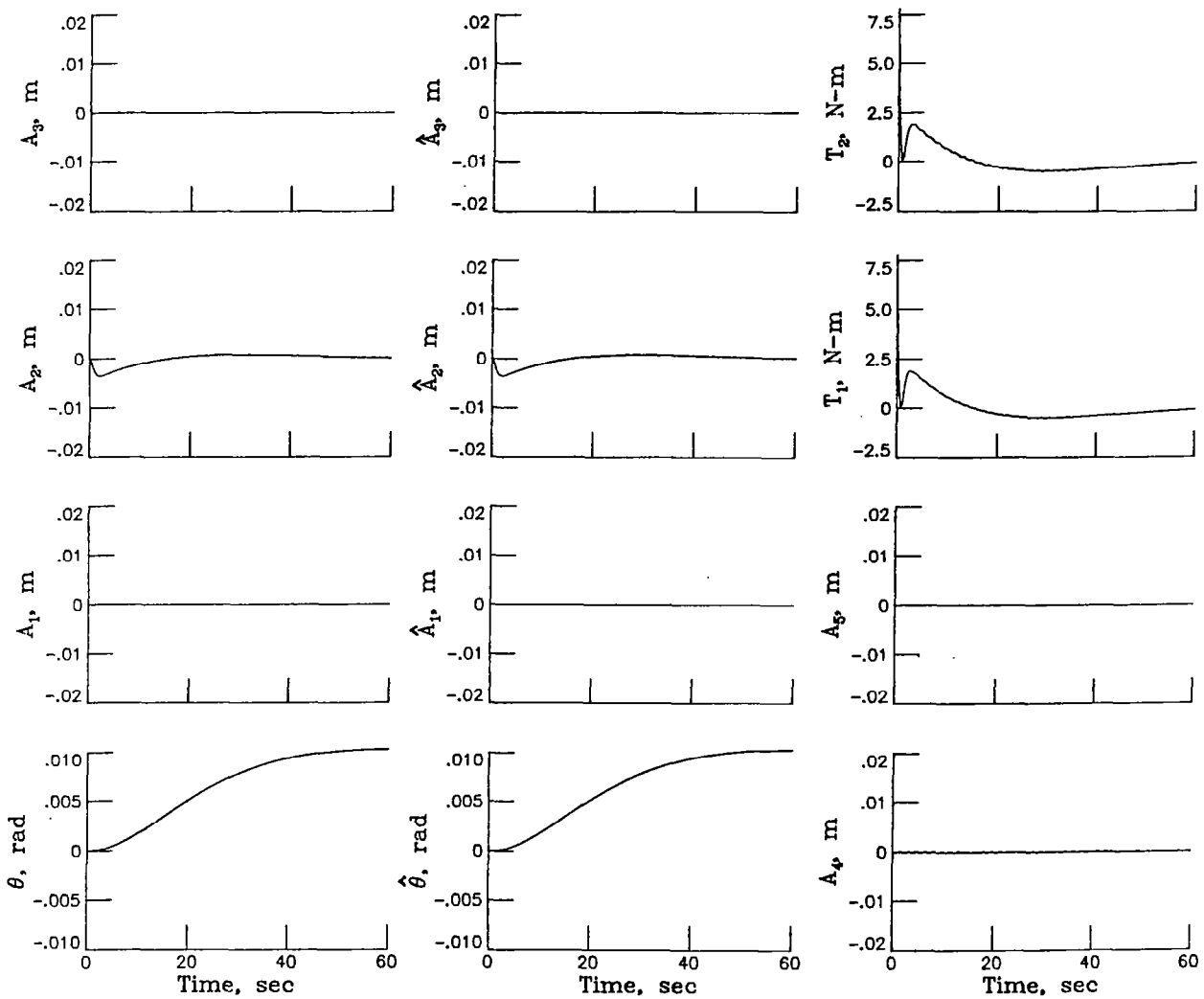

Figure 20

INITIAL PITCH DISTURBANCE - ESTIMATE AT 90 PERCENT

For the pitch command in figure 21, there is an initial pitch disturbance of -0.005 radian which is known only to an accuracy of 90 percent. The results illustrate the large effect of the initial estimate on the three modeled flexible modes. Also, the control-torque requirements are substantially increased over those of the previous figure. Doubling the error in the initial estimate would double the magnitude of these effects.

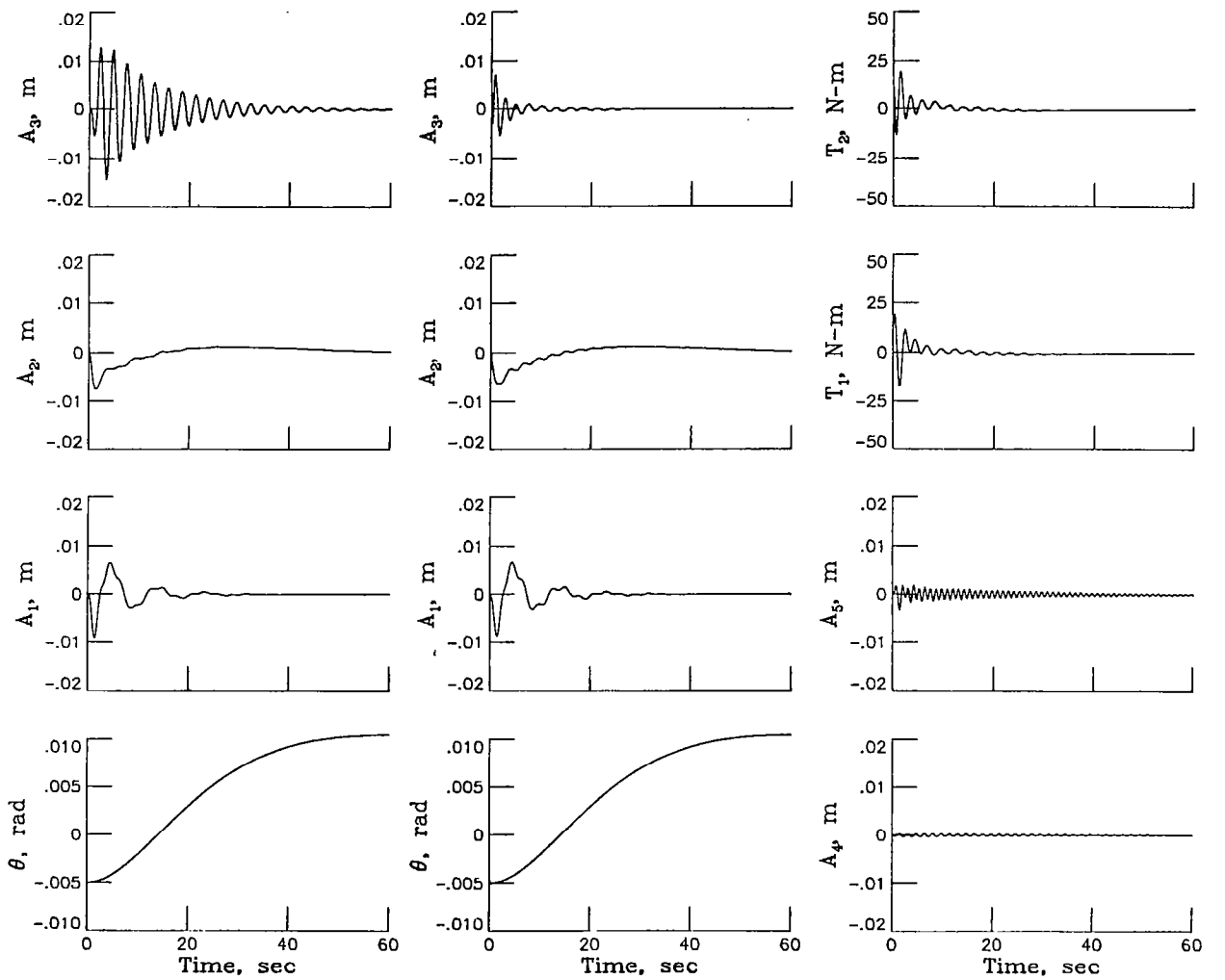

Figure 21

CONTROL REQUIREMENTS

Figure 22 compares the maximum peak actuator torques (absolute values) required for pitch and zero commands, assuming no lag in the system. The data apply to a four-actuator control system but are representative of any control arrangement. For the pitch-command data, there is an initial disturbance of -0.005 radian and the commanded value is 0.01 radian. The zero-command data pertain only to nulling initial disturbance in the flexible modes; i.e., no pitch disturbance. Except where noted, the peak torques occurred after the initial time.

As would be expected, the control requirements are essentially linearly related to the initial estimate. Also, the pitch commands require the higher control torques. Further, the results show that the requirements for zero commands increase as the accuracy of the initial estimate increase, while the opposite is true for pitch commands.

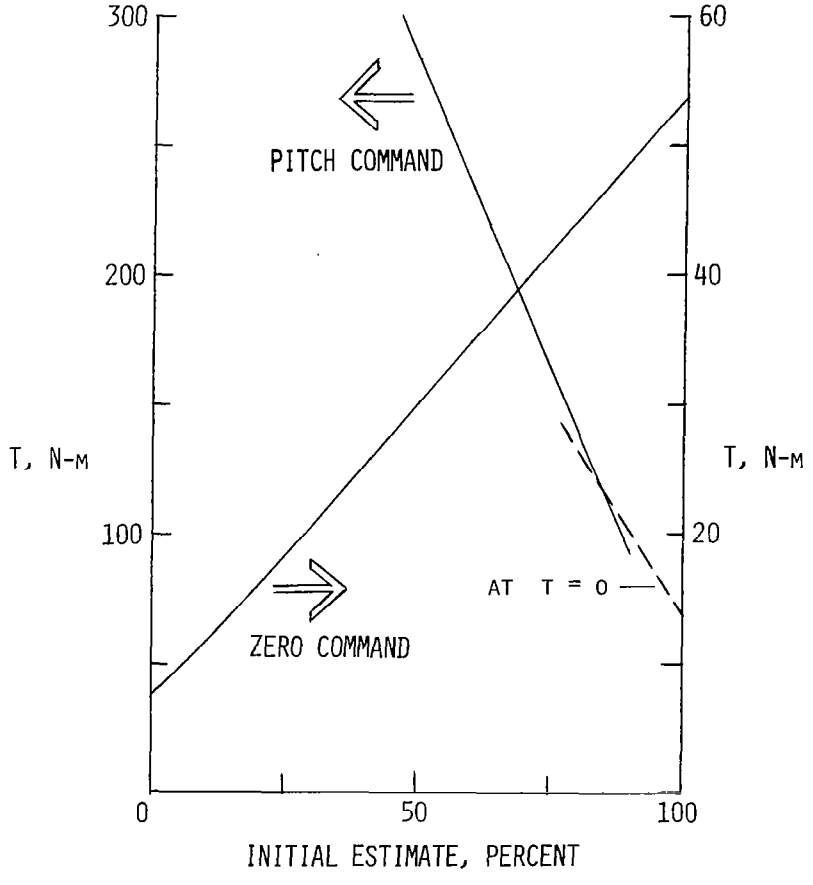

Figure 22

SENSOR LOCATION ERROR, 5 PERCENT TOWARDS LEFT

Figure 23 is similar to the zero command shown in figure 6, except for sensor-location error; i.e., the attitude sensors have been placed at locations other than those (nominal) used for the observer in calculating the Kalman gains. In this case the sensor locations have been moved 22.5 meters (5 percent of beam length), both in the same direction from nominal. Comparison with figure 6 shows that, except for A_5, this error produced negligible effects on system performance.

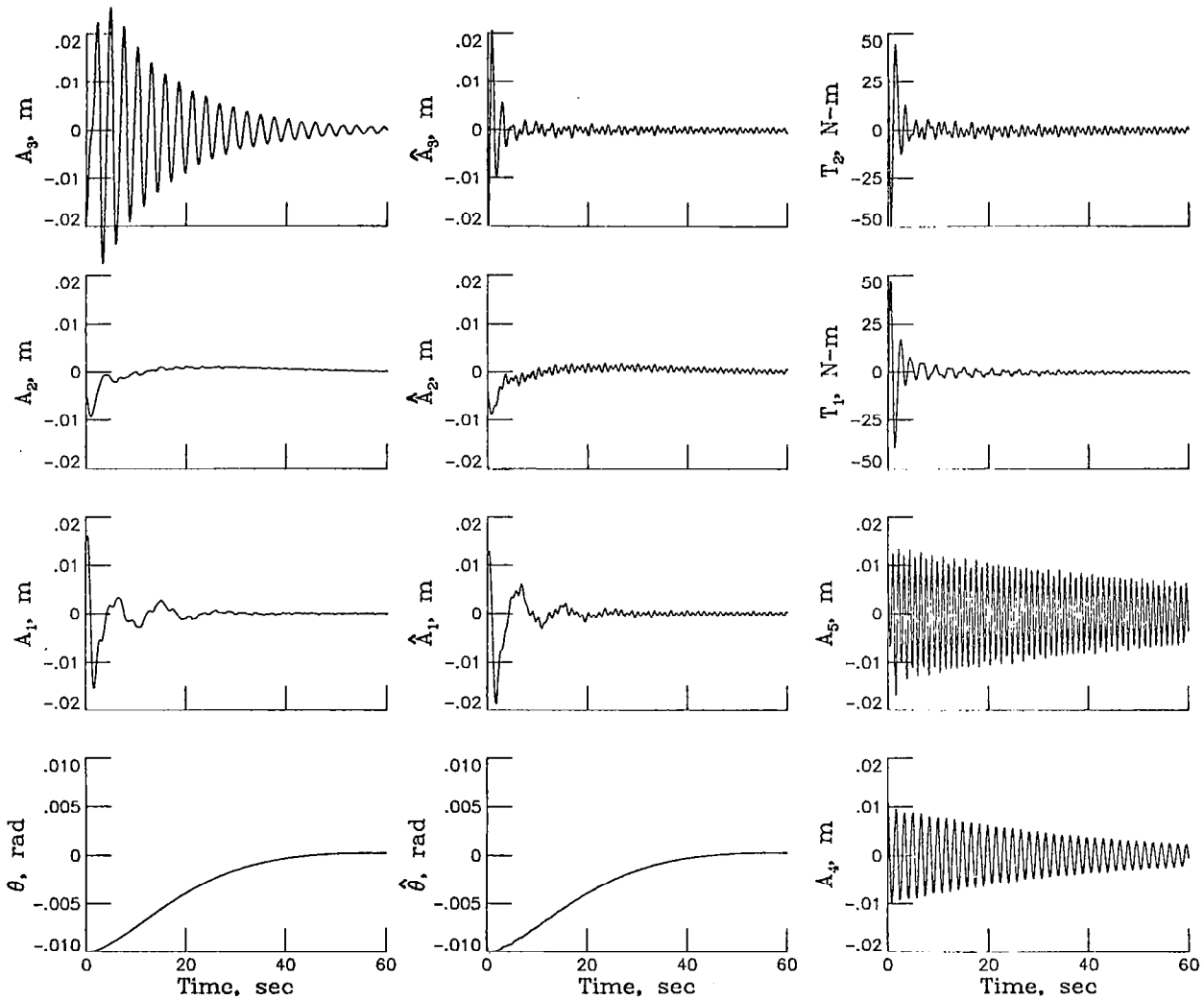

Figure 23

SENSOR LOCATION ERROR, 5 PERCENT TOWARDS ENDS

The case in figure 24 is the same as that for the previous figure, except the two sensors are moved in opposite directions, where the mode-slope differences from nominal (for example, sign changes) are more pronounced. Even though the system is eventually nulled, the performance is decreased as evidenced by the increased oscillations in A_3 and in the control actuators. These results can be attributed to the poor estimates in the three modeled flexible modes.

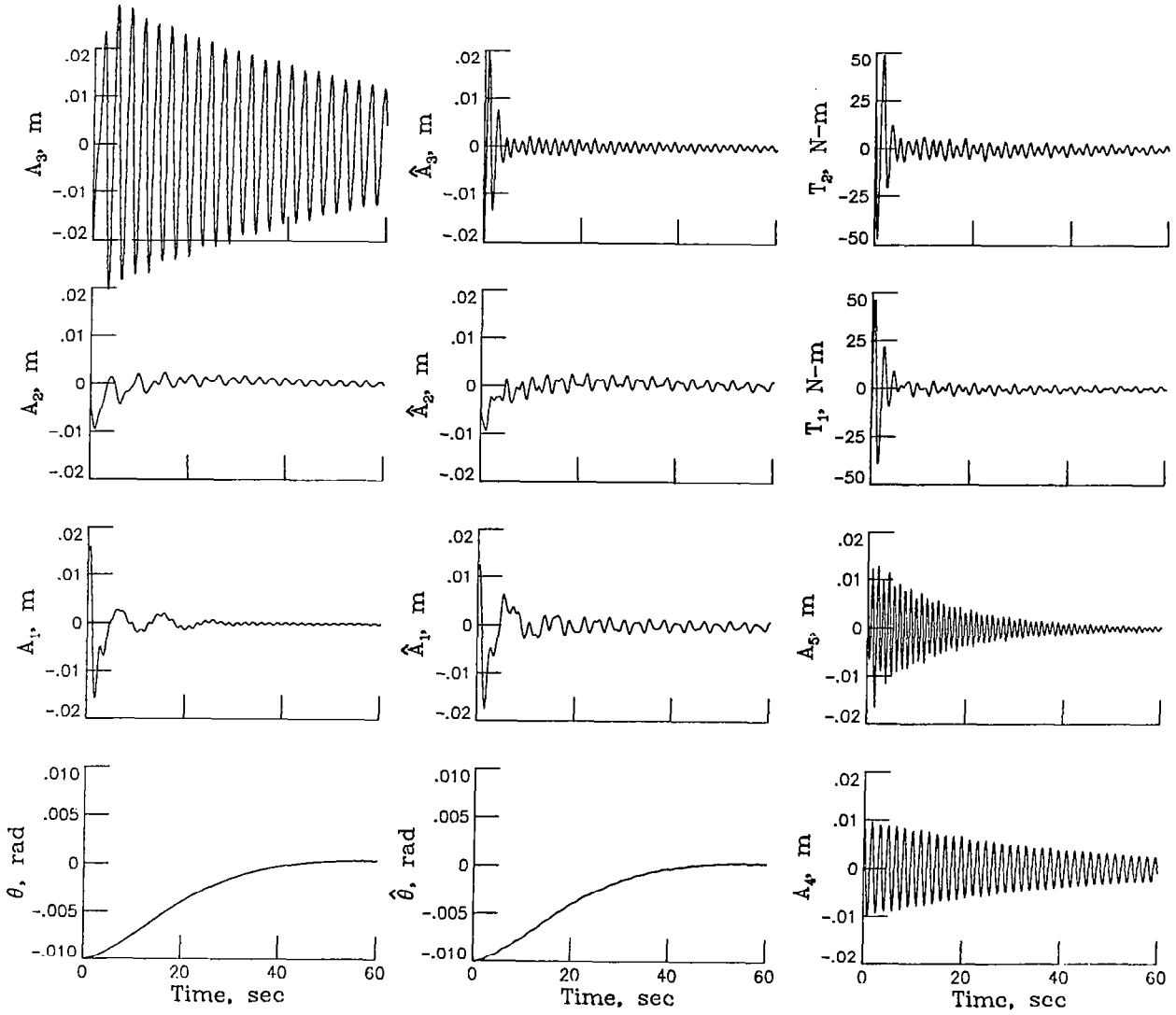

Figure 24

SENSOR LOCATION ERROR, 10 PERCENT TOWARDS ENDS

Relocation of the sensors 10 percent off the nominal position and in opposite directions leads to instability; this may be seen in figure 25.

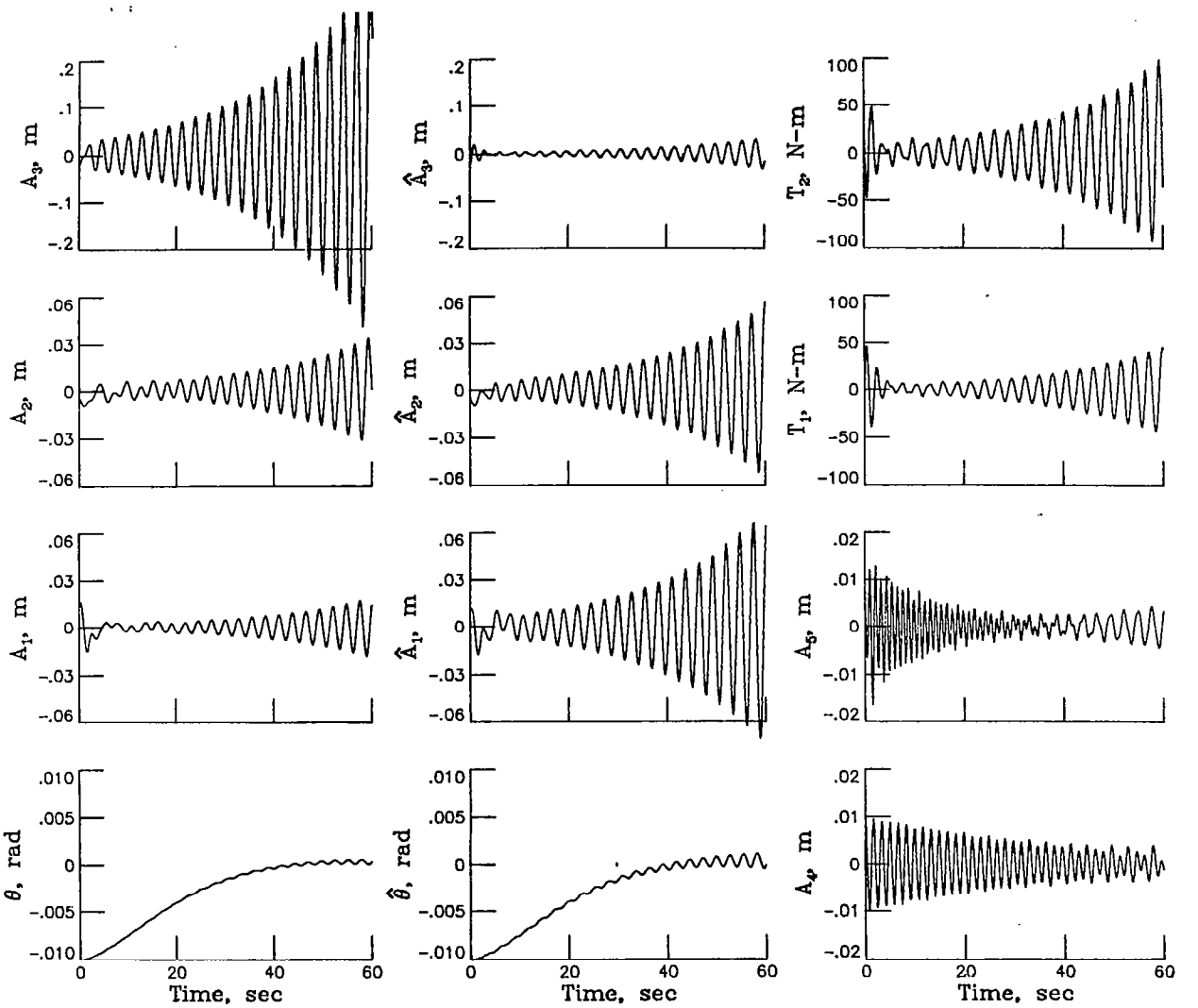

Figure 25

ACTIVE STABILIZATION OF A FLEXIBLE ANTENNA FEED TOWER

Arthur E. Bryson, Jr.
Stanford University
Stanford, California

ABSTRACT

Active stabilization logic is synthesized to hold a feed at the focus of a spacecraft antenna dish. The feed support structure is modeled as a tetrahedron made up of flexible bars and connected to the dish by six short legs containing force actuators. Using the symmetry of the structure, the model can be decomposed into four uncoupled subsystems: (1) pitch/forward motions with four degrees of freedom (DOF) and two controls, (2) roll/lateral motions with four DOF and two controls, (3) vertical motions with three DOF and one control, and (4) yaw motion with one DOF and one control. This greatly simplifies the synthesis of control logic.

INTRODUCTION

A spacecraft consists of a massive central body with a large antenna dish at one end; the feed for this antenna is mounted to the dish with a flexible support structure consisting of twelve bar-like members. (See fig. 1.) Six of the bars form a regular tetrahedron, with the feed at the apex. Two legs connect each of the three joints at the base of the tetrahedron to the antenna-dish/spacecraft, which we shall approximate as an inertial frame of reference due to its large mass. The mass of the structure will be lumped at the four joints of the tetrahedron, and the bars will be approximated as springs with axial deformation only.

The design objective is to control the four lowest frequency vibration modes that involve lateral motions of the feed so that they are at least 10 percent critically damped.

SEPARATION INTO SYMMETRIC AND ANTISYMMETRIC MOTIONS

Motions symmetric with respect to y-z plane involve seven degrees of freedom:

$$y_1,\ z_1,\ x_2 = -x_3,\quad y_2 = y_3,\quad z_2 = z_3,\ y_4,\ z_4$$

Motions antisymmetric with respect to y-z plane involve five degrees of freedom:

$$x_1,\ x_2 = x_3,\quad y_2 = -y_3,\quad z_2 = z_3,\ x_4$$

Three of the symmetric modes involve only vertical (z_1) motions of the apex, and one antisymmetric mode is symmetric about the z axis (a yaw mode), producing zero motion of the apex. The remaining eight modes consist of two sets of four modes that have identical frequencies, but one set involves symmetric motions and the other set involves antisymmetric motions.

The actuator forces can be arranged into six sets, one of which controls only the yaw mode, another that controls only z_1 motions, and two sets of two that control the remaining symmetric and antisymmetric modes, respectively. Thus the stabilization problem may be reduced to two almost identical problems of controlling four modes with two controls.

EQUATIONS OF MOTION

Let $\vec{r}_i$ be displacement vector of ith joint, $\vec{m}_{ij}$ be position vector from ith joint to jth joint, and k_1, k_2, k_ℓ be equal to EA/mL^3 for base members, vertical members, and legs, respectively. Then

$$\ddot{\vec{r}}_1 = -k_2\vec{m}_{1,2}\cdot(\vec{r}_1 - \vec{r}_2) - k_2\vec{m}_{1,3}\vec{m}_{1,3}\cdot(\vec{r}_1 - \vec{r}_3) - k_2\vec{m}_{1,4}\vec{m}_{1,4}\cdot(\vec{r}_1 - \vec{r}_4)$$

$$\ddot{\vec{r}}_2 = -k_2\vec{m}_{1,2}\vec{m}_{1,2}\cdot(\vec{r}_2 - \vec{r}_1) - k_1\vec{m}_{2,3}\vec{m}_{2,3}\cdot(\vec{r}_2 - \vec{r}_3) - k_1\vec{m}_{2,4}\vec{m}_{2,4}\cdot(\vec{r}_2 - \vec{r}_4)$$
$$- k_\ell\vec{m}_{2,5}\vec{m}_{2,5}\cdot\vec{r}_2 - k_\ell\vec{m}_{2,6}\vec{m}_{2,6}\cdot\vec{r}_2 + \vec{m}_{2,5}f_{2,5} + \vec{m}_{2,6}f_{2,6}$$

$$\ddot{\vec{r}}_3 = -k_2\vec{m}_{1,3}\vec{m}_{1,3}\cdot(\vec{r}_3 - \vec{r}_1) - k_1\vec{m}_{2,3}\vec{m}_{2,3}\cdot(\vec{r}_3 - \vec{r}_2) - k_1\vec{m}_{3,4}\vec{m}_{3,4}\cdot(\vec{r}_3 - \vec{r}_4)$$
$$- k_\ell\vec{m}_{3,7}\vec{m}_{3,7}\cdot\vec{r}_{3,7} - k_\ell\vec{m}_{3,8}\vec{m}_{3,8}\cdot\vec{r}_3 + \vec{m}_{3,7}f_{3,7} + \vec{m}_{3,8}f_{3,8}$$

$$\ddot{\vec{r}}_4 = -k_2\vec{m}_{1,4}\vec{m}_{1,4}\cdot(\vec{r}_4 - \vec{r}_1) - k_1\vec{m}_{2,4}\vec{m}_{2,4}\cdot(\vec{r}_4 - \vec{r}_2) - k_1\vec{m}_{3,4}\vec{m}_{3,4}\cdot(\vec{r}_4 - \vec{r}_3)$$
$$- k_\ell\vec{m}_{4,9}\vec{m}_{4,9}\cdot\vec{r}_4 - k_\ell\vec{m}_{4,10}\vec{m}_{4,10}\cdot\vec{r}_4 + \vec{m}_{4,9}f_{4,9} + \vec{m}_{4,10}f_{4,10}$$

For nominal configuration,

$$k_1 = \frac{(1)(1000)}{(2)(10)^3} = 0.5$$

$$k_2 = \frac{(1)(100)}{(2)(10)^3} = 0.05$$

$$k_\ell = \frac{(1)(100)}{(2)(2\sqrt{2})^3} = 2.2097$$

COMPUTER CODE "TETRA"

Calculates 12×12 K matrix, where

$$\frac{d^2}{dt^2}\begin{bmatrix} r_1 \\ \cdots \\ r_2 \\ \cdots \\ r_3 \\ \cdots \\ r_4 \end{bmatrix} = -K\begin{bmatrix} r_1 \\ \cdots \\ r_2 \\ \cdots \\ r_3 \\ \cdots \\ r_4 \end{bmatrix} + Gf$$

Calculates 7×7 K_S matrix and 5×5 K_A matrix, where

$$\ddot{d}_S = -K_S d_S + G_S f_S$$

$$\ddot{d}_A = -K_A d_A + G_A f_A$$

$$d_S \triangleq \left[y_1,\ z_1,\ \frac{x_2 - x_3}{2},\ \frac{y_2 + y_3}{2},\ \frac{z_2 + z_3}{2},\ y_4,\ z_4\right]^T$$

$$d_A \triangleq \left[x_1,\ \frac{x_2 + x_3}{2},\ \frac{y_2 - y_3}{2},\ \frac{z_2 - z_3}{2},\ x_4\right]^T$$

$$f_S \triangleq \left[\frac{H_2 - H_3}{2},\ \frac{V_2 + V_3}{2},\ V_4\right]^T$$

$$f_A \triangleq \left[\frac{H_2 + H_3}{2},\ \frac{V_2 - V_3}{2},\ H_4\right]^T$$

Note actuator forces resolved into vertical and horizontal components (V_i, H_i) at joints i = 2,3,4, which makes the determination of G_S,G_A quite simple.

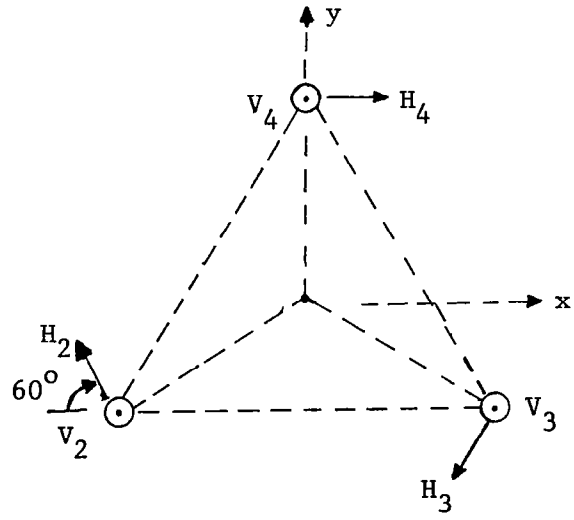

```
10 REM ***** TETRA **** 1/19/82 *****
20 REM * FINDS STIFFNESS MATRIX GIVEN
30 REM * JOINT COORDINATES & MEMBER
40 REM * STIFFNESSES FOR TETRAHEDRON
50 REM * ON LEGS; THEN FINDS STIFFNESS
60 REM * MATRICES FOR SYMMETRIC &
70 REM * ANTI-SYMMETRIC MOTIONS.
80 REM ********************************
90 DIMX(10,3),M(4,10,3),K(12,12):FORI=1TO10:FORJ=1TO3:READX(I,J):NEXTJ,I
100 READK1,K2,KL:DEFFNR(S)=INT(10000*S+.5)/10000
110 FORI=1TO4:FORJ=1TO10:FORK=1TO3:M(I,J,K)=X(I,K)-X(J,K):NEXTK,J,I
120 FORI=1TO3:FORJ=4TO6:K(I,J)=M(1,2,I)*M(1,2,J-3)*K2:NEXTJ,I
130 FORI=1TO3:FORJ=7TO9:K(I,J)=M(1,3,I)*M(1,3,J-6)*K2:NEXTJ,I
140 FORI=1TO3:FORJ=10TO12:K(I,J)=M(1,4,I)*M(1,4,J-9)*K2:NEXTJ,I
150 FORI=4TO6:FORJ=7TO9:K(I,J)=M(2,3,I-3)*M(2,3,J-6)*K1:NEXTJ,I
160 FORI=4TO6:FORJ=10TO12:K(I,J)=M(2,4,I-3)*M(2,4,J-9)*K1:NEXTJ,I
170 FORI=7TO9:FORJ=10TO12:K(I,J)=M(3,4,I-6)*M(3,4,J-9)*K1:NEXTJ,I
180 FORI=1TO3:FORJ=4TO12:K(J,I)=K(I,J):NEXTJ,I
190 FORI=4TO6:FORJ=7TO12:K(J,I)=K(I,J):NEXTJ,I
200 FORI=7TO9:FORJ=10TO12:K(J,I)=K(I,J):NEXTJ,I
210 FORI=1TO3:FORJ=1TO3:K(I,J)=-K(I,J+3)-K(I,J+6)-K(I,J+9):NEXTJ,I
220 FORI=4TO6:FORJ=4TO6:K(I,J)=-K(I,J-3)-K(I,J+3)-K(I,J+6):NEXTJ,I
230 FORI=4TO6:FORJ=4TO6:K(I,J)=K(I,J)-M(2,5,I-3)*M(2,5,J-3)*KL:NEXTJ,I
240 FORI=4TO6:FORJ=4TO6:K(I,J)=K(I,J)-M(2,6,I-3)*M(2,6,J-3)*KL:NEXTJ,I
250 FORI=7TO9:FORJ=7TO9:K(I,J)=-K(I,J-6)-K(I,J-3)-K(I,J+3):NEXTJ,I
260 FORI=7TO9:FORJ=7TO9:K(I,J)=K(I,J)-M(3,7,I-6)*M(3,7,J-6)*KL:NEXTJ,I
270 FORI=7TO9:FORJ=7TO9:K(I,J)=K(I,J)-M(3,8,I-6)*M(3,8,J-6)*KL:NEXTJ,I
280 FORI=10TO12:FORJ=10TO12:K(I,J)=-K(I,J-9)-K(I,J-6)-K(I,J-3):NEXTJ,I
290 FORI=10TO12:FORJ=10TO12:K(I,J)=K(I,J)-M(4,9,I-9)*M(4,9,J-9)*KL:NEXTJ,I
300 FORI=10TO12:FORJ=10TO12:K(I,J)=K(I,J)-M(4,10,I-9)*M(4,10,J-9)*KL:NEXTJ,I
310 PRINTTAB(10);"STIFFNESS/MASS MATRIX, UPPER LEFT QUADRANT"
320 FORI=1TO6:PRINTTAB(10);:FORJ=1TO6:PRINTFNR(K(I,J));:NEXTJ:PRINT:NEXTI
330 PRINTTAB(10);"UPPER RIGHT QUADRANT":FORI=1TO6:PRINTTAB(10);:FORJ=7TO12
335 PRINTFNR(K(I,J));:NEXTJ:PRINT:NEXTI
340 PRINTTAB(10);"LOWER RIGHT QUADRANT"
350 FORI=7TO12:PRINTTAB(10);:FORJ=7TO12:PRINTFNR(K(I,J));:NEXTJ:PRINT:NEXTI
360 REM *** CALCULATES ANTI-SYMMETRIC, SYMMETRIC STIFFNESS MATRICES: ***
370 DIMT(12,12),TI(12,12),L(12,12),L1(12,12):C=.5:T(1,1)=1:T(2,6)=1
380 T(3,7)=1:T(4,2)=1:T(4,8)=1:T(5,3)=1:T(5,9)=1:T(6,4)=1:T(6,10)=1:T(7,2)=1
390 T(7,8)=-1:T(8,9)=1:T(8,3)=-1:T(9,10)=1:T(9,4)=-1:T(10,5)=1:T(11,11)=1
400 T(12,12)=1:TI(1,1)=1:TI(2,4)=C:TI(2,7)=C:TI(3,5)=C:TI(3,8)=-C:TI(4,6)=C
410 TI(4,9)=-C:TI(5,10)=1:TI(6,2)=1:TI(7,3)=1:TI(8,4)=C:TI(8,7)=-C:TI(9,5)=C
420 TI(9,8)=C:TI(10,6)=C:TI(10,9)=C:TI(11,11)=1:TI(12,12)=1
430 FORI=1TO12:FORJ=1TO12:FORK=1TO12:L1(I,J)=L1(I,J)+K(I,K)*T(K,J):NEXTK,J,I
440 FORI=1TO12:FORJ=1TO12:FORK=1TO12:L(I,J)=L(I,J)+TI(I,K)*L1(K,J):NEXTK,J,I
450 PRINTTAB(10);"ANTI-SYMMETRIC STIFFNESS/MASS MATRIX:"
460 FORI=1TO5:PRINTTAB(10);:FORJ=1TO5:PRINTFNR(L(I,J));:NEXTJ:PRINT:NEXTI
470 PRINTTAB(10);"CROSS-COUPLING MATRIX:"
480 FORI=1TO5:PRINTTAB(10);:FORJ=6TO12:PRINTFNR(L(I,J));:NEXTJ:PRINT:NEXTI
490 PRINTTAB(10);"SYMMETRIC STIFFNESS/MASS MATRIX:"
500 FORI=6TO12:PRINTTAB(10);:FORJ=6TO12:PRINTFNR(L(I,J));:NEXTJ:PRINT:NEXTI
510 PRINTTAB(10);"CROSS-COUPLING MATRIX:"
520 FORI=6TO12:PRINTTAB(10);:FORJ=1TO5:PRINTFNR(L(I,J));:NEXTJ:PRINT:NEXTI:END
530 REM *** ENTER X,Y,Z COORDINATES OF JOINTS 1 THRU 10: ***
540 DATA 0,0,10.165,-5,-2.887,2,5,-2.887,2,0,5.7735,2,-6,-1.1547,0
550 DATA -4,-4.6188,0,4,-4.6188,0,6,-1.1547,0,2,5.7735,0,-2,5.7735,0
560 REM *** ENTER STIFFNESS/MASS FOR HEAVY MEMBERS, LIGHT MEMBERS, & LEGS: ***
570 DATA .5,.05,2.2097
READY.
```

PRINT-OUT FROM "TETRA"

```
STIFFNESS/MASS MATRIX, UPPER LEFT QUADRANT
-2.5  0  0  1.25  .7218  2.0413
 0 -2.5001 -2E-04  .7218  .4167  1.1786
 0 -2E-04 -10.0001  2.0413  1.1786  3.3334
 1.25  .7218  2.0413 -68.1694 -14.7184 -2.0413
 .7218  .4167  1.1786 -14.7184 -51.1771 -1.1764
 2.0413  1.1786  3.3334 -2.0413 -1.1764 -21.011
UPPER RIGHT QUADRANT
 1.25 -.7218 -2.0413  0  0  0
-.7218  .4167  1.1786  0  1.6667 -2.357
-2.0413  1.1786  3.3334  0 -2.357  3.3334
 50  0  0  12.5  21.6513  0
 0  0  0  21.6513  37.5021  0
 0  0  0  0  0  0
LOWER RIGHT QUADRANT
-68.1694  14.7184  2.0413  12.5 -21.6513  0
 14.7184 -51.1771 -1.1764 -21.6513  37.5021  0
 2.0413 -1.1764 -21.011  0  0  0
 12.5 -21.6513  0 -42.6776  0  0
-21.6513  37.5021  0  0 -76.6709  2.357
 0  0  0  0  2.357 -21.011

ANTI-SYMMETRIC STIFFNESS/MASS MATRIX:
-2.5  2.5  1.4435  4.0825  0
 1.25 -18.1694 -14.7184 -2.0413  12.5
 .7218 -14.7184 -51.1771 -1.1764  21.6513
 2.0413 -2.0413 -1.1764 -21.011  0
 0  25  43.3025  0 -42.6776
CROSS-COUPLING MATRIX:
 0  0  0  0  0  0  0
 0  0  0  0  0  0  0
 0  0  0  0  0  0  0
 0  0  0  0  0  0  0
 0  0  0  0  0  0  0
SYMMETRIC STIFFNESS/MASS MATRIX:
-2.5001 -2E-04  1.4435  .8335  2.3572  1.6667 -2.357
-2E-04 -10.0001  4.0825  2.3572  6.6667 -2.357  3.3334
 .7218  2.0413 -118.1694 -14.7184 -2.0413  21.6513  0
 .4167  1.1786 -14.7184 -51.1771 -1.1764  37.5021  0
 1.1786  3.3334 -2.0413 -1.1764 -21.011  0  0
 1.6667 -2.357  43.3025  75.0043  0 -76.6709  2.357
-2.357  3.3334  0  0  0  2.357 -21.011
CROSS-COUPLING MATRIX:
 0  0  0  0  0
 0  0  0  0  0
 0  0  0  0  0
 0  0  0  0  0
 0  0  0  0  0
 0  0  0  0  0
 0  0  0  0  0
```

EQUATIONS OF MOTION IN MODAL FORM

Using computer code "MODALSYS", the symmetric and antisymmetric equations of motion were put into modal form. Sketches of these mode shapes are given in figures 2 through 4. Only four modes involve fore-aft (y_1) motions of the apex (fig. 2). Another four modes involve only lateral (x_1) motions of the apex (fig. 3). Another three modes involve only vertical (z_1) motions of the apex (fig. 4). One mode involves no motion of the apex (fig. 5).

SEPARATION INTO FOUR SUBSYSTEMS

Only two linear combinations of actuator forces enter into the y_1 apex motions. (See first example of modal controllability matrix.) We shall call them f_{pitch} and f_{fwd}. Two different linear combinations of actuator forces enter into the x_1 apex motions. (See second example of modal controllability matrix.) They will be referred to as f_{roll} and f_{flat}. One different linear combination of actuator forces enters into the z_1 apex motions. It is called f_{vert}. One different linear combination of actuator forces involves no apex motion, and is called f_{yaw}. The equations of motion for these four subsystems are given elsewhere in this paper.

ANALYSIS OF TETRAHEDRON WITH CONSTRAINED MOTION

Symmetric Tetrahedron

Constraints

$$x_1 = x_4 = 0,\ x_3 = -x_2,\ y_3 = y_2,\ z_3 = z_2$$

$$h_3 = -h_2,\ v_3 = v_2,\ h_4 = 0$$

System equations

$$x = (y_1, z_1, x_2, y_2, z_2, y_4, z_4)$$

$$u = (H_2, v_2, v_4)$$

$$y = (y_1, y_2)$$

$$\dot{x} = Fx + Gu + G_A v$$

$$y = Hx$$

where

Units m ,sec

Dynamics Matrix F, is:

```
- 2.500 -  .000 + 1.443 +  .833 + 2.357 + 1.666 - 2.357
-  .000 -10.000 + 4.082 + 2.357 + 6.666 - 2.357 + 3.333
+  .721 + 2.041 -**.*** -14.718 - 2.041 +21.651 +  .000 (-118.1694)
+  .416 + 1.178 -14.718 -51.177 - 1.176 +37.502 +  .000
+ 1.178 + 3.333 - 2.041 - 1.176 -21.011 +  .000 +  .000
+ 1.666 - 2.357 +43.302 +75.004 +  .000 -76.670 + 2.357
- 2.357 + 3.333 +  .000 +  .000 +  .000 + 2.357 -21.011
```

Control Distribution Matrix, G, is:

```
+  .000 +  .000 +  .000
+  .000 +  .000 +  .000
-  .500 +  .000 +  .000
+  .866 +  .000 +  .000
+  .000 + 1.000 +  .000
+  .000 +  .000 +  .000
+  .000 +  .000 + 1.000
```

Feedback Gain Matrix C, is:

```
+  .000 +  .000 +  .000 +  .000 +  .000 +  .000 +  .000
+  .000 +  .000 +  .000 +  .000 +  .000 +  .000 +  .000
+  .000 +  .000 +  .000 +  .000 +  .000 +  .000 +  .000
```

Output Distribution Matrix, H, is:

```
+ 1.000 +  .000 +  .000 +  .000 +  .000 +  .000 +  .000
+  .000 + 1.000 +  .000 +  .000 +  .000 +  .000 +  .000
```

Disturbance Distribution Matrix GA, is:

```
+ 1.000 +  .000
+  .000 + 1.000
+  .000 +  .000
+  .000 +  .000
+  .000 +  .000
+  .000 +  .000
+  .000 +  .000
```

Modal Analysis

Eigenvalues are:

Real	Imaginary	Mode no.
-151.8372 +	.0000	12
- 85.5752 +	.0000	10
- 23.3724 +	.0000	9
- 21.7350 +	.0000	7
- 8.7456 +	.0000	4
- 7.4730 +	.0000	3
- 1.8009 +	.0000	1

Eigenvector Matrix, T, is:

```
y1 + .0000 - .0317 + .0000 + .1979 - .2629 - .0000 +1.0000  m12
z1 + .0512 - .0000 - .7307 - .0001 - .0008 +1.0000 - .0000  m10
x2 - .8659 + .9673 - .0275 + .0057 + .0832 + .0107 + .0165  m9
y2 - .5000 - .6753 - .0160 - .1190 + .8557 + .0064 + .0997  m7
z2 - .0193 + .0188 + .9994 - .4997 - .1214 + .2440 + .0534  m4
y4 +1.0000 +1.0000 + .0316 - .1090 +1.0000 - .0120 + .1283  m3
z4 - .0193 - .0376 +1.0000 +1.0000 + .2424 + .2441 - .1069  m1
```

```
Inverse of the Eigenvector Matrix is:
+ .0000 + .0170 - .5766 - .3329 - .0128 + .3329 - .0064
- .0083 + .0000 + .5109 - .3566 + .0099 + .2640 - .0099
- .0000 - .2067 - .0155 - .0090 + .5656 + .0089 + .2826
+ .1253 + .0000 + .0072 - .1507 - .6334 - .0690 + .6331
- .0997 - .0003 + .0631 + .6493 - .0921 + .3793 + .0920
- .0000 + .8480 + .0182 + .0109 + .4138 - .0102 + .2070
+ .9486 - .0000 + .0313 + .1892 + .1014 + .1218 - .1014

The Modal Dynamics Matrix Fq, Inv(T)*F*T, is:
-*.**** + .0000 + .0000 + .0000 + .0005 + .0000 + .0000 (-151.8)
+ .0000 -*.**** - .0000 - .0000 + .0005 + .0000 + .0000  (-85.57)
+ .0000 + .0000 -*.**** - .0003 + .0000 - .0002 + .0000  (-23.37)
+ .0000 + .0000 + .0003 -*.**** + .0002 + .0000 - .0000  (-21.73)
+ .0000 + .0000 + .0000 + .0000 -8.7466 + .0000 + .0000
+ .0000 + .0000 - .0002 - .0002 - .0000 -7.4721 + .0000
+ .0000 + .0000 - .0000 - .0000 - .0002 + .0000 -1.8009
The Modal Controllability Matrix Gq, Inv(T)*G, is:
- .0000 - .0128 - .0064
- .5643 + .0099 - .0099
- .0000 + .5656 + .2826
- .1341 - .6334 + .6331
+ .5307 - .0921 + .0920
+ .0004 + .4138 + .2070
+ .1482 + .1014 - .1014
The Modal Observability Matrix Hq, H*T, is:
+ .0000 - .0317 + .0000 + .1979 - .2629 - .0000 +1.0000
+ .0512 - .0000 - .7307 - .0001 - .0008 +1.0000 - .0000
The Modal Disturbability Matrix GAq, Inv(T)*(GA), is:
+ .0000 + .0170
- .0083 + .0000
- .0000 - .2067
+ .1253 + .0000
- .0997 - .0003
- .0000 + .8480
+ .9486 - .0000
```

Antisymmetric Tetrahedron

Constraints

$x_3 = x_2$, $y_3 = -y_2$, $z_3 = -z_2$, $z_1 = 0$, $y_1 = 0$, $y_4 = 0$, $z_4 = 0$,

$h_3 = h_2$, $v_3 = -v_2$, $v_4 = 0$

System equations

$x = (x_1, x_2, y_2, z_2, x_4)$

$u = (h_2, v_2, h_4)$

Modal amplitudes

$$q = [m_{12}, m_{10}, m_9, m_7, m_4, m_3, m_1]$$

$$\ddot{q} = F_q q + G_q u + G_{Aq} v$$

$$y = H_q q$$

where

Units m ,sec

Dynamics Matrix F, is:

```
- 2.500 + 2.500 + 1.443 + 4.082 +  .000
+ 1.250 -18.169 -14.718 - 2.041 +12.500
+  .721 -14.718 -51.177 - 1.176 +21.651
+ 2.041 - 2.041 - 1.176 -21.011 +  .000
+  .000 +25.000 +43.302 +  .000 -42.677
```

Control Distribution Matrix, G, is:

```
+  .000 +  .000 +  .000
-  .500 +  .000 +  .000
+  .866 +  .000 +  .000
+  .000 + 1.000 +  .000
+  .000 +  .000 + 1.000
```

Feedback Gain Matrix C, is:

```
+  .000 +  .000 +  .000 +  .000 +  .000
+  .000 +  .000 +  .000 +  .000 +  .000
+  .000 +  .000 +  .000 +  .000 +  .000
```

Output Distribution Matrix, H, is:

```
+ 1.000 +  .000 +  .000 +  .000 +  .000
```

Disturbance Distribution Matrix GA, is:

```
+ 1.000
+  .000
+  .000
+  .000
+  .000
```

Eigenvalues are:

Real	Imaginary	Mode no.
- 85.5753 +	.0000	11
- 21.7350 +	.0000	8
- 17.6775 +	.0000	6
- 8.7462 +	.0000	5
- 1.8009 +	.0000	2

Eigenvector Matrix, T, is:

```
+ .0256 - .2286 - .0001 - .2761 +1.0000
- .3579 + .1300 - .4998 +1.0000 + .1188
- .7840 - .0068 + .8659 + .0874 + .0165
- .0264 +1.0000 + .0004 - .2207 + .0926
+1.0000 + .1409 +1.0000 + .8483 + .0901
```

x_1		m_{11}
x_2		m_8
y_2		m_6
z_2		m_5
z_4		m_2

Inverse of the Eigenvector Matrix is:

```
+ .0103 - .2877 - .6303 - .0212 + .4019
- .1085 + .1234 - .0065 + .9496 + .0669
```

```
- .0000 - .3333 + .5774 + .0002 + .3334
- .0949 + .6875 + .0601 - .1518 + .2916
+ .9487 + .2254 + .0313 + .1757 + .0855
The Modal Dynamics Matrix, Inv(T)*F*T, is:
-*.**** + .0000 + .0000 + .0000 + .0000     (-85.58)
+ .0000 -*.**** + .0000 + .0000 + .0000     (-21.73)
+ .0000 + .0000 -*.**** + .0000 + .0000     (-17.68)
+ .0000 + .0000 + .0000 -8.7462 + .0000
+ .0000 + .0000 + .0000 + .0000 -1.8009
The Modal Controllability Matrix, Inv(T)*G, is:
- .4020 - .0212 + .4019
- .0673 + .9496 + .0669
+ .6667 + .0002 + .3334
- .2917 - .1518 + .2916
- .0855 + .1757 + .0855
The Modal Observability Matrix, H*T, is:
+ .0256 - .2286 - .0001 - .2761 +1.0000
The Modal Disturbability Matrix Inv(T)*(GA), is:
+ .0103
- .1085
- .0000
- .0949
+ .9487
Residues;All Outputs, Ctrl 1,Then Ctrl 2, etc.
- .0103 + .0154 - .0000 + .0805 - .0855
- .0005 - .2171 + .0000 + .0419 + .1757
+ .0103 - .0153 - .0000 - .0805 + .0855
Residues;All Outputs, Dist. 1, Then Dist. 2, etc.
+ .0002 + .0248 + .0000 + .0262 + .9487
```

PITCH/FORWARD TRANSLATION SUBSYSTEM

$$\ddot{m}_1 = -(1.342)^2 m_1 + 0.1907 f_p$$

$$\ddot{m}_4 = -(2.957)^2 m_4 + 0.6652 f_F$$

$$\ddot{m}_7 = -(4.662)^2 m_7 - 0.9848 f_p + 0.7914 f_F$$

$$\ddot{m}_{10} = -(9.251)^2 m_{10} - 0.1320 f_p - 0.5788 f_F$$

where

$$\begin{bmatrix} y_1 \\ z_1 \\ x_2 \\ y_2 \\ z_2 \\ y_4 \\ z_4 \end{bmatrix} = \begin{bmatrix} 1 & -0.2629 & 0.1979 & -0.0317 \\ 0 & 0 & 0 & 0 \\ 0.0165 & 0.0832 & 0.0057 & 0.9673 \\ 0.0997 & 0.8557 & -0.1190 & -0.6753 \\ 0.0534 & -0.1214 & -0.5000 & 0.0188 \\ 0.1283 & 1 & -0.1090 & 1 \\ -0.1069 & 0.02424 & 1 & -0.0376 \end{bmatrix} \begin{bmatrix} m_1 \\ m_4 \\ m_7 \\ m_{10} \end{bmatrix}$$

and

$$\begin{bmatrix} H_z \\ V_2 \\ V_4 \end{bmatrix} = \begin{bmatrix} 0.02602 & 1 \\ 0.5000 & -0.4872 \\ -1 & 0.9744 \end{bmatrix} \begin{bmatrix} f_p \\ f_F \end{bmatrix} \qquad \begin{aligned} H_3 &= -Hz \\ V_3 &= V_2 \\ H_4 &= 0 \end{aligned}$$

ROLL/LATERAL TRANSLATION SUBSYSTEM

$$\ddot{m}_2 = -(1.342)^2 m_2 + 0.2202 f_R$$

$$\ddot{m}_5 = -(2.957)^2 m_5 + 0.5482 f_L$$

$$\ddot{m}_8 = -(4.662)^2 m_8 + 0.9845 f_R - 0.5925 f_L$$

$$\ddot{m}_{11} = -(9.251)^2 m_{11} + 0.1880 f_R + 0.6184 f_L$$

where

$$\begin{bmatrix} x_1 \\ x_2 \\ y_2 \\ z_2 \\ x_4 \end{bmatrix} = \begin{bmatrix} 1 & -0.2761 & -0.2286 & 0.0256 \\ 0.1188 & 1 & 0.1300 & -0.3579 \\ 0.0165 & 0.0874 & -0.0068 & -0.7840 \\ 0.0926 & -0.2207 & 1 & -0.0264 \\ 0.0901 & 0.8483 & 0.1409 & 1 \end{bmatrix} \qquad \begin{bmatrix} m_2 \\ m_5 \\ m_8 \\ m_{11} \end{bmatrix} \qquad \begin{aligned} x_3 &= x_2 \\ y_3 &= -yz \\ z_3 &= z_2 \end{aligned}$$

and

$$\begin{bmatrix} H_2 \\ V_2 \\ H_4 \end{bmatrix} = \begin{bmatrix} -0.1735 & -0.5000 \\ 1 & -0.7299 \\ 0.3470 & 1 \end{bmatrix} \begin{bmatrix} f_R \\ f_L \end{bmatrix} \qquad \begin{aligned} H_3 &= Hz \\ V_3 &= -V_z \\ V_4 &= 0 \end{aligned}$$

VERTICAL SUBSYSTEM

$$\ddot{m}_3 = -(2.734)^2 m_3 + 0.6208 f_V$$

$$\ddot{m}_9 = -(4.835)^2 m_9 + 0.8476 f_V$$

$$\ddot{m}_{12} = -(12.322)^2 m_{12} + 0.0192 f_V$$

where

$$\begin{bmatrix} y_1 \\ z_1 \\ x_2 \\ y_2 \\ z_2 \\ y_4 \\ z_4 \end{bmatrix} = \begin{bmatrix} 0 & 0 & 0 \\ 1 & -0.7307 & 0.0512 \\ 0.0107 & -0.0275 & -0.8659 \\ 0.0064 & -0.0160 & -0.5000 \\ 0.2440 & 0.9994 & -0.0193 \\ -0.0120 & 0.0316 & 1 \\ 0.2440 & 1 & -0.0193 \end{bmatrix} \begin{bmatrix} m_3 \\ m_9 \\ m_{12} \end{bmatrix} \qquad \begin{aligned} x_3 &= -x_2 \\ y_3 &= y_2 \\ z_3 &= z_2 \end{aligned}$$

and

$$\begin{bmatrix} V_2 \\ V_3 \\ V_4 \end{bmatrix} = \begin{bmatrix} 1 \\ 1 \\ 1 \end{bmatrix} \begin{bmatrix} f_V \end{bmatrix}$$

YAW SUBSYSTEM

$$\ddot{m}_6 = -(4.204)^2 m_6 + 1.000 f_Y$$

where

$$\begin{bmatrix} x_1 \\ x_2 \\ y_2 \\ z_2 \\ x_4 \end{bmatrix} = \begin{bmatrix} 0 \\ -0.5000 \\ 0.8660 \\ 0 \\ 1.000 \end{bmatrix} \begin{bmatrix} m_6 \end{bmatrix} \qquad \begin{aligned} x_3 &= x_2 \\ y_3 &= -yz \\ z_3 &= z_2 \end{aligned}$$

and

$$\begin{bmatrix} H_2 \\ H_3 \\ H_4 \end{bmatrix} = \begin{bmatrix} 1 \\ 1 \\ 1 \end{bmatrix} \begin{bmatrix} f_Y \end{bmatrix} \qquad \begin{aligned} V_2 &= 0 \\ V_3 &= 0 \\ V_4 &= 0 \end{aligned}$$

Figure 6 shows the combinations of controls that control only modes 1 and 4 (and also modes 7 and 10). Figure 7 shows the combinations of controls that control modes 2 and 5 (and also 8 and 11). Figure 8 shows the combinations of controls that control the vertical and yaw modes.

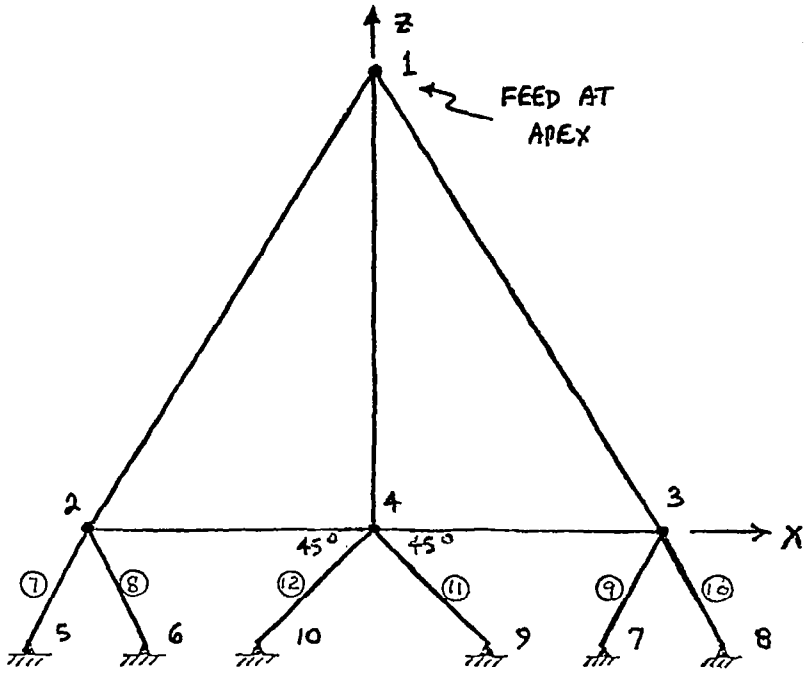

Rear view.

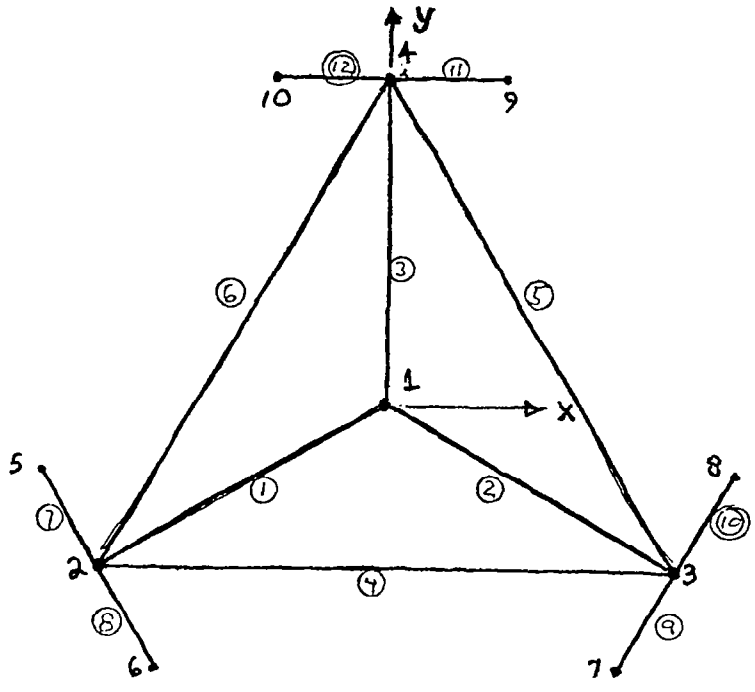

Top view

Figure 1.- Antenna feed tower.

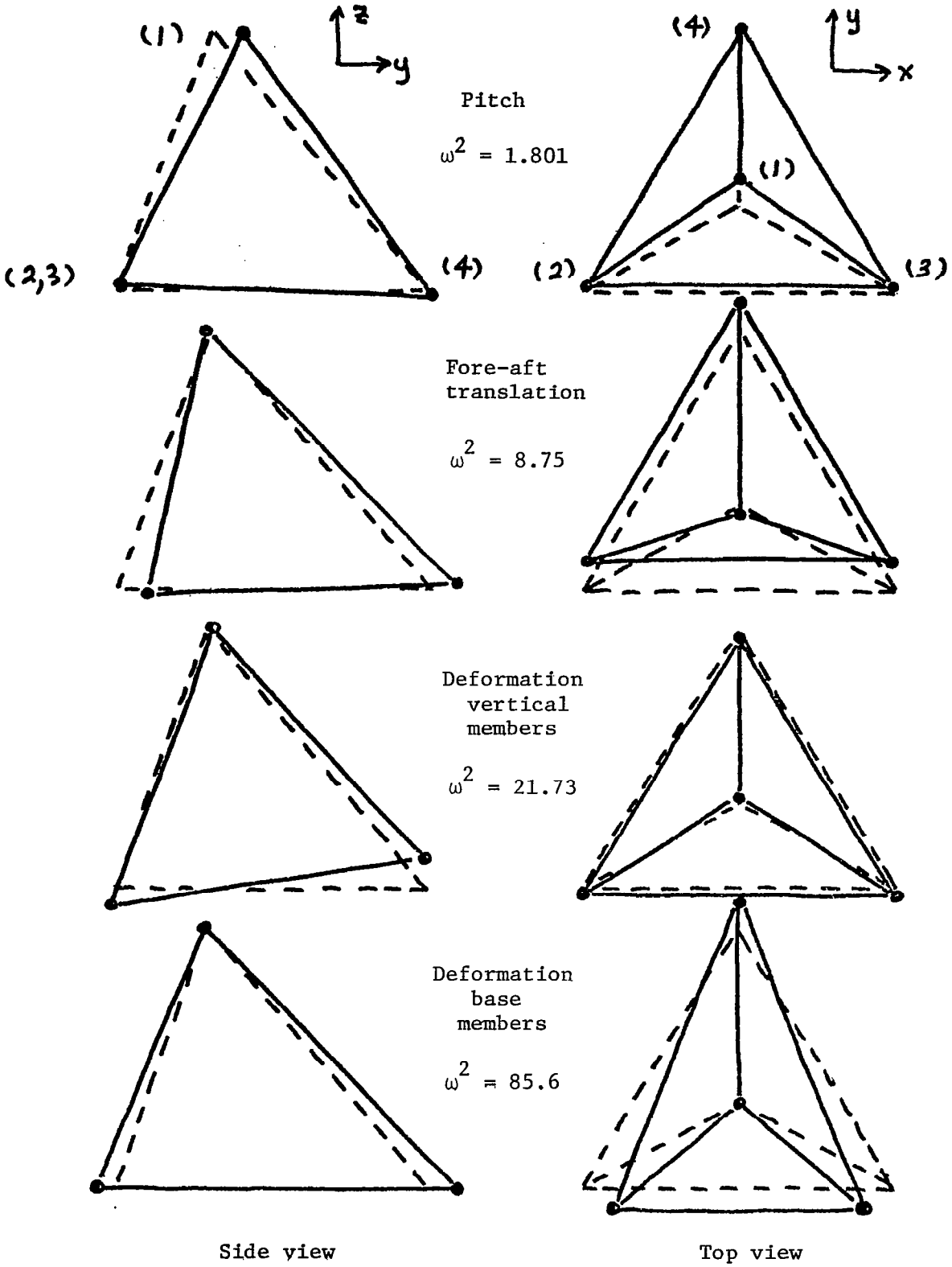

Figure 2.- Modes that involve only y motions of the apex.

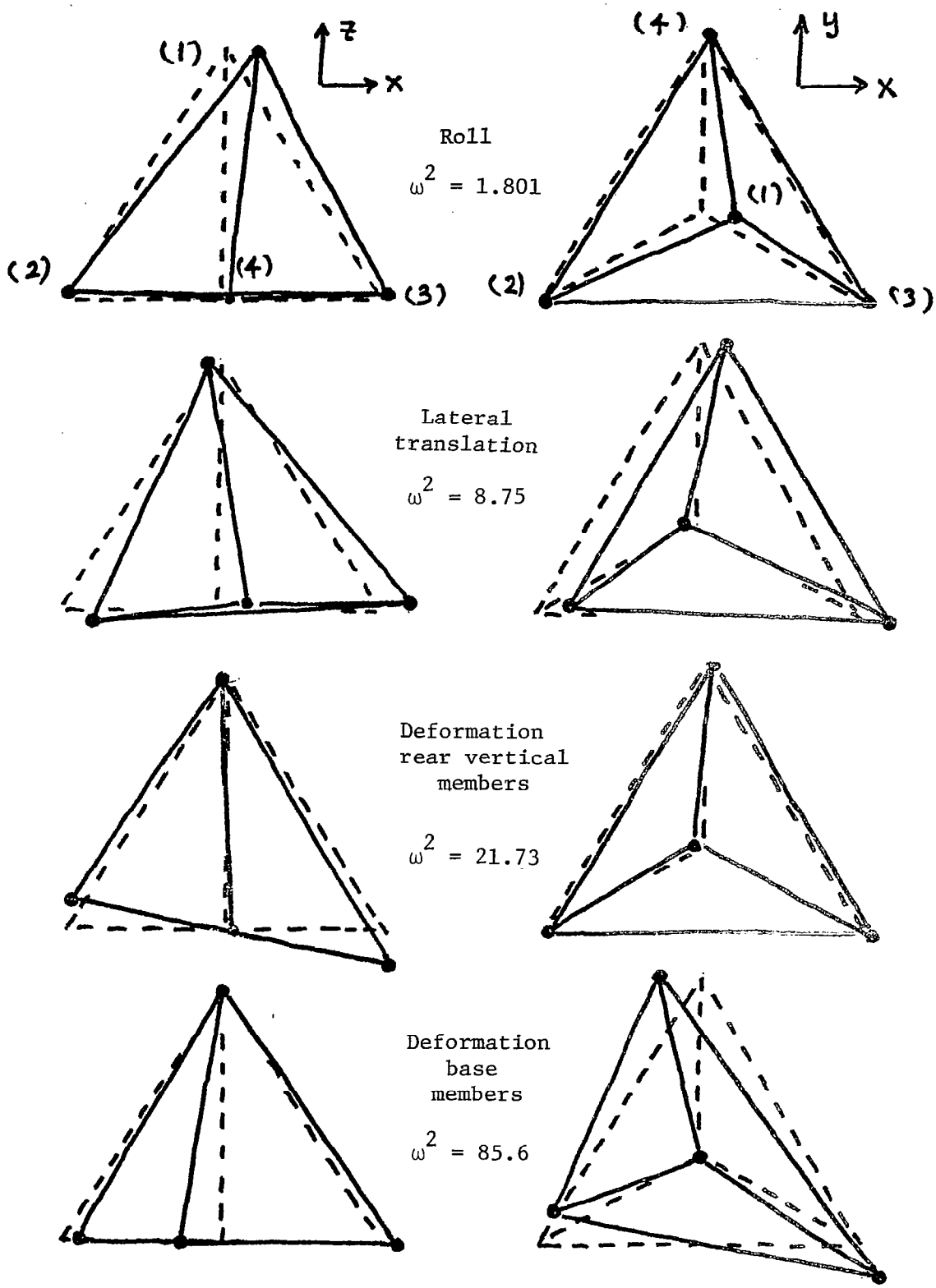

Figure 3.- Modes that involve only x motions of the apex.

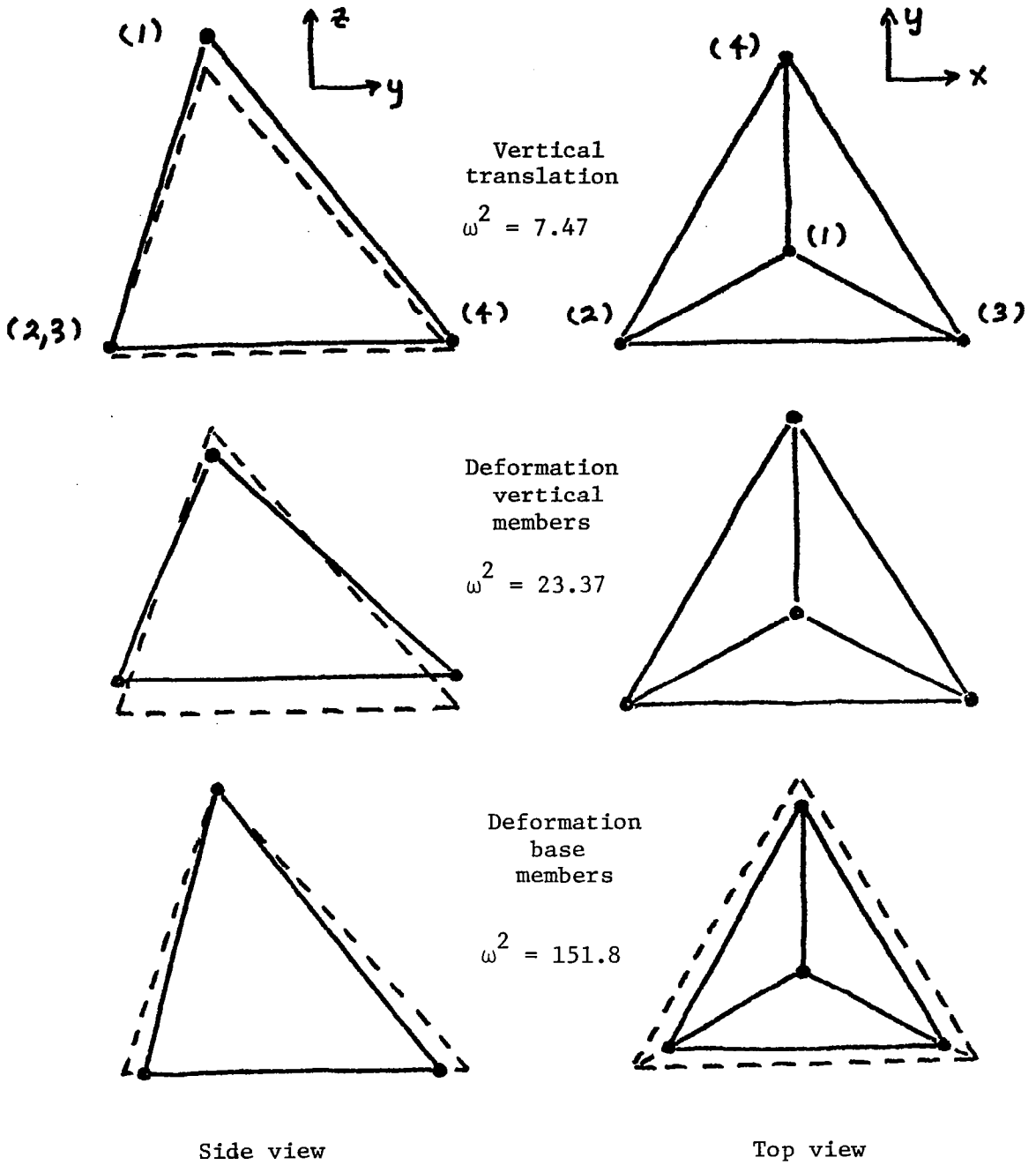

Figure 4.- Modes involving only z motions of the apex.

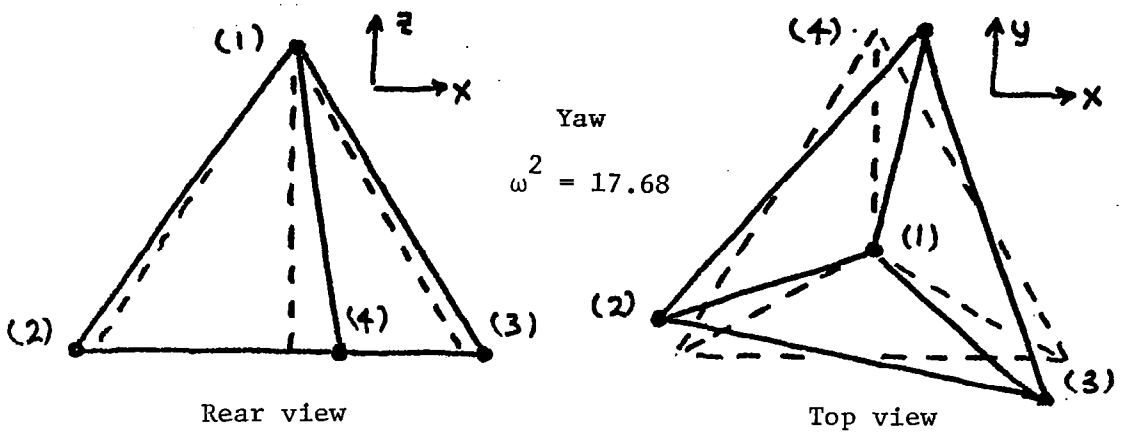

Figure 5.- Antisymmetric mode involving no motion of apex.

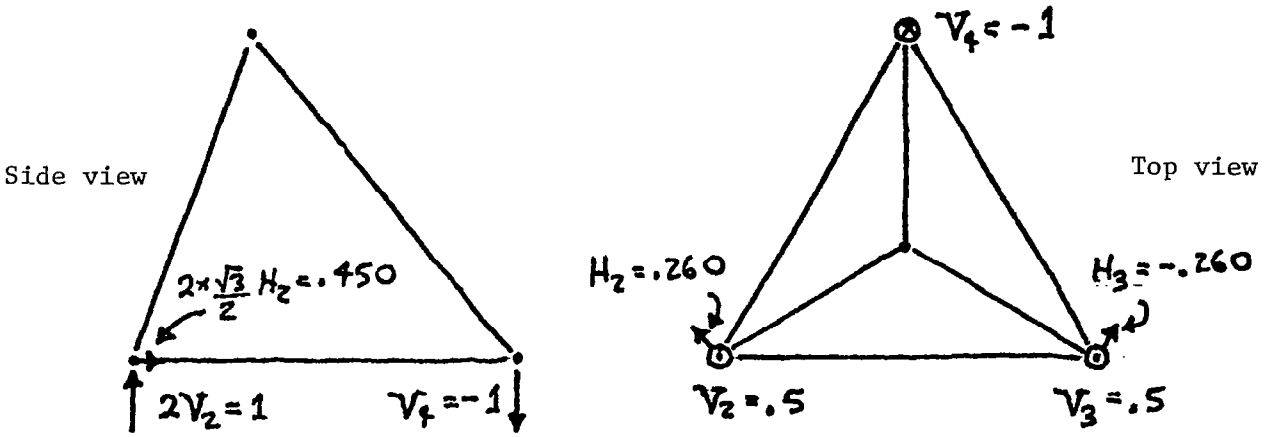

(a) Mode m_1 (pitch) controls (f_p).

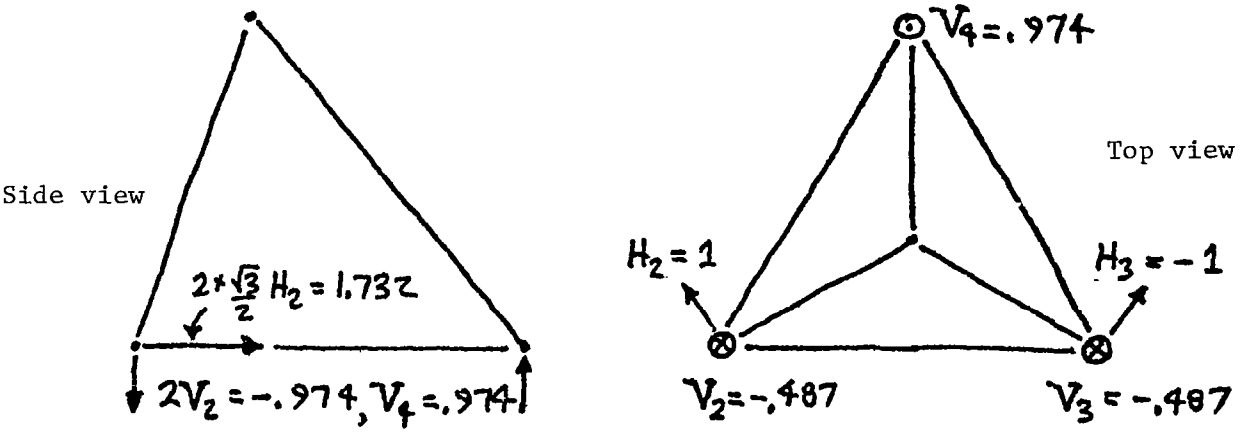

(b) Mode m_4 (forward translation) controls (f_F).

Figure 6.- Pitch and forward translation controls.

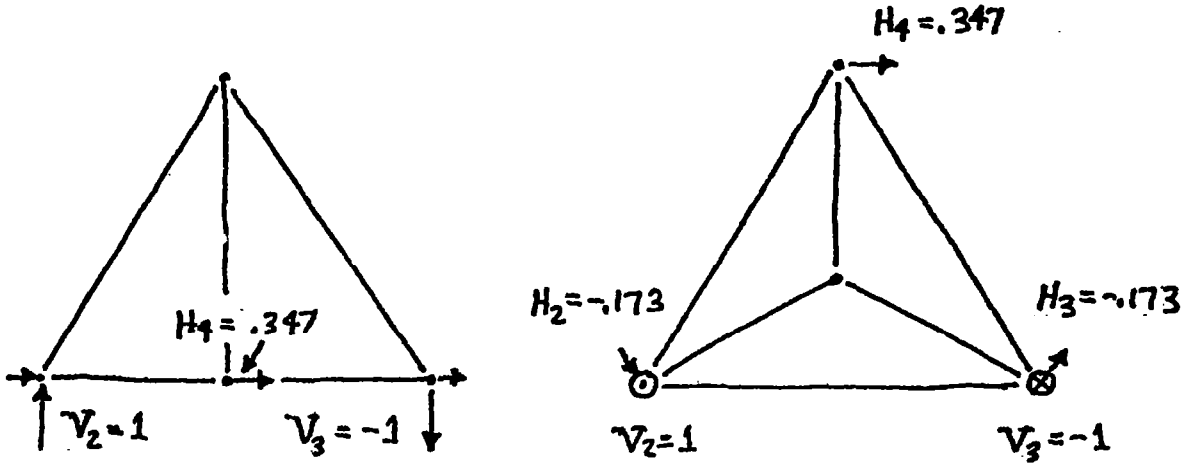

Rear view

Top view

(a) Mode m_2 (roll) controls (f_R).

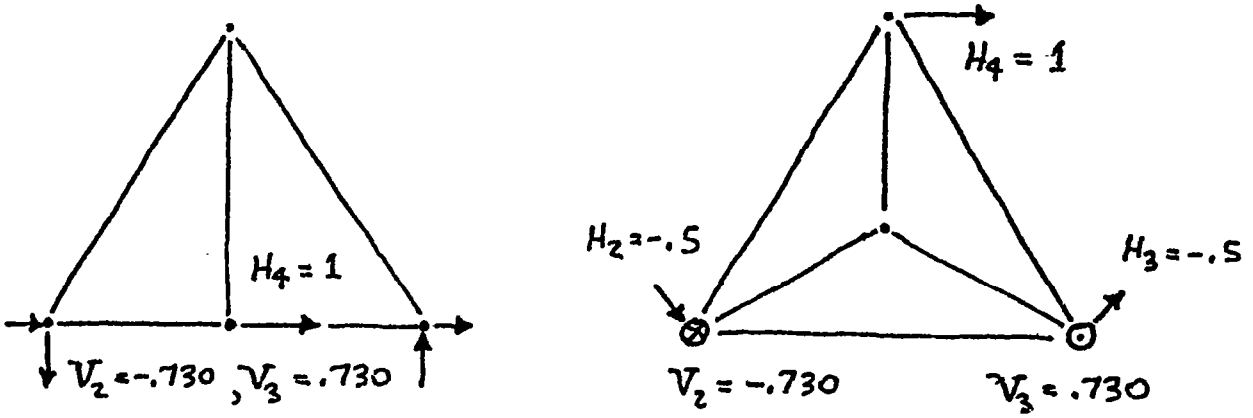

Rear view

Top view

(b) Mode m_5 (lateral translation) controls (f_L).

Figure 7.- Roll and lateral translation controls.

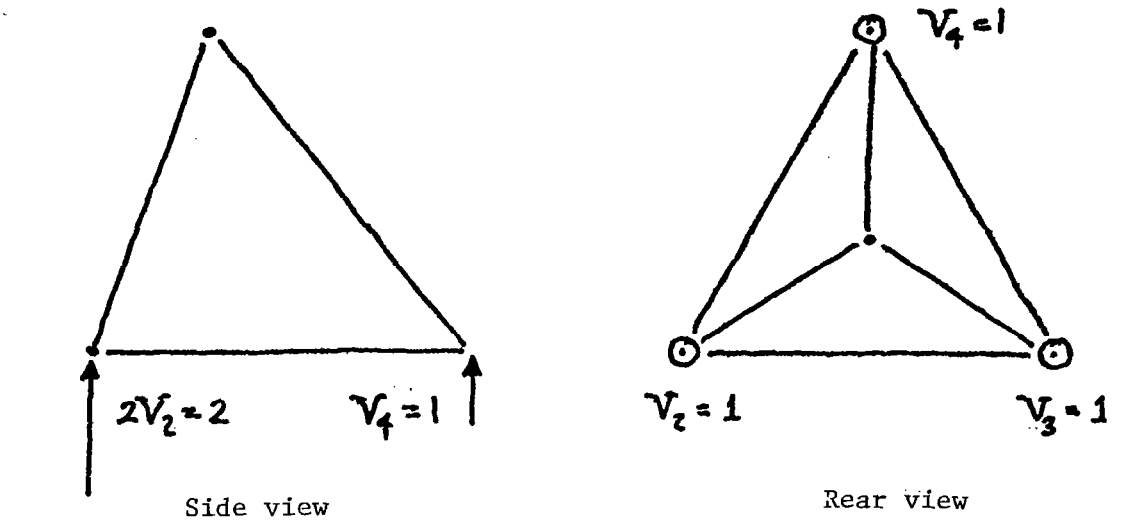

(a) Vertical modes control (f_v).

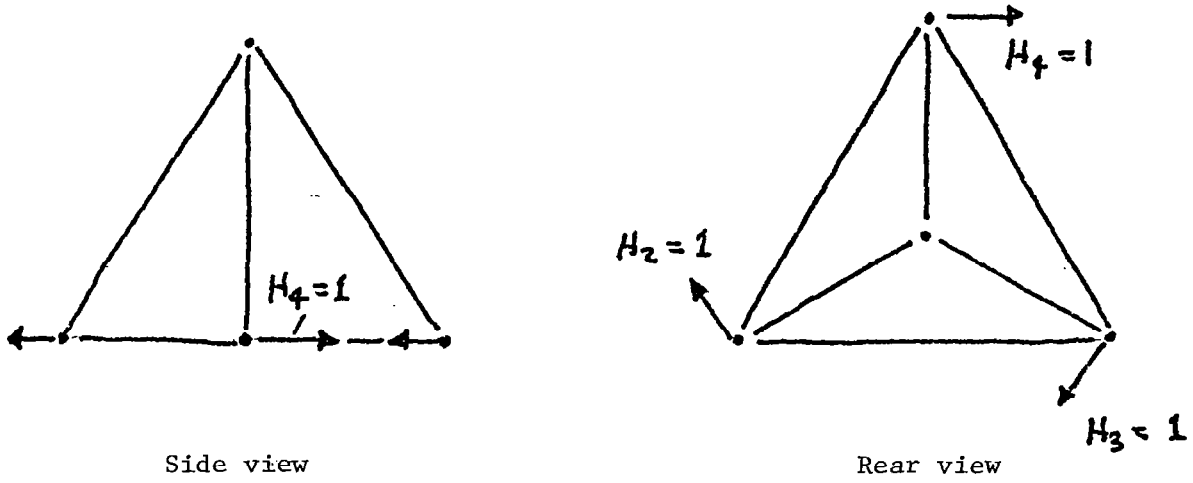

(b) Yaw mode controls (f_y).

Figure 8.- Vertical and yaw controls.

ACTIVE CONTROL OF FLEXIBLE STRUCTURES WITH SEPARATED SENSORS AND ACTUATORS

R. H. Cannon and D. Rosenthal
Stanford University
Stanford, California

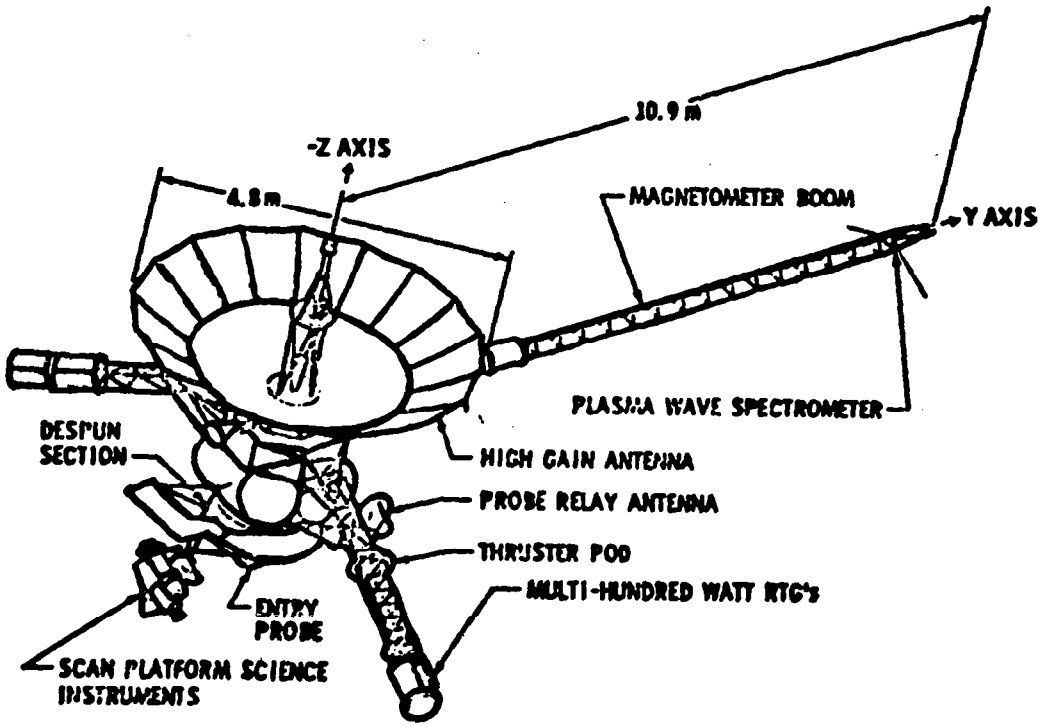

The Galileo spacecraft.

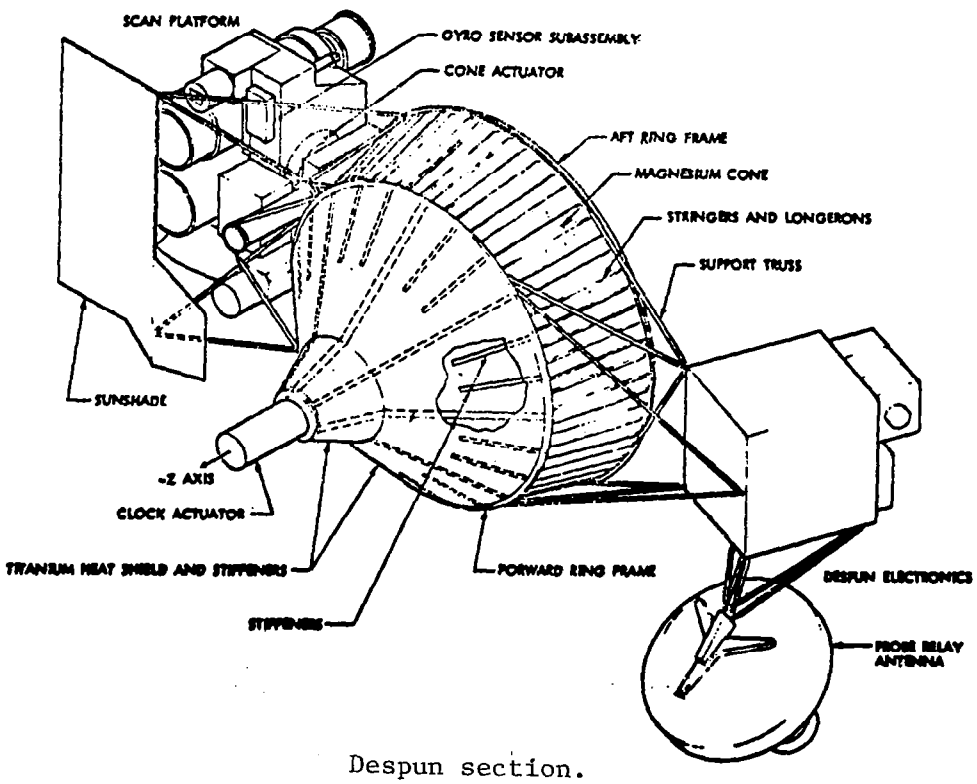

Despun section.

KEY CONTROL PROBLEMS OF FLEXIBLE SPACECRAFT

- Very flexible
- Low damping
- Noncolocated sensor and actuator
- Uncertain parameters
- Nearly equal modes

APPROACH TO CONTROL

- Kalman filter
- Adaptive control
  - Identify plant frequency
  - Tune Kalman filter

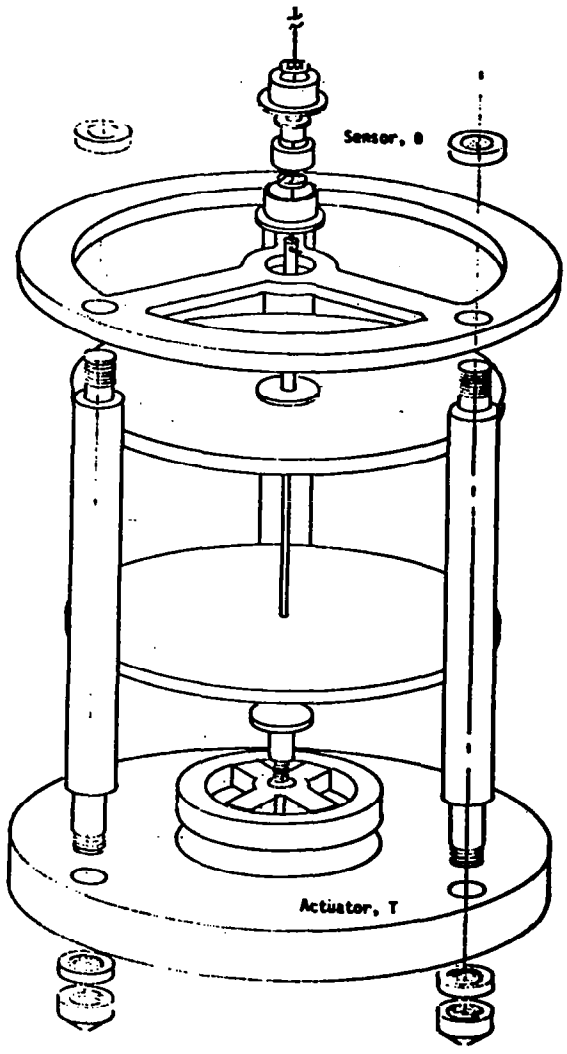

Initial laboratory two-disk plant.

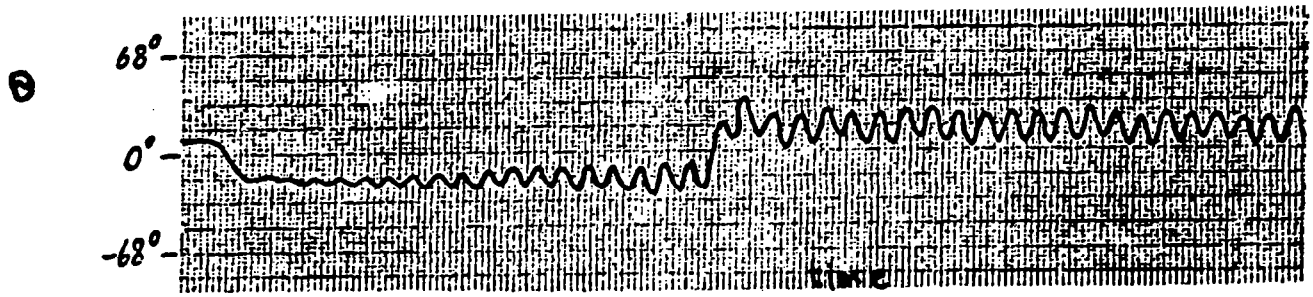

(a) Natural frequency modeled 10 percent lower than actual.

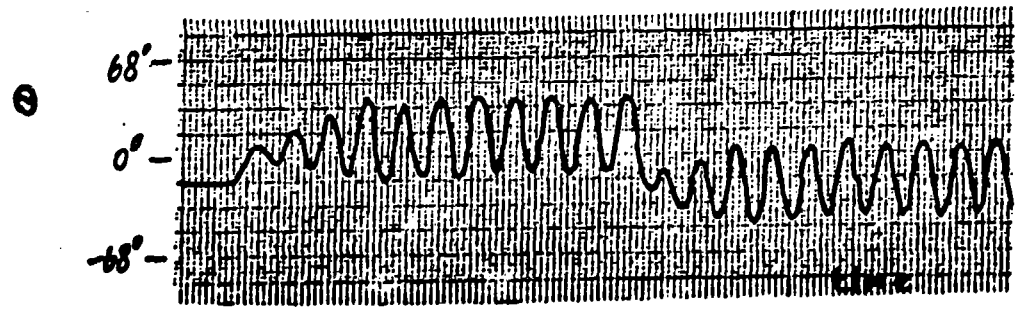

(b) Natural frequency modeled 20 percent higher than actual.

Step response of closed-loop system with mismatch in actual and modeled natural frequency.

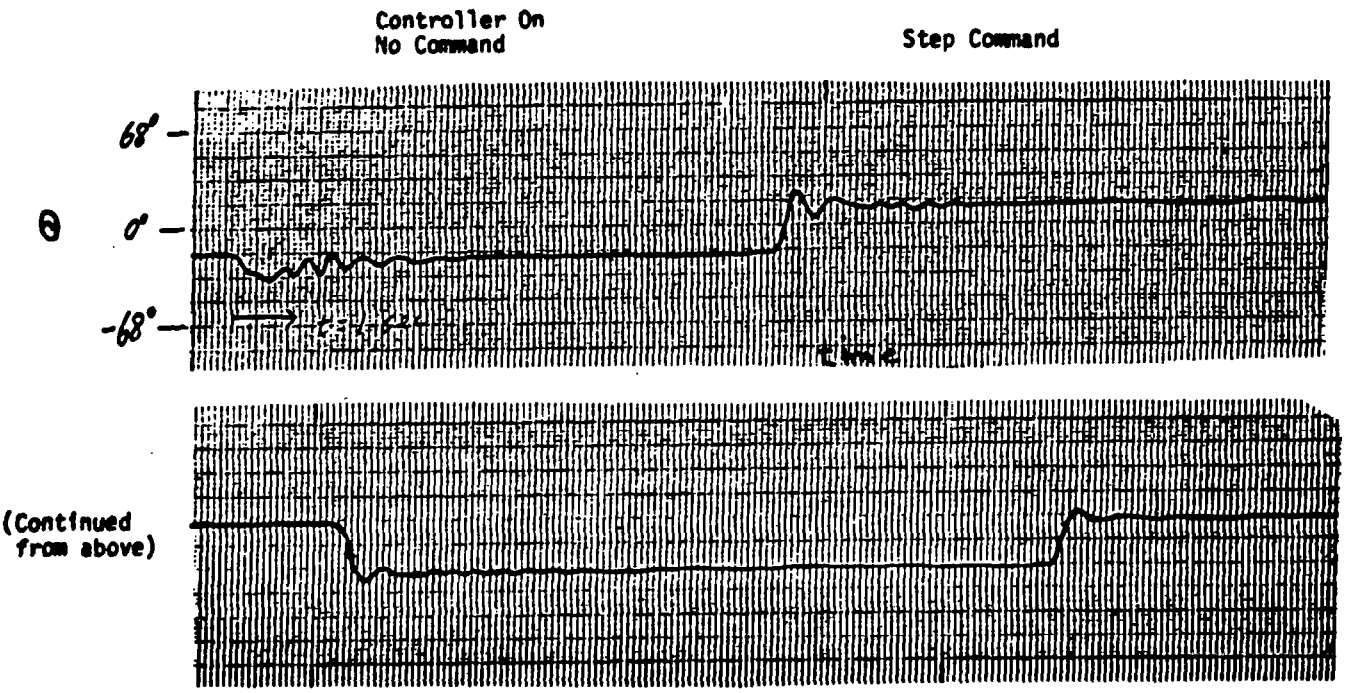

Step response of closed-loop system with self-tuning adaptive optimal controller. Vibration frequency in Kalman filter was incorrectly assumed to be 1.7 Hz (-25 percent error) initially. Parameter error in model was corrected in real time by frequency-locked loop.

DOCKING OF A RIGID SPACECRAFT WITH UNRESTRAINED ORBITING FLEXIBLE STRUCTURE

T. R. Kane
Stanford University
Palo Alto, California

Purpose:

Establish a methodology for producing simulations of the docking of a rigid spacecraft with any unrestrained flexible structure.

Method:

Produce a detailed algorithm for the simulation of the docking of a rigid body with a nonuniform unrestrained beam.

Background:

Predocking and postdocking motions can be simulated with algorithms given in references 1 and 2.

Tasks:

(1) Determine the values acquired during docking by the variables characterizing the motions of the rigid body and the unrestrained beam.

(2) Transform to the variables used in connection with the cantilever beam.

(3) Perform simulations of the total process.

REFERENCES

1. Levinson, David A.; and Kane, Thomas R.: Simulation of Large Motions of Nonuniform Beams in Orbit. Part 1 - The Cantilever Beam. J. Astronaut. Sci., vol. 29, no. 3, July-September 1981, pp. 213-244.

2. Kane, Thomas R.; and Levinson, David A.: Simulation of Large Motions of Nonuniform Beams in Orbit. Part 2 - The Unrestrained Beam. J. Astronaut. Sci., vol. 29, no. 3, July-September 1981, pp. 245-275.

Beam

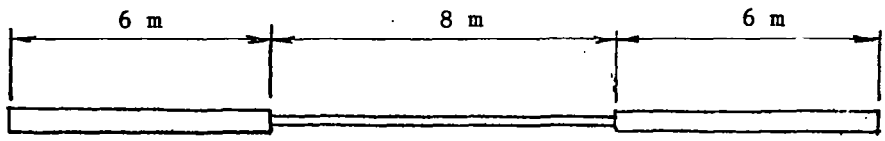

Variables

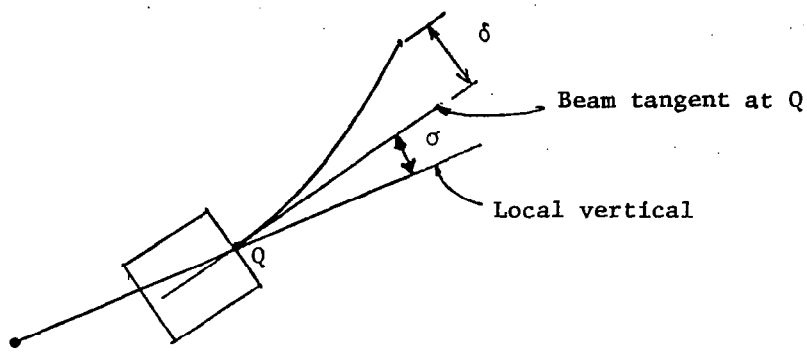

Initially undeformed beam

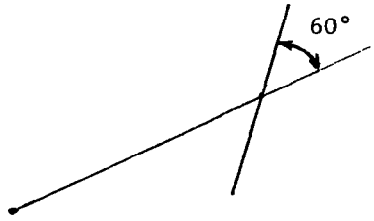

Initially deformed beam

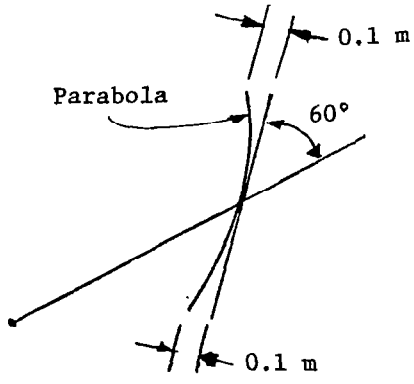

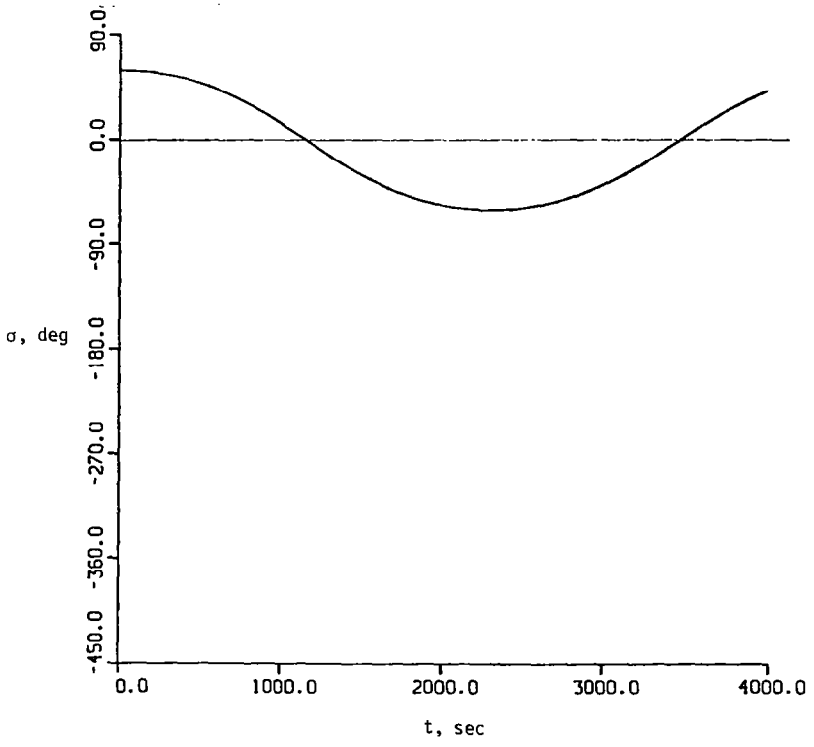

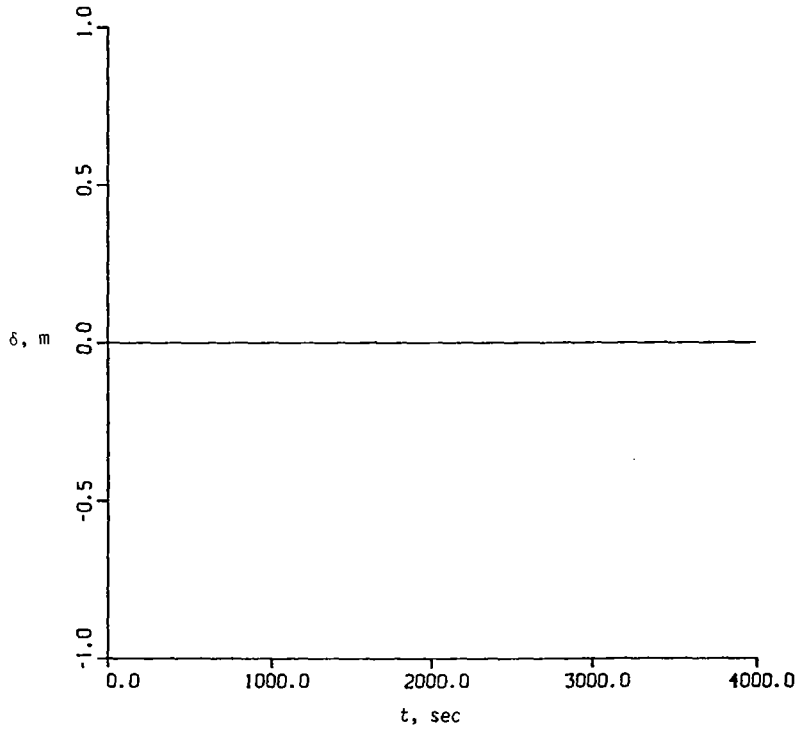

Libration of initially undeformed beam; no docking.

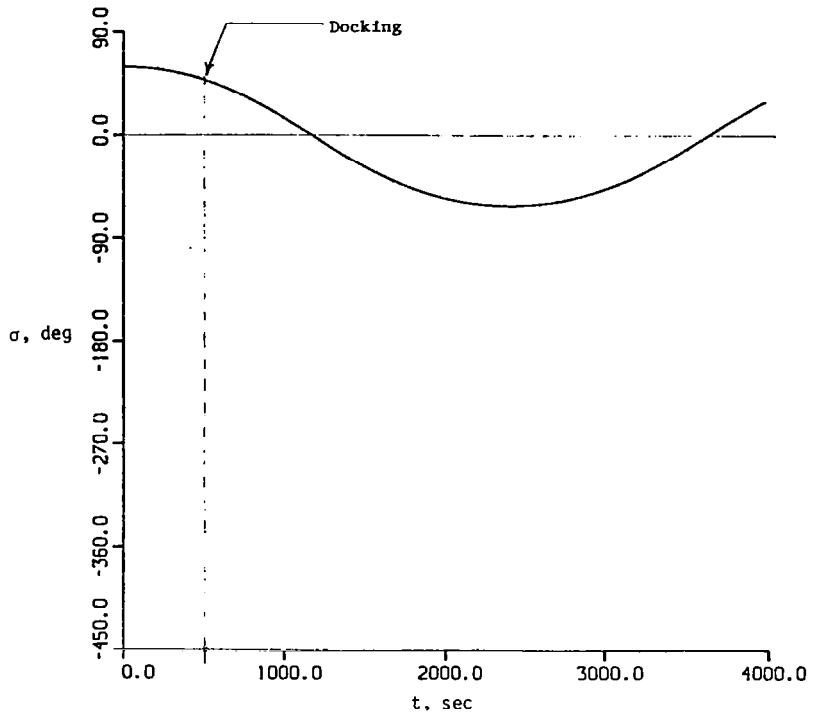

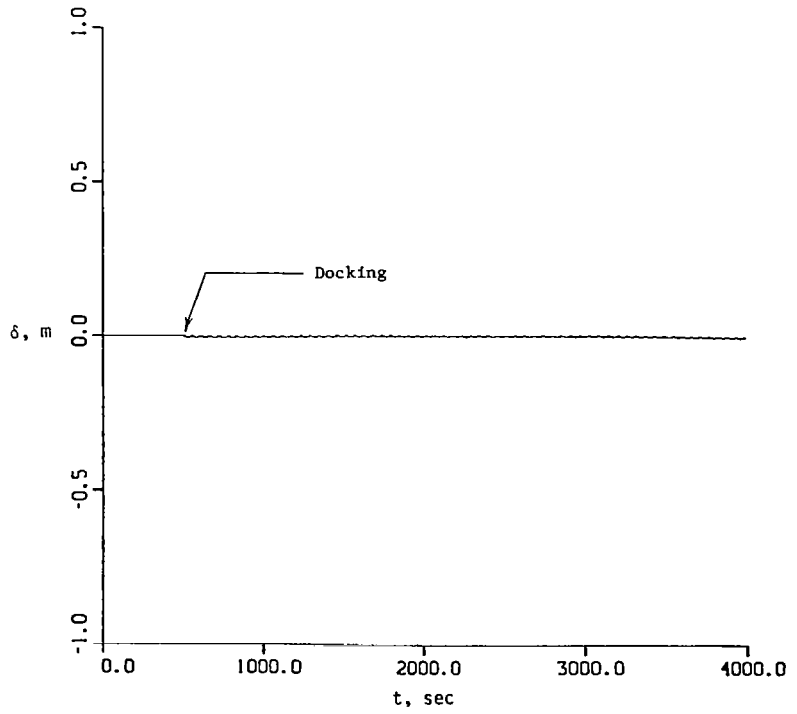

Libration of initially undeformed beam; perfect docking.

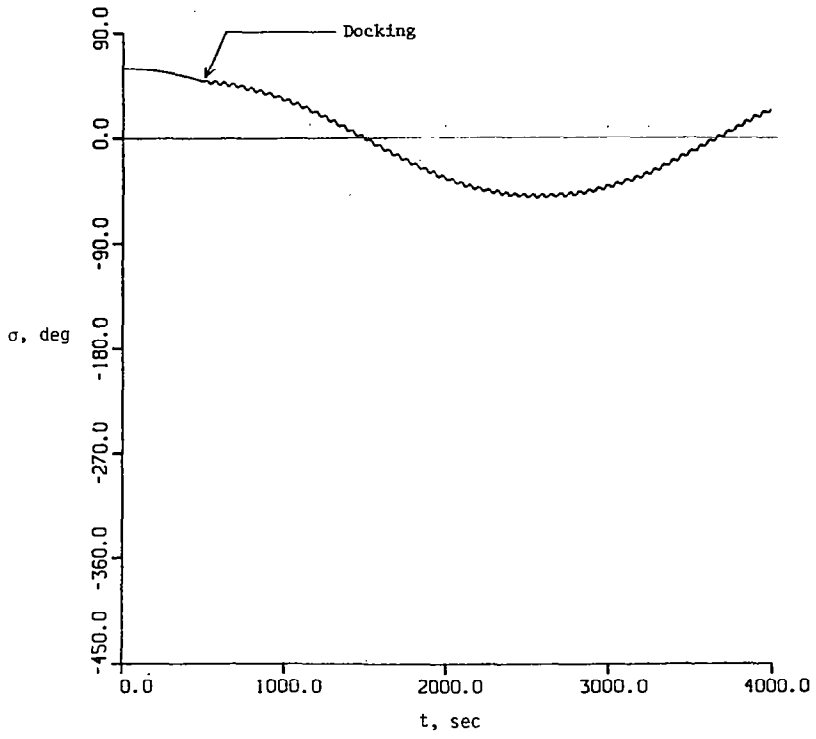

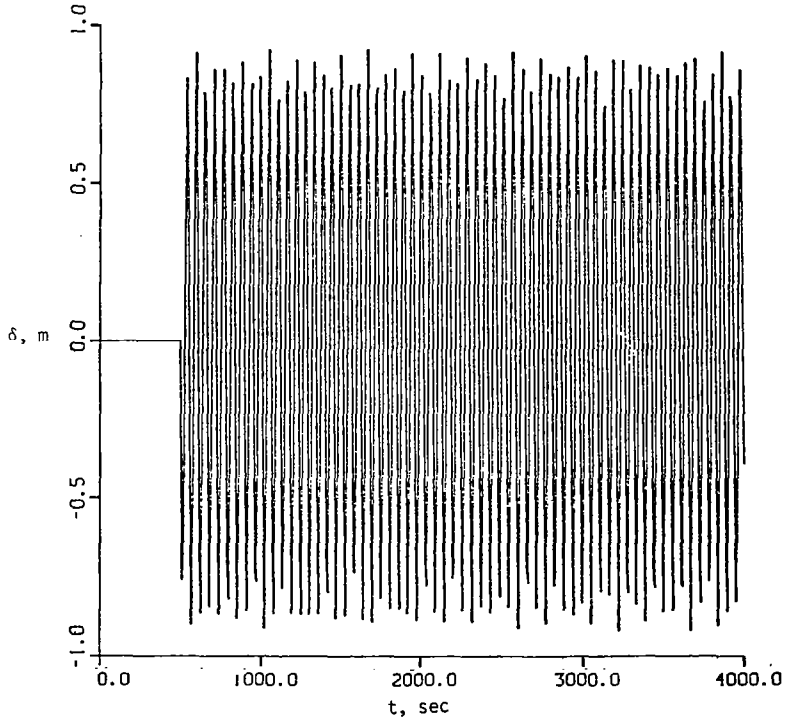

Libration of initially undeformed beam; imperfect docking. Velocity mismatch approximately 1 cm/sec; angular velocity mismatch approximately 0.01 rad/sec.

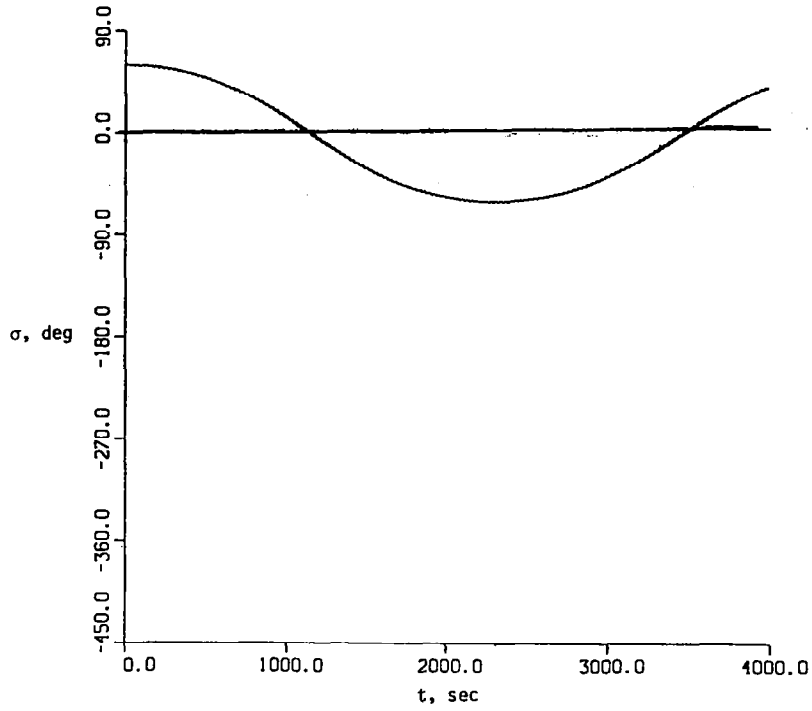

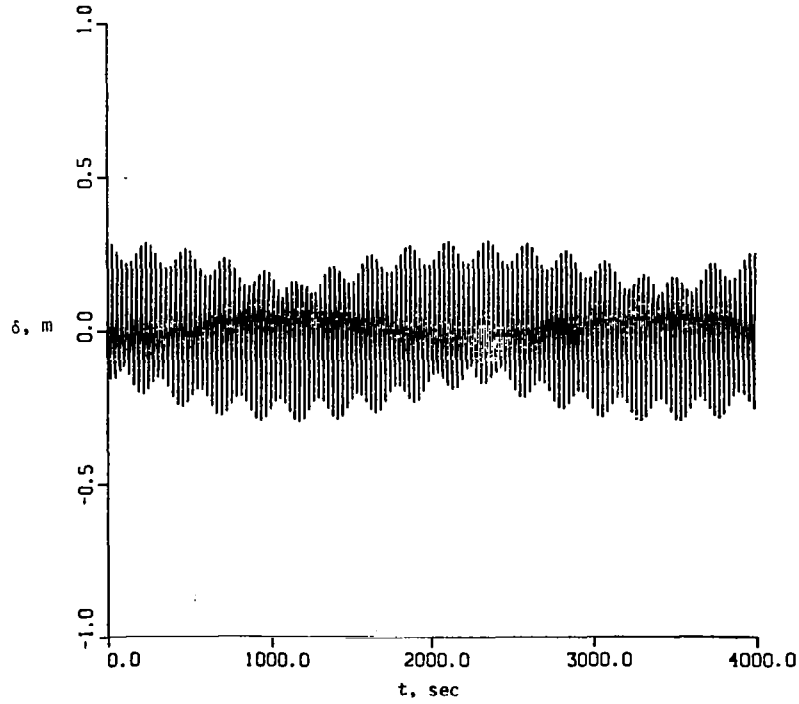

Libration of initially undeformed beam; no docking.

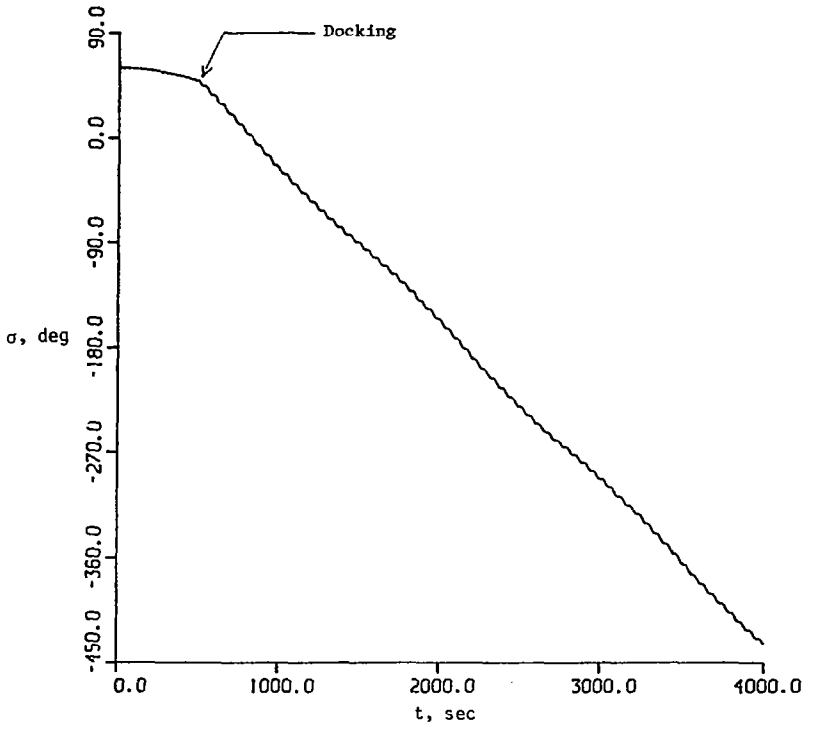

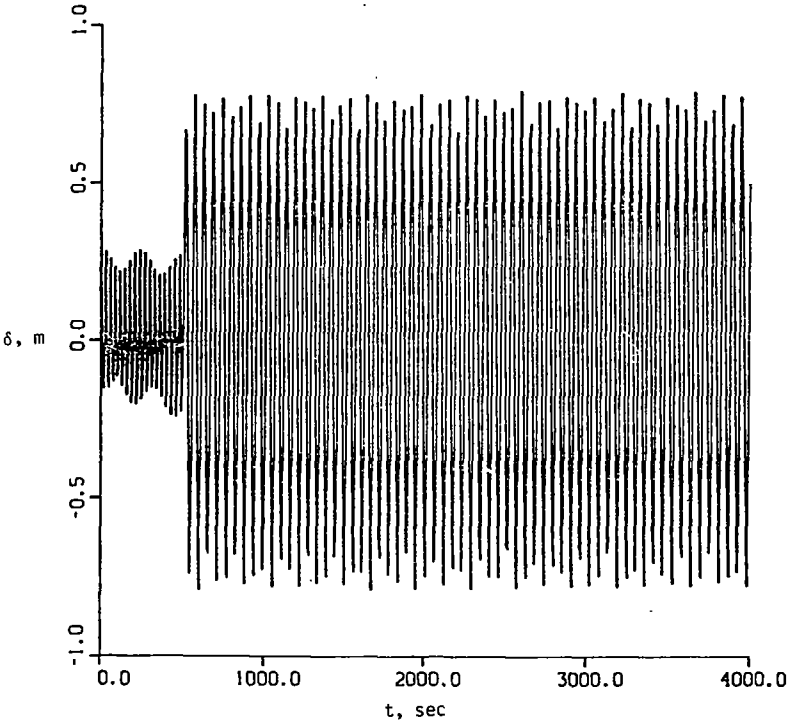

Libration of initially deformed beam; perfect docking.

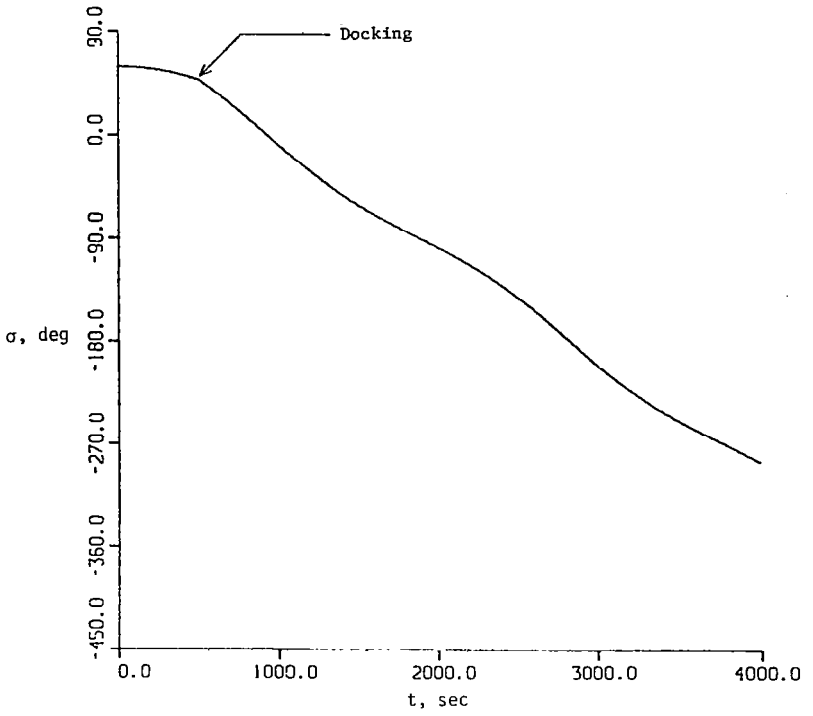

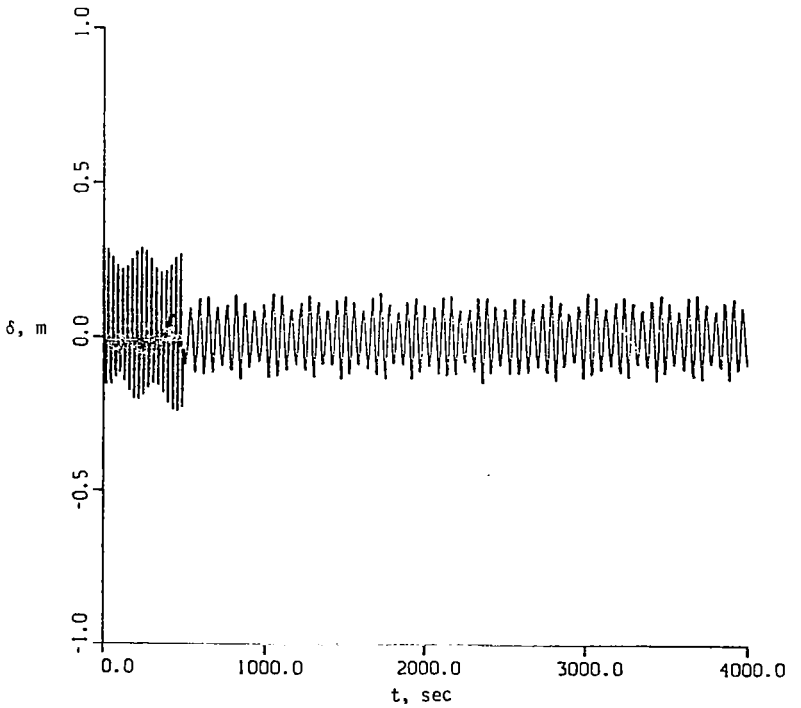

Libration of initially deformed beam; imperfect docking.

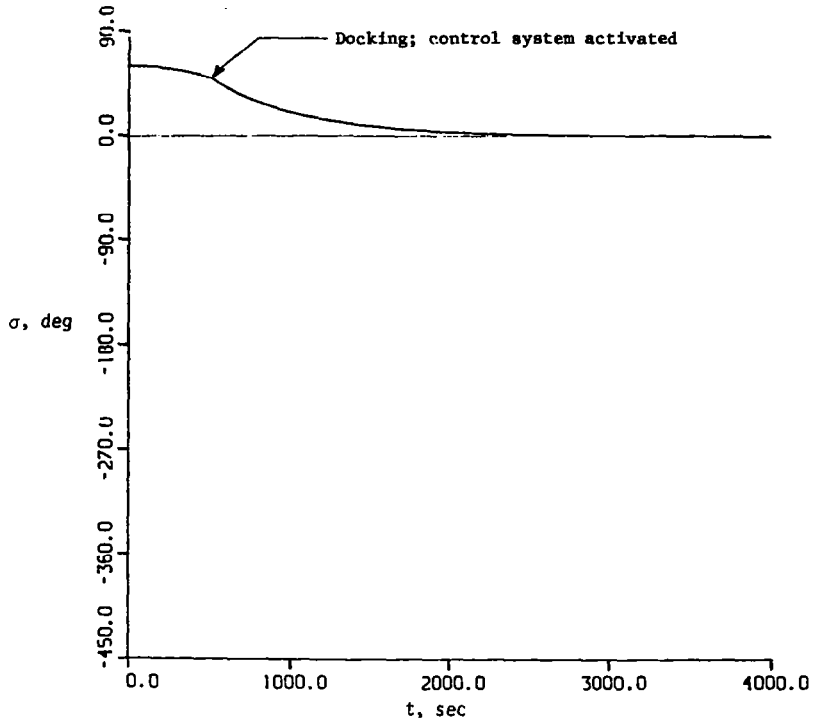

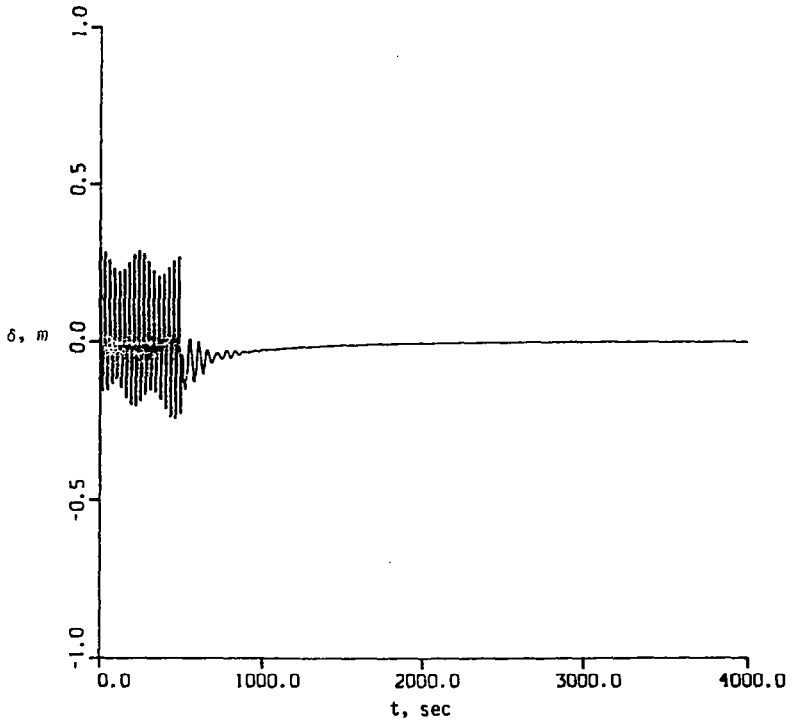

Libration of initially deformed beam; postdocking control proportional to $-\dot{\sigma}$.

RESEARCH ON ELASTIC LARGE SPACE STRUCTURES

AS "PLANTS" FOR ACTIVE CONTROL

H. Ashley and A. von Flotow

Stanford University
Stanford, California

INTRODUCTION

- Modeling of large space structures (LSS) in terms of elastic wave propagation
- Scale effects on structural damping
- "Loss coefficients" of monolithic LSS
- Wave propagation in nondispersive and dispersive media (1-D and 2-D)
- Spectral separation of system response:

$$x(s) = H(s)[u(s) + iC(s)] \cong H_R(s)[u(s) + iC(s)] + \underbrace{[H(s) - H_R(s)][u_F(s) + iC_F(s)]}_{\text{correction term}}$$

where $H_R(s)$ is a reduced-order transfer function

- Reflection of waves from boundaries
- Modeling of discrete structures as equivalent continuous structures
- Dynamics of networks of elastic waveguides
- Control of systems with wave-related time delays
- Application to a 1-D system under active control: 0.12-sec lag predicted with Timoshenko beam idealization and empirically determined shear rigidity
- Significance of passive damping (ref. 1):

  1. A LSS with exactly zero damping is uncontrollable unless sensors and actuators are all collocated (often impractical)

  2. Even very small amounts of damping are important to practical success of control

- Some approximate effects of LSS linear scale L on a typical modal damping ratio ζ:

  1. For a "monolithic" element, ζ is proportional to material damping and decreases with decreasing frequency ω (i.e., with increasing L)

  2. Viscous friction dominates at joints; thus $\zeta \sim 1/L$

  3. Coulomb frection at joints and joint preload is dependent on rotational rate $\Omega \rightarrow \zeta \sim (\Omega L)^2$

  4. All sources active $\rightarrow$ ζ between a constant and $\sim L^{-1}$

STUDY OF INTRINSIC DAMPING IN MONOLITHIC METALLIC STRUCTURE

- Two "semi-reversible" mechanisms seem feasible for LSS:

  1. Thermal relaxation

  2. Grain boundary relaxation (can give large values of ζ but required temperatures may be too high)

- Work in progress on thermal damping

- Properties of thermal damping

  1. Involves coupling between mechanical and entropy waves; e.g., for isotropic solid with $T = T_o + \Delta T$ and displacement $\vec{q} \equiv u\vec{i} + v\vec{j} + w\vec{k}$,

$$\frac{k}{\rho}\nabla^2(\Delta T) - c_v\frac{\partial \Delta T}{\partial t} - \frac{T_o \alpha E}{\rho[1 - 2\nu]}\nabla\cdot\frac{\partial \vec{q}}{\partial t} = 0$$

$$\frac{\partial u}{\partial x} \equiv E_{xx} = \alpha\Delta T + \frac{\sigma_{xx} - \nu(\sigma_{yy} + \sigma_{zz})}{E}$$

$$\frac{\partial \sigma_{xx}}{\partial x} + \frac{\partial \sigma_{xy}}{\partial y} + \frac{\partial \sigma_{xz}}{\partial z} = \frac{\partial^2 u}{\partial t^2}$$

  2. ζ is configuration-dependent (e.g., 10^{-2} to 10^{-3} for beams and plates, 10^{-7} to 10^{-8} for bars and rods). Composite beams are under study.

  3. The value of ζ depends on frequency ω and material properties. E.g., for a rectangular beam of depth b:

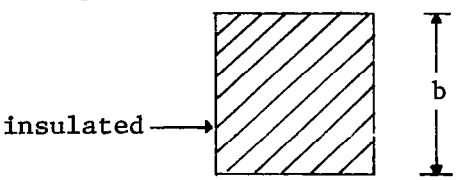

$$\zeta \approx 0.55\,\frac{T_o E \alpha^2}{\rho c_v}\left[\frac{\omega\mu}{\omega^2 + \mu^2}\right] \quad \text{with} \quad \mu \equiv \left(\frac{\pi}{b}\right)^2 \frac{k}{\rho c_v} \quad \text{sec}^{-1}$$

Metal (R.T.)	b, cm	$\zeta_{max} \times 10^{-3}$	ω for ζ_{max}, rad sec^{-1}
Al and alloys	10	1.53	0.083
	5	1.53	2.08
	1	1.53	8.31
Cu	10	0.73	0.112
Low-carbon steel	10	0.675	0.0225
Ti and alloys	10	0.18	0.0075
Ni and alloys	10	0.79	0.0141
Be	10	0.5 (est.)	0.061 (est.)
Mg	10	1.35	0.0844
Al at 1000 K	10	4.12	0.0755

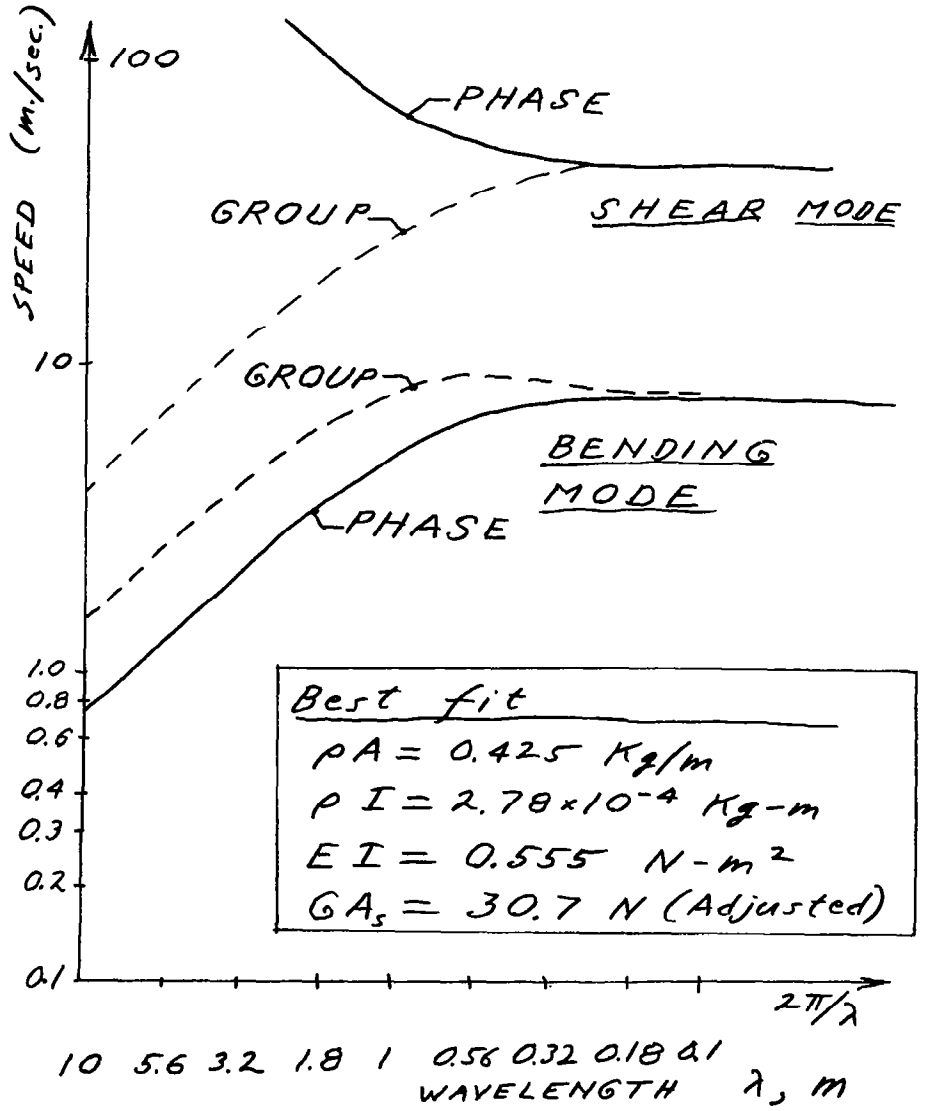

Timoshenko beam waves.

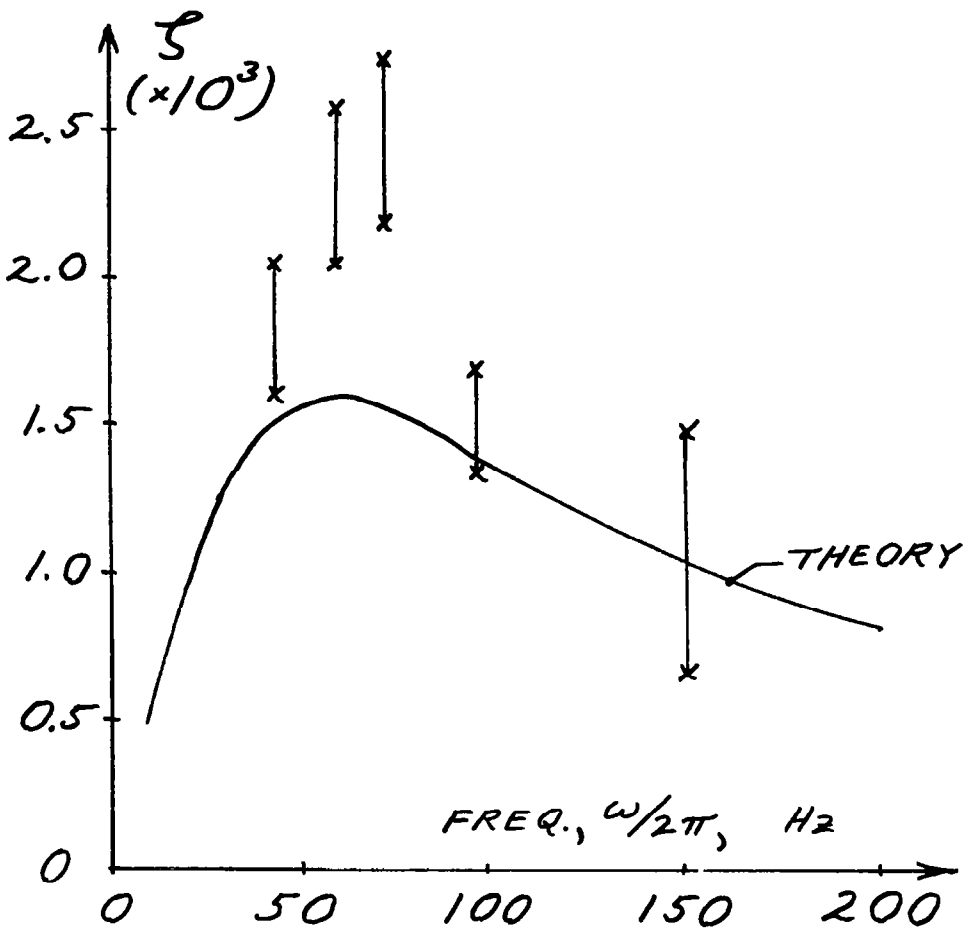

Thermal damping theory compared with recent tests on free-free Al beams in vacuo.

IDENTIFICATION AND CONTROL OF SPACECRAFT

C. S. Greene
M. F. Barrett
Honeywell Systems and Research
Minneapolis, Minnesota

IDENTIFICATION & CONTROL OF SPACECRAFT

* THE PROBLEM

* CONTROL
  - CLASSICAL
  - MODERN

* IDENTIFICATION

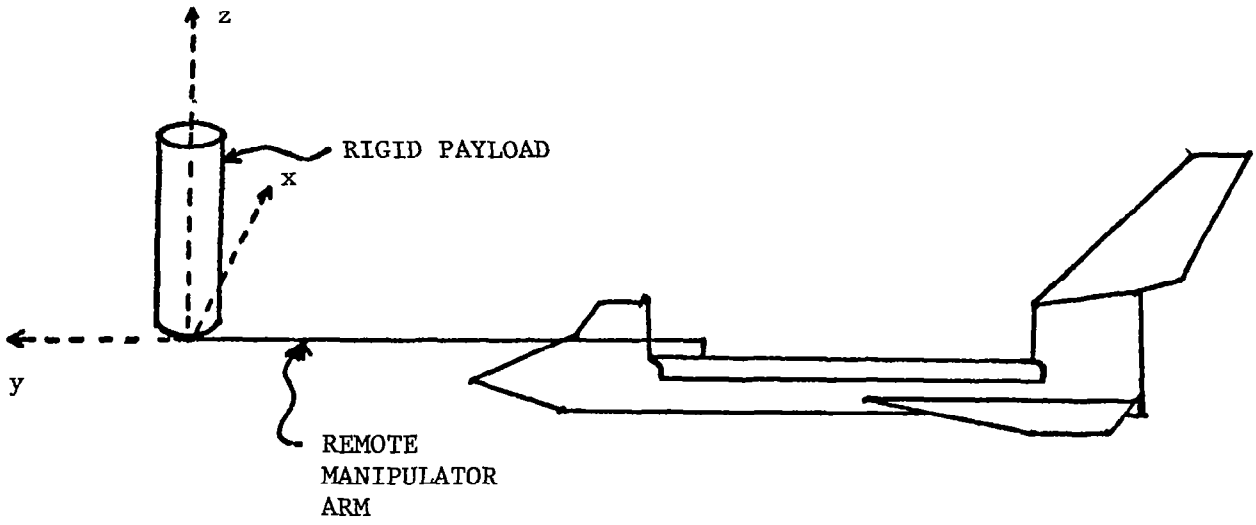

CLASSICAL CONTROL

* SCALAR FEEDBACK DESIGN

* LEAD-LAG CONTROLLER

$$K(s) = \frac{k(s+a)}{(s^2+2\zeta b+b^2)}$$

* BANDWIDTH AROUND 1 RAD/SEC

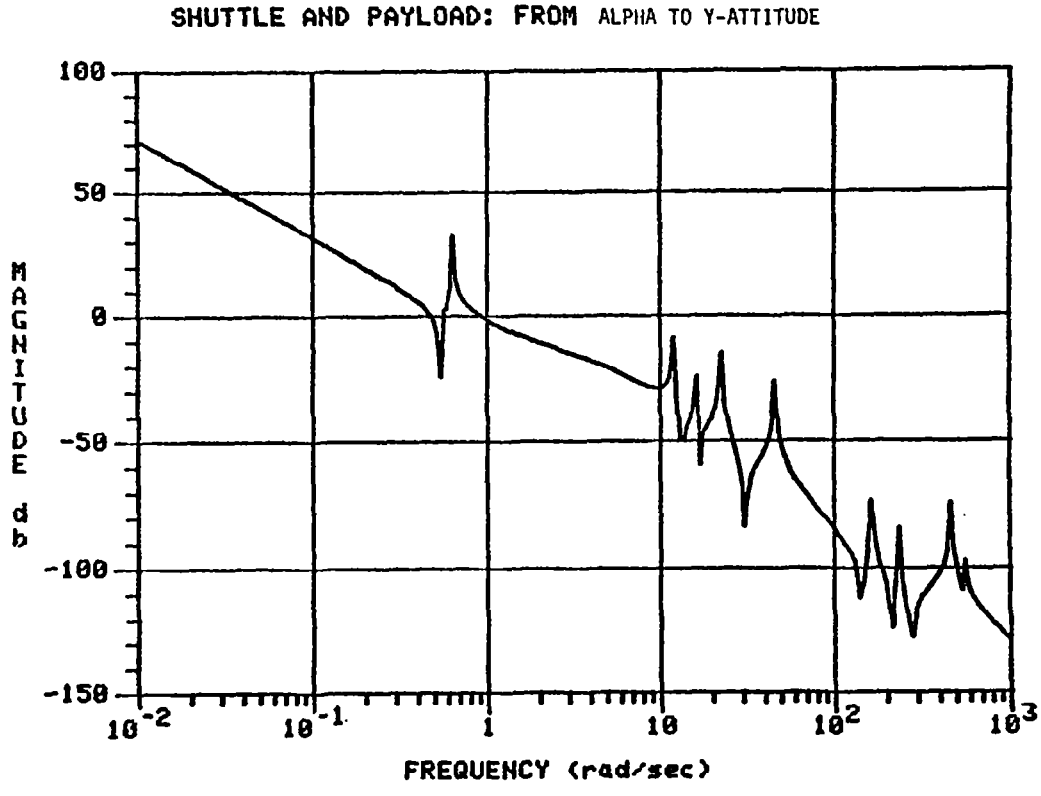

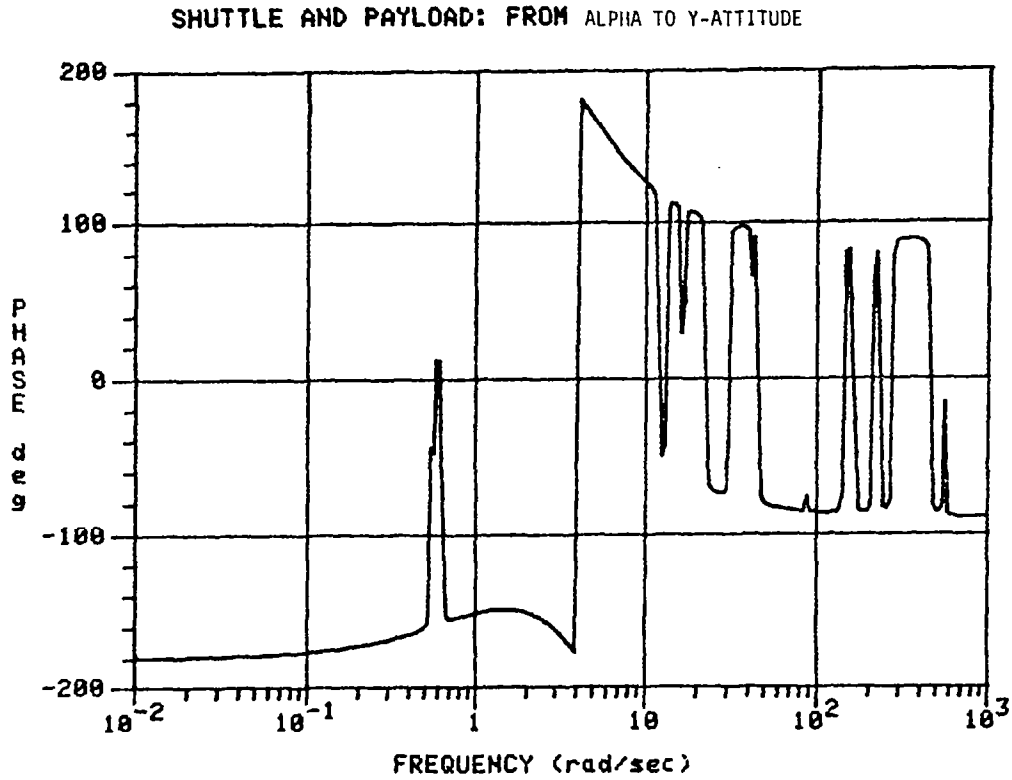

MODERN CONTROL

* START WITH FULL-STATE DESIGN
  - GOAL: MINIMIZE PAYLOAD ATTITUDE ERRORS
  - ITERATE ON CONTROL PENALTY TO ACHIEVE BW OF 5 R/S

* DESIGN FILTER TO RECOVER LQ RESPONSE
  - USE STEIN/DOYLE ROBUSTNESS RECOVERY RESULTS

* TEST ROBUSTNESS

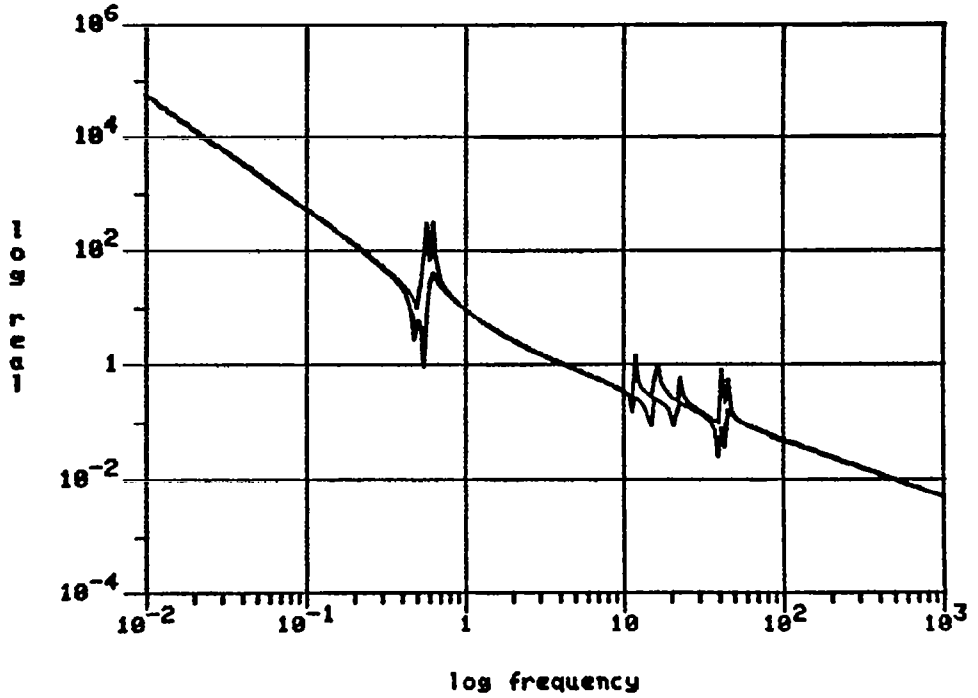
10^6
10^4
10^2
1
10^{-2}
10^{-4}
log sval
10^{-2}
10^{-1}
1
10
10^2
10^3
log frequency

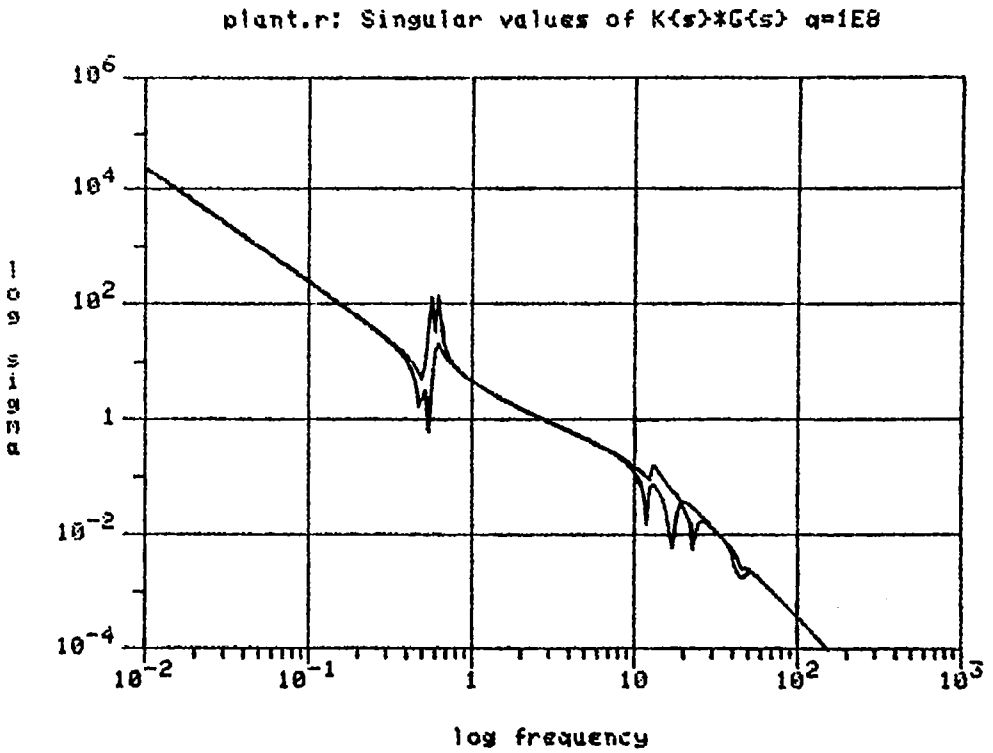
plant.r: Singular values of K(s)*G(s) q=1E8
10^6
10^4
10^2
1
10^{-2}
10^{-4}
log sigma
10^{-2}
10^{-1}
1
10
10^2
10^3
log frequency

I + KG

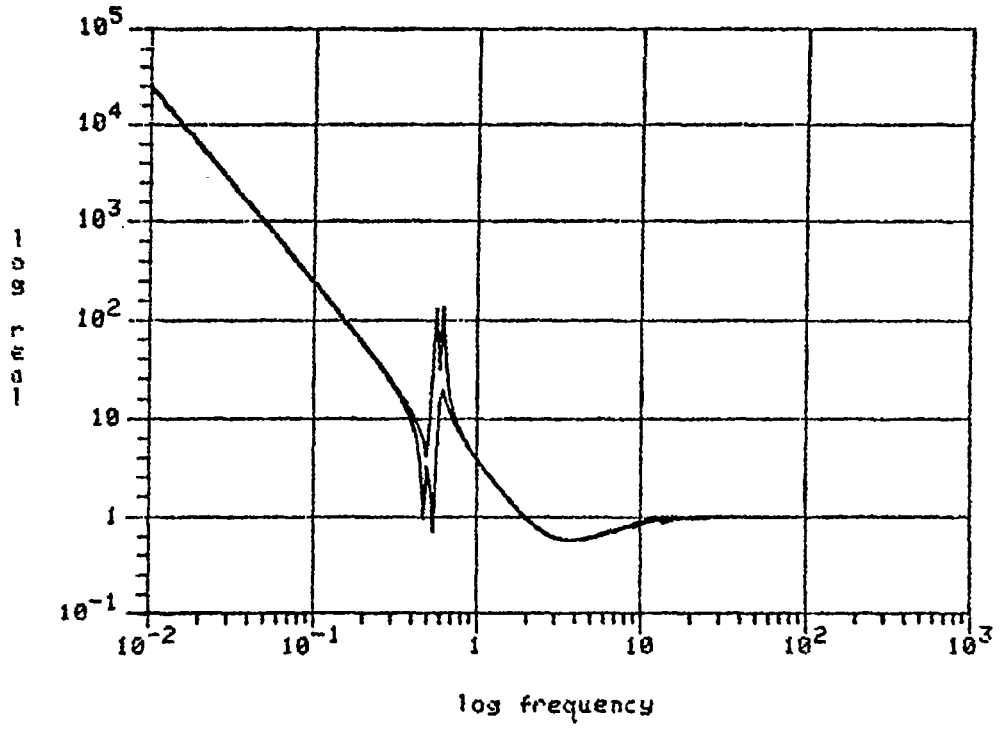

CONTROLLER

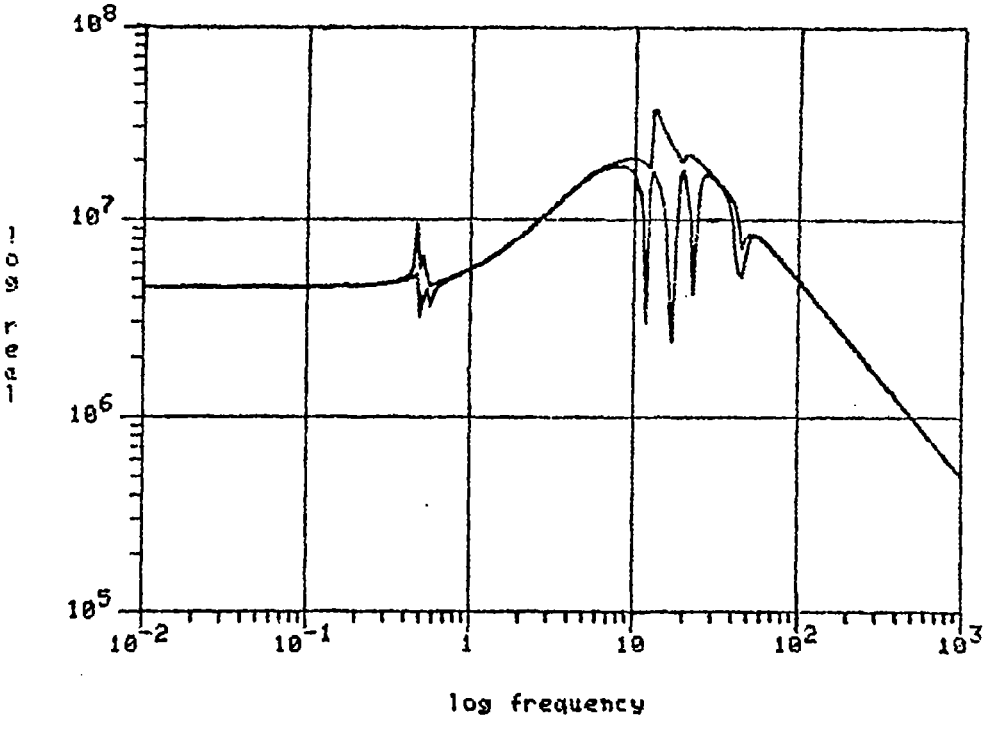

IDENTIFICATION

MAXIMUM LIKELIHOOD ESTIMATION (MLE)

IDENTIFICATION

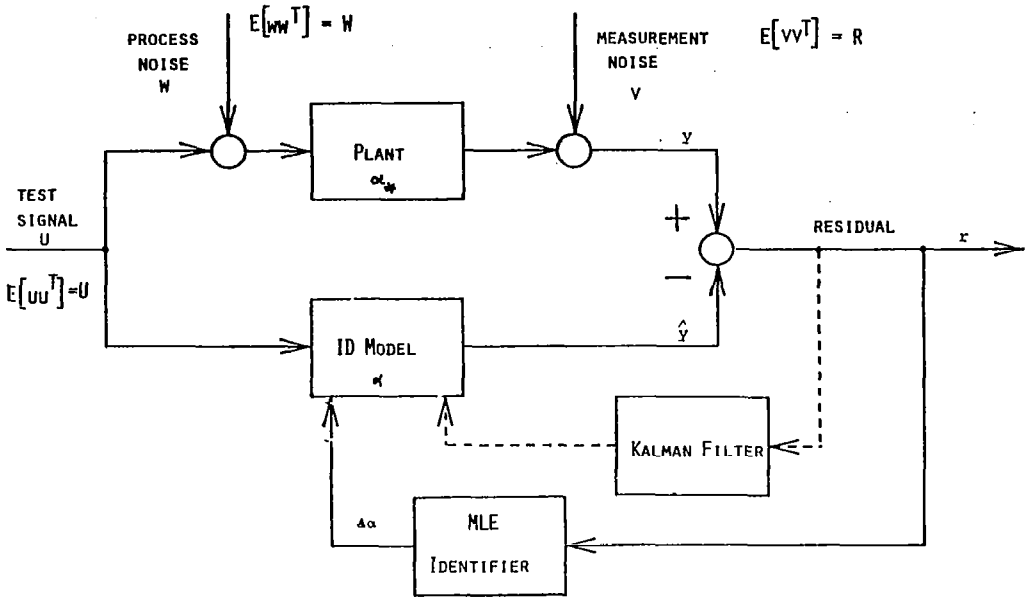

MODEL STRUCTURE

- STATE SPACE

  n_* MODES (2x2 BLOCKS)

  m INPUTS

  p OUTPUTS

$$\begin{bmatrix} \vdots \\ \dot{x}_i \\ \ddot{x}_i \\ \vdots \end{bmatrix}(t) = \begin{bmatrix} \ddots & & 0 \\ & \begin{matrix} 0 & 1 \\ -\omega_i^2 & -2\zeta_i\omega_i \end{matrix} & \\ 0 & & \ddots \end{bmatrix} \begin{bmatrix} \vdots \\ x_i \\ \dot{x}_i \\ \vdots \end{bmatrix}(t) + \begin{bmatrix} \vdots \\ \begin{matrix} 0 \\ b_i^T \end{matrix} \\ \vdots \end{bmatrix} [u(t) + w(t)]$$

$$\begin{bmatrix} y \end{bmatrix}(t) = \begin{bmatrix} \cdots & c_i\ 0 & \cdots \end{bmatrix} \begin{bmatrix} \vdots \\ x_i \\ \dot{x}_i \\ \vdots \end{bmatrix}(t) + \begin{bmatrix} v \end{bmatrix}(t)$$

- FREQUENCY DOMAIN

$$y(s) = (G_*(s)[u(s)+w(s)] + v(s)$$

$$G_*(s) = \sum_{i=1}^{n_*} \frac{c_i\, b_i^T}{s^2+2\zeta_i\omega_i s+\omega_i^2}$$

- PARAMETER VECTOR

$$\alpha_* = \{\omega_{*i}^2,\ 2\zeta_{*i}\omega_{*i},\ b_{*i},\ c_{*i};\ i = 1, \ldots, n_*\}$$

MLE IDENTIFICATION SETUP

- RESIDUAL DEFINITION

$$r_k \triangleq y(kT) - \hat{y}(kT)$$

- LIKELIHOOD FUNCTION (NEGATIVE LOG)

$$L(\alpha) \triangleq \sum_{k=0}^{N} L_k(\alpha)$$

$$\triangleq \sum_{k=0}^{N} \frac{1}{2}\left[\text{LOG DET } S_k + r_k^T S_k r_k\right]$$

WHERE

$\alpha \triangleq \{\omega_i^2,\ 2\zeta_i\omega_i,\ b_i,\ c_i;\ i = 1, \ldots, n\}$ = UNKNOWN PARAMETERS

$S_k \triangleq E_\alpha\{r_k r_k^T\}$ = PREDICTED RESIDUAL COVARIANCE

MLE IDENTIFICATION SOLUTION

- PARAMETER ESTIMATE (THEORETICAL)

$$\hat{\alpha} \triangleq \text{ARG}\left\{\min_{\alpha} L(\alpha)\right\} = \text{PARAMETER ESTIMATE}$$

- ITERATIVE ALGORITHMS

GRADIENT: $\hat{\alpha}_{J+1} = \hat{\alpha}_J - \epsilon_J \nabla L(\hat{\alpha}_J)$

NEWTON-RHAPSON: $\hat{\alpha}_{J+1} = \hat{\alpha}_J - \left[\nabla^2 L(\hat{\alpha}_J)\right]^{-1} \nabla L(\hat{\alpha}_J)$

WHERE

$$\nabla L(\alpha) \triangleq \frac{\partial L}{\partial \alpha}(\alpha)$$

$$\nabla^2 L(\alpha) \triangleq \frac{\partial^2 L}{\partial \alpha^2}(\alpha)$$

IDENTIFICATION ACCURACY ISSUES

- SYSTEMATIC ERRORS: $E_*(\hat{\alpha}) - \alpha_*$
  - MODEL-ORDER MISMATCH
  - TEST SIGNAL AMPLITUDE AND SHAPING
  - SYSTEMATIC DISTURBANCES
  - SENSOR/ACTUATOR MODEL ERRORS
- STOCHASTIC ERRORS: $\sigma_\alpha \sim \frac{1}{\sqrt{TN}}$
  - RANDOM DISTURBANCES AND SENSOR NOISE
  - TEST SIGNAL AMPLITUDE AND SHAPING
  - IDENTIFICATION TIME INTERVAL

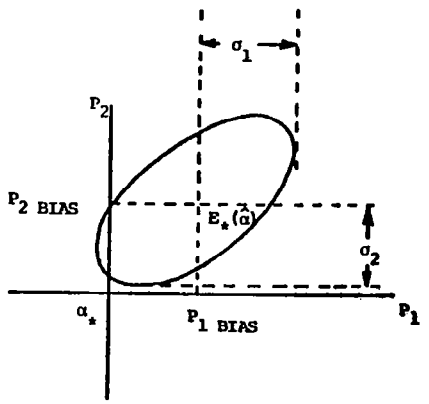

STEADY-STATE IDENTIFIABILITY ANALYSIS (YARED)

- EXPECTED LIKELIHOOD FUNCTION

$$I^*(\alpha) = E_* \left\{ L_k(\alpha) \right\}$$
$$= \frac{1}{2} \left[\text{LOG DET } S + \text{TR}(S^{-1} S_*) \right]$$

- RESIDUAL COVARIANCES

$S = E_\alpha \left\{ r_K r_K^T \right\}$ = KALMAN FILTER PREDICTED RESIDUAL COVARIANCE MATRIX

$S_* = E_* \left\{ r_K r_K^T \right\}$ = ACTUAL RESIDUAL COVARIANCE MATRIX

NOTE: S_* AND $I^*(\alpha)$ CAN ONLY BE COMPUTED WHEN THE TRUE PLANT PARAMETERS ARE KNOWN.

EXPECTED MLE IDENTIFICATION SOLUTION

- EXPECTED PARAMETER ESTIMATE (THEORETICAL)

$$\hat{\alpha}_* \triangleq E_* \left\{ \hat{\alpha} \right\} = \text{ARG} \left\{ \min_{\alpha} \; I^*(\alpha) \right\}$$

- ITERATIVE ALGORITHMS

GRADIENT: $\hat{\alpha}_{*_{J+1}} = \hat{\alpha}_{*_J} - \epsilon_J \nabla I^*(\hat{\alpha}_{*_J})$

NEWTON-RHAPSON: $\hat{\alpha}_{*_{J+1}} = \hat{\alpha}_{*_J} - \left[\nabla^2 I^*(\hat{\alpha}_{*_J}) \right]^{-1} \nabla I^*(\hat{\alpha}_{*_J})$

WHERE $\nabla I^*(\alpha) = \dfrac{\partial^2 I^*}{\partial \alpha}(\alpha)$

$\nabla^2 I^*(\alpha) = \dfrac{\partial^2 I^*}{\partial \alpha^2}(\alpha)$

STEADY STATE IDENTIFICATION ACCURACY

- SYSTEMATIC ERRORS (BIASES)
  - PARAMETER ERRORS

$\alpha_{BIAS} \triangleq \hat{\alpha}_* - \alpha_* = 0$ WHEN NO MODEL MISMATCH

  - INFORMATION MEASURE (YARED)

$I(\alpha_* ; \hat{\alpha}_*) \triangleq I^*(\hat{\alpha}_*) - I^*(\alpha_*) \geq 0$

- STOCHASTIC ERRORS

$$\begin{aligned} C_{OV}\{\hat{\alpha}\} &\triangleq \lim_{N \to \infty} E_* \left\{ (\hat{\alpha} - \hat{\alpha}_*)(\hat{\alpha} - \hat{\alpha}_*)^T \right\} \\ &\triangleq \left[\nabla^2 I^*(\hat{\alpha}_*) \right]^{-1} E_* \left\{ \left[\frac{\partial L}{\partial \alpha}(\hat{\alpha}_*) \right] \left[\frac{\partial L}{\partial \alpha}(\hat{\alpha}_*) \right]^T \right\} \left[\nabla^2 I^*(\hat{\alpha}_*) \right]^{-1} \frac{1}{(N+1)^2} \\ &= \left[\nabla^2 I^*(\hat{\alpha}_*) \right]^{-1} \frac{1}{(N+1)} \quad \text{WHEN NO MODEL MISMATCH} \end{aligned}$$

STOCHASTIC ERROR WITH PROCESS NOISE

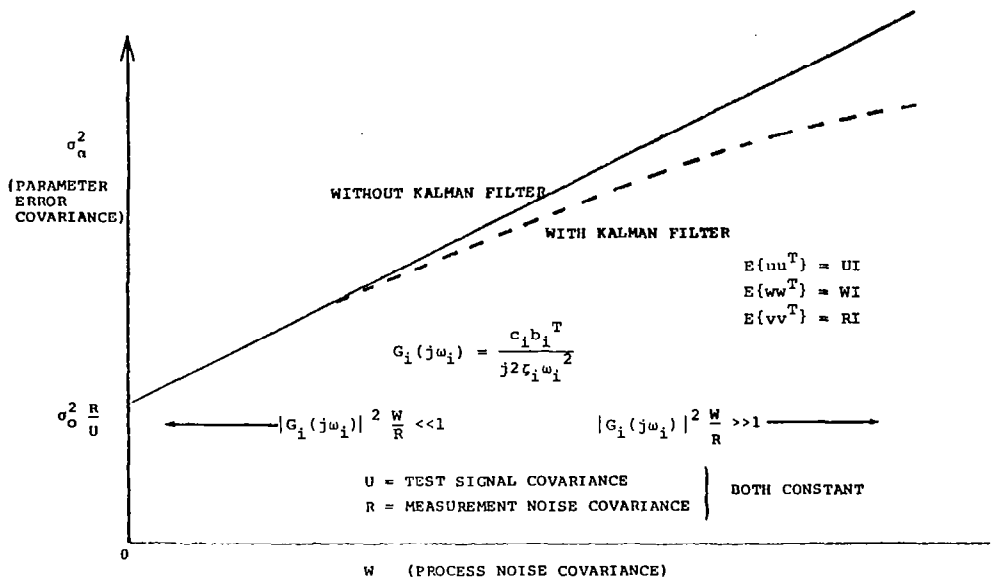

SIMPLIFIED IDENTIFICATION ACCURACY ANALYSIS
(FOR EACH MODE)

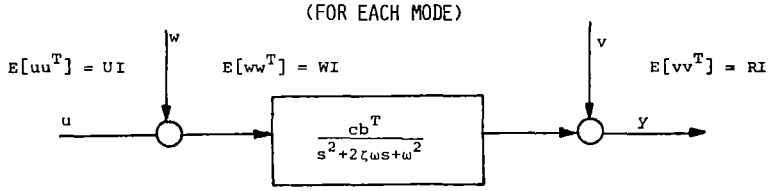

$$\alpha \triangleq \{\omega^2,\ 2\zeta\omega,\ b_1, \ldots b_m,\ c_1, \ldots,\ c_p\} - \{b_L \text{ or } c_M\}$$

$$\frac{\sigma_{\omega^2}^2}{(\omega^2)^2} = \frac{8\zeta^2}{SNR}\ \frac{1}{(N+1)T}\ ;\quad \rho \triangleq \max_{\ell,m}\left\{\frac{b_\ell^2}{|b|^2},\ \frac{c_m^2}{|c|^2}\right\} \leq 1$$

$$\frac{\sigma_{2\zeta\omega}^2}{(2\zeta\omega)^2} = \frac{4}{SNR}\ \frac{1}{(N+1)T}\ ;\quad SNR \triangleq \begin{cases} \dfrac{|c|^2|b|^2}{4\zeta\omega^3}\ \dfrac{U}{R} & \text{(MEAS. NOISE)} \\ \zeta\omega\ \dfrac{U}{W} & \text{(PROC. NOISE)} \end{cases}$$

$$\frac{\sigma_{b\ell}^2}{b_\ell^2} = \frac{1}{SNR}\left[\frac{|b|^2}{b_\ell^2} + \rho^{-1}\right]\ \frac{1}{(N+1)T}$$

$$\frac{\sigma_{cm}^2}{c_m^2} = \frac{1}{SNR}\left[\frac{|c|^2}{c_m^2} + \rho^{-1}\right]\ \frac{1}{(N+1)T}$$

NOTE: THIS ANALYSIS ASSUMES THAT $\omega T << 1$, $\zeta << 1$ AND APPLIES FOR EACH MODE

NUMERICAL RESULTS

- PROBLEM SIZE

  12 MODES (=22 - 8R.B. - 2 SMALL)
  2 INPUTS (α, β GIMBAL ANGLES)
  2 OUTPUTS (x, y ATTITUDES)
  60 PARAMETERS (=12 MODES x 5 PARAMETERS/MODE)

- TEST SIGNAL, NOISE STATISTICS

  SAMPLE TIME: T = 0.1 SEC
  TEST SIGNAL: $U = 4000(\text{IN-LB})^2$
  PROCESS NOISE: $W = 40(\text{IN-LB})^2$
  MEASUREMENT NOISE: $R = 4 \times 10^{-12}$ RAD^2

- WORST-CASE RELATIVE ERRORS AT TIME (MODE 9):

PARAMETER	1 SEC	14 SEC	0.39 HRS
ω^2	0.0265	0.007	0.0007
$2\zeta\omega$	3.75	1.0	0.1
b_1	13.6	3.6	0.36
c_1	2.7	0.7	0.07
c_2	11.7	3.1	0.31

SUMMARY

- CONTROL PROBLEM
  - MODERN LQ CONTROL DESIGN WITH ROBUSTNESS RECOVERY PRODUCES ROBUST CONTROLLERS FOR LSS
  - ACCURATE ID ALLOWS A FIVE-FOLD INCREASE IN LOOP BW
- IDENTIFICATION PROBLEM
  - STRUCTURAL MODES MAY BE IDENTIFIED ONE AT A TIME FOR SMALL DAMPING
  - LSS ID W/O KF
    --GREATLY REDUCES PARAMETER BIASES
    --GIVES ONLY MODEST INCREASE IN STOCHASTIC ERRORS
  - RELATIVE ERRORS IN PARAMETERS AFTER ID ARE SMALLER FOR FREQUENCY THAN FOR DAMPING OR MODE SHAPES
- OPEN ISSUE: HOW ACCURATE MUST ID BE FOR ROBUST CONTROL DESIGN?

THE DYNAMICS AND CONTROL OF

LARGE FLEXIBLE SPACE STRUCTURES

Peter M. Bainum, V. K. Kumar, R. Krishna,
A. S. S. R. Reddy, and C. M. Diarra
Howard University
Washington, D. C.

INTRODUCTION

Large, flexible orbiting systems have been proposed for possible use in communications, electronic orbital-based mail systems, and solar energy collection. The size and low weight-to-area ratio of such systems indicate that system flexibility is now the main consideration in the dynamics and control problem. For such large, flexible systems, both orientation and surface shape control will often be required.

Figure 1 illustrates a conceptual development plan of a system software capability for use in the analysis of the dynamics and control of large space structures technology (LSST) systems. This concept can be subdivided into four different stages: (1) system dynamics; (2) structural dynamics; (3) application of control algorithms; and (4) simulation of environmental disturbances. Modeling the system dynamics of such systems in orbit is the most fundamental component.

SOLAR RADIATION PRESSURE EFFECTS

The equations for determining the effects of solar radiation pressure on a flexible beam are summarized below.

Forces:

$$\bar{F}_a = -h_o \bar{\tau} \int_s (\hat{\tau} \cdot \hat{n})\, ds \qquad \text{(absorbing surface)}$$

$$\bar{F}_\gamma = -2h_o \int_s \hat{n}(\hat{\tau} \cdot \hat{n})^2\, ds \qquad \text{(reflecting surface)}$$

$$\bar{F}_\varepsilon = \bar{F}_a + \varepsilon(\bar{F}_\gamma - \bar{F}_a) \qquad \text{(surface with reflectivity } \varepsilon\text{)}$$

Moments:

$$\bar{M}_a = h_o \hat{\tau} x \int_s \bar{R}(\hat{\tau} \cdot \hat{n})\, ds \qquad \text{(absorbing surface)}$$

$$\bar{M}_\gamma = 2h_o \int_s \hat{n} \times \bar{R}(\hat{\tau} \cdot \hat{n})^2\, ds \qquad \text{(reflecting surface)}$$

$$\bar{M}_\varepsilon = \bar{M}_a + \varepsilon(\bar{M}_\gamma - \bar{M}_a) \qquad \text{(surface with reflectivity } \varepsilon\text{)}$$

where

$\hat{\tau}$ = unit vector in the direction of solar radiation

$\hat{n}$ = unit vector normal to the surface ds

$h_o = 4.64 \times 10^{-6}$ N/m^2

Results for a flexible beam:

$$\bar{F}_a = -a_o h_o \left[a_o(z_1 - z_o) - b_o\right]\hat{i} + h_o b_o \left[a_o(z_1 - z_o) - b_o\right]\hat{k}$$

$$\bar{M}_a = -h_o a_o b_o \left\{(z_1 + z_o)/2 - 2/\Omega_n \left[\sigma(\cos h\Omega_n - \cos \Omega_n)\right] + \sin \Omega_n + \sin h\Omega_n\right\}$$

$$\bar{F}_\gamma = -2h_o \int_s z' \frac{(a_o z' - b_o)^2}{(1 + z')^2} dx\, \hat{i} - 2h_o \int_s \frac{(a_o z' - b_o)^2}{(1 + z')^2} dx\, \hat{k}$$

$$\bar{M}_\gamma = 2h_o \int_s \frac{(a_o z' - b_o)^2}{(1 + z')^2} \left(z'z - x + \frac{1}{2}\right) dx\, \hat{k}$$

where

$a_o = \sin \theta \qquad b_o = \cos \theta$

$z(x)$ = flexural deflection

$z' = \frac{dz}{dx}$

Ω_n = nth modal frequency

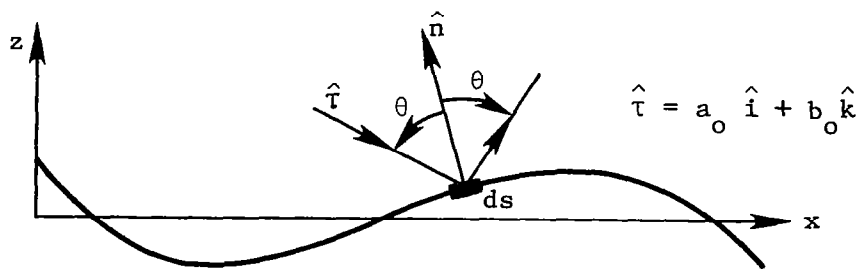

Figure 2 shows the variation of the resultant horizontal and normal force components of a beam with a completely absorbing surface as the solar incidence angle θ is varied from 0^o to 90^o. Here, θ represents the angle between the normal to the undeflected beam and $\bar{\tau}$. The horizontal and normal force components are measured relative to the beam's undeflected axes. As expected, for small tip deflections of the beam, the resultant horizontal absorbing force component becomes zero for incidence angles of 0^o and 90^o, while the normal component has a maximum amplitude at zero incidence angle. In figures 2 and 3 the individual effect of each mode is illustrated, with the assumed beam tip deflection as indicated in the figures.

The magnitude of the resultant moments as the solar incidence angle is varied is shown in figure 3 for the assumed tip deflection of 0.01ℓ. Large moments can result for larger deflections, whereas these moments would be zero for a rigid beam. For small pitch angle displacements, the moment due to solar radiation pressure may become greater than the moment due to the gravity-gradient forces, as shown in figure 4. It is seen that at geosynchronous altitudes, the moment due to solar radiation may become predominant even for deflections on the order of 0.01ℓ. With the aid of moment diagrams such as those in figure 3, it is possible to determine the disturbance torques due to solar radiation pressure once the number of modes and the associated modal deflections are specified for a model.

MODELING ERRORS - ORBITAL AND GRAVITY-GRADIENT EFFECTS

One of the principal sources of (disturbance) torques acting on an orbiting space structure is the orbital (gyroscopic) and gravity-gradient effects. Such effects associated with the orbital (angular) motion do not need to be considered when developing a system model for an Earth-based large flexible system. Many investigators, however, model the pitch, roll, and yaw modes (rigid body motion) of large, flexible orbiting systems as double integrator plants (two poles at the origin), and the subsequent control system design is based on these models. It is the purpose of this section to evaluate the effects of omitting the orbital and gravity-gradient effects when designing shape and orientation control laws for flexible systems in orbit. Models of flexible square plates and shallow spherical shells in orbit are selected as examples.

The effects of designing control laws without the orbital and gravity-gradient torques included in the system models of square plates and shallow spherical shells in low Earth orbit (250 nautical miles) are illustrated in figures 5 to 10. A square plate was also considered in a geosynchronous orbit. The analysis was performed by first calculating the control law, which was in the form $\bar{u} = F\bar{x}$, for the case where the orbital and gravity-gradient effects are not included in the model. The same control law is then applied to the model that includes these effects.

For figure 4, the control law was selected such that the overall response time constant of the system is 2.22 hours (which may be reasonable for a large space structure). The shift in the closed loop poles of the plate model due to the presence of the orbital and gravity-gradient effects is illustrated in this figure. It can be seen that some of the poles move to the right half plane, leading to instability and thus emphasizing the importance of including the orbital and gravity-gradient effects in the model. The poles due to the rigid body modes are shifted considerably, but the flexible modes remain virtually unaffected. This can be attributed to the high frequency of the flexible modes. (Note that the orbital and gravity-gradient effects are of a relatively low frequency.) This result gives an

indication that by designing a more robust (faster response) control system, the shift of the actual closed loop poles would be relatively less pronounced.

This phenomenon can be demonstrated by designing the gain matrix, F, such that the desired response time constant is reduced to 460 seconds. The shift in the closed loop poles for this case is shown in figure 6. In figure 7 the control forces are shown for the second (more robust) control law, where the closed loop response with orbital and gravity-gradient effects is degraded but does not become unstable. (It should be noted that time has been nondimensionalized with respect to the orbital frequency of the 250-nautical-mile low Earth orbit, in order to provide a basis for comparison.) The difference in the total control force impulse as applied to the two models (a) and (b) is minimal because of the robustness of the controller. The slowly varying orbital and gravity-gradient torques have a relatively greater impact on the less robust systems, and can even lead to possible instabilities, as was illustrated in figure 5.

As expected, the orbital and gravity-gradient effects are less pronounced in the case of a structure in geosynchronous orbit than in the case of a structure in low Earth orbit. However, if the control systems are designed with response times comparable to the orbital periods, under the influence of orbital and gravity-gradient effects the closed loop systems may become unstable.

The shift in the closed loop poles of the spherical shell model due to the presence of the orbital and gravity-gradient effects is shown in figure 8. One of the closed loop poles is moved to the right-hand side of the S-plane, causing instability. As compared to the case of the plate, the effect of the orbital and gravity-gradient torques on the shell is more pronounced, as the instability due to movement of the poles occurs at the relatively fast designed response time constant of 615 seconds (compared to 8000 seconds in the case of plate). When the control is redesigned for a response time constant of 400 seconds, the shift in the poles is as shown in figure 9. A general shift in the rigid body motion poles is observed, but the system remains stable.

The control forces associated with both models (a) and (b) of figure 9 are compared in figure 10. A considerable increase in the control effort is observed when the model includes the effect of the orbital gyroscope and gravity-gradient torques. This may be explained by the fact that the mass distribution of the shell is more complex than that of the plate, resulting in relatively greater dynamic coupling when the gyroscopic and gravity-gradient effects are included in the shell model.

THE DEVELOPMENT OF AN ALGORITHM TO EVALUATE COUPLING COEFFICIENTS FOR A LARGE FLEXIBLE ANTENNA

The generic mode equations and the equations of rotational motion of a flexible orbiting body contain both coupling terms between the rigid and flexible modes and terms due to the coupling within the flexible modes that are assumed to be small and thus are usually neglected when a finite element analysis of the dynamics of the system is undertaken. In this section a computational algorithm is developed which permits the evaluation of the coefficients in these coupling terms in the equations of motion as applied to a finite element model of a hoop/column antenna system (ref. 1).

Using a Newton-Euler approach, one can express the equations of motion of an elemental mass of the system, in the frame moving with the body, as:

$$\left\{\bar{a}_{cm} + \ddot{\bar{r}} + 2\bar{\omega} + \dot{\bar{r}} + \dot{\bar{\omega}} \times \bar{r} + \bar{\omega} \times (\bar{\omega} \times \bar{r})\right\}\rho \, dv = \left\{\bar{f} + \bar{e} + L(\bar{q})/\rho\right\}\rho \, dv \qquad (1)$$

where

ρ = mass per unit volume

$\bar{e}$ = external forces per unit mass

$\bar{q}$ = elastic transverse displacements of the element of volume

$\bar{f}$ = force due to the gravity on the unit mass

L = the linear operator which when applied to $\bar{q}$ yields the elastic forces acting on the element of volume considered

$\bar{r}$ = position vector of element dv

$\bar{\omega}$ = inertial angular velocity of the body frame

$\bar{a}_{cm}$ = acceleration of the center of mass

Equations of Rotational Motion

The equations of rotational motion of the body are obtained by taking the moments of all the external, internal, and inertial forces acting on the body; i.e., from equation (1):

$$\int \bar{r} \times \left[\bar{a}_{cm} + \ddot{\bar{r}} + (2\bar{\omega} \times \dot{\bar{r}}) + (\dot{\bar{\omega}} \times \bar{r}) + \left(\bar{\omega} \times (\bar{\omega} \times \bar{r})\right)\right] \rho \, dv = \int_v \bar{r} \times \left[L(\bar{q})/\rho + \bar{f} + \bar{e}\right]\rho \, dv \qquad (2)$$

One can obtain the following form for the equations of rotational motion:

$$\bar{R} + \sum_{n=1}^{\infty} \bar{Q}^{(n)} + \sum_{n=1}^{\infty} \bar{D}^{(n)} = \bar{G}_R + \sum_{n=1}^{\infty} \bar{G}^{(n)} + \bar{C} \qquad (3)$$

where

$$\bar{R} = \int_v \left[\bar{r}_o \times (\dot{\bar{\omega}} \times \bar{r}_o) - (\bar{r}_o \cdot \bar{\omega})(\bar{\omega} \times \bar{r}_o)\right] \rho \, dv$$

$$\sum_{n=1}^{\infty} \bar{Q}^{(n)} = \int_v \left\{ \bar{r}_o \times \ddot{\bar{q}} + 2\bar{r}_o \times \left(\bar{\omega} \times \dot{\bar{q}}\right) + \bar{r}_o \times \left(\dot{\bar{\omega}} \times \bar{q}\right) + \bar{q} \times \left(\dot{\bar{\omega}} \times \bar{r}_o\right) \right.$$
$$\left. - \left(\bar{r}_o \cdot \bar{\omega}\right)\left[\left(\bar{\omega} \times \bar{q}\right) - \left(\bar{q} \cdot \bar{\omega}\right)\right]\left(\bar{\omega} \times \bar{r}_o\right) \right\} \rho \, dv$$

$$\sum_{n=1}^{\infty} \bar{D}^{(n)} = \int_v \bar{q}\rho \, dv \times \left(\bar{a}_{cm} - \bar{f}_o\right) + \sum_{n=1}^{\infty} \omega_n^2 A_n \int_v \bar{r}_o \times \bar{\Phi}^{(n)} \rho \, dv$$

$$\bar{G}_R = \int \bar{r}_o \times M\bar{r}_o \, \rho \, dv$$

$$\sum_{n=1}^{\infty} \bar{G}^{(n)} = \int_v \left(\bar{r}_o \times M\bar{q} + \bar{q} \times M\bar{r}_o\right)\rho \, dv$$

$$\bar{C} = \int_v \bar{r} \times \bar{e} \, \rho \, dv$$

$$\bar{r} = \bar{r}_o + \bar{q}$$

M = matrix operator which when applied to $\bar{r}$ yields gravity-gradient forces

$\bar{a}_{cm}$ = acceleration of the center of mass

$\bar{f}_o$ = force/mass due to gravity at the undeformed center of mass

$\bar{\Phi}^{(n)}$ = modal shape vector for the nth mode

ω_n = frequency of the nth mode

A_n = time-dependent modal amplitude function

Generic Mode Equations

The generic mode equation is obtained by taking the modal components of all internal, external, and inertial forces acting on the body, i.e.,

$$\int_v \bar{\Phi}^{(n)} \cdot \left[\bar{a}_{cm} + \ddot{\bar{r}} + 2\bar{\omega} \times \dot{\bar{r}} + \dot{\bar{\omega}} \times \bar{r} + \bar{\omega} \times \left(\bar{\omega} \times \bar{r}\right)\right] \rho \, dv$$
$$= \int_v \bar{\Phi}^{(n)} \cdot \left[L(\bar{q})/\rho + \bar{f} + \bar{e}\right]\rho \, dv \qquad (4)$$

The generic mode equation is obtained in the following form:

$$\ddot{A}_n + \omega_n^2 A_n + \psi_n/M_n + \sum_{m=1}^{\infty} \psi_{mn}/M_n = \left(g_n + \sum_{m=1}^{\infty} g_{mn} + E_n + D_n'\right)\Big/ M_n \qquad (5)$$

where

$$\psi_n = \int_v \left[\bar{\Phi}^{(n)} \cdot \dot{\bar{\omega}} \times \bar{r}_o + \bar{\Phi}^{(n)} \cdot \bar{\omega} \times (\bar{\omega} \times \bar{r}_o)\right] \rho \, dv$$

$$\sum_{m=1}^{\infty} \psi_{mn} = \int_v \left[2\bar{\Phi}^{(n)} \cdot \bar{\omega} \times \dot{\bar{q}} + \bar{\Phi}^{(n)} \cdot \dot{\bar{\omega}} \times \bar{q} + \bar{\Phi}^{(n)} \cdot \bar{\omega} \times (\bar{\omega} \times \bar{q})\right] \rho \, dv$$

$$g_n = \int \bar{\Phi}^{(n)} \cdot M\bar{r}_o \, \rho \, dv$$

$$\sum_{m=1}^{\infty} g_{mn} = \int_v \bar{\Phi}^{(n)} \cdot M\bar{q}\rho \, dv$$

$$E_n = \int \bar{\Phi}^{(n)} \cdot \bar{e}\rho \, dv$$

$$D_n' = \int_v \bar{\Phi}^{(n)} \rho \, dv \cdot (\bar{a}_{cm} - \bar{f}_o)$$

Here ψ_n is the inertia coupling between rigid body modes and the nth structural mode and ψ_{mn} is the inertia coupling between the mth and nth structural modes.

Cartesian Components of the Different Coupling Terms

The expressions for $\bar{R}$, $\bar{Q}^{(n)}$, $\bar{G}_R$, $\bar{G}^{(n)}$, ψ_n, ψ_{mn}, g_n, and g_{mn} in Cartesian components are presented in this section. The following vectors can be expressed in their Cartesian component form as:

$$\bar{r}_o = \xi_x \hat{i} + \xi_y \hat{j} + \xi_z \hat{k}; \quad \bar{\omega} = \omega_x \hat{i} + \omega_y \hat{j} + \omega_z \hat{k}$$

$$\bar{q} = \sum_{n=1}^{\infty} A_n(t)\bar{\Phi}^{(n)}(\bar{r}_o); \quad \bar{\Phi}^{(n)} = \phi_x^{(n)}\hat{i} + \phi_y^{(n)}\hat{j} + \phi_z^{(n)}\hat{k}$$

$$\bar{Q}^{(n)} = Q_x^{(n)}\hat{i} + Q_y^{(n)}\hat{j} + Q_z^{(n)}\hat{k}$$

$$\bar{G}^{(n)} = G_x^{(n)}\hat{i} + G_y^{(n)}\hat{j} + G_z^{(n)}\hat{k}$$

where $\hat{i}$, $\hat{j}$, and $\hat{k}$ are unit vectors along the body principal axes of inertia in the undeformed state, and ξ_x, ξ_y, and ξ_z are the coordinates of a point in the undeformed state.

With the use of the component forms of the vectors given above, one can expand the various vector expressions given in equations (3) and (5) to obtain

$$\bar{R} = \left[J_x\dot{\omega}_x + (J_z - J_y)\omega_y\omega_z\right]\hat{i} + \left[J_y\dot{\omega}_y + (J_x - J_z)\omega_z\omega_x\right]\hat{j} + \left[J_z\dot{\omega}_z + (J_y - J_x)\omega_x\omega_y\right]\hat{k} \tag{6}$$

$$\begin{aligned} Q_x^{(n)} = {} & \ddot{A}_n\left(H_{yz}^{(n)} - H_{zy}^{(n)}\right) + 2\dot{A}_n\left[\left(H_{yy}^{(n)} + H_{zz}^{(n)}\right)\omega_x - H_{yx}^{(n)}\omega_y - H_{zx}^{(n)}\omega_z\right] \\ & + A_n\left[2\left(H_{yy}^{(n)} + H_{zz}^{(n)}\right)\dot{\omega}_x - \left(H_{xy}^{(n)} + H_{yx}^{(n)}\right)\dot{\omega}_y - \left(H_{zx}^{(n)} + H_{xz}^{(n)}\right)\dot{\omega}_z\right. \\ & - 2\omega_y\omega_z\left(H_{zz}^{(n)} - H_{yy}^{(n)}\right) - \omega_x\omega_y\left(H_{xz}^{(n)} + H_{zx}^{(n)}\right) + \omega_x\omega_z\left(H_{xy}^{(n)} + H_{yx}^{(n)}\right) \\ & \left. + \left(\omega_z^2 - \omega_y^2\right)\left(H_{yz}^{(n)} + H_{zy}^{(n)}\right)\right] \end{aligned} \tag{7}$$

$$\bar{G}_R = (J_z - J_y)M_{23}\hat{i} + (J_x - J_z)M_{31}\hat{j} + (J_y - J_x)M_{21}\hat{k} \tag{8}$$

$$G_x^{(n)} = A_n\Big[(M_{33} - M_{22})\Big(H_{yz}^{(n)} + H_{zy}^{(n)}\Big) - M_{21}\Big(H_{xz}^{(n)} + H_{zx}^{(n)}\Big)$$

$$+ M_{31}\Big(H_{xy}^{(n)} + H_{yx}^{(n)}\Big) + 2M_{23}\Big(H_{yy}^{(n)} - H_{zz}^{(n)}\Big)\Big] \tag{9}$$

$$\psi_n = \dot{\omega}_x\Big(H_{yz}^{(n)} + H_{zy}^{(n)}\Big) + \dot{\omega}_y\Big(H_{zx}^{(n)} - H_{xz}^{(n)}\Big) + \dot{\omega}_z\Big(H_{xy}^{(n)} - H_{yx}^{(n)}\Big)$$

$$+ \omega_x\omega_y\Big(H_{xy}^{(n)} + H_{yx}^{(n)}\Big) + \omega_y\omega_z\Big(H_{yz}^{(n)} + H_{zy}^{(n)}\Big) + \omega_z\omega_x\Big(H_{zx}^{(n)} + H_{xz}^{(n)}\Big)$$

$$- \omega_x^2\Big(H_{yy}^{(n)} + H_{zz}^{(n)}\Big) - \omega_y^2\Big(H_{zz}^{(n)} + H_{xx}^{(n)}\Big) - \omega_z^2\Big(H_{xx}^{(n)} + H_{yy}^{(n)}\Big) \tag{10}$$

$$\psi_{mn} = 2\dot{A}_m\Big[\omega_x\Big(L_{yz}^{(mn)} - L_{zy}^{(mn)}\Big) + \omega_y\Big(L_{zx}^{(mn)} - L_{xz}^{(mn)}\Big) + \omega_z\Big(L_{xy}^{(mn)} - L_{yx}^{(mn)}\Big)\Big]$$

$$+ A_m\Big[\dot{\omega}_x\Big(L_{yz}^{(mn)} - L_{zy}^{(mn)}\Big) + \dot{\omega}_y\Big(L_{zx}^{(mn)} - L_{xz}^{(mn)}\Big) + \dot{\omega}_z\Big(L_{xy}^{(mn)} - L_{yx}^{(mn)}\Big)$$

$$+ \omega_x\omega_y\Big(L_{xy}^{(mn)} + L_{yx}^{(mn)}\Big) + \omega_y\omega_z\Big(L_{yz}^{(mn)} + L_{zy}^{(mn)}\Big) + \omega_z\omega_x\Big(L_{zx}^{(mn)} + L_{xz}^{(mn)}\Big)$$

$$- \omega_x^2\Big(L_{yy}^{(mn)} + L_{zz}^{(mn)}\Big) - \omega_y^2\Big(L_{zz}^{(mn)} + L_{xx}^{(mn)}\Big) - \omega_z^2\Big(L_{xx}^{(mn)} + L_{yy}^{(mn)}\Big)\Big] \tag{11}$$

$$g_n = \sum_{\alpha\beta}\sum H_{\alpha\beta}^{(n)} M_{\alpha\beta}$$

$$g_{mn} = A_m \sum_{\alpha\beta}\sum L_{\alpha\beta}^{(mn)} M_{\alpha\beta}$$

where

$$H_{\alpha\beta}^{(n)} = \int_v \xi_\alpha \phi_\beta^{(n)} dm$$

$$L_{\alpha\beta}^{(mn)} = \int_v \phi_\alpha^{(m)} \phi_\beta^{(n)} dm$$

$\alpha, \beta = x, y, z$ or $1, 2, 3$

When α is x in $H_{\alpha\beta}^{(n)}$ or $L_{\alpha\beta}^{(mn)}$, the corresponding value of α in $M_{\alpha\beta}$ is 1. In a similar manner, when α is y in $H_{\alpha\beta}^{(n)}$ or $L_{\alpha\beta}^{(mn)}$, α is 2 in $M_{\alpha\beta}$, and when α is z in $H_{\alpha\beta}^{(n)}$ or $L_{\alpha\beta}^{(mn)}$, α is 3 in $M_{\alpha\beta}$. The same reasoning holds for β.

The expressions for $Q_y^{(n)}$ and $Q_z^{(n)}$ are obtained by the cyclic permutation of x, y, z in the expression for $Q_x^{(n)}$ in equation (7), and the expressions for $G_y^{(n)}$ and $G_z^{(n)}$ are obtained by the cyclic permutation of x, y, z in the expression for $G_x^{(n)}$ in equation (9).

For a discretized model, the expressions for the volume integrals are replaced by the following summations:

$$H_{\alpha\beta}^{(n)} = \sum_{i=1}^{k} (\xi_\alpha)_i \left(\phi_\beta^{(n)}\right)_i m_i \qquad (12)$$

$$(\alpha,\beta = x,y,z)$$

$$L_{\alpha\beta}^{(mn)} = \sum_{i=1}^{k} \left(\phi_\alpha^{(m)}\right)_i \left(\phi_\beta^{(n)}\right)_i m_i \qquad (13)$$

where

k = total number of discrete masses

i = index identifying a nodal point

m_i = mass concentrated at the ith node

ξ_α = coordinates of m_i in the undeformed state

REFERENCE

1. Bainum, Peter M.; Reddy, A. S. S. R.; Krishna, R.; Diarra, Cheick M.; and Kumar, V. K.: The Dynamics and Control of Large Flexible Space Structures - V. NASA CR-169360, 1982.

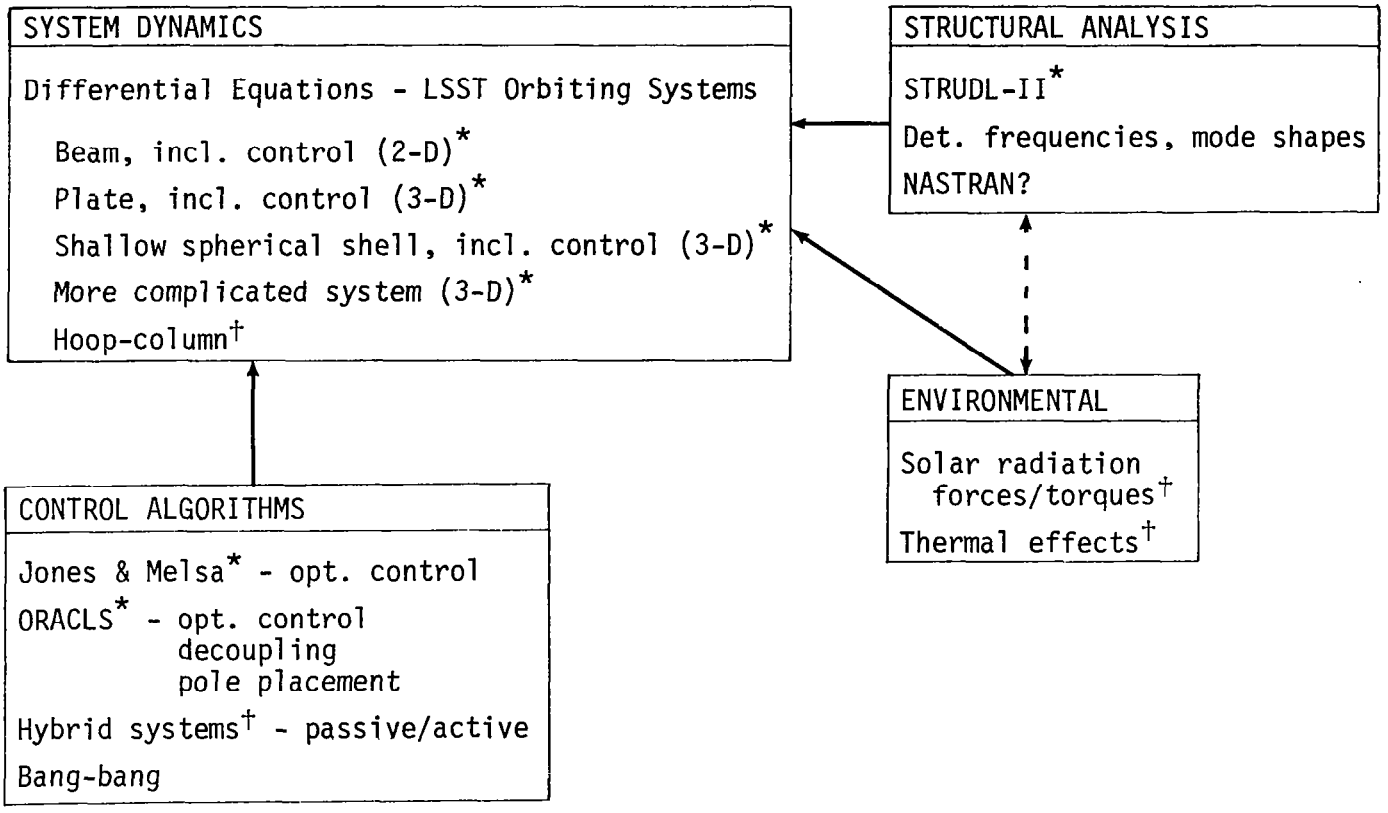

*Operational.
†In progress.

Figure 1.- Development of system software for LSST dynamics analysis.

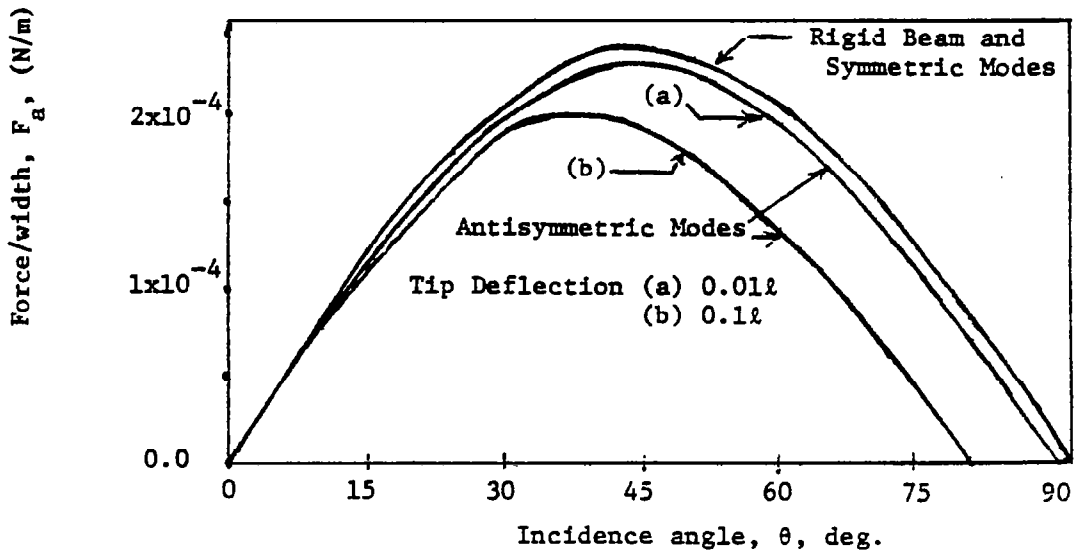

(a) Horizontal component.

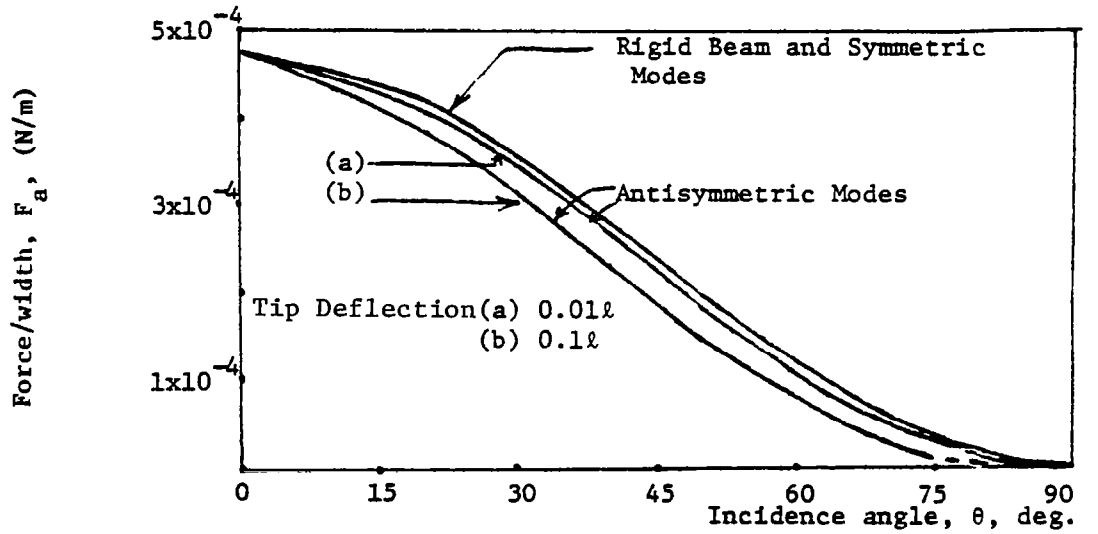

(b) Normal component.

Figure 2.- Variation of solar force components with incidence angle. Totally absorbing surface - free-free beam (length ℓ = 100 m).

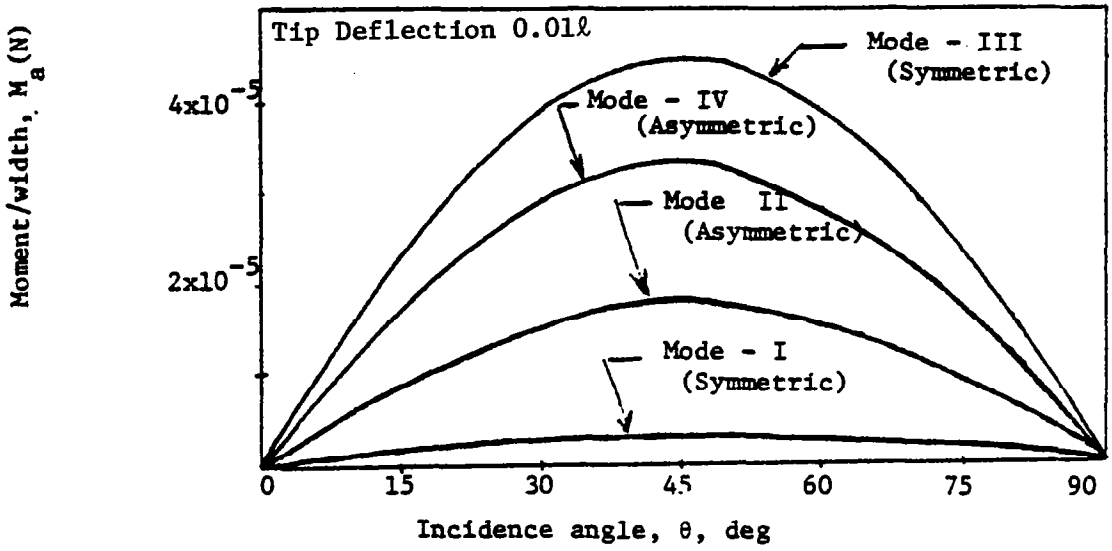

Figure 3.- Pitch moment due to solar radiation pressure (completely absorbing surface). Effect of individual modes in the system - free-free beam.

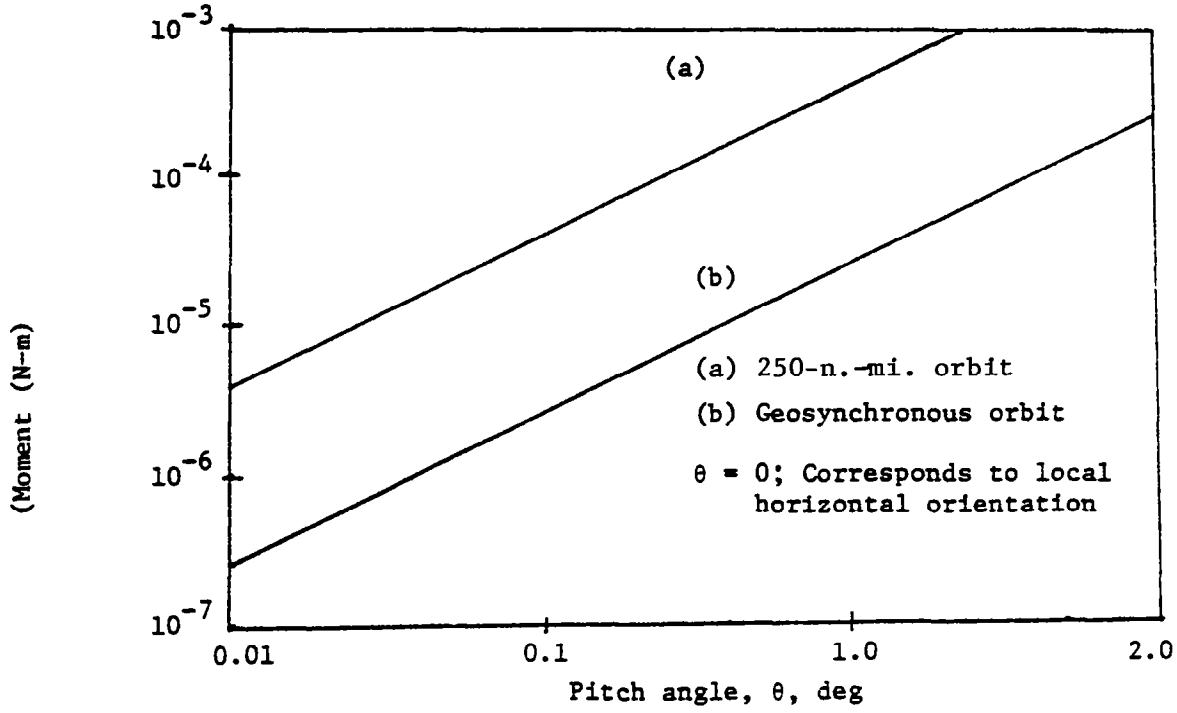

Figure 4.- Moment due to gravity-gradient force as a function of pitch angle (100-m rigid beam).

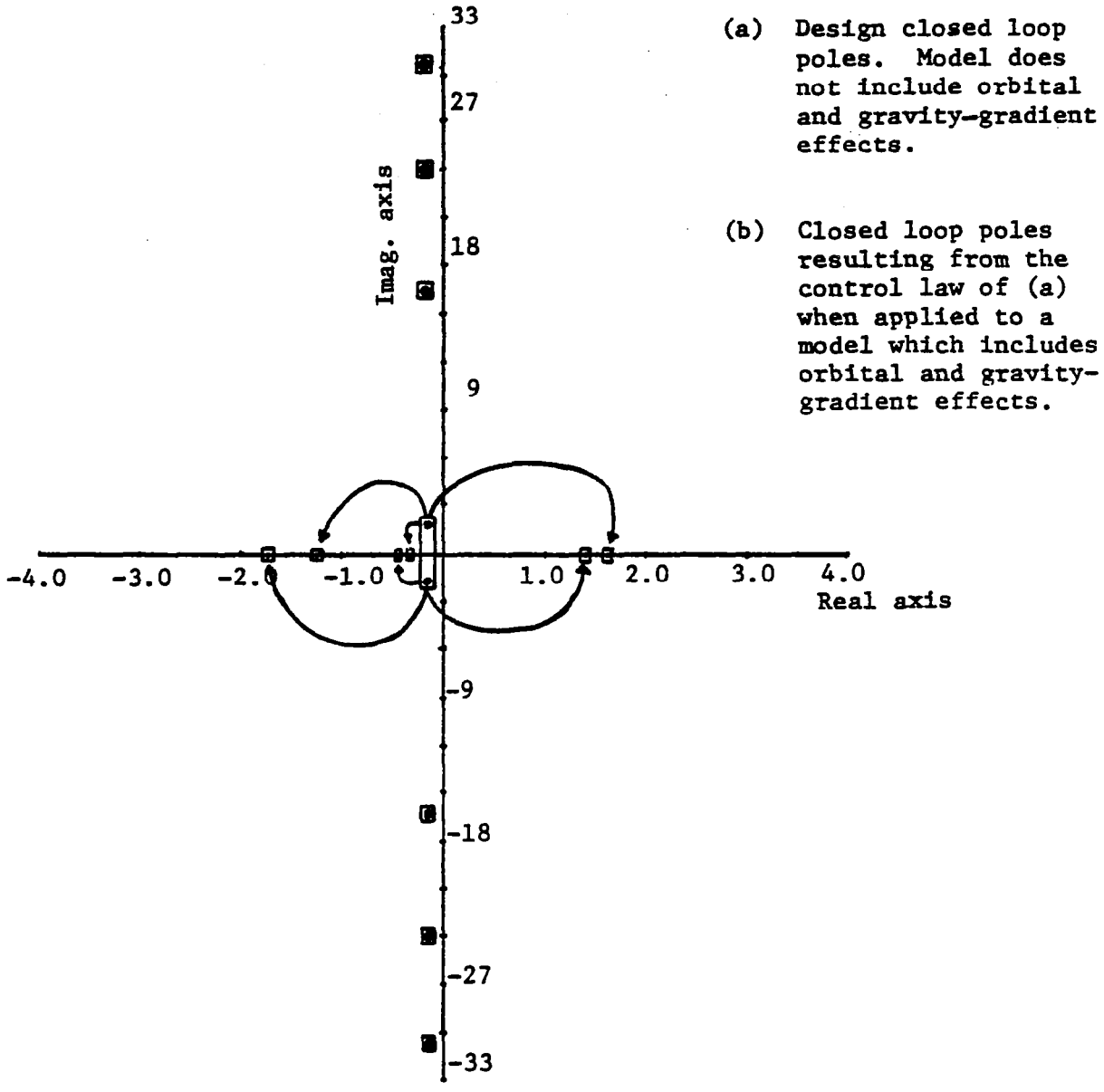

Figure 5.- Shift in closed loop poles due to orbital and gravity-gradient torques. Square plate in 250-n.-mi. orbit. Overall designed response time constant of the system = 8000 sec.

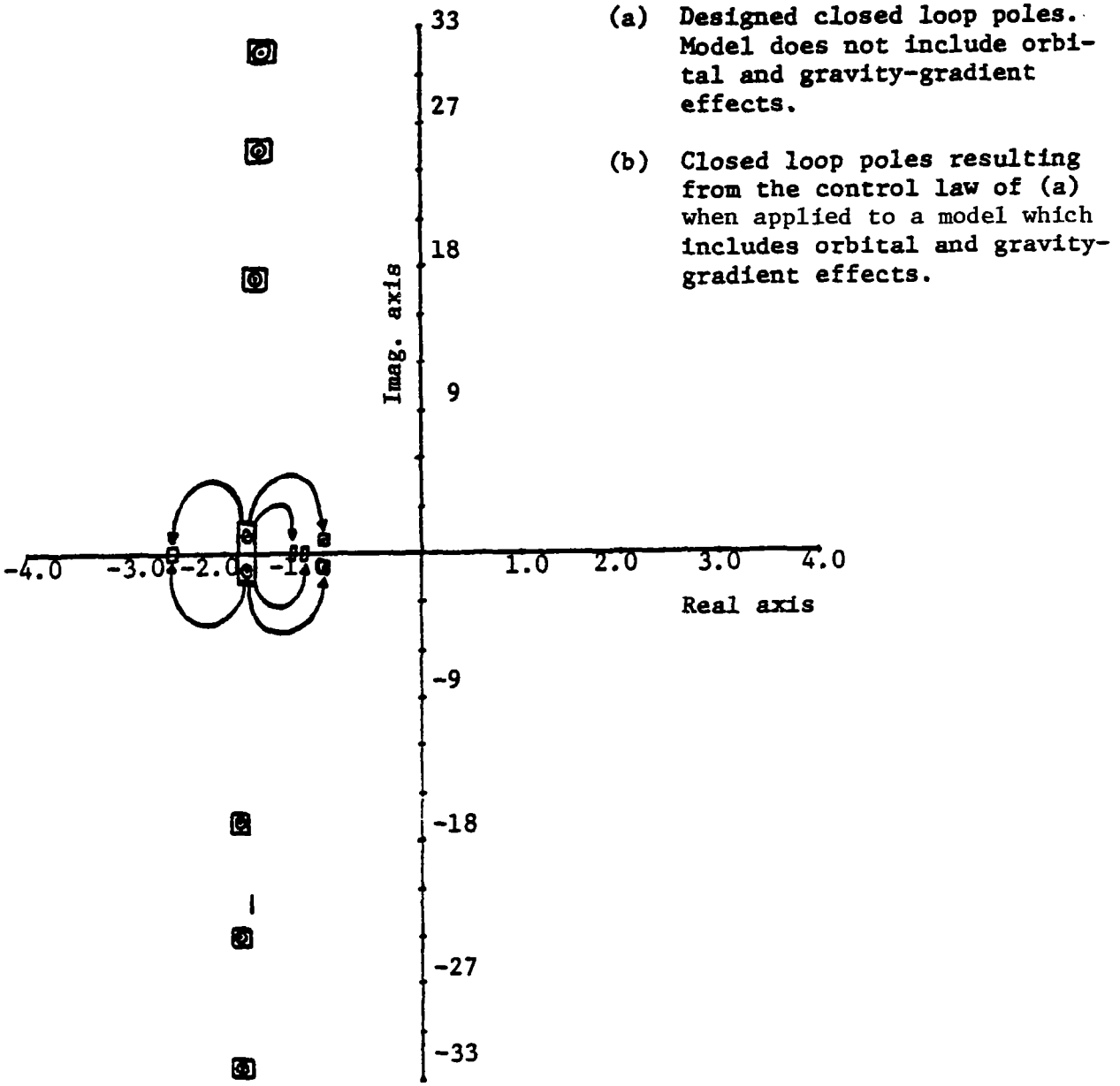

Figure 6.- Shift in closed loop poles due to orbital and gravity-gradient torques. Square plate in 250-n.-mi. orbit. Overall designed response time constant of the system = 460 sec.

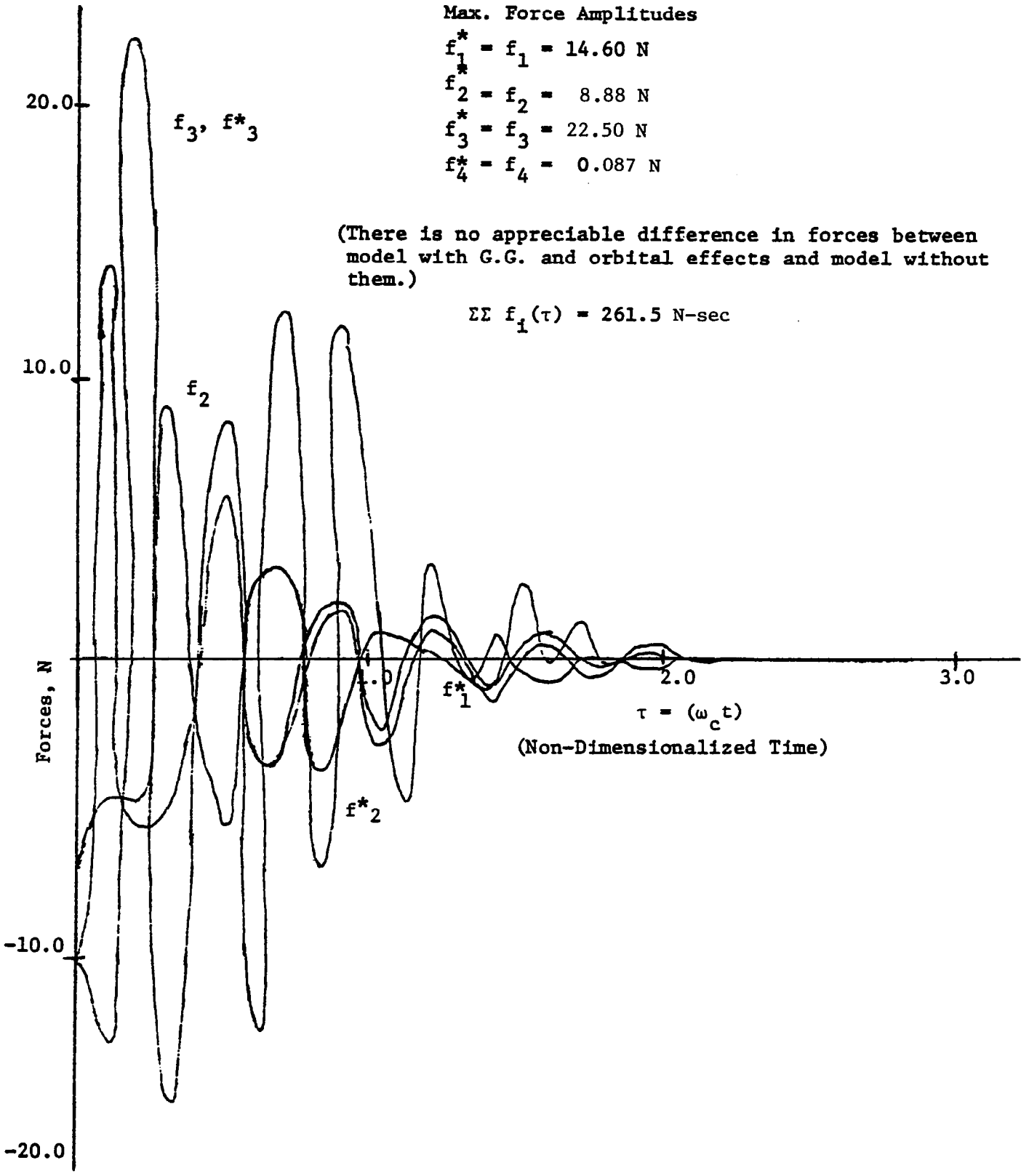

Figure 7.- Time history of control forces. Square plate.

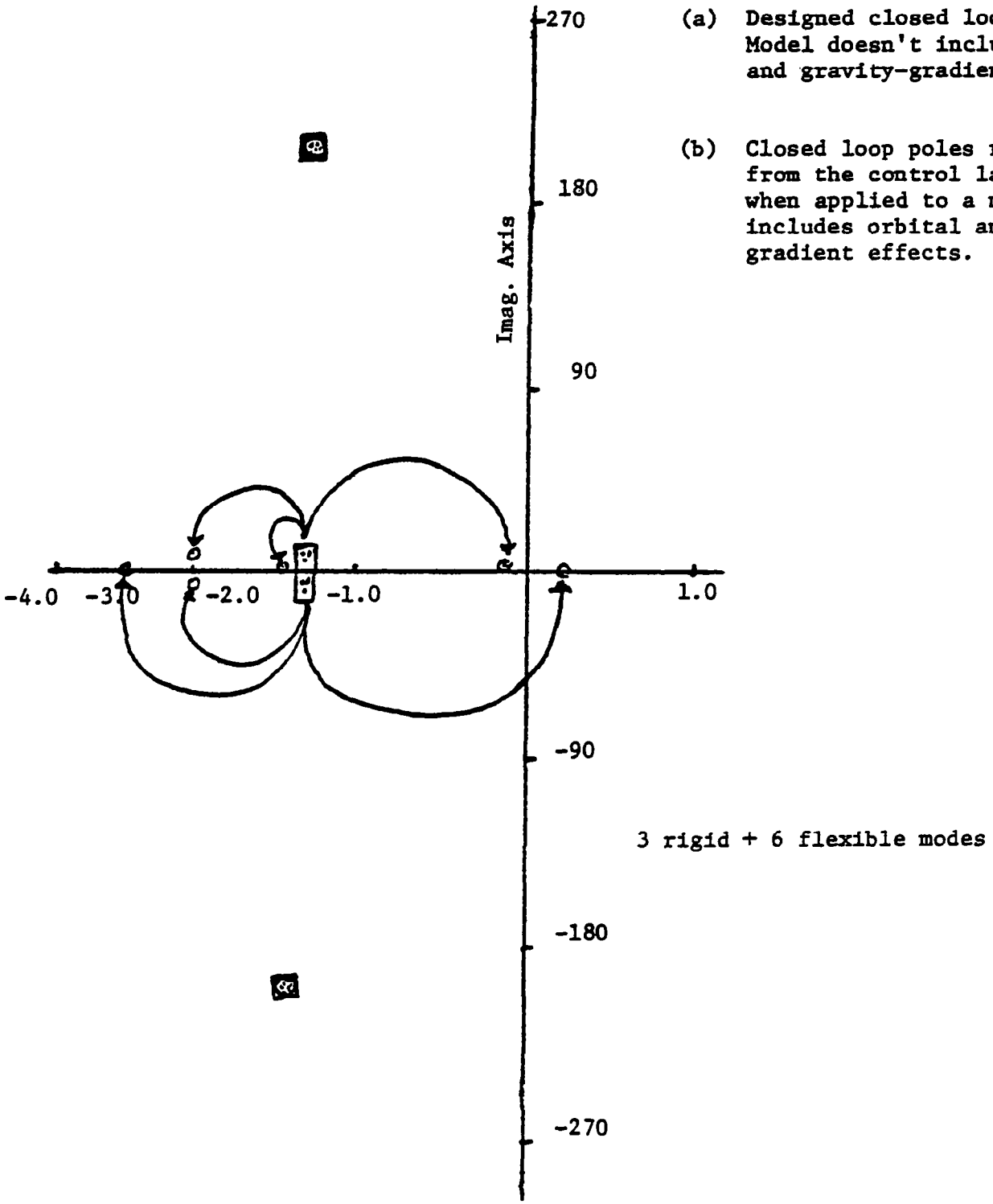

Figure 8.- Shift in closed loop poles due to orbital and gravity-gradient torques. Shallow spherical shell in 250-n.-mi. orbit. Overall designed response time constant of the system = 615.0 sec.

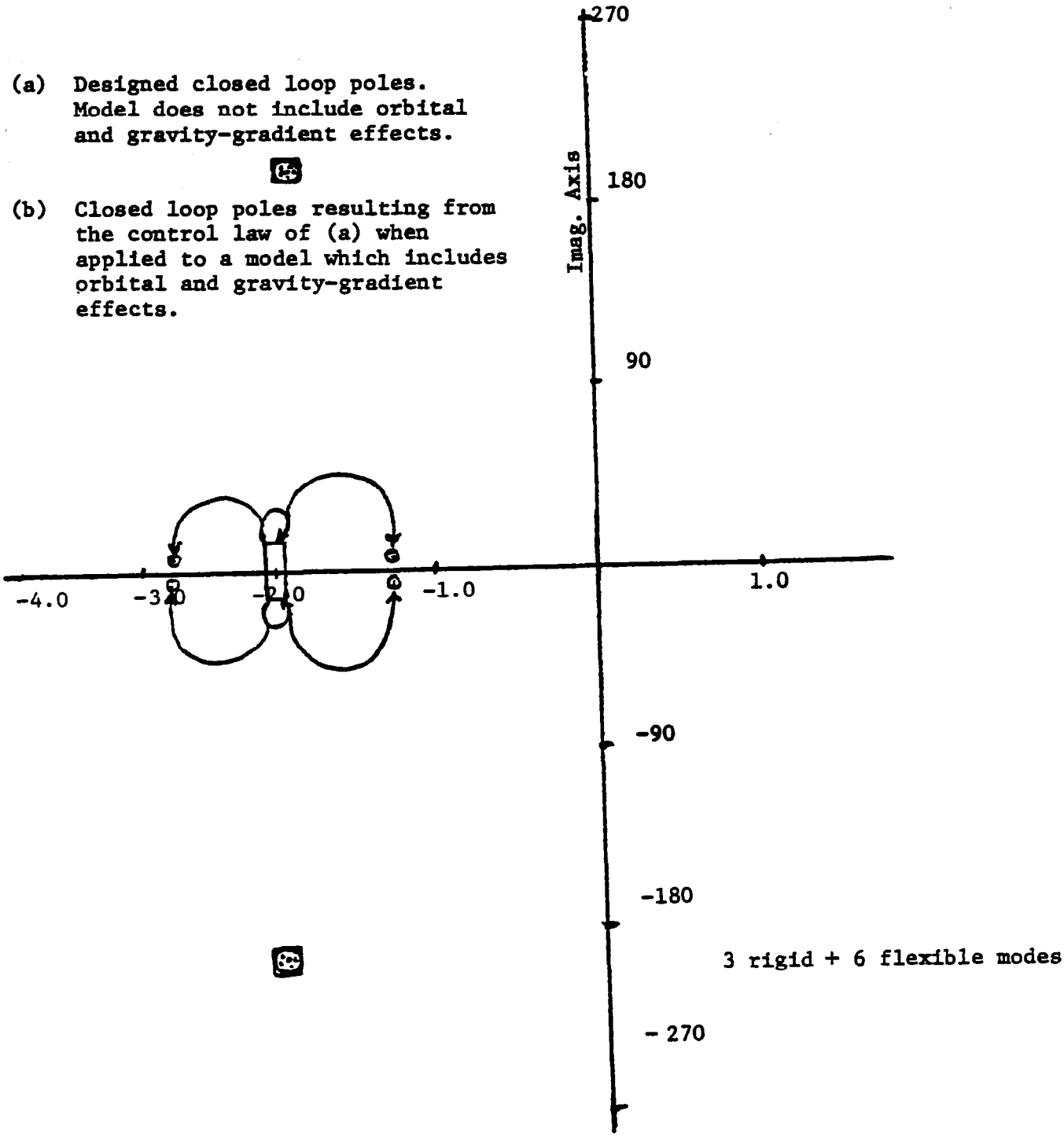

Figure 9.- Shift in closed loop poles due to orbital and gravity-gradient torques. Shallow spherical shell in 250-n.-mi. orbit. Overall designed response time constant of the system = 400 sec.

PEAK FORCE AMPLITUDES-CONTROL LAW DEVELOPED WITHOUT ORBITAL AND GRAVITY-GRADIENT EFFECTS IN THE MODEL AND THEN APPLIED TO A MODEL WITH THEM (Shell in orbit).

Without Orbital and G.G. Effects	With Orbital and G.G. Effects*
f_1: 516.40 N	f_1^*: 565.63 N
f_2: 73.30 N	f_2^*: 164.76 N
f_3: 239.50 N	f_3^*: 321.11 N
f_4: 117.54 N	f_4^*: 117.07 N
f_5: 132.45 N	f_5^*: 153.84 N
f_6: 146.82 N	f_6^*: 431.61 N
$\sum\sum_{ti} f_i$ = 7020.8 N-sec	$\sum\sum_{ti} f_i^*$ = 19373.0 N-sec

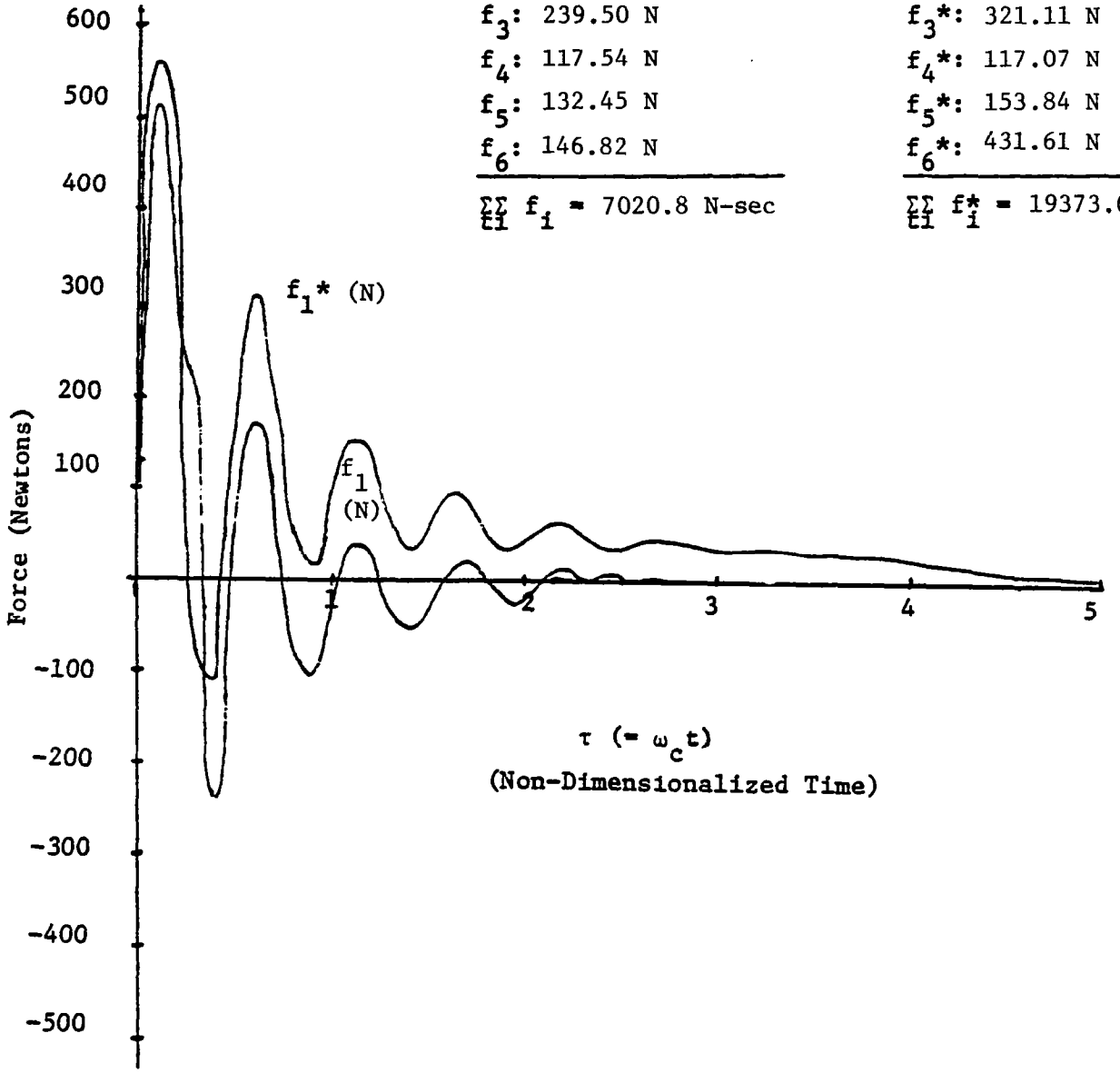

Figure 10.- Time history of control forces. Shallow spherical shell.

CONTROL OF STRUCTURES IN SPACE

L. Meirovitch and H. Barun
Department of Engineering Science and Mechanics
Virginia Polytechnic Institute and State University
Blacksburg, Virginia

EQUATION OF MOTION FOR DISTRIBUTED SYSTEMS

Differential equation: $Lu(P,t) + M(P)\partial^2 u(P,t)/\partial t^2 = f(P,t)$, $P \in D$

Boundary conditions: $B_i u(P,t) = 0$, $i=1,2,\ldots,p$, $P \in S$

$u(P,t)$ = displacement at point P

L, B_i = differential operators (L is self-adjoint of order 2p)

M = mass density

$f(P,t)$ = distributed control force

EIGENVALUE PROBLEM

Differential equation: $L\phi = \lambda M\phi$

Boundary conditions: $B_i \phi = 0$, $i = 1,2,\ldots,p$

Solution: eigenvalues $\lambda_r = \omega_r^2$, eigenfunctions ϕ_r $(r=1,2,\ldots)$

Because L is self-adjoint, eigenfunctions are orthogonal

L is generally positive semidefinite $\rightarrow \lambda_r$ are all nonnegative

$\lambda_r = 0$ for rigid-body modes

$\omega_r = \sqrt{\lambda_r}$ = natural frequencies

Orthonormality conditions: $\int_D M\phi_s\phi_r \, dD = \delta_{rs}$, $\int_D \phi_s L\phi_r \, dD = \lambda_r \delta_{rs}$

MODAL EQUATIONS

Expansion theorem: $u(P,t) = \sum_{r=1}^{\infty} \phi_r(P) u_r(t)$

$u_r(t)$ = modal coordinates

Modal equations: $\ddot{u}_r(t) + \omega_r^2 u_r(t) = f_r(t)$, $r=1,2,...$

Modal controls: $f_r(t) = \int_D \phi_r(P) f(P,t) dD$, $r=1,2,...$

Coupled controls: $f_r(t) = f_r(u_1, \dot{u}_1, u_2, \dot{u}_2, ...)$, $r=1,2,...$

Independent modal-space control (IMSC): $f_r(t) = f_r(u_r, \dot{u}_r)$, $r=1,2,...$

CONTROL IMPLEMENTATION

Distributed actuators: $f(P,t) = \sum_{r=1}^{\infty} M(P) \phi_r(P) f_r(t)$

Coupled controls: unable to design distributed controls

IMSC: design modal controls first, then use above formula
no control spillover

Discrete actuators: $f(P,t) = \sum_{j=1}^{m} F_j(t)\, \delta(P-P_j)$

$$f_r(t) = \sum_{j=1}^{m} \phi_r(P_j) F_j(t) = \sum_{j=1}^{m} B_{rj} F_j(t) \quad , \quad r=1,2,...,n$$

n = number of controlled modes

$$\underset{\sim}{F} = [F_1\ F_2\ \dots\ F_m]^T \quad \underset{\sim}{f} = [f_1\ f_2\ \dots\ f_n]^T \quad B = B_{rj}$$

Coupled controls: Design $\underset{\sim}{F}(t)$ so as to ensure controllability
IMSC: Design $\underset{\sim}{f}(t)$ so as to control a given number of modes
Then, $\underset{\sim}{F}(t) = B^{\dagger} \underset{\sim}{f}(t)$, $B^{\dagger}$ = pseudo-inverse of B
To avoid pseudo-inverses, let $m = n$, or the number of actuators must equal the number of controlled modes.

CONTROL IMPLEMENTATION (CONT'D)

Distributed measurements:

Measurements: $u(P,t)$, $\dot{u}(P,t)$ for all P and at any t

Then, modal coordinates and velocities, $u_r(t)$ and $\dot{u}_r(t)$, are computed by using the modal filters

$$u_r(t) = \int_D M(P)\,\phi_r(P)u(P,t)dD,\quad \dot{u}_r(t) = \int_D M(P)\,\phi_r(P)\dot{u}(P,t)dD,\quad r=1,2,\ldots$$

Discrete measurements:

Measurements: $y_j(t) = u(P_j,t)$, $\dot{y}_j(t) = \dot{u}(P_j,t)$, $j = 1,2,\ldots,k$

k = number of sensors

Standard approach: Use Luenberger observer to estimate state

Discrete measurements treated as distributed:

Use interpolation functions to compute estimate $\hat{u}(P,t)$ of $u(P,t)$

Then, use modal filters to compute estimates $\hat{u}_r(t)$ of $u_r(t)$

Divide structure into s segments (elements)

Approximate displacement: $\hat{u}(P,t) = \sum_{j=1}^{S} \underset{\sim}{L}_j^T(P)\underset{\sim}{y}_j(t)$

$\underset{\sim}{y}_j$ = measurements at the boundaries of j'th interval

$\underset{\sim}{L}_j$ = vector of interpolation functions (from the finite element method)

Estimated modal coordinates:

$$\hat{u}_r(t) = \int_D M(P)\phi_r(P)\sum_{j=1}^{S}\underset{\sim}{L}_j^T\underset{\sim}{y}_j(t)dD = \sum_{j=1}^{S}\underset{\sim}{I}_{rj}\underset{\sim}{y}_j(t),\quad r = 1,2,\ldots,n$$

Similarly $\dot{\hat{u}}_r(t) = \sum_{j=1}^{S}\underset{\sim}{I}_{rj}\dot{\underset{\sim}{y}}_j(t)$

$$\underset{\sim}{I}_{rj} = \int_D M(P)\phi_r(P)\underset{\sim}{L}_j(P)dD = \text{const}$$

$\underset{\sim}{I}_{rj}$ are computed off-line, in advance.

CONTROL IMPLEMENTATION (CONT'D)

Rearrange $\underset{\sim}{I}_{rj}$ such that

$$\hat{u}_r(t) = \sum_{j=1}^{k} C_{rj} y_j(t) \ , \quad \hat{\dot{u}}_r(t) = \sum_{j=1}^{k} C_{rj} \dot{y}_j(t)$$

Let

$$\underset{\sim}{\hat{u}}(t) = [\hat{u}_1 \ \hat{u}_2 \ldots \hat{u}_n]^T, \quad \underset{\sim}{\hat{\dot{u}}}(t) = [\hat{\dot{u}}_1 \ \hat{\dot{u}}_2 \ \ldots \ \hat{\dot{u}}_n]^T$$

$$C = C_{rj} \ , \quad r=1,2,\ldots,n; \ j=1,2,\ldots,k$$

$$\underset{\sim}{y}(t) = [y_1 \ y_2 \ \ldots \ y_k]^T, \quad \underset{\sim}{\dot{y}}(t) = [\dot{y}_1 \ \dot{y}_2 \ \ldots \ \dot{y}_k]^T$$

$$\underset{\sim}{\hat{u}}(t) = C\underset{\sim}{y}(t) \ , \quad \underset{\sim}{\hat{\dot{u}}}(t) = C\underset{\sim}{\dot{y}}(t)$$

The way C is assembled depends on the nature of the interpolation functions (see example later).

THE LANGLEY BEAM EXPERIMENT

Free-free beam controlled by using 4 actuators and 9 sensors

Use IMSC to control four modes, two rigid-body and two elastic modes

Actuator forces $F_j(t) = \sum_{r=1}^{4} (B^{-1})_{rj} f_r(t), \quad j = 1,2,3,4$

Modal forces:

1) For rigid body modes

$\eta_r = |\hat{u}_r| + |\hat{\dot{u}}_r|/c_r \ , \quad r=1,2$

c_r = weighting factor

if $\eta_r < d_r$, then $f_r = 0$

if $\eta_r > d_r$ and

i) $\hat{u}_r > 0$, $\hat{\dot{u}}_r > 0$, or $\hat{u}_r > 0 > \hat{\dot{u}}_r$ and $|\hat{\dot{u}}_r| < \varepsilon_r$, then $f_r = -k_r$

ii) $\hat{u}_r < 0$, $\hat{\dot{u}}_r < 0$, or $\hat{u}_r < 0 < \hat{\dot{u}}_r$ and $|\hat{\dot{u}}_r| < \varepsilon_r$, then $f_r = k_r$

d_r = magnitude of the deadband region

ε_r = threshold velocity, k_r = modal control force

THE LANGLEY BEAM EXPERIMENT (CONT'D)

2) for elastic modes

$$f_r(t) = -k_r \quad , \quad |\hat{u}_r| \geq d_r \text{ and } \dot{\hat{u}}_r > 0$$

$$0 \quad , \quad -d_r < \hat{u}_r < d_r$$

$$k_r \quad , \quad |\hat{u}_r| \geq d_r \text{ and } \dot{\hat{u}}_r < 0$$

For simulation purposes, the response is available in closed form both for rigid-body and elastic modes.

Actuator locations immaterial when IMSC is used.

$$\underset{\sim}{F}(t) = B^{-1}\underset{\sim}{f}(t) \qquad F_j(t) = \sum_{r=1}^{4} (B^{-1})_{jr} f_r(t) \quad j=1,2,3,4$$

Actual control forces are a combination of on-off functions of the type

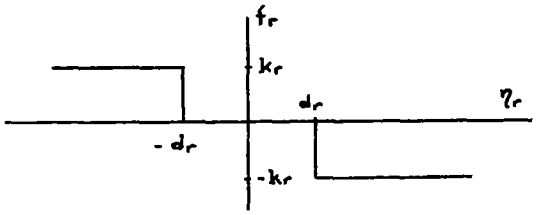

Actuators available at LARC have four components, which can be assigned to each modal control force. As a result, each actuator command becomes a linear combination of 4 modal on-off control forces.

THE LANGLEY BEAM EXPERIMENT (CONT'D)

Sensors measure displacements alone. Ideally, for bending they should measure displacements and slopes (velocities and slopes of velocities too)

Divide the beam into four equal segments (elements) and measure displacements at the ends and middle point of the element, so that the nine sensors are spaced at equal intervals.

As interpolation functions use

$$\underset{\sim}{L}_j = [\zeta(2\zeta-1) \quad 4\zeta(1-\zeta) \quad 1-3\zeta+2\zeta^2]^T, \quad 0 < \zeta < 1$$

where ζ is a local coordinate related to the global coordinate x by

$\zeta = j - \frac{4}{L}x$, in which j is the segment number

The C matrix is assembled from $\underset{\sim}{I}_{rj}$ tensor as

$$C_{rp} = \sum_{j=1}^{s} \sum_{\ell=1}^{3} \underset{\sim}{I}_{rj\ell}\, \delta_{2j+\ell-2,p} \qquad \begin{array}{l} r = 1,2,\ldots,n \ , \ n=4 \\ s = 4 \\ p = 1,2,\ldots,k, \ k = 9 \end{array}$$

ℓ = index denoting the interpolation function

j = index denoting the element number

Because velocity measurements are not available estimate velocities by using the relation

$$\hat{\dot{u}}_r(jT) = \frac{\hat{u}_r(jT) - \hat{u}_r(jT-T)}{T}$$

T = sampling time = 1/33 sec.

Or, one could use a modal Luenberger type observer. Because the controls are nonlinear, the convergence of the observer can only be determined by trial and error.

THE LANGLEY BEAM EXPERIMENT (CONT'D)

Parameters associated with the beam:

L = 12 ft. cross-section = 6 x 3/16 in

6061 aluminum: $\rho = 0.1$ lb/in^3 $E = 1 \times 10^7$ lb/in^2

The free-free, uniform beam admits a closed-form solution. The transcendental equation was solved numerically to yield the eigenvalues

$\omega_1 = 0$

$\omega_2 = 0$

$\omega_3 = 11.47979$ rad/s

$\omega_4 = 31.64450$ rad/s

$\omega_5 = 62.03586$ rad/s

$\omega_6 = 102.5484$ rad/s

$\omega_7 = 153.1897$ rad/s

Simulation of the Beam motion:

The first 7 modes are included in the simulation: 4 controlled + 3 residual modes

Control Gain Parameters:

$d_1 = d_2 = 0.002$, $d_3 = d_4 = 0.0005$

$k_1 = k_2 = 0.3$, $k_3 = 0.12$, $k_4 = 0.03$

$\varepsilon_1 = \varepsilon_2 = 0.01$

$\gamma_r = |\hat{u}_r| + |\dot{\hat{u}}_r| /10$, r=1,2

Sampling time = 1/33 sec.

Viscous damping was added to each flexible mode

Damping factor $\xi_r = 0.002$, r=3,4,5,6,7

Disturbance of the beam was taken in the form of a unit impulse of magnitude 1/12 lb applied at $x_0 = 0.67L$.

The displacement of the beam cannot exceed 1 in at any time because of the location of the sensors and actuators in the experimental setup.

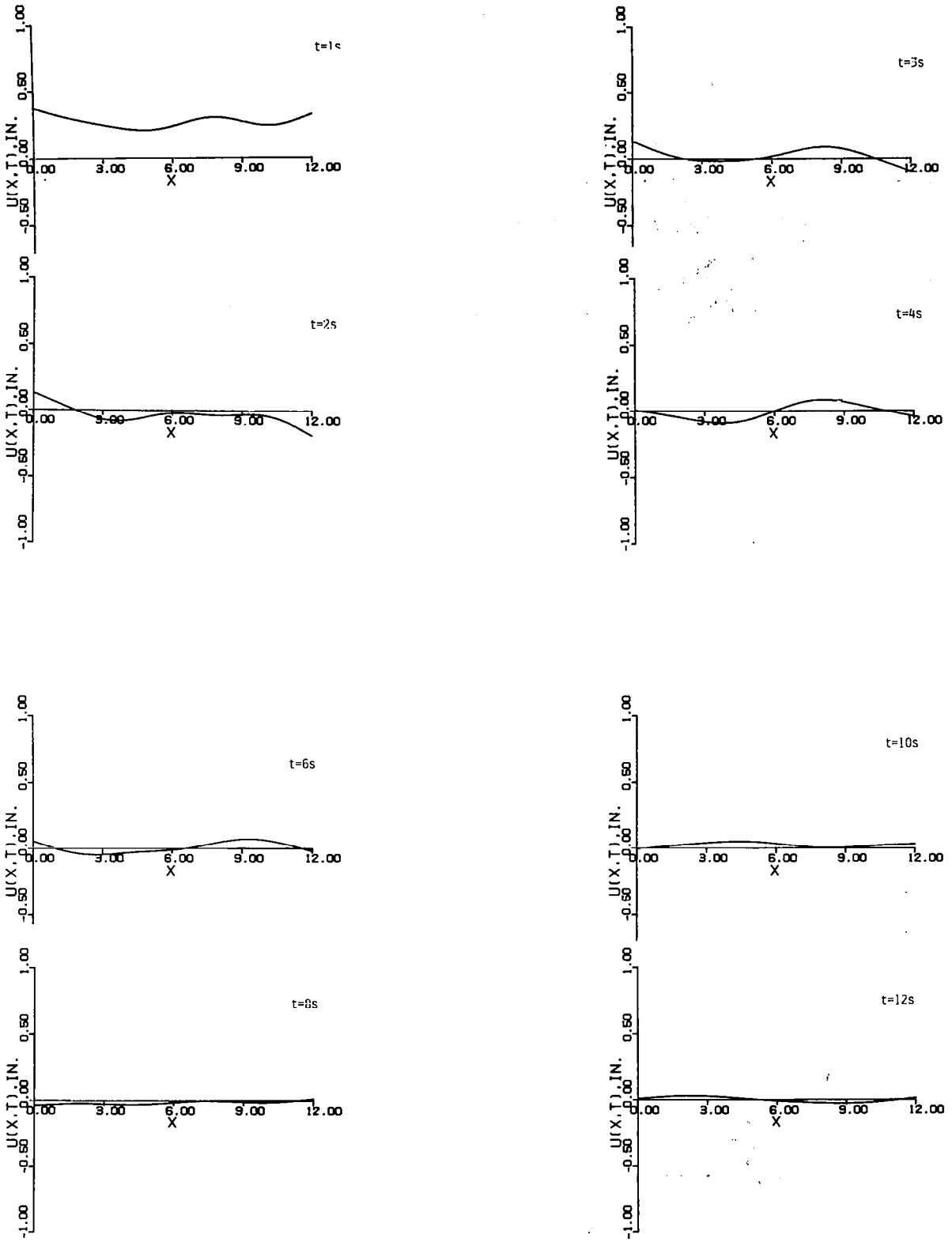

RESPONSE OF THE LANGLEY BEAM

THE LANGLEY BEAM EXPERIMENT (CONT'D)

Results

- The main contribution to the response is from the rigid-body modes.
- The second elastic mode shows noticeable participation. This participation will eventually disappear due to internal damping.
- Control of the second elastic mode can be enhanced by sensing velocities, or estimating velocitites via a Luenberger observer.
- Observation spillover (which may arise from the need of more sensors) was found to be negligible. So was the control spillover into the residual modes. Simulations of the beam with and without the residual modes indicated that spillover effects are infinitesimal. The reasons for this are:

    1) IMSC is used
    2) Modal filters are used
    3) Residual modes have very high frequencies

Conclusion

The IMSC method in conjunction with on-off modal controls does a good job in controlling the motion of the beam, where the motion consists primarily of the rigid-body modes.

ROBUST PRECISION POINTING CONTROL OF LARGE SPACE PLATFORM PAYLOADS

S. M. Joshi
Old Dominion University Research Foundation
Norfolk, Virginia

LSS CONTROLLER DESIGN STRATEGY

- INHERENT DAMPING PLAYS A VERY IMPORTANT ROLE IN STABILITY. THEREFORE IT IS HIGHLY DESIRABLE TO ENHANCE INHERENT DAMPING USING A SECONDARY CONTROLLER.

- DESIGN PRIMARY CONTROLLER FOR CONTROLLING RIGID-BODY MODES AND POSSIBLY SOME SELECTED STRUCTURAL MODES.

SECONDARY CONTROLLER - VELOCITY FEEDBACK

- FLEXIBLE PART OF DYNAMICS:

$$\underset{n_q \times 1}{\ddot{q}} + D\dot{q} + \Lambda q = \underset{n_q \times n_f}{\Phi^T} f$$

$$D = D^T \geq 0 \quad , \quad \Lambda = \mathrm{diag}(\omega_1^2, \omega_2^2, \cdots, \omega_{n_q}^2)$$

- SENSOR OUTPUT:

$$y_r = \Phi \dot{q}$$

CONTROL LAW:

$$f = -K_r y_r = -K_r \Phi \dot{q}$$

- WITH PERFECT (LINEAR, INSTANTANEOUS) ACTUATORS/SENSORS:

  - STABLE IF $K_r \geq 0$

  - ASYMPTOTICALLY STABLE (AS) IF

$K_r > 0$ AND (Λ, Φ^T) CONTROLLABLE

- WHAT IS THE EFFECT OF

  NONLINEARITIES

  ACTUATOR/SENSOR DYNAMICS

EFFECT OF SENSOR/ACTUATOR NONLINEARITIES:

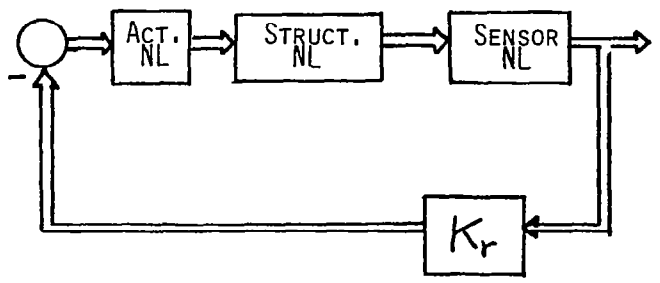

ACTUATOR NONLINEARITIES: LET $\psi_a(0) = 0$ [$\psi_a(a)$ = ACTUATOR]

a) ORIGIN STABLE IF $\nu^T K_r^{-1} \psi_a(\nu) \geq 0$

b) ORIGIN ASIL* IF $\nu^T K_r^{-1} \psi_a(\nu) > 0$ for $\nu \neq 0$

AND (Λ, Φ^T) CONTROLLABLE

(FOR DIAGONAL K_r, $\nu_i \psi_{a_i}(\nu_i) > 0$)

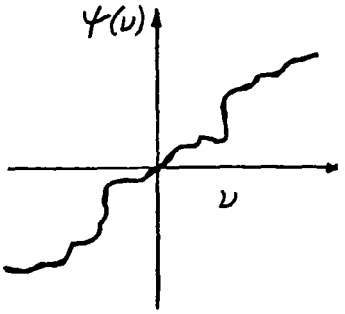

NONLINEARITIES IN ACTUATORS AND SENSORS:

LET K_r BE DIAGONAL

a) ORIGIN STABLE IF $\sigma \psi(\sigma) \geq 0$ FOR EACH ACTUATOR AND SENSOR

b) ORIGIN ASIL* IF $\sigma \psi(\sigma) > 0$ " "

AND (Λ, Φ^T) IS CONTROLLABLE

CONSIDER ACTUATOR/SENSOR DYNAMICS GIVEN BY

$$\mu \dot{x}_a = A_a x_a + B_a u_a$$

WHERE $\mu > 0$, SMALL; A_A STRICTLY HURWITZ

- IF THE CLOSED-LOOP SYSTEM WITH <u>PERFECT</u> ACTUATORS/SENSORS IS AS, THEN THE TRAJECTORY WITH FINITE-BANDWIDTH ACTUATORS/SENSORS IS $O(\mu)$ CLOSE TO TRAJECTORY WITH PERFECT ACTUATORS/SENSORS (REF. 1).
  HOW TO DETERMINE μ THAT WILL GUARANTEE STABILITY?

*ASYMPTOTICALLY STABLE IN THE LARGE

- CONSIDER THE SINGLE-INPUT SINGLE-OUTPUT CASE (SISO)

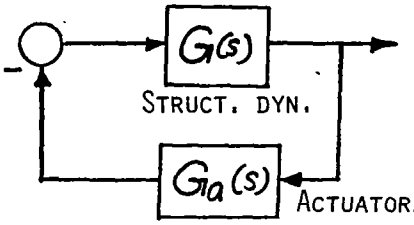

ASSUME SIMPLE STRUCTURAL MODE FREQUENCIES, NO DAMPING, AND NO POLE-ZERO CANCELLATIONS (I.E. CONTROLLABILITY)

- THEOREM THE CLOSED-LOOP SYSTEM IS AS FOR SUFFICIENTLY SMALL $K_r > 0$ IF

$$-90^\circ < \phi_a(\omega) < 90^\circ$$

AT $\omega = \omega_i \quad (i = 1, 2, \cdots, n_q)$

WHERE $\phi_a(\omega) = \angle G_a(j\omega)$

- ALWAYS STABLE FOR 1ST ORDER $G_a(s)$
- WHEN ACTUATOR/SENSOR HAVE n_a REAL POLES AT $s = -\sigma_a$ AND NO ZEROS. THE SYSTEM IS AS FOR SMALL $K_r > 0$ IF

$$\sigma_a > \frac{\omega_{MAX}}{\tan(\pi/2n_a)}$$

GIVES SOME INSIGHT INTO ACTUATOR/SENSOR BANDWIDTH REQUIREMENTS. ADDITIONAL INVESTIGATION NEEDED FOR OBTAINING MORE USEFUL RESULTS.

n_a	σ_a/ω_{MAX} (MIN. REQD.)
1	0
2	1
3	1.73
4	2.48
5	3.09
6	3.76
7	4.4
8	5.07

CONTROL OF PPS/LSS

- ATTITUDE AND VIBRATION CONTROL OF LSS
- POINTING CONTROL OF EACH PPS
- SINCE THE MASS OF EACH PPS MAY BE OF THE SAME ORDER AS THAT OF LSS, INSTABILITY IS POSSIBLE IF CONTROL SYSTEMS ARE DESIGNED INDEPENDENTLY.

SECONDARY CONTROLLER USING ANNULAR MOMENTUM CONTROL DEVICES (AMCD'S)

ASSUMPTIONS

- AMCD RIMS ARE RIGID
  - RIM DIA $\simeq$ 2 M (SMALL COMPARED TO LSS)
- ACTUATORS AND SENSORS PERFECT
  - ELECTROMAGNETIC ACTUATORS AND POSITION SENSORS ARE ALMOST PERFECTLY LINEAR IN THE OPERATING RANGE. BANDWIDTH IS SEVERAL HUNDRED Hz.
- ACTUATORS/SENSORS COLLOCATED
  - INHERENT DESIGN CHARACTERISTIC OF AMCD
- CONTROL LAW:

$$f = K_p \delta + K_r \dot{\delta}$$

WHERE δ IS THE ACTUATOR CENTERING ERROR VECTOR

- STABLE IF $K_p > 0$, $K_r \geq 0$

ASYMPTOTICALLY STABLE (AS) IF

a) $K_p > 0$, $K_r > 0$

b) LSS STRUCTURAL MODEL STABILIZABLE

c) NO UNDAMPED LSS MODES AT $2j\Omega_i$ (Ω_i = SPIN FREQ.)

d) $\sum_{1}^{\nu} H_i \neq 0$

PRIMARY ATTITUDE CONTROLLER (PAC)

- USING TORQUE ACTUATORS
  - COLLOCATED ACTUATORS/SENSORS
  - NONCOLLOCATED ACTUATORS/SENSORS
- USING AMCD'S

PAC USING TORQUE ACTUATORS

- SEVERAL TORQUE ACTUATORS AT VARIOUS POINTS OF LSS
  - COLLOCATED ACTUATORS/SENSORS:
  - EQUATIONS OF MOTION:

$$A_s \ddot{x}_s + B_s \dot{x}_s + C_s x_s = \Gamma T$$

$$x_s = (\phi_s, \theta_s, q^T)^T$$

- COLLOCATED ACTUATORS/SENSORS

  MEASUREMENTS CONSIST OF:
  - ATTITUDE VECTOR: $\alpha = \Gamma^T x_s$
  - ATTITUDE RATE VECTOR: $\dot{\alpha} = \Gamma^T \dot{x}_s$

  CONTROL LAW: $T = -(G_p \alpha + G_r \dot{\alpha})$

- STABLE IF $G_p > 0$, $G_r \geq 0$
  - AS IF $G_p > 0$, $G_r > 0$, (C_s, Γ^T) CONTROLLABLE

- CONTROL LAW MINIMIZES

$$J = \int_0^\infty (x_s^T, \dot{x}_s^T, T^T) \begin{bmatrix} Q_1 & 0 & S \\ 0 & Q_2 & 0 \\ S^T & 0 & R \end{bmatrix} \begin{pmatrix} x_s \\ \dot{x}_s \\ T \end{pmatrix} dt$$

- EFFECT OF ACTUATOR/SENSOR DYNAMICS

  SISO CASE, NO REPEATED FREQS., CONTROLLABLE

  Let $\phi_a(\omega) = \angle G_a(j\omega)$, $\phi_a(0) = 0$

  $G_p = k g_p$, $G_r = k g_r$

  - AS FOR SMALL $k > 0$ IF

$$-\phi_{zi} < \phi_a(\omega_i) < 180^\circ - \phi_{zi}$$

  WHERE ϕ_{zi} IS A FUNCTION

  OF ω_i AND POSITION RATE GAINS

- ADDITIONAL INVESTIGATION IS NEEDED

- IF TORQUE ACTUATORS AND ATTITUDE/RATE SENSORS ARE NOT COLLOCATED
  - STABILITY NOT GUARANTEED
  - MUST USE LQG-BASED APPROACHES INVESTIGATED EARLIER
    - KNOWLEDGE OF FREQUENCIES AND MODE-SHAPES REQUIRED
    - ▲ TRUNCATION: "RESIDUAL" MODES IGNORED IN THE DESIGN PROCESS

▲ MODEL ERROR SENSITIVITY SUPPRESSION (REF. 2), "SPILLOVER" IS INCLUDED IN THE QUADRATIC PERFORMANCE FUNCTION:

$$\dot{x}_c = A_c x_c + B_c u$$

$$\dot{x}_r = A_r x_r + B_r u$$

$$J = \int_0^\infty \left\{ x_c^T Q x_c + u^T R u + (B_r u)^T Q_r (B_r u) \right\} dt$$

- IT CAN BE SHOWN THAT THE SAME AMCD'S CAN BE USED FOR PRIMARY CONTROL
- ATTITUDE AND RATE SENSORS LOCATED ON LSS AT MIDPOINTS OF AMCD ACTUATORS
- APPROXIMATES TORQUE ACTUATORS AND COLLOCATED SENSORS— PROVEN TO BE STABLE
- CLOSED-LOOP RIGID-BODY BANDWIDTH DEPENDS ON TOTAL MOMENTUM, ALLOWABLE GAPS, ETC.

PRELIMINARY MATH MODEL OF LSS/MPPS

- ASSUME LUMPED POINT-MASSES AT POINTS OF ATTACHMENT OF PPS'S (FOR LSS MODEL)
- ALL PPS RIGID
- EACH PPS CONSISTS OF GIMBALS AND TORQUERS (ONLY X-AXIS GIMBAL ASSUMED IN PRELIMINARY STUDY).

- MATH MODEL GIVEN BY:

$$A\ddot{x} + B\dot{x} + Cx = \Gamma f$$

$$x = (\phi_s, \theta_s, \phi_1, \phi_2, \cdots, \phi_p, q^T)^T \quad q: n_q \times 1$$

$$A = \begin{bmatrix} A_{11} & 0 \\ 0 & I_{n_q} \end{bmatrix} \quad B = \begin{bmatrix} 0 & 0 \\ 0 & D \end{bmatrix} \quad C = \begin{bmatrix} 0 & 0 \\ 0 & \Lambda \end{bmatrix}$$

$$\Lambda = \text{diag}(\omega_1^2, \omega_2^2, \cdots, \omega_{n_q}^2)$$

$$f = (T_1^T, T_2^T, \cdots, T_m^T, T_{g1}, T_{g2}, \cdots, T_{gp})^T$$

$$T_i = (T_{xi}, T_{yi})^T$$

OBSERVATIONS

- INERTIAL ATTITUDE AND RATE SENSORS ON EACH PPS PAYLOAD
- m INERTIAL ATTITUDE AND RATE SENSORS ON LSS (COLLOCATED WITH LSS TORQUE ACTUATORS)
- SENSORS FOR MEASURING RELATIVE ANGLE BETWEEN EACH GIMBAL AND LSS

CONTROL OF MULTIPLE PRECISION - POINTED STRUCTURES (MPPS) MOUNTED ON LSS

- MPPS USED FOR COMMUNICATIONS, ASTRONOMY, EARTH RESOURCES, AND WEATHER PAYLOADS

- ADVANTAGES:
  - LESS ORBITAL SLOT SPACE AT GEO
  - SAVINGS IN POWER, CYROGENICS, GROUND DATA LINKS, AND SMALLER GROUND TERMINALS

CONTROL LAWS

- CONTROL LAW I: DECENTRALIZED CONTROL OF LSS/PPS:
  - USE LSS ATTITUDE AND RATE SIGNALS AND DESIGN LSS CONTROL LAW (COLLOCATED ACTUATORS/SENSORS)
  - USE PPS ATTITUDE AND RATE SIGNALS AND DESIGN CONTROL LAW (TO GENERATE DESIRED GIMBAL TORQUER TORQUES)
  - THE RESULTING CLOSED-LOOP SYSTEM CAN BE <u>UNSTABLE</u>
- CONTROL LAW II: ROBUST COMPOSITE CONTROL
  - USE INERTIAL PPS AND LSS SENSORS, AND ALSO GIMBAL-ANGLE SENSORS AND COMBINE THE SIGNALS TO OBTAIN

$$y = \Gamma^T x$$

  - CONTROL LAW:

$$f = -K_p y - K_r \dot{y}$$

  - CLOSED-LOOP SYSTEM LYAPUNOV-STABLE if $K_p > 0, K_r \geq 0$
  - ASYMPTOTICALLY STABLE (AS) IF $K_p, K_r > 0$, AND LSS STRUCTURAL MODEL STABILIZABLE, <u>REGARDLESS</u> OF NUMBER OF MODES AND NUMBER OF PPS. THEREFORE, CONTROLLER IS ROBUST.

NUMERICAL RESULTS

- 100' x 100' x 0.1" COMPLETELY FREE ALUMINUM PLATE
- TWO PPS EACH WITH MASS = LSS MASS
- THREE LSS TORQUE ACTUATORS WITH COLLOCATED ATTITUDE AND RATE SENSORS
- CONTROL LAW I: DECENTRALIZED CONTROL
  - LSS BW ≈ 0.05 rad/sec
  - PPS BW INCREASED GRADUALLY - A STRUCTURAL MODE WAS DRIVEN UNSTABLE FOR PPS BW > 0.1 rad/sec
- CONTROL LAW II: COMPOSITE CONTROL
  - LSS BW ≈ 0.05 rad/sec
  - PPS BW OF 1 rad/sec ($\rho = 0.7$) WAS EASILY OBTAINED WITHOUT SIGNIFICANT EFFECT ON CLOSED-LOOP LSS STRUCTURAL MODES

CONCLUDING REMARKS

- TWO-LEVEL LSS CONTROL IS STABLE AND ROBUST AND OFFERS PROMISE
- FURTHER INVESTIGATION NEEDED ON EFFECTS OF ACTUATOR/SENSOR BANDWIDTH
- COMPOSITE LSS/MPPS CONTROLLER IS STABLE AND ROBUST

PLANS FOR CONTINUED RESEARCH

- COMPLETE INVESTIGATION OF LSS/MPPS COMPOSITE CONTROL, INCLUDING PERFORMANCE EVALUATION
- INVESTIGATE ANNULAR SUSPENSION AND POINTING SYSTEM (ASPS) FOR PPS CONTROL ACTUATION
- START INVESTIGATION OF HOOP-COLUMN ANTENNA CONTROL

REFERENCES

1. Chow, J. H.; and Kotovic, P. V.: A Decomposition of Near Optimum Regulators for Systems With Slow and Fast Modes. IEEE Transactions on Automatic Control, vol. 21, no. 5, 1976, pp. 701-705.
2. Sesak, J. R.; Likens, P. W.; and Coradetti, T.: Flexible Spacecraft Control by Model Error Sensitivity Suppression (MESS). J. Astronaut. Sci., vol. 27, no. 2, pp. 131-156.

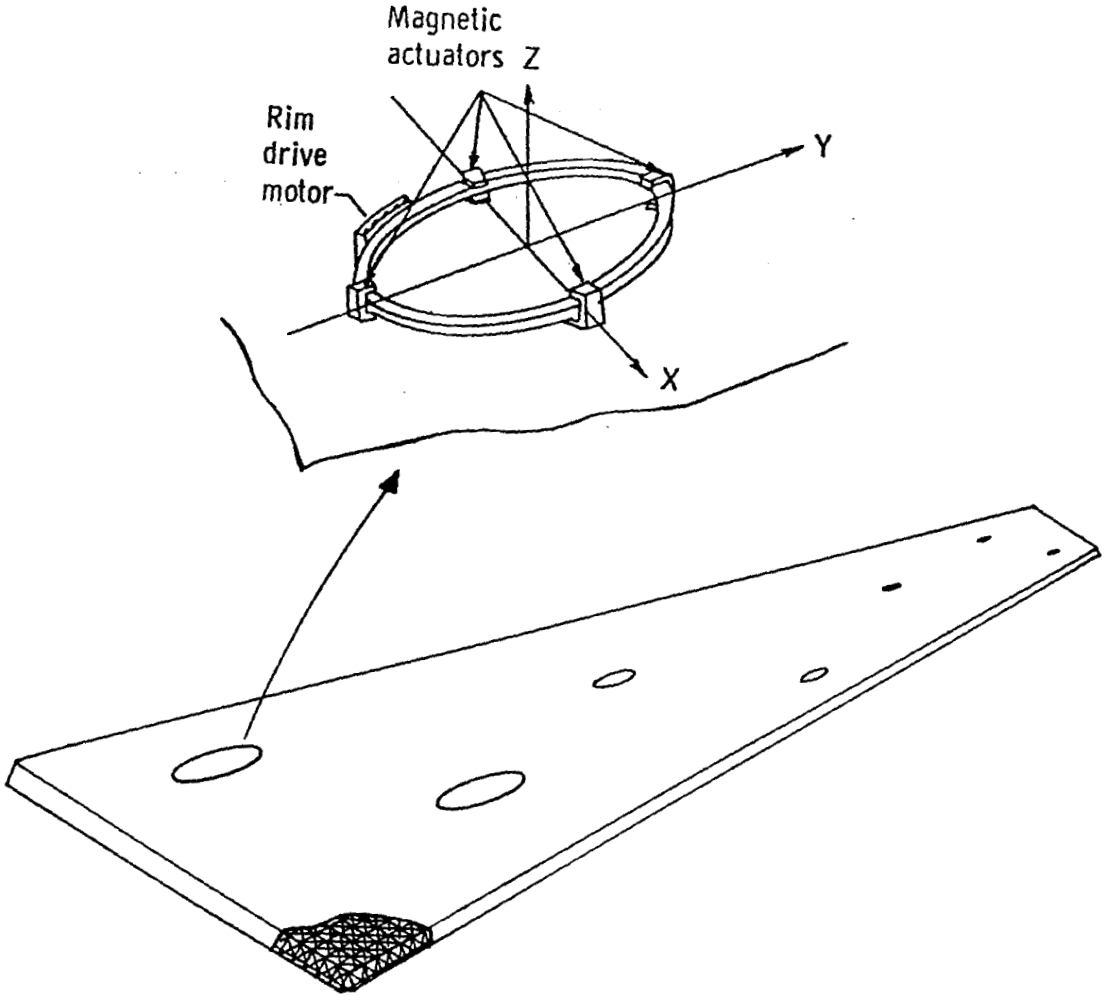

AMCD/ LSS CONFIGURATION

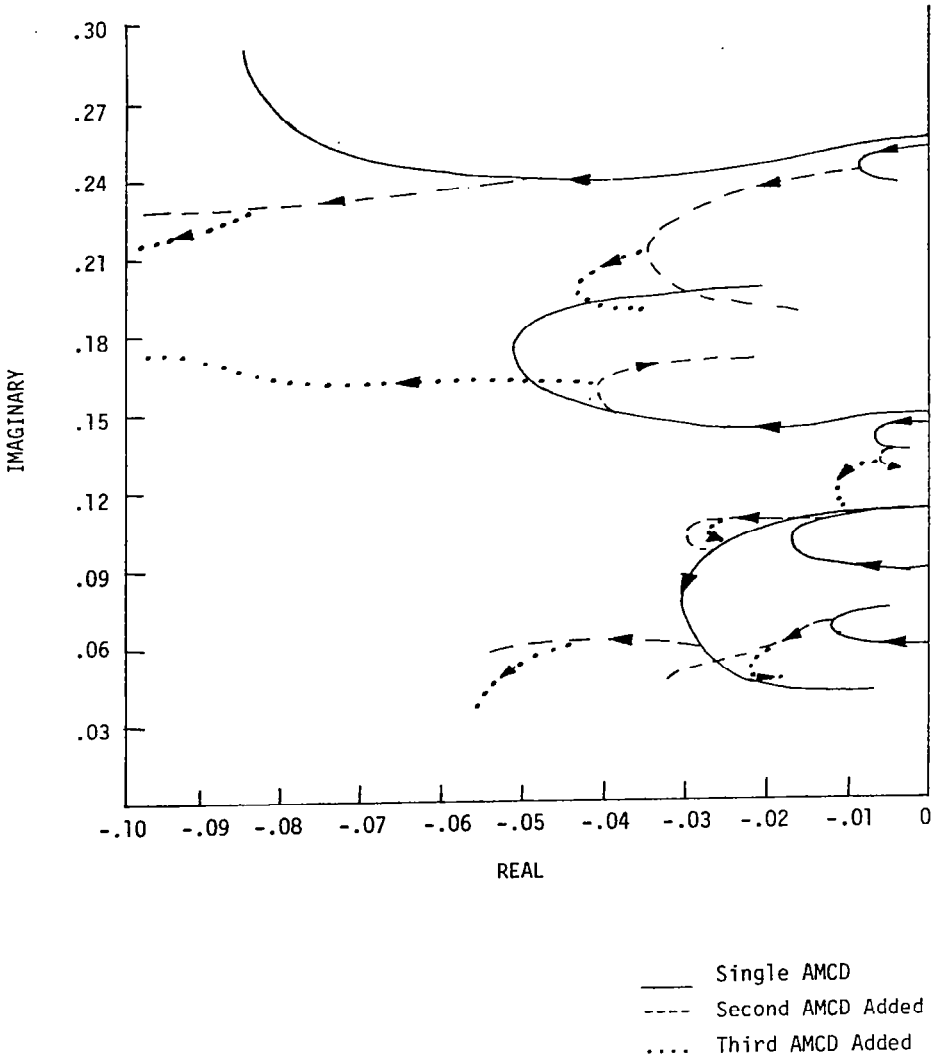

SECONDARY CONTROLLER ROOT LOCI

NONLINEAR EFFECT ON MODAL DATA ANALYSIS METHOD

Lucas G. Horta
NASA Langley Research Center
Hampton, Virginia

NONLINEAR EFFECT ON MODAL DATA ANALYSIS METHODS

OBJECTIVES:

1 - DETERMINE HOW THE PRESENCE OF NONLINEARITIES IN STRUCTURAL TEST DATA CAN BE DETECTED WHEN USING MODERN LINEAR MODAL DATA ANALYSIS METHODS.

2 - EVALUATE THE EXTENT TO WHICH LINEAR ALGORITHMS CAN PROVIDE USEFUL INFORMATION ON NONLINEAR SYSTEMS.

APPROACH:

1 - GENERATE SIMULATED TEST DATA BY A NONLINEAR ANALYTICAL MODEL.

2 - USE LINEAR METHODS (IBRAHIM TIME DOMAIN ALGORITHM (ITD) AND FREQUENCY-DOMAIN TRANSFER FUNCTION TECHNIQUES) TO ANALYZE SETS OF THIS DATA WITH CONTROLLED PARAMETRIC VARIATION.

SINGLE DEGREE OF FREEDOM MODEL

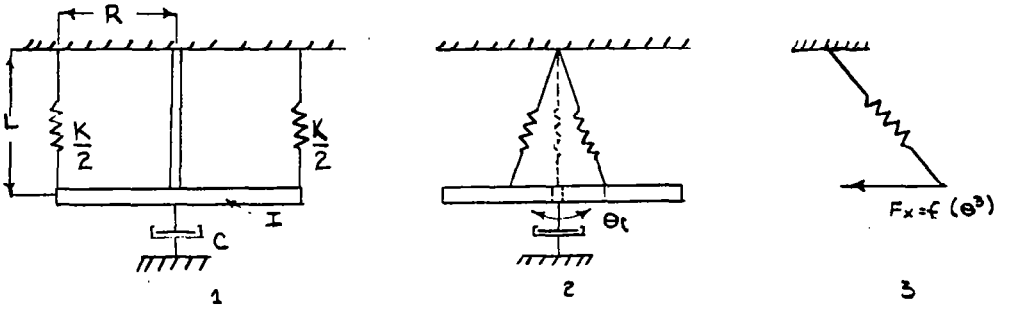

SYSTEM DIFFERENTIAL EQUATION FOR SMALL DISPLACEMENT

$$\frac{d^2\theta}{dt^2} = -\frac{1}{2}\frac{KR^4\theta^3}{L^2I} - \frac{JG}{LI}\theta - \frac{c}{I}\frac{d\theta}{dt}$$

GENERAL FORM

$$\ddot{\theta} = C_1\theta^3 + C_2\theta + C_3\dot{\theta}$$

LINEAR NATURAL FREQUENCY = 0.288 HZ

LINEAR MODAL DAMPING = 0.01

SINGLE DEGREE OF FREEDOM RESPONSE

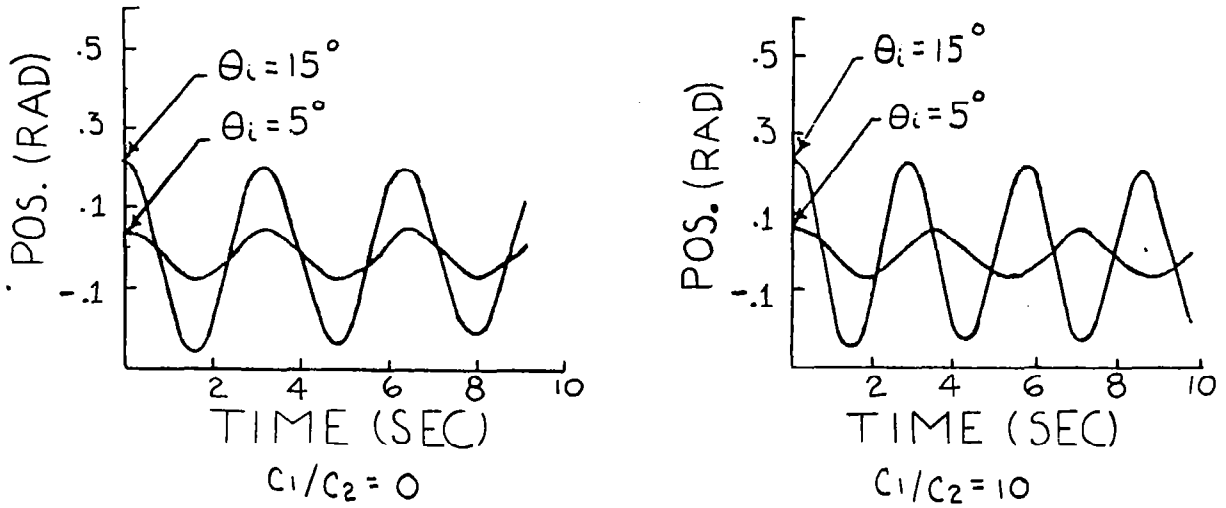

THE IBRAHIM-TIME-DOMAIN (ITD) MODAL DATA ANALYSIS METHOD

- AN OFF-LINE LARGE-SCALE DATA ANALYSIS METHOD DEVELOPED FOR STRUCTURAL DYNAMICS TESTS.
- OPERATES ON FREE-DECAY RESPONSES SOLVING MANY DATA CHANNELS SIMULTANEOUSLY.
- HAS PROVEN MORE SUCCESSFUL THAN OTHER LABORATORY METHODS FOR HANDLING NOISE, LARGE SYSTEMS, AND CLOSELY SPACED MODES.

SINGLE DEGREE OF FREEDOM RESULTS

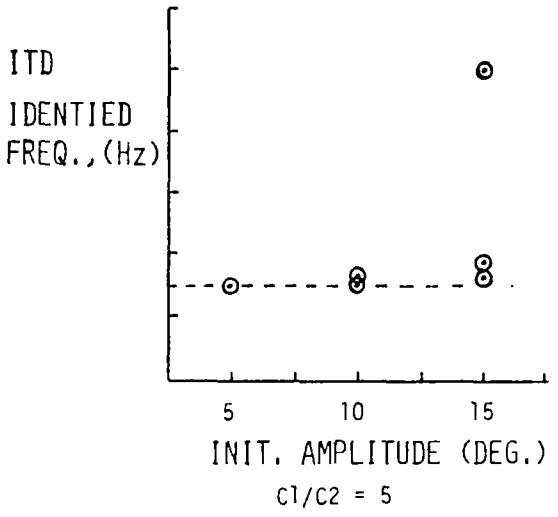

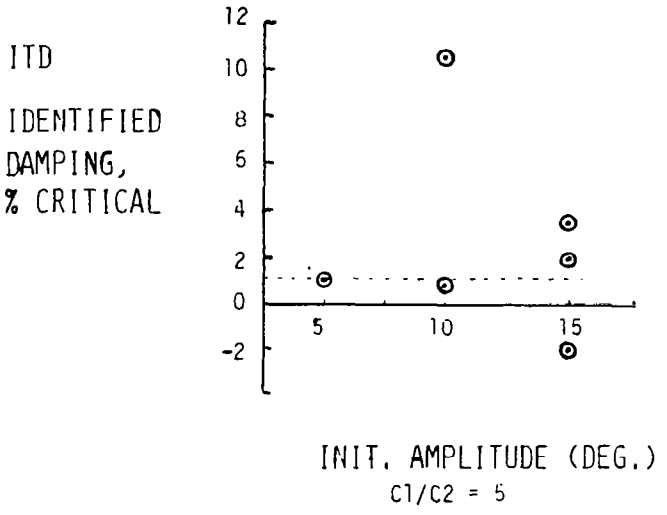

SINGLE DEGREE OF FREEDOM RESULTS COMPARISON

	F_1 (HZ)	F_2 (HZ)	F_3 (HZ)
ANALYTICAL	0.3042	0.9127	1.52
ITD	0.3030	0.8970	1.562
% DIFFERENCE	0.39	1.72	2.76

$C_1/C_2 = 5 \quad IC = 10^{\circ}$

TWO DEGREE OF FREEDOM ANALYTICAL MODEL

SYSTEM

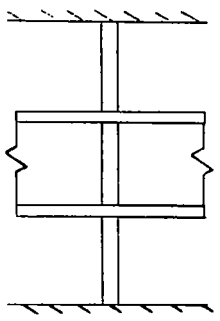

EQUATION OF MOTION

$$\begin{bmatrix} I_1 & 0 \\ 0 & I_2 \end{bmatrix}\begin{Bmatrix} \ddot{\theta}_1 \\ \ddot{\theta}_2 \end{Bmatrix} + \begin{bmatrix} C_{11} & -C_{12} \\ -C_{21} & C_{22} \end{bmatrix}\begin{Bmatrix} \dot{\theta}_1 \\ \dot{\theta}_2 \end{Bmatrix} + \begin{bmatrix} K_{11} & -K_{12} \\ -K_{21} & K_{22} \end{bmatrix}\begin{Bmatrix} \theta_1 \\ \theta_2 \end{Bmatrix}$$

$$+ \begin{bmatrix} \varepsilon & 0 \\ 0 & -\varepsilon \end{bmatrix}\begin{Bmatrix} (\theta_1-\theta_2)^3 \\ (\theta_1-\theta_2)^3 \end{Bmatrix} = \begin{Bmatrix} 0 \\ 0 \end{Bmatrix}$$

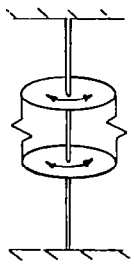

LINEAR Mode
$F_1 = .100$ HZ

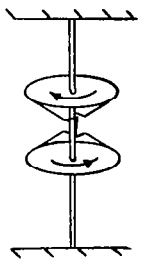

NON LINEAR Mode
$F_2 = .199$ HZ

TWO DEGREE OF FREEDOM RESULTS

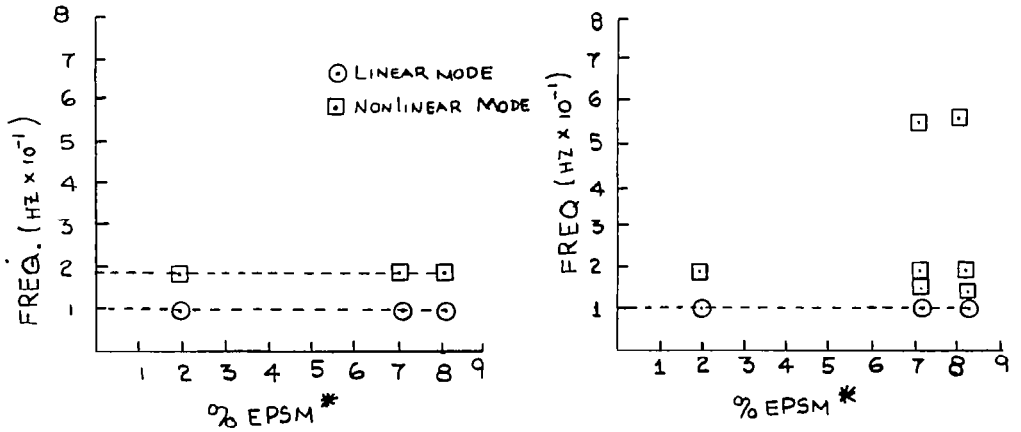

ASSUMED DOF = 6

ASSUMED DOF = 10

* EPSM = ENERGY PROVIDED TO SECOND MODE

SUMMARY

1 - THE ITD MODAL DATA ANALYSIS METHOD SUCCESSFULLY IDENTIFIED THE FREQUENCY COMPONENTS (BUT NOT DAMPING) OF THE TRUE SOLUTION OF A NONLINEAR SYSTEM FROM SIMULATED TEST DATA.

2 - THE APPROXIMATE MODAL PARAMETERS OF THE LINEAR SYSTEM CAN BE IDENTIFIED BY THE ITD METHOD WHEN LOW LEVELS OF NONLINEARITIES ARE PRESENT.

3 - THE ITD METHOD SUCCESSFULLY IDENTIFIED THE MODAL PARAMETERS OF A LINEAR MODE IN THE PRESENCE OF A NONLINEAR RESPONSE.

FUTURE RESEARCH THRUST

1 - EXPERIMENTAL EVALUATION OF ITD METHOD ON A TWO-DEGREE-OF-FREEDOM NONLINEAR LABORATORY MODEL.

2 - APPLICATION OF FREQUENCY-DOMAIN TRANSFER-FUNCTION TECHNIQUES TO THE SAME ANALYTICAL AND EXPERIMENTAL DATA.

STRUCTURAL DESIGN FOR DYNAMIC RESPONSE REDUCTION

Brantley R. Hanks
NASA Langley Research Center
Hampton, Virginia

OBJECTIVE: STUDY STIFFNESS AUGMENTATION BY MATHEMATICAL DESIGN

APPROACH: APPLY LINEAR REGULATOR THEORY WITH PROPORTIONAL FEEDBACK

JUSTIFICATION: STIFFNESS IS READILY AVAILABLE TO DESIGNER AS PREDICTABLE PASSIVE CONTROL

TIME-INVARIANT LINEAR REGULATOR---GENERAL

SYSTEM:

$$\dot{x} = Ax + Bu + Dw$$

CONTROLLED VARIABLES:

$$y = Cx$$

OBJECTIVE:

$$\min_u J \quad \text{where} \quad J = x_f^T S_f x_f + \int_o^{t_f} \left[y^T Q y + u^T R u \right] dt$$

OPTIMAL CONTROL (ASSUMING w IS RANDOM):

$$u = -R^{-1} B^T P x$$

WHERE P IS SOLUTION TO

$$\dot{P} = -PA - A^T P + PBR^{-1} B^T P - C^T Q C \qquad P(t_f) = S_f$$

IF $t_f \rightarrow \infty$, GET <u>STEADY-STATE</u> P (AND U) FROM

$$0 = -PA - A^T P + PBR^{-1} B^T P - C^T Q C$$

POSITIVE DEFINITE P EXISTS IF

- A IS DETECTABLE IN C, STABILIZABLE IN B
- RESPONSE WEIGHTING MATRIX, Q, IS POSITIVE SEMIDEFINITE
- CONTROL WEIGHTING MATRIX, R, IS POSITIVE DEFINITE

LINEAR REGULATOR ADAPTED TO STRUCTURES

SYSTEM:

$$\begin{Bmatrix} \dot{x} \\ \ddot{x} \end{Bmatrix} = \begin{bmatrix} o & I \\ -M^{-1}K & -M^{-1}G \end{bmatrix} \begin{Bmatrix} x \\ \dot{x} \end{Bmatrix} + \begin{Bmatrix} o \\ M^{-1}B \end{Bmatrix} u + \begin{Bmatrix} o \\ M^{-1}D \end{Bmatrix} w \qquad w \sim N(0, \sigma^2)$$

OBJECTIVE FUNCTION:

$$J = \int_o^{t_f} \left[\begin{pmatrix} x^T & \dot{x}^T \end{pmatrix} \begin{bmatrix} K & 0 \\ 0 & M \end{bmatrix} \begin{Bmatrix} x \\ \dot{x} \end{Bmatrix} + (u^T)[R](u) \right] dt$$

ASSUME:

- RANDOM INITIAL CONDITIONS
- COMPLETE STATE FEEDBACK WITH NO ROTATIONAL COUPLING
- $t_f \longrightarrow \infty$ (TIME-INVARIANT STRUCTURAL CHANGE)

CONTROL:

$$\begin{Bmatrix} 0 \\ M^{-1}B \end{Bmatrix} u = \begin{bmatrix} 0 & 0 \\ -M^{-1}BR^{-1}B^T M^{-1} T_{P_{21}} & -M^{-1}BR^{-1}B^T M^{-1} T_{P_{22}} \end{bmatrix} \begin{Bmatrix} x \\ \dot{x} \end{Bmatrix}$$

WHERE P_{21} AND P_{22} ARE SOLUTIONS TO

$$P_{21}^T A_{21} + A_{21}^T P_{21}^T - P_{21}^T M^{-1} BR^{-1}B^T(M^{-1})^T P_{21} + C_1^T Q_1 C_1 = 0 \qquad (1)$$

AND

$$P_{22}A_{22} + A_{22}^T P_{22} - P_{22}M^{-1}BR^{-1} B^T(M^{-1})^T P_{22} + (P_{21} + P_{21}^T + C_2 Q_2 C_2) = 0 \qquad (2)$$

IN THESE EQUATIONS $A_{21} = M^{-1} K$ AND $A_{22} = M^{-1} G$

NOTE THAT (1) IS NOT SYMMETRIC; ALSO THAT (1) IS INDEPENDENT OF (2).

Q WEIGHTING MATRIX CONSIDERATIONS

$$\min_{u} J \quad \text{where} \quad J = \int_0^\infty \left[y^T Q y + u^T R u \right] dt$$

$$y^T Q y = \begin{pmatrix} x^T & \dot{x}^T \end{pmatrix} \begin{bmatrix} C_{11}^T & C_{21}^T \\ C_{12}^T & C_{22} \end{bmatrix} \begin{bmatrix} Q_{11} & Q_{12} \\ Q_{21} & Q_{22} \end{bmatrix} \begin{bmatrix} C_{11} & C_{12} \\ C_{21} & C_{22} \end{bmatrix} \begin{Bmatrix} x \\ \dot{x} \end{Bmatrix}$$

- If rate and displacement considered independently and Q chosen so as not to couple x and $\dot{x}$

$$y^T Q y = \begin{pmatrix} x^T & \dot{x}^T \end{pmatrix} \begin{bmatrix} C_{11}^T Q_{11} C_{11} & 0 \\ 0 & C_{22}^T Q_{22} C_{22} \end{bmatrix} \begin{Bmatrix} x \\ \dot{x} \end{Bmatrix}$$

- <u>For design</u>, selection of C is governed by desired minimum response points. Hence, C and Q <u>may</u> be assigned similar functions.
- Diagonal C and Q minimizes weighted square response at selected coordinates.
- Choice of $Q_n = K$ and $Q_{22} = M$ minimizes sum of strain and kinetic energy at locations determined and (optionally) weighted by C.

REGULATOR FOR STRUCTURES--MODAL COORDINATES

TRANSFORMATION $x = \phi q$ WHERE $q = q_k e^{(\sigma_i + j\omega_i)t}$

WHERE ϕ IS NORMALIZED $\phi^T M \phi = I$

AND σ_i IS ASSUMED PROPORTIONAL TO ω_i $\left(\text{I.E., } \sigma_i = -2\xi_i\omega_i \text{ OR } \phi^T G \phi = \left[-2\xi_i\omega_i\right]\right)$

OBJECTIVE FUNCTION BECOMES

$$J = \int_0^{t_f} \left[\left(q^T \dot{q}^T\right) \begin{bmatrix} \phi^T K \phi & 0 \\ 0 & \phi^T M \phi \end{bmatrix} \begin{Bmatrix} q \\ \dot{q} \end{Bmatrix} + \left(u^T R u\right) \right] dt$$

NOTE THAT

$$\phi^T K \phi = \left[\omega_i^2\right] = \left[\Omega^2\right]$$

HENCE, WEIGHTING MATRIX $Q = \begin{bmatrix} \Omega^2 & 0 \\ 0 & I \end{bmatrix}$

RICCATI EQUATIONS BECOME

$$P_{21}^T \Omega^2 + \Omega^2 P_{21} + P_{21}^T B R^{-1} B^T P_{21} - C_1^T \Omega^2 C_1 = 0 \qquad (3)$$

AND

$$P_{22}\left[2\xi\Omega\right] + \left[2\xi\Omega\right] P_{22} + P_{22} B R^{-1} B^T P_{22} - \left(P_{21} + P_{21}^T + C_2^T C_2\right) = 0 \qquad (4)$$

WHERE P, B, R, AND C ARE MODAL EQUIVALENTS OF P, B, R, AND C.

BY CHOOSING P, B, R, AND C DIAGONAL, WE DECOUPLE THE SOLUTION AND GET PURE "MODAL CONTROL."

CANTILEVER BEAM MODEL

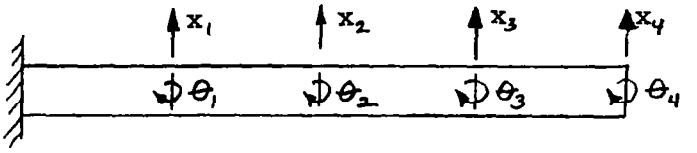

ASSUMED:

- CONSISTENT MASS FINITE ELEMENTS
- UNIFORM INITIAL STIFFNESS & MASS DISTRIBUTION
- FIRST NATURAL FREQUENCY = .047 Hz (.297 RAD/SEC)

PHYSICAL IMPLEMENTATION OF STIFFNESS CONTROL

X_3, θ_4 COUPLING

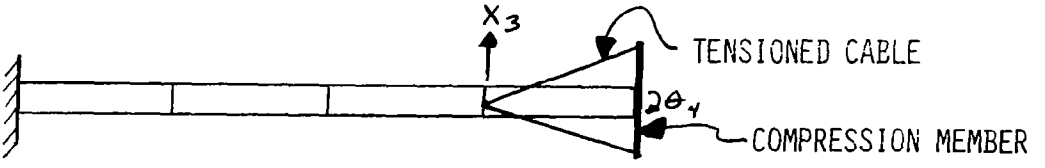

θ_1, θ_3 COUPLING

PRACTICAL OPTIMUM?

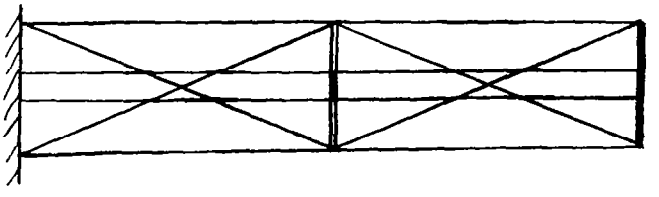

CONTROL WEIGHTING EFFECTS ON DESIGN

UNDAMPED NATURAL FREQUENCIES

MODE	INITIAL FREQ., $\frac{RAD}{SEC}$	FINAL FREQUENCY, $RAD/_{SEC}$			
		R = 10I	R = I	R = .1 I	R = .01 I
1	.297	.359	.557	.972	1.725
2	1.867	1.880	1.989	2.619	4.538
3	5.262	5.267	5.309	5.684	7.711
4	10.382	10.384	10.406	10.615	12.233

DAMPING RATIOS

MODE	INITIAL DAMPING % C/C_R	FINAL DAMPING, % C/C_{CR}			
		R = 10I	R = I	R = .1 I	R = .01 I
1	2	59.3	108	176	298
2	2	12.0	35.0	78.1	131
3	2	4.7	13.4	38.6	82.9
4	2	2.9	7.1	21.0	55.4

*NOTE: SOLUTIONS OBTAINED SEPARATELY FOR STIFFNESS AND DAMPING COMPARED EXACTLY TO FULL ORDER CONTROLLER SOLUTION

STIFFNESS MATRIX COMPARISON (ASSUMED CONSTANT MASS)

ORIGINAL K

X_1	θ_1	X_2	θ_2	X_3	θ_3	X_4	θ_4	
125	-1250	-125	-1250	0	0	0	0	X_1
	16667	1250	8333	0	0	0	0	θ_1
		250	0	-125	-1250	0	0	X_2
			33333	1250	8333	0	0	θ_2
				250	0	-125	-1250	X_3
	$\omega = .297$ rad/sec				33333	1250	8333	θ_3
						250	0	X_4
							33333	θ_4

FINAL K FOR R = .1 I

129.7	-1261	-127.8	-1241	-1.74	-3.83	-.166	-.71	X_1
	16719	1254	8278	6.41	12.85	.84	2.94	θ_1
		260.3	-5.22	-127	-1239	-1.58	-3.84	X_2
			33528	1236	8249	2.45	4.58	θ_2
				246.3	-2.06	-124.6	-1239	X_3
	$\omega = .972$ rad/sec				33540	1234	8252	θ_3
						268	-3.37	X_4
							33543	θ_4

R WEIGHTING EFFECT ON STIFFNESS MATRIX

(FIRST ROW ONLY SHOWN)

ORIG. K_{ij}	125	-1250	-125	-1250	0	0	0	0
R = 10 I	125.1	-1250	-125	-1250	-.008	-.009	-.002	-.005
R = I	125.7	-1252	-125.1	-1249	-.21	-.27	-.06	-.13
R = .1 I	129.7	-1261	-127.8	-1241	-1.74	-3.83	-17	-.71
R = .01 I	150.8	-1310	-150.3	-1220	-3.19	-24.0	-1.8	-2.9

RELATED SPONSORED RESEARCH

- KAMAN AEROSPACE CORPORATION - AUTOMATED MATH MODEL IMPROVED FOR MATCHING EXPERIMENTAL DATA.
- INSTITUTE FOR COMPUTER APPLICATIONS IN SCIENCE AND ENGINEERING - IDENTIFICATION OF EQUIVALENT PDE SYSTEMS TO MATCH MEASURED DATA.

SUMMARY

- COMPUTER PROGRAM FOR REDESIGNING STRUCTURAL MODES TO REDUCE RESPONSE HAS BEEN INITIATED.
- LINEAR REGULATOR APPROACH IN MODAL COORDINATES HAS BEEN IMPLEMENTED. TRANSFORMATION OF SOLUTION TO PHYSICAL STRUCTURE IS A MAJOR PROBLEM.
- SOLUTION OF STIFFNESS EQUATIONS AND DAMPING EQUATIONS CAN BE DONE SEPARATELY AS NXN SET OF (MATRIX RICCATI) EQUATIONS.

PLANNED EFFORT FOR '82

- INCLUDE MASS OF CONTROL
- STUDY WEIGHTING TO MINIMIZE OR SELECT CROSS-TERMS
- IMPLEMENT PHYSICAL COORDINATE SOLUTION
- STUDY POTENTIAL FOR "BENEFICIAL" CROSS TERMS

ALGORITHMS FOR ON-LINE

PARAMETER AND MODE SHAPE ESTIMATION

Frederick E. Thau
The City University of New York
New York, N.Y.

One of the schemes that has been proposed for the adaptive control of large flexible space structures is shown in figure 1. This approach is based upon a modal decomposition of the dynamic response of the flexible structure and is designed to make use of the parallel processing features of modern minicomputers. Satisfactory performance of the parallel structure identification technique shown in figure 1 can be achieved only when the approximation functions noted in the figure correspond to the natural modes of the flexible structure. The work summarized here presents a technique for estimating both mode shapes and modal parameters.

$$w(s,t) = \sum_{i=1}^{NM} q_i(t, p_i)\, \epsilon_i(s) + \sqrt{}(s,t)$$

(a) Motion of flexible structure.

$$q(k+1) = A_1 q(k) + A_2 q(k-1) + B_1 U(k) + B_2 U(k-1)$$

$$y(k) = H_q(k) + w(k)$$

(b) Modal description.

Figure 1.- Problem formulation.

Figure 2 shows the analytic background for the formulation of the on-line identification problem. The motion of the flexible structure is expressed as a sum of NM terms involving the modal shape function $\xi_i(s)$ and the modal amplitudes $q_i(t,p_i)$ where s denotes the spatial variable and t represents time. The parameter vector p_i represents a set of parameters $[A_{1i},A_{2i},\tilde{B}_{1i},\tilde{B}_{2i}]$ for each mode. The identification problem is formulated in terms of the modal description shown in figure 2(b), where the $A_i, i=1,2$ are diagonal matrices of order NM, U(k) denotes a vector of actuator signals and the B_i are rectangular matrices. Matrix H, relating the modal amplitudes to the measurement vector y(k), has columns that are linearly independent in the modal model. On-line measurements $\{y(k)\},\{U(k)\}$ are to be processed in order to obtain estimates of the matrices A_i, B_i, and H.

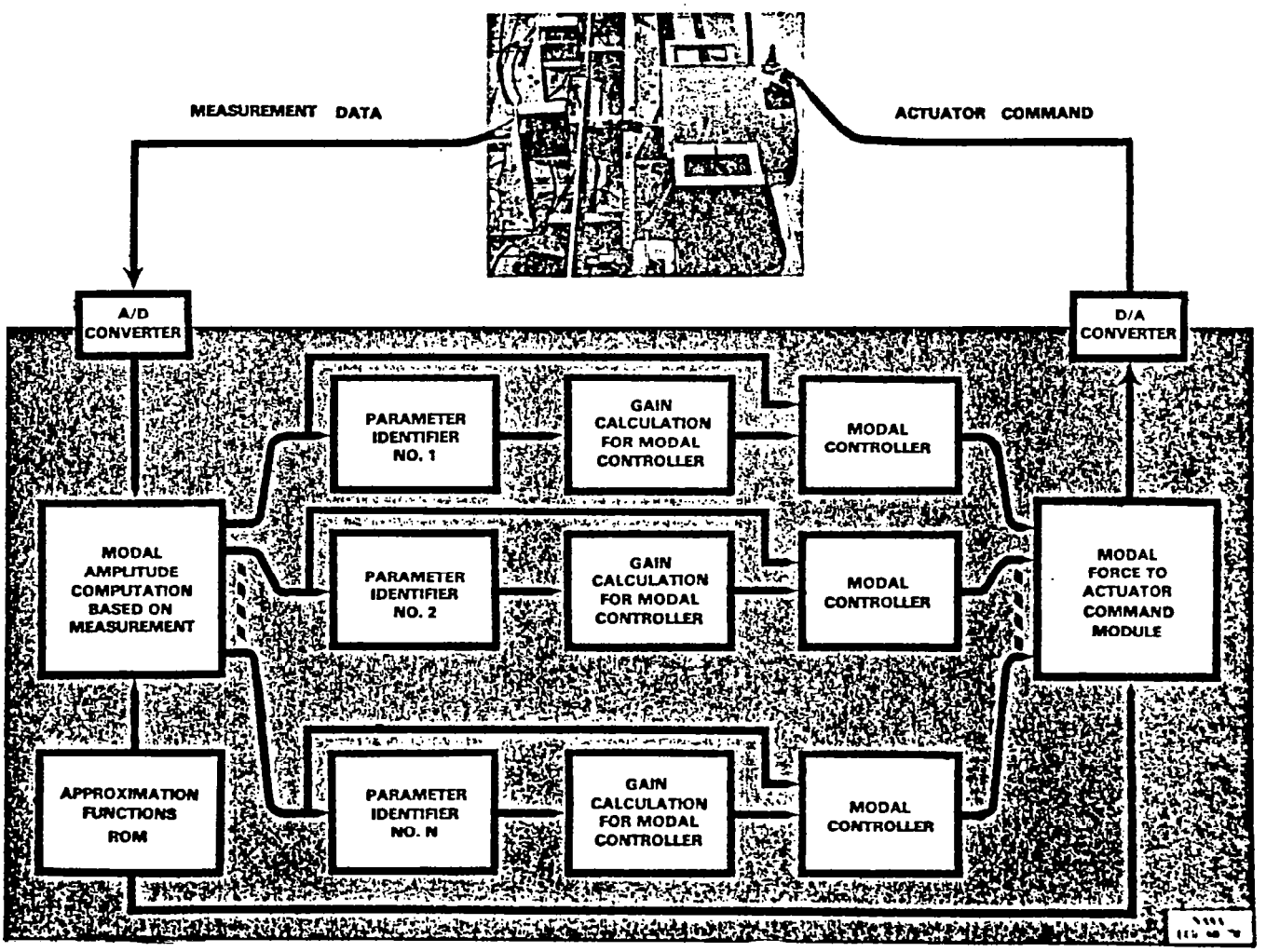

Figure 2.- Distributed adaptive control.

Algorithms for on-line parameter identification are shown in figure 3. Assuming that the approximation functions are given, the modal parameters are updated using an output error formulation where the error e_i is given by

$$e_i(k-1) = q_i(k-1) - A_{1i}q_i(k-2) - A_{2i}q_i(k-3) - \tilde{B}_{1i}F_i(k-2) - \tilde{B}_{2i}F_i(k-3)$$

where $F_i(k)$ denotes a modal force component. The weights W_i are selected to satisfy

$$W_1q_i^2(k-2) + W_2q_i^2(k-3) + W_3F_i^2(k-2) + W_4F_i^2(k-3) < 2$$

to insure stability of the identification algorithm.

The approach for updating the approximation functions is based on combining the modal equations shown in figure 2 into the single relation involving matrices M_i and N_i where

$$M_i = HA_iH^+ \qquad i = 1,2$$
$$N_i = HB_i$$

and $(H)^+$ denotes the pseudo-inverse of H. Using a regression analysis approach, data are collected over a time interval of length N and a least-squares estimate of M_i and N_i is obtained. When the number of modes in the modal approximation is the same as the number of sensors, the eigenvectors of M_i correspond to the columns of H.

$$p_i(k) = p_i(k-1) + e_i(k-1)\cdot\begin{bmatrix} W_1q_i(k-2) \\ W_2q_i(k-3) \\ W_3F_i(k-2) \\ W_4F_i(k-3) \end{bmatrix}$$

(a) Pole-zero characteristics - output error formulation.

$$y(k+1) = M_1y(k) + M_2y(k-1) + N_1U(k) + N_2U(k-1) + n(k+1)$$

$$N \updownarrow Y(N) = S(N)M^T + V(N);\quad M^T = \begin{bmatrix} M_1^T \\ M_2^T \\ N_1^T \\ N_2^T \end{bmatrix}$$

$$\hat{M}^T = S^+(N)Y(N)$$

(b) Approximation functions - regression analysis.

Figure 3.- On-line parameter identification.

A schematic diagram of the flexible beam used to test the identification algorithms is shown in figure 4. Sensor and actuator locations along the beam are shown along with the modal frequencies and mode shapes for the first three flexible modes obtained from the SPAR analysis program.

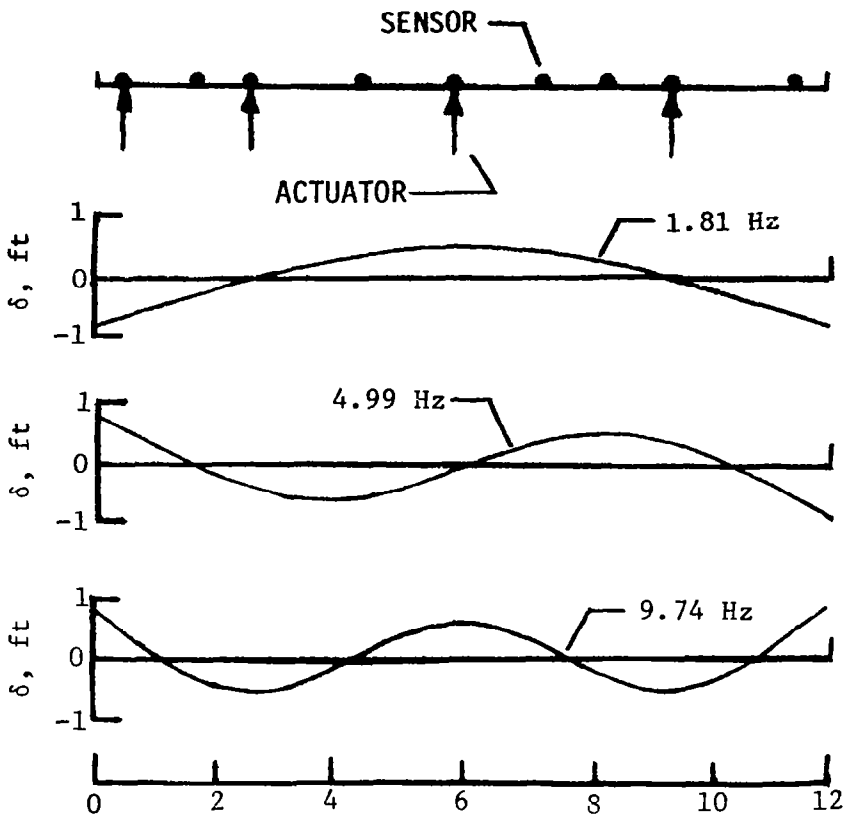

Figure 4.- Modes of interest.

Figure 5 shows the modal decomposition for mode 3 unforced response. A set of approximation functions obtained from the SPAR analysis was used and eight modes were assumed in the real-time program that produced the modal amplitude signals shown. For this response there is some excitation of modes 1 and 2. However, higher frequency modes do not appear to be excited.

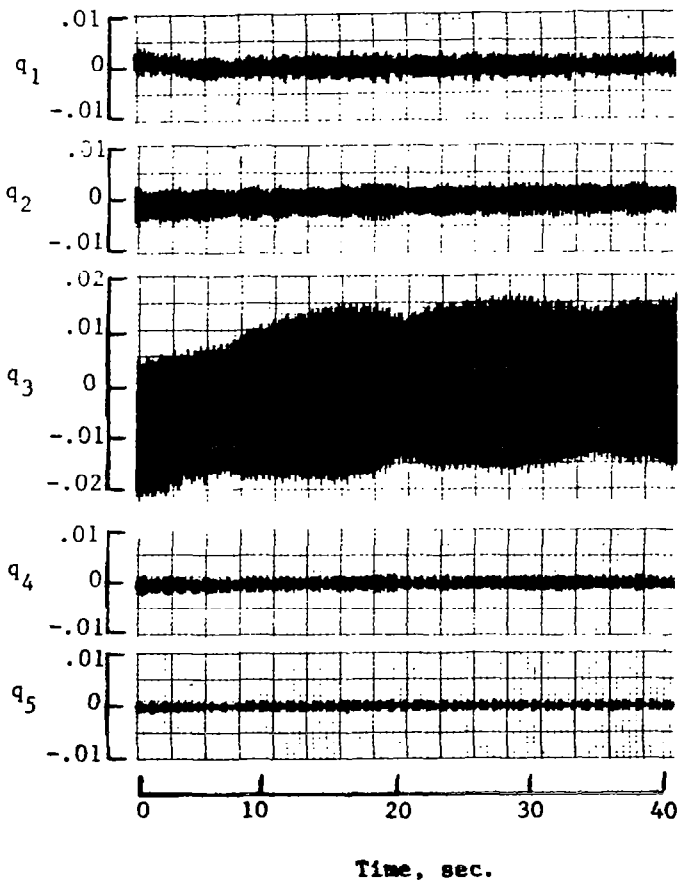

Figure 5.- Modal decomposition.

Eight SPAR modes; mode 3 excited.

Outputs of four on-line identifiers that result from self-sustained oscillation of the third vibration mode are shown in figure 6. Note that before the sustained oscillation occurs the identifiers are responding to measurement noise. Upon initiation of the sustained oscillation the parameters of the vibrating mode are rapidly identified. The parameters p_j^i correspond to the j^{th} diagonal element of the matrix A_i, $i = 1,2$, shown in figure 2. Also shown in the figure are the modal parameters derived from the structural analysis program.

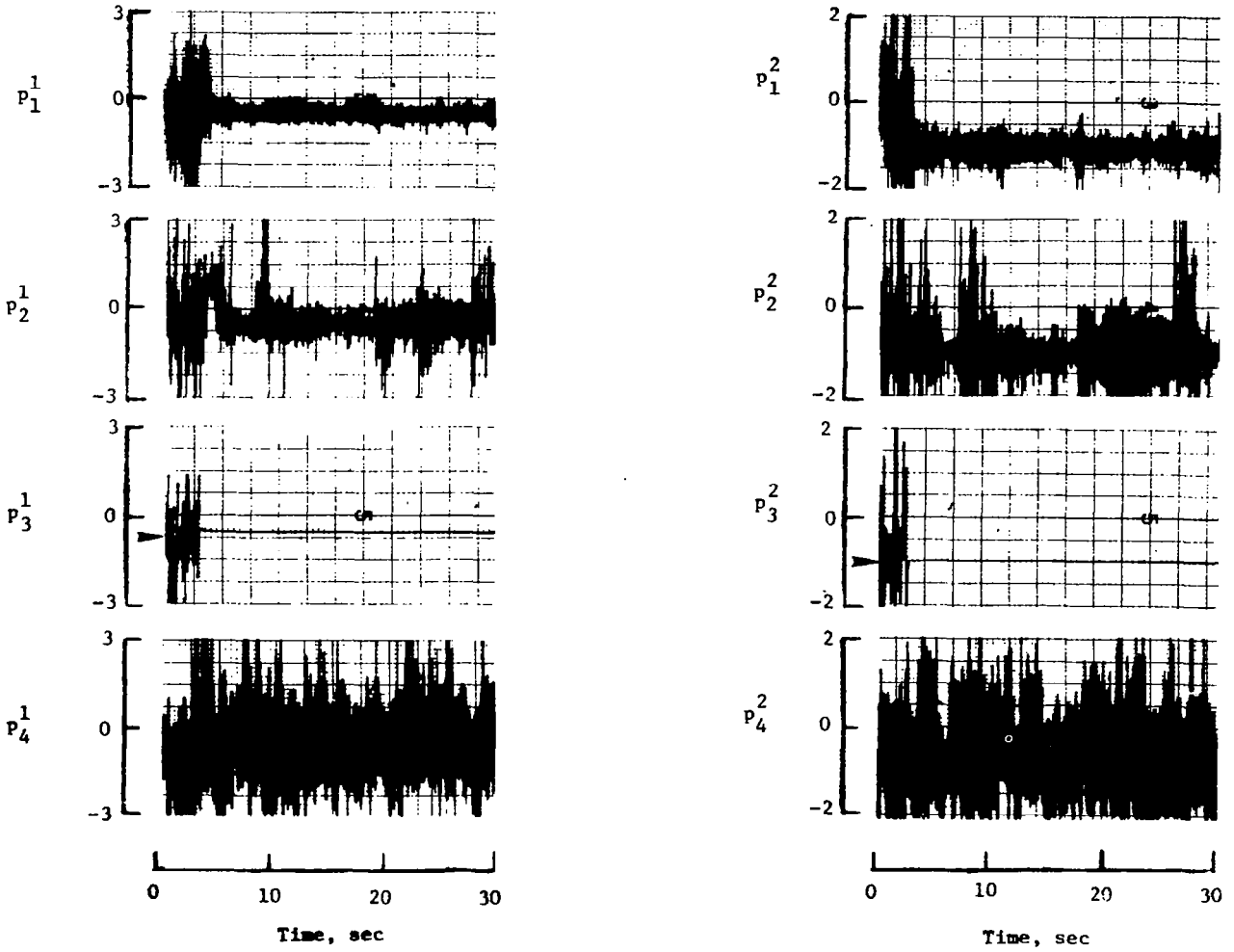

Figure 6.- Output of parameter identifiers. SPAR derived values; mode 3 excited.

Figure 7 shows the outputs of four on-line identifiers resulting from a 5-Hz excitation produced by actuator 1. Note that the parameters of the first vibration mode are identified but the high frequency modal parameters are not found as a result of the 5-Hz excitation.

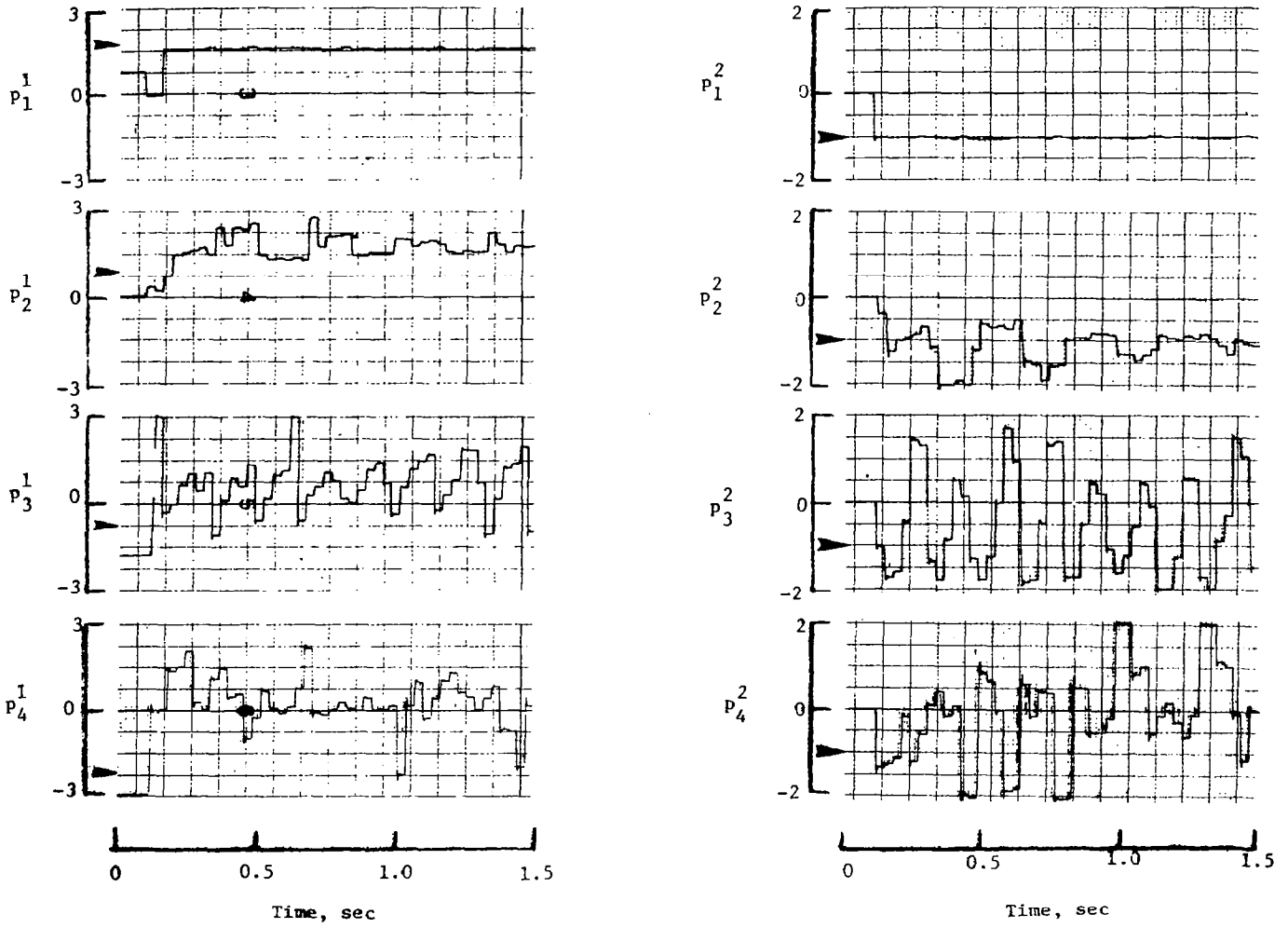

Figure 7.- Output of parameter identifiers. SPAR derived values. Sinusoidal excitation by actuator 1 at 5 Hz.

Figure 8 demonstrates the result of applying the mode shape identification procedure (a) to a simulation wherein the beam was given an arbitrary displacement and (b) in an experiment wherein only the first flexible mode was excited. In the simulation the normalized mode shape obtained agreed with that produced by the SPAR analysis. However, in the laboratory experiment a distortion in the identified mode shape was observed. In both cases the mode shape was identified on line after approximately 1 second of data processing.

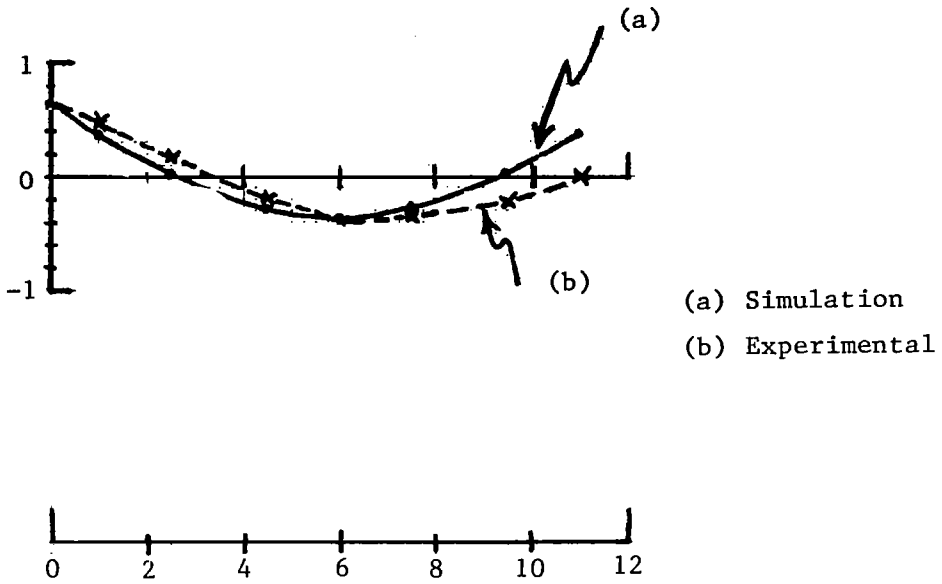

Figure 8.- Identification of mode shape.
First flexible mode.

A table of identified modal parameter values that resulted from a simulation incorporating both the mode shape and modal parameter identification schemes is shown in figure 9. Identification of mode shapes and parameters was accomplished in approximately 1 second of processing measurements from eight sensors distributed along the beam.

[Simulation - all modes excited at parameter values]

Flexible mode	Initial	Final	Actual
1	-0.8495	1.8726	1.87267
2	-1.7194	1.0991	1.099181
3	0.09918	-0.71936	-0.71940
4	0.83907	-1.9960	-1.9960
5	0.8726	0.15047	0.15049
6	-2.996	1.8387	1.83907

Figure 9.- Identification of modal parameters.

SUMMARY

- Presented algorithms for on-line parameter and mode-shape estimation
- Examined identification performance using computer simulations and a limited number of laboratory experiments
- Future work will include:

  (1) Further experimental studies

  (2) Development of separable nonlinear least-squares approach to identification

  (3) Development of on-line performance measures for sequential processing decisions

COMPONENT NUMBER AND PLACEMENT IN LARGE SPACE STRUCTURE CONTROL

Wallace E. VanderVelde
Department of Aeronautics and Astronautics
Massachusetts Institute of Technology
Cambridge, Massachusetts

PURPOSE:

PROVIDE AN OBJECTIVE MEANS OF ASSISTING THE DESIGNER OF THE CONTROL SYSTEM FOR A LARGE FLEXIBLE SPACE STRUCTURE IN HIS CHOICE OF HOW MANY ACTUATORS AND SENSORS TO INCORPORATE IN THE SYSTEM, AND WHERE TO LOCATE THEM ON THE STRUCTURE.

WHAT WE NEED IS:

- A QUANTITATIVE MEASURE OF HOW WELL A SYSTEM CAN BE CONTROLLED WITH A SPECIFIED SET OF ACTUATORS
- A QUANTITATIVE MEASURE OF HOW WELL A SYSTEM CAN BE OBSERVED WITH A SPECIFIED SET OF SENSORS
- A MEANS OF RECOGNIZING THE EFFECTS OF COMPONENT FAILURES IN THESE MEASURES
- A MEANS OF OPTIMIZING THE LOCATIONS OF ACTUATORS AND SENSORS SO AS TO MAXIMIZE THESE MEASURES

A MEASURE OF THE DEGREE OF CONTROLLABILITY

1. FIND THE MINIMUM CONTROL ENERGY STRATEGY FOR DRIVING THE SYSTEM FROM A GIVEN INITIAL STATE TO THE ORIGIN IN A PRESCRIBED TIME.

2. DEFINE THE REGION OF INITIAL STATES WHICH CAN BE RETURNED TO THE ORIGIN WITHIN SPECIFIED LIMITS ON CONTROL ENERGY AND TIME USING THE OPTIMAL STRATEGY.

3. DEFINE THE DEGREE OF CONTROLLABILITY TO BE SOME MEASURE OF THE SIZE OF THIS REGION.

STEP 1. MINIMUM ENERGY CONTROL

Problem statement: $\quad \text{Min } E = \frac{1}{2} \int_0^T \underline{u}^T R \, \underline{u} \, dt$

$$\text{subject to } \dot{\underline{x}} = A\underline{x} + B\underline{u}$$

$$\underline{x}(0) \text{ , } T \text{ given}$$

$$\underline{x}(T) = 0$$

Solution: $\quad \underline{u}(t) = R^{-1} B^T \Phi_{pp}(t) \Phi_{xp}(T)^{-1} \Phi_{xx}(T) \, \underline{x}(0)$

The $\Phi_{ij}(t)$ are partitions of the transition matrix for the system

$$\frac{d}{dt}\begin{bmatrix} \underline{x} \\ \underline{p} \end{bmatrix} = \begin{bmatrix} A & -BR^{-1}B^T \\ 0 & -A^T \end{bmatrix} \begin{bmatrix} \underline{x} \\ \underline{p} \end{bmatrix}$$

STEP 2. THE RECOVERY REGION

Using optimal control, the cost to return to the origin can be expressed:

$$E = \frac{1}{2}\, \underline{x}(0)^T\, V(0)^{-1}\, \underline{x}(0)$$

with $$\dot{V} = AV + VA^T - BR^{-1}B^T \qquad V(T) = 0$$

For specified values of time, T, and control energy, E_s, the recovery region is the interior of the space bounded by the surface

$$\underline{x}(0)^T\, V(0)^{-1}\, \underline{x}(0) = 2\, E_s$$

STEP 3. THE SIZE OF THE RECOVERY REGION

First scale the state variables such that equal displacements in all directions are equally important.

$$\underline{z} = D\underline{x}$$

$$D = \begin{bmatrix} \frac{1}{x_{1_{min}}} & & & \\ & \frac{1}{x_{2_{min}}} & & \\ & & \ddots & \\ & & & \frac{1}{x_{n_{min}}} \end{bmatrix}$$

where $x_{i_{min}}$ is the minimum initial value of x_i one would like to be able to drive to the origin with constrained time and control energy.

STEP 3 (CONTINUED)

Then define a weighted measure of the volume of the recovery region in the scaled space.

$$Vol = V_S + \frac{V_S}{V_R} (V_R - V_S)$$

V_S = volume of the largest sphere which can be inscribed in the elliptical boundary of the recovery region

V_R = volume of the recovery region

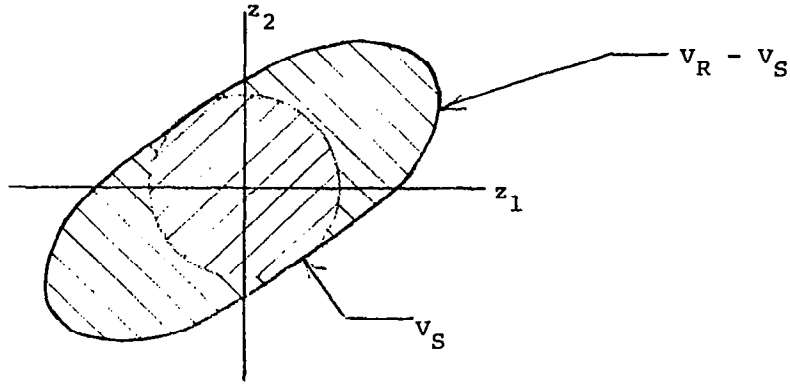

The Degree of Controllability is defined to be the n^{th} root of this weighted volume.

$$DC = \sqrt[n]{Vol}$$

Also $$V_R \approx \prod_i (\lambda_i)^{-1/2}$$

where the λ_i are the eigenvalues of $D^{-1} V(0)^{-1} D^{-1}$.

Alternatively

$$V_R \approx \pi_i (\nu_i)^{1/2}$$

where the ν_i are the eigenvalues of $DV(0)D$.

Then $$V_S \approx (\nu_{i_{min}})^{n/2}$$

An analytic solution is available for V(0).

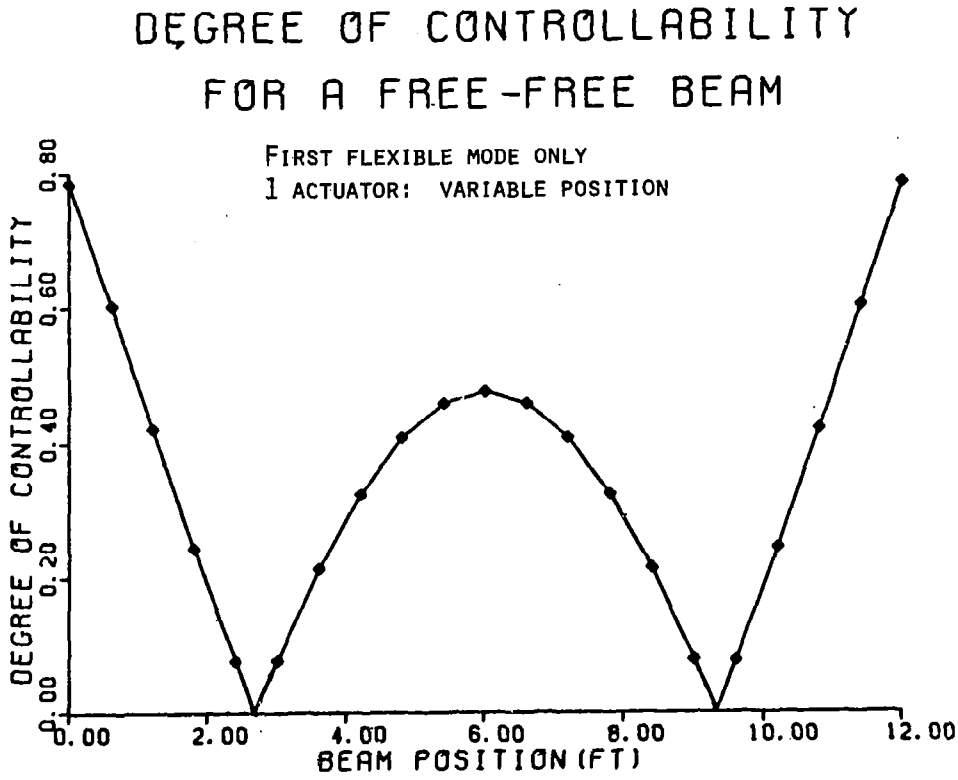
DEGREE OF CONTROLLABILITY
FOR A FREE-FREE BEAM
FIRST FLEXIBLE MODE ONLY
1 ACTUATOR: VARIABLE POSITION
DEGREE OF CONTROLLABILITY
0.00
0.20
0.40
0.60
0.80
0.00
2.00
4.00
6.00
8.00
10.00
12.00
BEAM POSITION (FT)

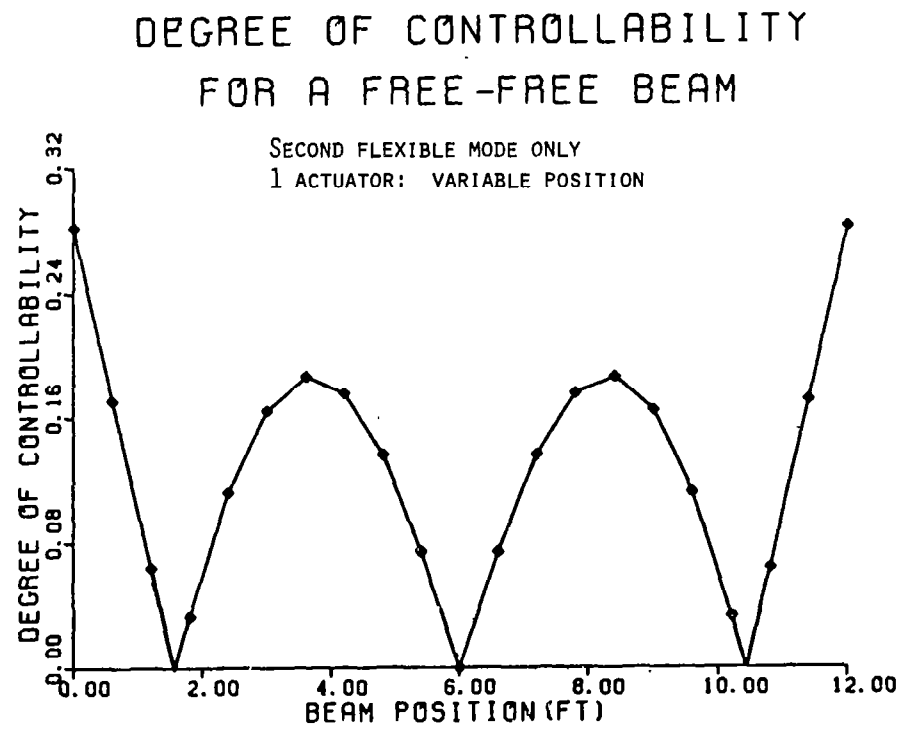
DEGREE OF CONTROLLABILITY
FOR A FREE-FREE BEAM
SECOND FLEXIBLE MODE ONLY
1 ACTUATOR: VARIABLE POSITION
DEGREE OF CONTROLLABILITY
0.00
0.08
0.16
0.24
0.32
0.00
2.00
4.00
6.00
8.00
10.00
12.00
BEAM POSITION (FT)

DEGREE OF CONTROLLABILITY
FOR A FREE-FREE BEAM

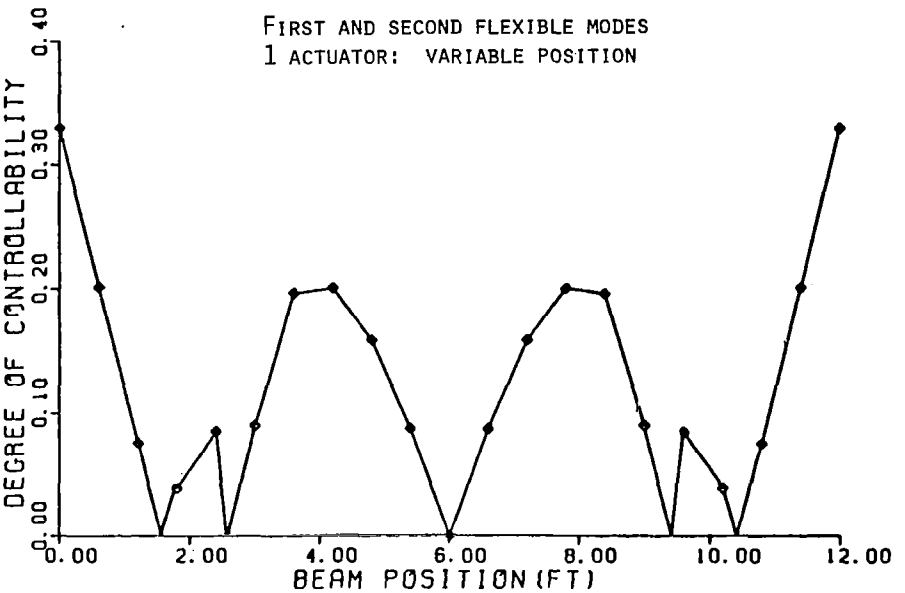

DEGREE OF CONTROLLABILITY
FOR A FREE-FREE BEAM

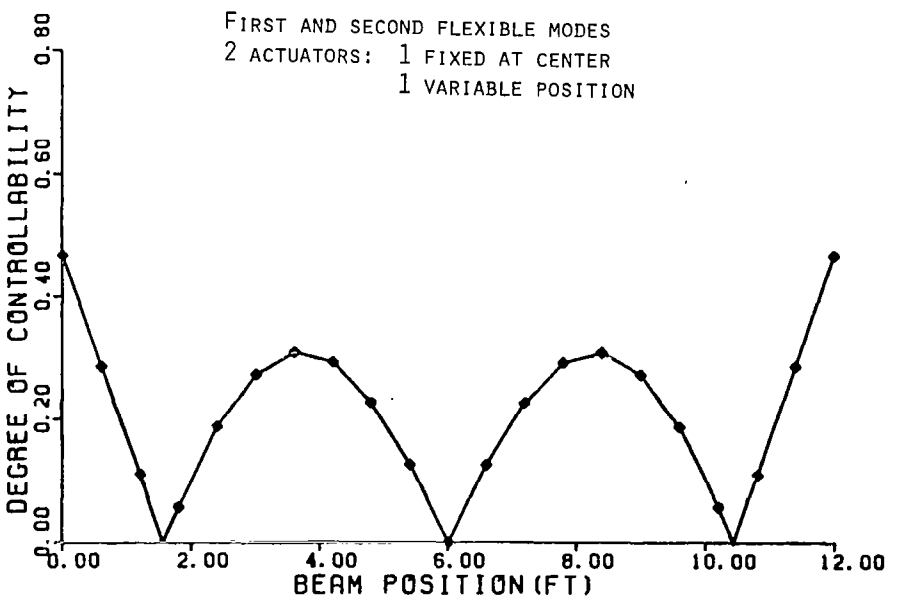

DEGREE OF CONTROLLABILITY FOR A FREE-FREE BEAM

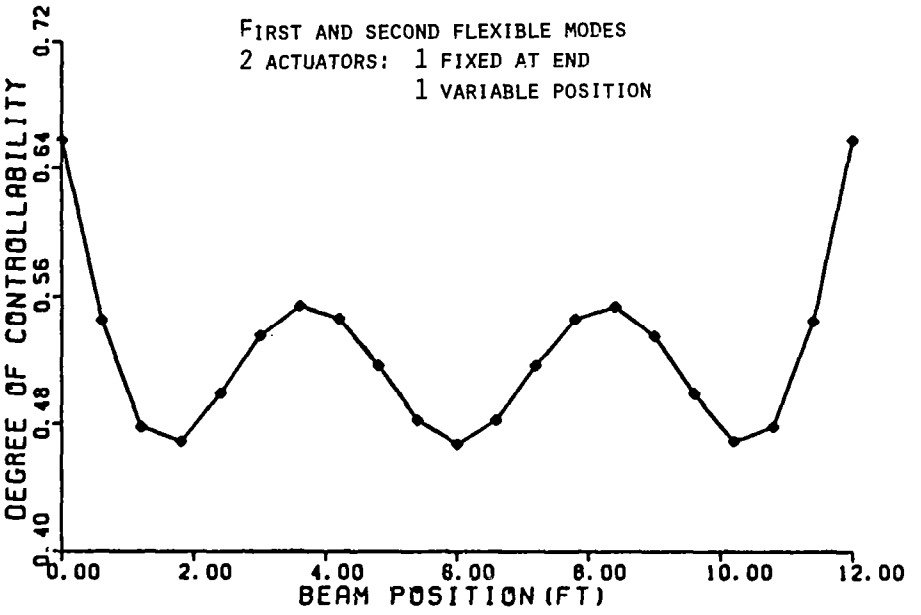

ONE MORE CONSIDERATION

WE WANT THE MEASURE OF CONTROLLABILITY TO REFLECT THE FACT THAT A SYSTEM WITH MORE ACTUATORS OF EQUAL EFFECTIVENESS HAS GREATER CONTROL CAPABILITY THAN ONE WITH FEWER ACTUATORS.

THE DC JUST DEFINED IS MADE PROPORTIONAL TO THE NUMBER OF ACTUATORS PLACED AT THE SAME LOCATIONS IF THE ELEMENTS OF R ARE SCALED INVERSELY WITH THE NUMBER OF ACTUATORS.

FOR DIAGONAL R, CHOOSE $R_{o_{ii}}$ TO REFLECT THE RELATIVE COST OF THE DIFFERENT CONTROLS. THEN

$$R_{ii} = R_{o_{ii}}/m$$

m = total number of actuators

A MEASURE OF THE DEGREE OF OBSERVABILITY

1. IN TERMS OF AN INFORMATION MATRIX, DETERMINE HOW MUCH INFORMATION CAN BE DERIVED ABOUT THE SYSTEM STATE IN TIME T, STARTING FROM ZERO INFORMATION, USING THE GIVEN SET OF SENSORS.

2. DEFINE THE DEGREE OF OBSERVABILITY TO BE A MEASURE OF THE SIZE OF THIS INFORMATION MATRIX.

STEP 1. THE INFORMATION MATRIX

WE WANT THE DEGREE OF OBSERVABILITY TO BE A PROPERTY OF THE SYSTEM, NOT OF THE ENVIRONMENT IN WHICH IT OPERATES. SO DO NOT CONSIDER STATE DRIVING NOISE.

THEN

$$\dot{J} = -JA - A^T J + C^T N^{-1} C$$

$$J(0) = 0$$

CORRESPONDING TO THE SYSTEM MODEL

$$\dot{\underline{x}} = A\underline{x} + B\underline{u}$$

$$\underline{y} = C\underline{x} + \underline{n}$$

$$\overline{\underline{n}(t_1)\underline{n}(t_2)^T} = N\delta(t_2 - t_1)$$

AN ANALYTIC SOLUTION IS AVAILABLE FOR J(T).

STEP 2. THE SIZE OF THE MATRIX

ONE WAY TO MEASURE THE SIZE OF J(T) IS TO INDICATE THE VOLUME CONTAINED WITHIN THE SURFACE

$$\underline{v}^T J(T)^{-1} \underline{v} = 1$$

BUT THE VARIABLES SHOULD BE SCALED TO REFLECT THE RELATIVE IMPORTANCE OF ERRORS IN THE DIFFERENT STATE VARIABLES.

$$\underline{w} = F \underline{v}$$

$$F = \begin{bmatrix} e_{1_{max}} & & & \\ & e_{2_{max}} & & \\ & & \ddots & \\ & & & e_{n_{max}} \end{bmatrix}$$

WHERE $e_{i_{max}}$ IS THE MAXIMUM TOLERABLE ERROR IN THE ESTIMATE OF x_i.

THE DEGREE OF OBSERVABILITY IS DEFINED WITH RESPECT TO THIS VOLUME IN THE SPACE OF EQUALLY IMPORTANT ERRORS ($\underline{w}$) JUST AS THE DEGREE OF CONTROLLABILITY WAS DEFINED FOR THE VOLUME OF THE RECOVERY REGION IN THE SPACE OF EQUALLY IMPORTANT CONTROL CHARACTERISTICS.

$$DO = \sqrt[n]{V_S + \frac{V_S}{V_R}(V_R - V_S)}$$

$$V_R = \prod_i (\nu_i)^{1/2}$$

$$V_S = (\nu_{i_{min}})^{n/2}$$

WHERE THE ν_i ARE THE EIGENVALUES OF FJ(T)F.

DEGREE OF OBSERVABILITY FOR A FREE-FREE BEAM

FIRST FLEXIBLE MODE ONLY
1 SENSOR: VARIABLE POSITION

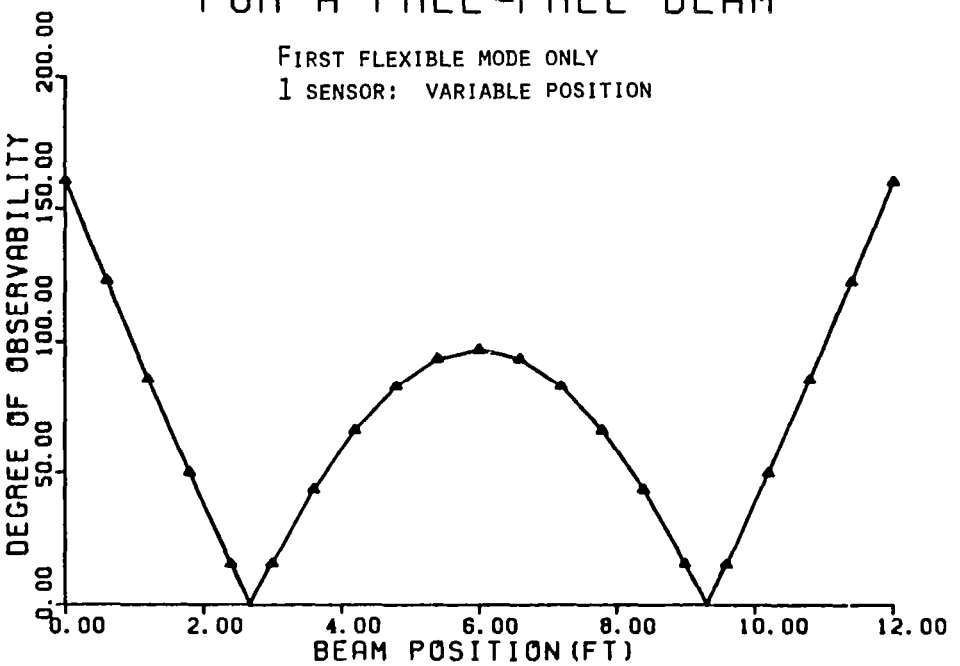

DEGREE OF OBSERVABILITY FOR A FREE-FREE BEAM

FIRST AND SECOND FLEXIBLE MODES
2 SENSORS: 1 FIXED AT CENTER
1 VARIABLE POSITION

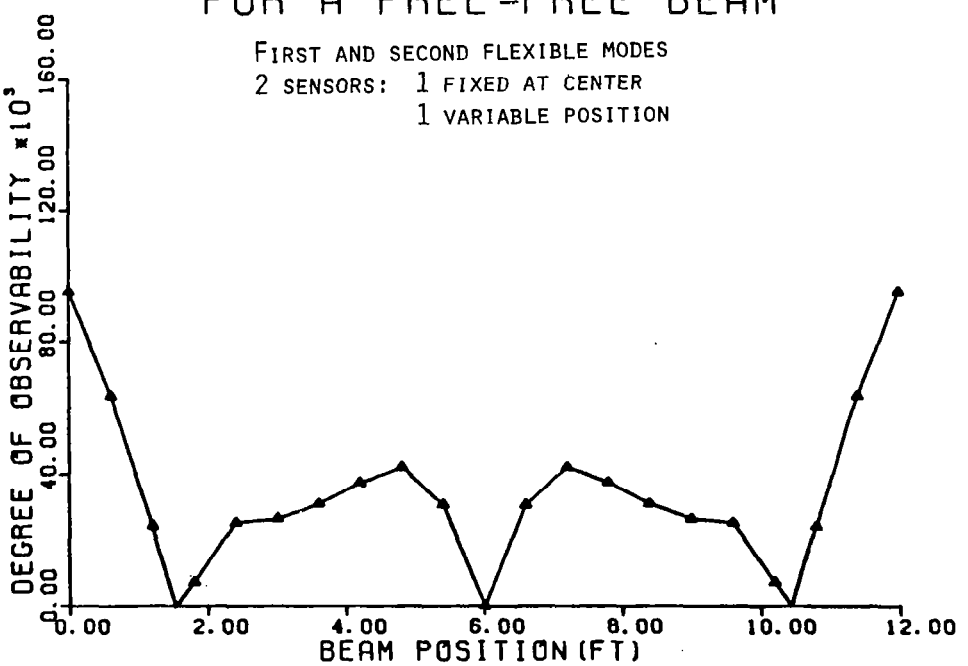

RECOGNITION OF COMPONENT FAILURES IN THESE MEASURES

LET f INDICATE THE STATE OF FAILURES AMONG THE ACTUATORS OR SENSORS. THEN FOR EVERY f, $DC(f)$ OR $DO(f)$ CAN BE COMPUTED AS JUST DESCRIBED.

FROM THE STATISTICAL MODEL FOR FAILURES OF THE DIFFERENT COMPONENTS ONE CAN EXPRESS $P[f(t) = f_i]$.

THE AVERAGE, OVER THE MISSION PERIOD, OF THE EXPECTED DEGREE OF CONTROLLABILITY OR OBSERVABILITY IS TAKEN AS THE FINAL MEASURE.

$$ADC = \frac{1}{T_m}\int_0^{T_m} \overline{DC(t)}\, dt$$

$$= \frac{1}{T_m}\int_0^{T_m} \sum_i DC(f_i)\, P[f(t) = f_i]\, dt$$

$$= \sum_i DC(f_i)\, \frac{1}{T_m}\int_0^{T_m} P[f(t) = f_i]\, dt$$

THE DEGREE OF OBSERVABILITY IS COMPUTED IN THE SAME WAY.

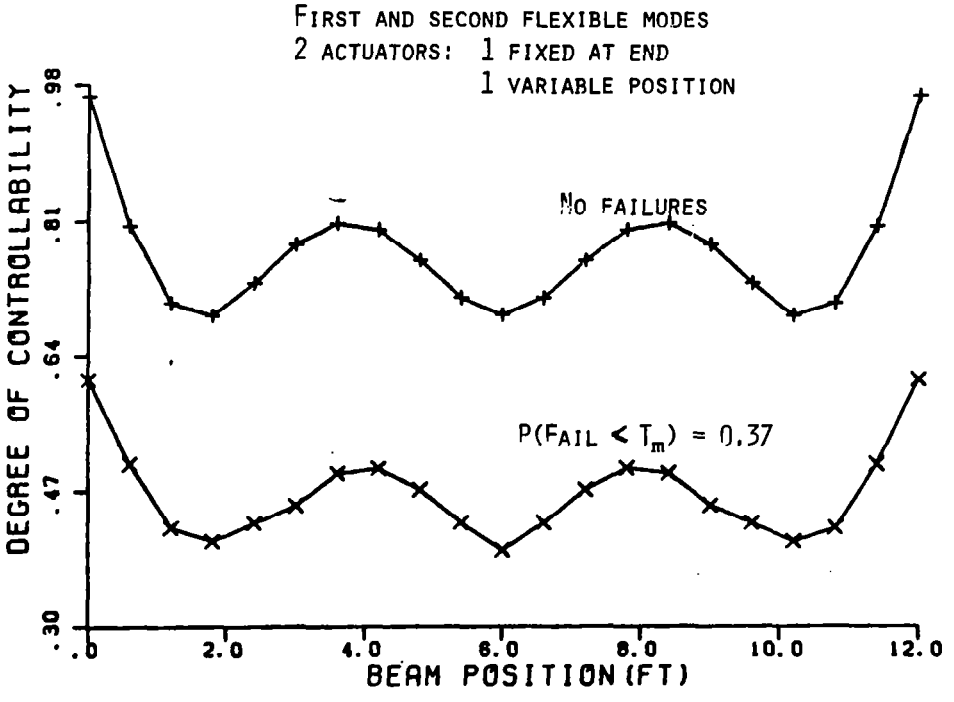

OPTIMIZING COMPONENT LOCATIONS

THE AVERAGE DEGREE OF CONTROLLABILITY IS A FUNCTION OF THE CHOICE OF ACTUATOR LOCATIONS; LET ℓ INDICATE THE VARIOUS ADMISSIB LE CHOICES.

$$\text{ADC} \Rightarrow \text{ADC}(\ell)$$

AN OPTIMIZATION ROUTINE IS REQUIRED TO FIND THE OPTIMUM LOCATIONS.

$$\text{ADC}^* = \max_{\ell \in L} \text{ADC}(\ell)$$

THE OPTIMUM SENSOR LOCATIONS ARE DEFINED IN THE SAME WAY USING THE AVERAGE DEGREE OF OBSERVABILITY.

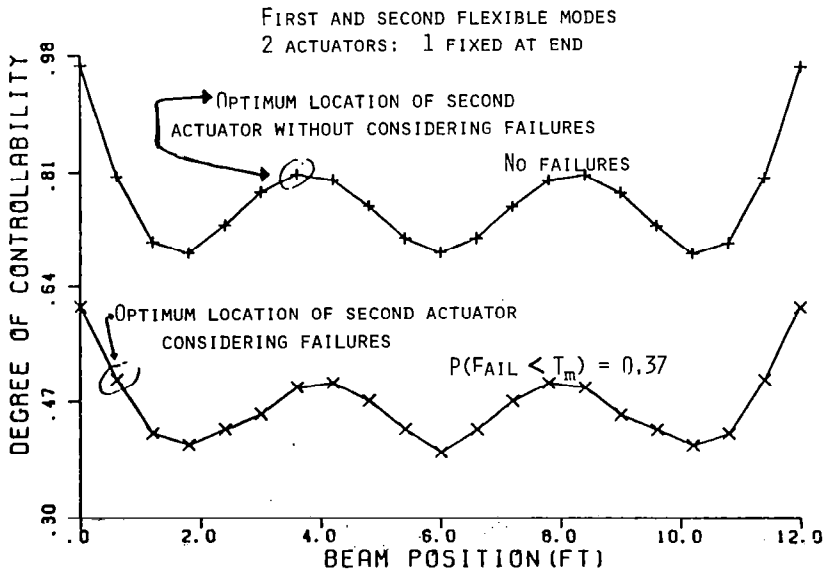

CHOICE OF THE NUMBER OF COMPONENTS

THE OPTIMUM AVERAGE DEGREE OF CONTROLLABILITY IS A FUNCTION OF THE NUMBER OF ACTUATORS IN THE SYSTEM.

$$ADC^* \Rightarrow ADC^*(m)$$

WITH THE LIKELY CONSTRAINT THAT MULTIPLE ACTUATORS CANNOT BE PLACED IN THE SAME LOCATION, $ADC^*(m)$ SHOWS DIMINISHING RETURNS WITH INCREASING m.

THE SAME IS TRUE FOR THE OPTIMUM AVERAGE DEGREE OF OBSERVABILITY.

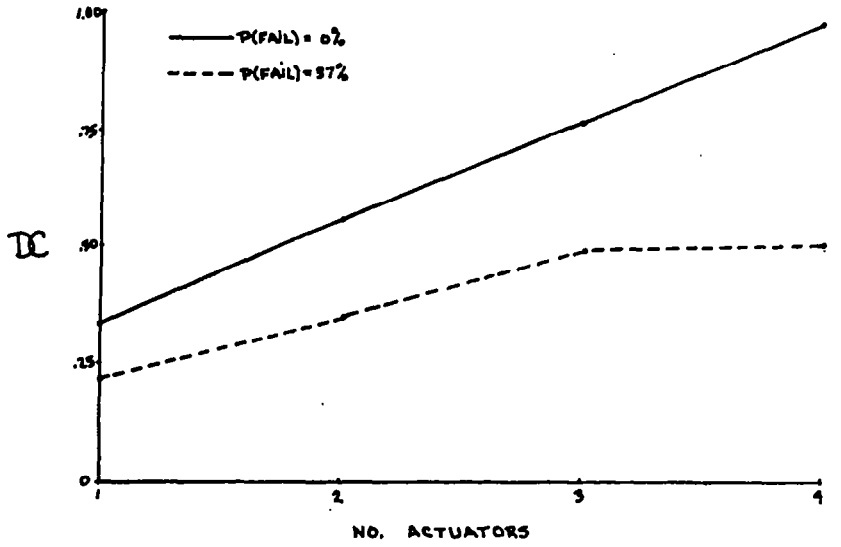

A PROGRAM PLAN FOR THE DEVELOPMENT OF FAULT TOLERANT LARGE SPACE SYSTEMS

Paul Motyka
Charles Stark Draper Laboratory, Inc.
Cambridge, Massachusetts

Objectives

- Establish the need for fault tolerance in LSS
- Discuss the unique characteristics of LSS which affect fault tolerance
- Summarize the status of fault tolerant systems for LSS
- Discuss a program plan to validate and demonstrate the concept of fault tolerance for LSS

Establishment of the Need for Fault Tolerant LSS

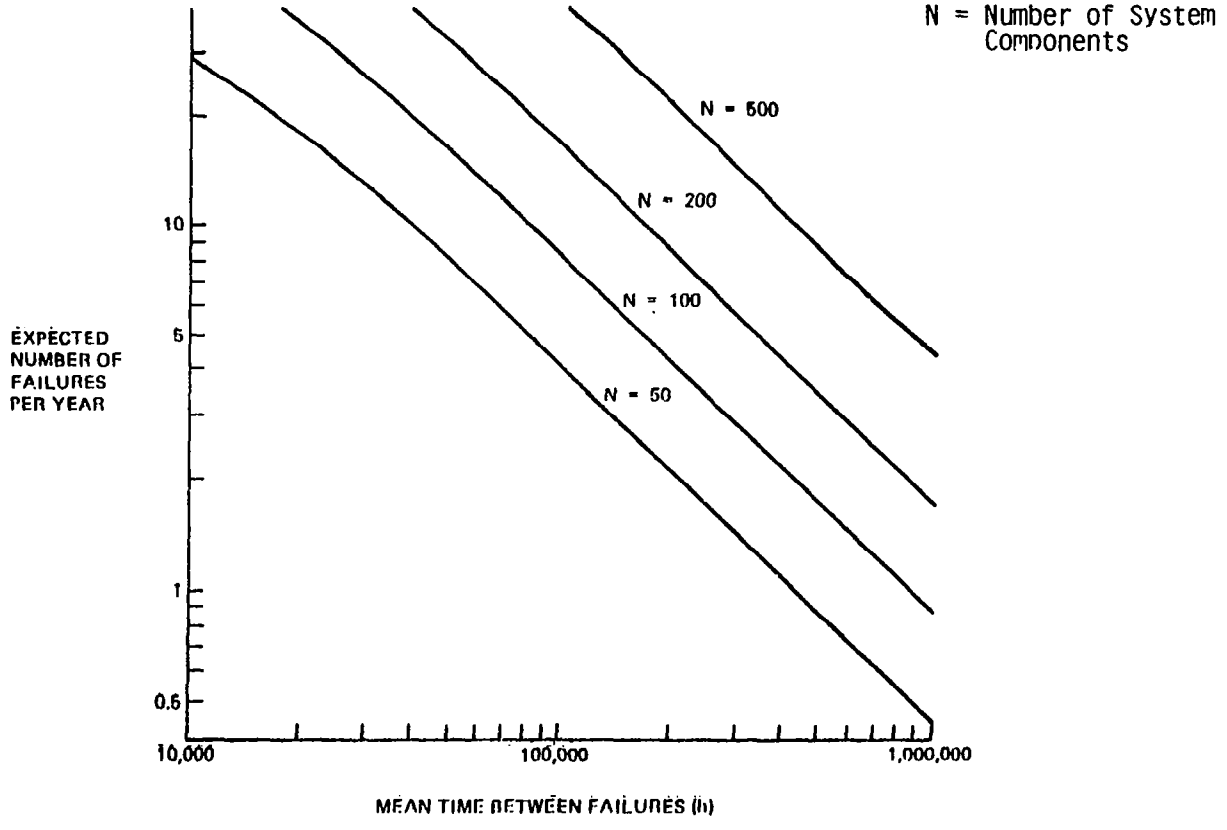

Characteristics of LSS That Affect Fault Tolerance

- Dimensionality
  - Will have to consider a much larger number of components than in any previous application
  - May affect the achievement of real time operation and computational accuracy
- Precise accuracy and stability requirements
  - Small failures will have to be detected and isolated quickly
- Structural mode and physical displacement effects on sensors
  - May be comparable in magnitude to the failures which must be detected
- Environmental effects
  - Dynamic effects such as large angle slewing maneuvers
  - Thermal effects may produce changes in modal characteristics
- Spillover (Model Order Reduction) effects
  - May introduce uncertainties which can be falsely interpreted as failures
- Many diverse types of sensors present
  - Must be collectively accounted for if system wide fault tolerant capability is to be achieved
- Multiple experiments operating on a single LSS
  - Interactions among experiments may result in false alarms
  - A robust fault tolerant system may be required to tolerate changes in modal characteristics with experiments
- The modal frequencies may be in the controller bandwidth
  - Filtering to reduce modal effects and improve fault tolerant capability may not be possible

Status of Fault-Tolerant Technology for LSS

- Little work has been done in this area
- A large body of knowledge concerning fault tolerant systems has evolved in spacecraft and avionics applications
- This material forms a solid foundation for the development of fault tolerant technology for LSS

Elements of a Program Plan to Validate the Concept of Fault Tolerance for LSS

- System modeling
  - Generate an analytic model of the LSS
- Environment modeling
  - Define LSS tasks, maneuvers and disturbances
- Requirements definition
  - Define LSS accuracy, stability and reliability requirements
- Component modeling
  - Define analytic models, error effects, noise, flexibility effects, etc.
  - Uncertainties establish the fault tolerant capability of LSS
- Fault tolerant techniques development
  - Develop algorithms to detect and isolate faults and reconfigure LSS
- Simulation development
  - Both nonreal time and real time capabilities will be needed
- Development of a fault tolerant data processing capability
  - Needed to carry out computations associated with the LSS
  - A firm basis for this technology exists

Elements of a Program Plan to Validate the Concept of Fault Tolerance for LSS (concluded)

- Conceptual design
  - Preliminary definition of algorithms, components, architectures, etc. and assessment of design alternatives
- System design
  - Detailed and specific determination of parameters, components, architectures and algorithms for selected LSS
- Preliminary implementation
  - Definition of system software and hardware
  - Partitioning of functions among subsystems
- Validation of fault tolerance concept and demonstration of capability
  - Use simulation of complete LSS
- Requirements evaluation
  - Use simulation to assess ability of fault tolerant LSS to meet accuracy and stability requirements
  - Analytic techniques must be employed to evaluate the reliability of the LSS

Conclusions

- There is a definite need for fault tolerance in LSS
- LSS have unique characteristics which impact fault tolerance
- Very little work has been done regarding fault tolerance for LSS although a solid base exists from spacecraft and avionics applications
- A program plan for the validation and demonstration of the concept of fault tolerance for LSS has been developed

LARGE SPACE STRUCTURES

CONTROL ALGORITHM CHARACTERIZATION

E. Fogel
Charles Stark Draper Laboratory, Inc.
Cambridge, Massachusetts

Computation Consideration in LSS Control/Identification

- Algorithms
- Structures
- Computation considerations

Spillover Effect

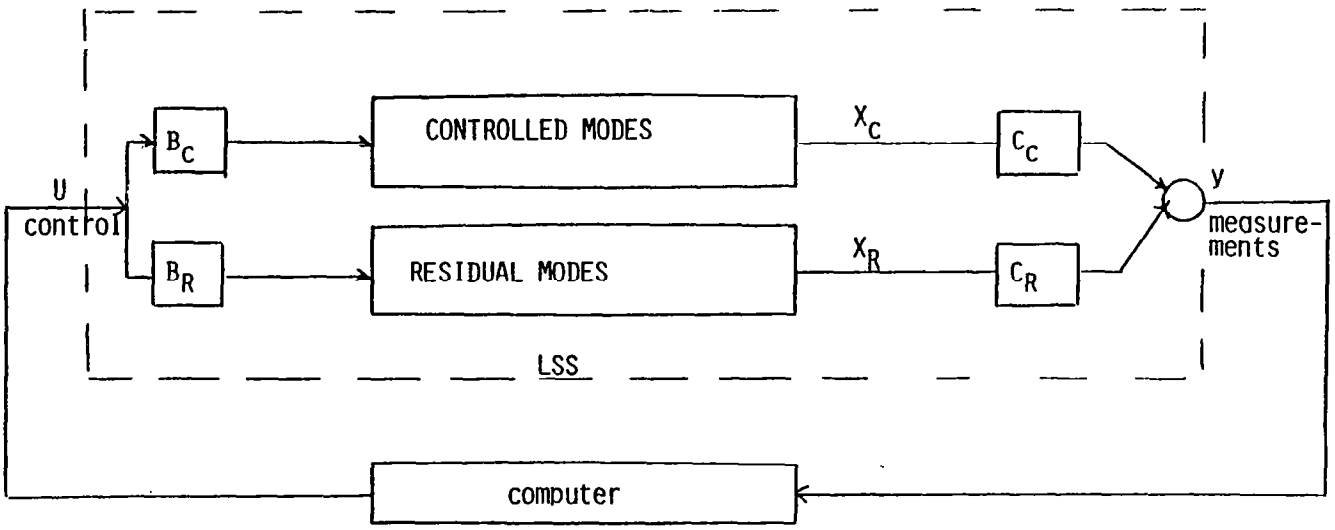

MODEL

$\dot{X} = AX + BU$ $\qquad$ $y = CX$

$A = \text{diag}\ \ H_j$ $\qquad$ $H_j = \begin{bmatrix} 0 & 1 \\ -\omega^2 & 0 \end{bmatrix}$

Separation to : controlled modes

X_C

: residual modes

X_R

$$X = \begin{bmatrix} X_C \\ X_R \end{bmatrix} \qquad \begin{cases} \dot{X} = \begin{bmatrix} A_C & \\ & A_R \end{bmatrix} X + \begin{bmatrix} B_C \\ B_R \end{bmatrix} U \\ y = C_C X_C + C_R X_R \end{cases}$$

LAC/HAC

LAC: local feedback colocated sensor/actuator pairs

→ Augment damping

HAC: dynamic feedback to control a reduced order model

* frequency shaped K.F.

HAC/LAC Control Algorithm

LAC: $U_L = \bar{G}\, y \qquad \bar{G} = \bar{G}^T > 0$

HAC:

$$\dot{\varphi} = \Omega\ \varphi + M\, X_C$$

$$\dot{\hat{X}}_C = A_C \hat{X}_C + BU + K(y - C_C \hat{X}_C)$$

$$U_H = G_1 \hat{X}_C + G_2 \varphi$$

$$U = U_L + U_H$$

Rate HAC rate = 1/2 LAC rate

LAC/HAC BASED COMPUTATION REQUIREMENTS

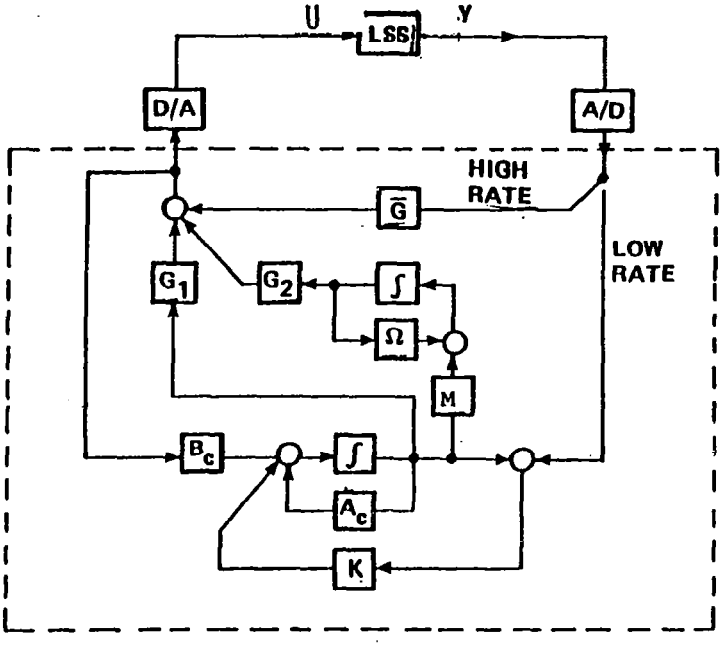

COMPUTER

LQG APPROACH

Solution

$$\text{solve} \quad \text{LQG} \qquad \text{for } X_C$$

$$J = \int \left[\| X_C \|_Q^2 + \| U \|_R^2 \right] dt$$

Implementation

$$U = \check{T} K \hat{X}_C$$

$$\dot{\hat{X}}_C = A_C \hat{X}_C + B_C U + \bar{K} \check{\bar{T}} (y - C_C \hat{X}_C)$$

$$K = - R^{-1} B_C^T P$$

$$PA_C + A_C^T P + Q - PTB_C R^{-1} T B_C^T P = 0$$

$$\left.\begin{array}{lll} T: & B_R T = 0 & B_C T \neq 0 \\ \bar{T}: & \bar{T} C_R = 0 & \bar{T} C_C \neq 0 \end{array}\right\} \quad \text{orthogonality conditions}$$

Closed loop:

$$\frac{d}{dt} \begin{bmatrix} X_C \\ X_R \\ e \end{bmatrix} = \begin{bmatrix} A_C - B_C TK & 0 & B_C TK \\ 0 & A_R & 0 \\ 0 & 0 & A_C - \bar{K} \bar{T} C_C \end{bmatrix} \begin{bmatrix} X_C \\ X_R \\ e \end{bmatrix}$$

$$e = \overset{\Delta}{X}_C - \hat{X}_C$$

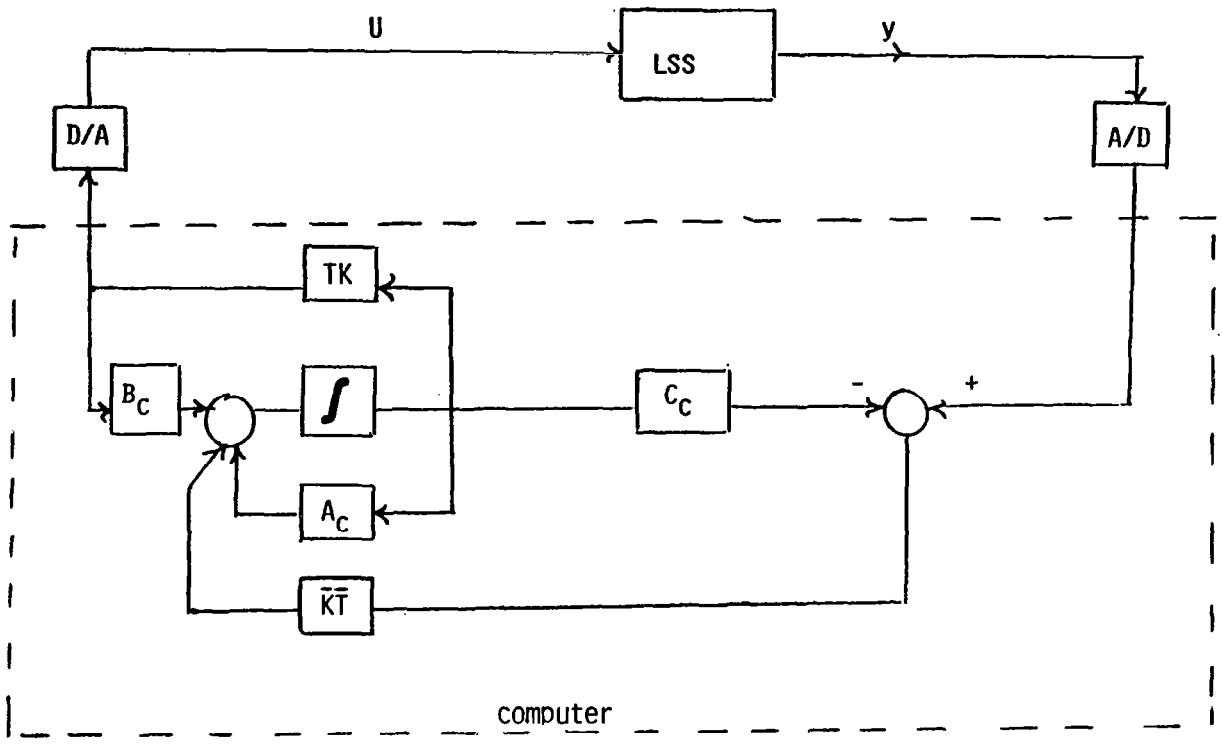

STRUCTURES USED AS EXAMPLES

- 100-METER BEAM
- 50-METER REFLECTOR ANTENNA

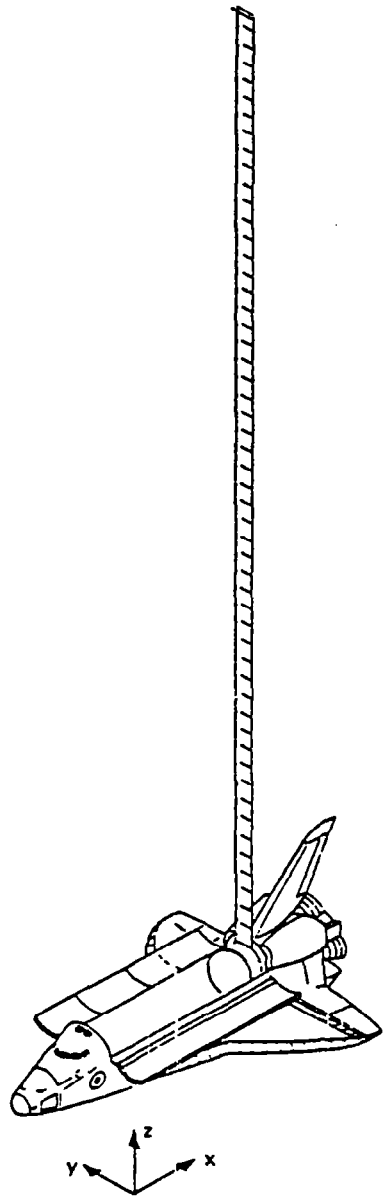

Beam Instrumentation

3 clusters of x y { accelerometer (sensor) / proof mass (actuator) }

at: Top, Middle, Bottom

DIMENSION (M) OF SENSOR VECTOR AND ACTUATOR VECTOR = 3 x 2 = 6

50m REFLECTOR

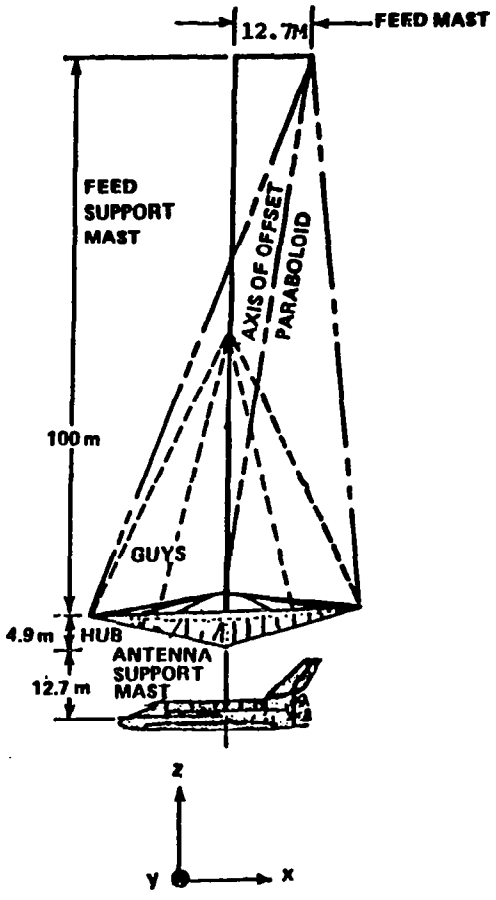

OFF SET FEED
F/D = 2.0
NONMETALLIC FEEDMAST
TAPERED TENSION TRUSS

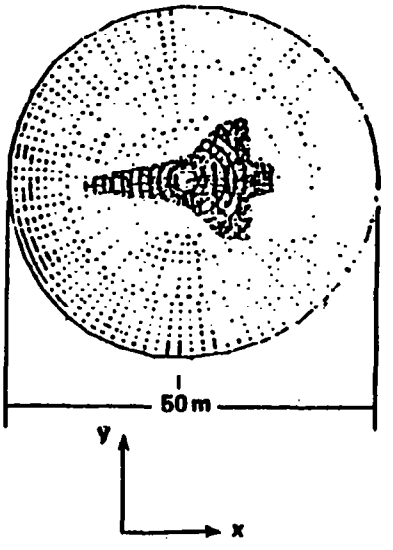

Antenna Instrumentation (detail)

13 CLUSTERS OF COLOCATED SENSORS/ACTUATORS AS FOLLOWS:

1. MAST/ORBITER ATTACHMENT:

SENSORS	2 DOF	ACCELEROMETER PKG (x, y)
ACTUATOR	2 DOF	PROOF MASS

2. REFLECTOR HUB (WHERE FEED SUPPORT MAST IS ATTACHED TO ANTENNA SUPPORT MAST)

SENSORS	2 DOF	ACCELEROMETER PKG (x, y)
	1 DOF	RATE GYRO (TORSION AXIS)
ACTUATOR	2 DOF	PROOF MASS PKG
	1 DOF	TORQUE WHEEL

3. 8 CLUSTERS OF INSTRUMENTS AROUND RIM OF REFLECTOR:

SENSORS	2 DOF	ACCELEROMETER (TANGENTIAL,+ z) TENSIOMETERS ON GUY WIRES
ACTUATORS	2 DOF	PROOF MASS (tangential +Z), Guy Tensioner

4. MIDDLE OF FEED SUPPORT:

SENSORS	2 DOF	ACCELEROMETER PKG (x,y)
ACTUATORS	2 DOF	PROOF MASS (x,y)

5. FEED MAST/SUPPORT MAST ATTACHMENT:

SENSORS:	2 DOF	ACCELEROMETER	(x,y)
	1 DOF	RATE GYRO	(TORSION)
ACTUATORS	2 DOF	PROOF MASS	(x,y)
	1 DOF	TORQUE WHEEL	(TORSION)

6. AT FEED:

SENSORS	2 DOF	ACCELEROMETER	(y,z)
ACTUATORS	2 DOF	PROOF MASS	(y,z)

- DIMENSION OF SENSOR/ACTUATOR VECTORS (M) = 2+3+2+3+2+8x3 = 36

LQG AND HAC/LAC COMPUTATIONAL SIZING

- THESE ALGORITHMS HAVE BEEN SIZED IN TERMS OF
  - FLOATING POINT OPERATION (FLOP) DEMANDS
  - STORAGE FOR VARIABLES
  - INPUT/OUTPUT DATA FLOW
- FLOP SIZING (PER CONTROL CYCLE) DONE AS A FUNCTION OF THE NUMBER OF CONTROL STATES AND THE NUMBER OF SENSOR/ACTUATOR PAIRS
- STORAGE FOR VARIABLES AND I/O SIZING DONE FOR SPECIFIC STRUCTURE EXAMPLES

Input/Output Data Flow Rates

Assumption
- Control bandwidth 50 Hz
- Accuracy - 2 byte/word

→ { Sampling frequency 250 Hz
  { Command frequency

Data Flow rate per { sensor / actuator } 500 [Bytes/sec]

Total: Beam: 3,000 [Bytes/sec]
Antenna: 18,000 [Bytes/sec]

1553B bus capacity 48,000 [Bytes/sec]

LQG SIZING

	BEAM	ANTENNA
SENSOR/ACTUATOR PAIRS (m)	6	36
CONTROL STATES (n_c)	20	20
FLOP PER CYCLE*	1420	4420
VARIABLES**	752	2312
I/O PER CYCLE	12	72

*INCLUDES SENSOR COMPENSATION FLOP (120 FOR BEAM, 720 FOR ANTENNA)

**INCLUDES SENSOR COMPENSATION VARIABLES (60 FOR BEAM, 360 FOR ANTENNA)

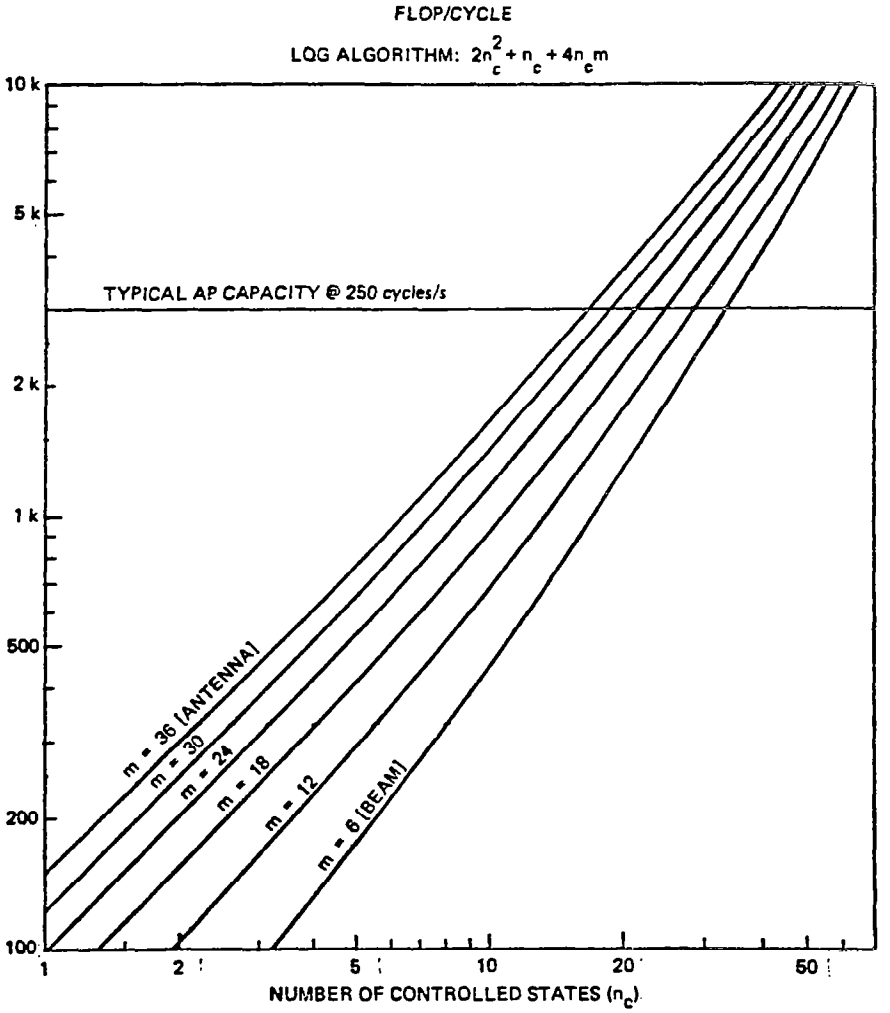

HAC/LAC SIZING

	BEAM	ANTENNA
SENSOR/ACTUATOR PAIRS (m)	6	36
CONTROL STATES (n_c)	12	12
FLOP PER CYCLE*	633	4608
VARIABLES**	570	3060
I/O	12	72

*INCLUDES SENSOR COMPENSATION FLOP (120 FOR BEAM, 720 FOR ANTENNA)

**INCLUDES SENSOR COMPENSATION VARIABLES (60 FOR BEAM, 360 FOR ANTENNA)

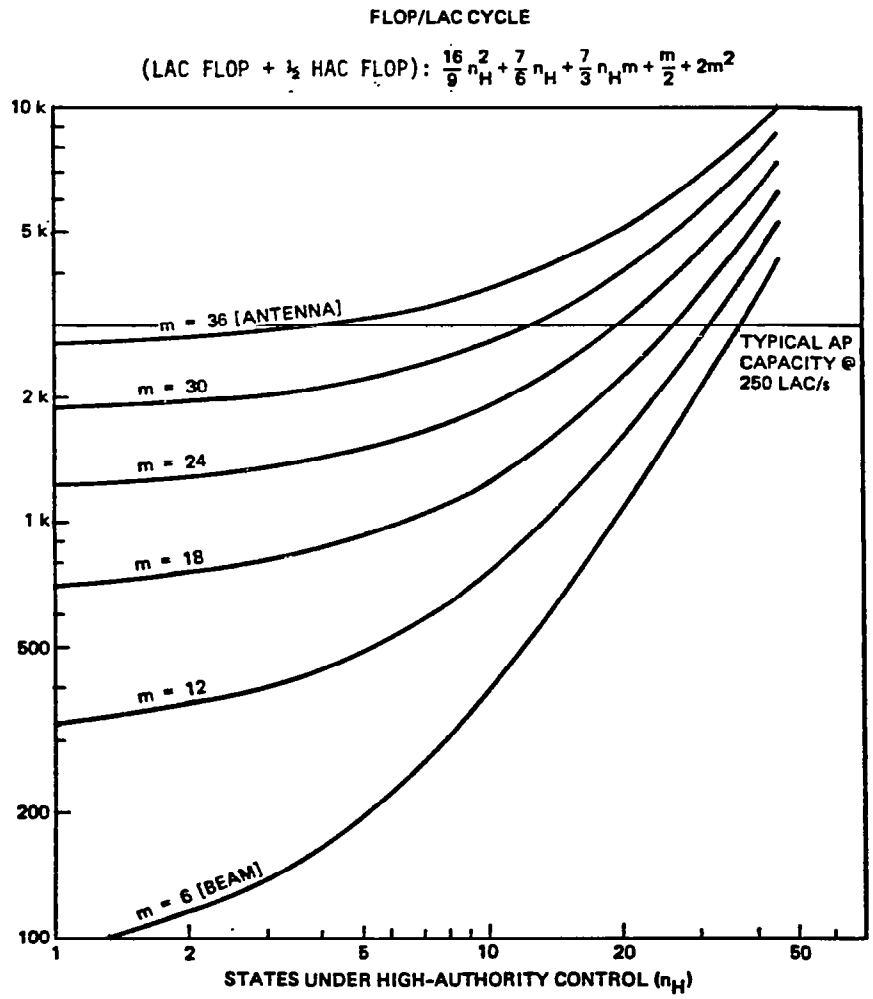

COMPUTATION LOAD

Structure	Algorithm	m	n	n_c (n_H)	rate K Flops/sec	% GPC capacity	% typical AP capacity
Beam	LQG	6	12	6	55	67	7
		6	16	10	112	135	14
	HAC/LAC	6	12	6	34.	41	4
		6	16	10	57	69	7
Antenna	LQG	36	42	6	260	300	36
	HAC/LAC	36	42	6	750	900	100

m = # of sensors/actuators
n = # of modes in model

n_c, n_H = # of controlled modes

SYSTEM IDENTIFICATION COMPUTATIONAL SIZING

- ARMA-LEAST SQUARES ALGORITHM SIZED FOR FLOP AS FUNCTION OF MODEL ORDER (N) AND NUMBER OF SENSOR/ACTUATOR PAIRS (m)
- FLOP REQUIREMENTS FOR THIS ALGORITHM ARE SO LARGE THAT IMPLEMENTATION IN A FLIGHT SYSTEM OR ITS GTF ANALOG IS PRECLUDED
- EVEN IMPLEMENTATION IN GROUND-BASED COMPUTERS IS CONSIDERED QUESTIONABLE, BUT THIS STUDY ASSUMES A GROUND-BASED IMPLEMENTATION

- NOTE: SOME OTHER SYSTEM IDENTIFICATION ALGORITHM MAY BE IMPLEMENTABLE IN A FLIGHT SYSTEM

- Algorithm Assessed - Least Squares

  Motivation for choosing LS

  - Relative high spectral resolution
  - Comparable to other algorithm in computation complexity

    e.g.: Covariance algorithm
    : Maximum Entropy
  - "Better" algorithms - considerably more complicated
  - Less complex algorithms - considerable penalty in performance
  - LS - robust to order reduction
  - Useful for - control design
    - self tuning regulators

Identification Algorithm Sizing

Assume the ARMA model

$$y_k = \sum_{l=1}^{N} A_l y_{k-l} + \sum_{l=0}^{N-1} B_l U_{k-l}$$

where y_k = vector of measurements (sensors) at cycle k

U_k = vector of control influence at cycle k

we can write

$$y_k = \left[A_1 \vdots \cdots \vdots A_n \vdots B_o \vdots \cdots B_{n-1}\right] \begin{bmatrix} y_{k-1} \\ \vdots \\ y_{k-n} \\ U_k \\ \vdots \\ U_{k-n+1} \end{bmatrix}$$

$$= \alpha \cdot z_k$$

Use least squares identification

SYSTEM IDENTIFICATION ALGORITHM FLOP REQUIREMENTS

	BEAM	ANTENNA
SENSOR/ACTUATOR PAIRS (m)	6	36
MODES MODELLED (N)	12	42
OFF-LINE MEGAFLOP FOR 4000 CYCLES	354.2	297,779
OFF-LINE FLOP/CYCLE	88,552	74,444,881
OFF-LINE MEGAFLOPS (@ 250 CPS)	22.1	18,611
ON-LINE FLOP/CYCLE	169,784	73,601,174
ON-LINE MEGAFLOPS (@ 250 CPS)	42.5	18,400

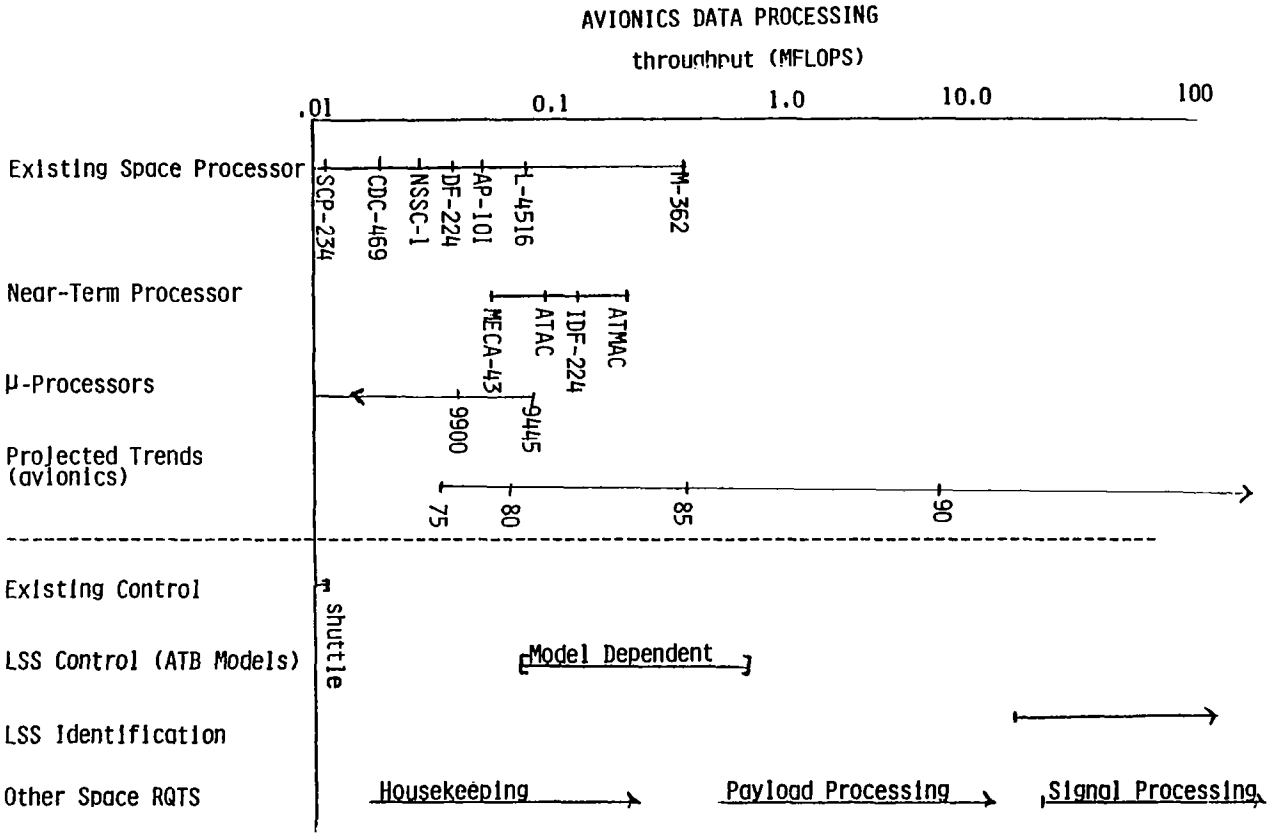

PARTITIONING OF LARGE SPACE STRUCTURES

VIBRATION CONTROL COMPUTATIONS

J. Kernan
Charles Stark Draper Laboratory, Inc.
Cambridge, Massachusetts

LQG SIZING

	BEAM	ANTENNA
SENSOR/ACTUATOR PAIRS (m)	6	36
CONTROL STATES (n_c)	20	20
FLOP PER CYCLE*	1420	4420
VARIABLES**	752	2312
I/O PER CYCLE	12	72

*INCLUDES SENSOR COMPENSATION FLOP (120 FOR BEAM, 720 FOR ANTENNA)
**INCLUDES SENSOR COMPENSATION VARIABLES (60 FOR BEAM, 360 FOR ANTENNA)

HAC/LAC SIZING

	BEAM	ANTENNA
SENSOR/ACTUATOR PAIRS (m)	6	36
CONTROL STATES (n_c)	12	12
FLOP PER CYCLE*	633	4608
VARIABLES**	570	3060
I/O	12	72

*INCLUDES SENSOR COMPENSATION FLOP (120 FOR BEAM, 720 FOR ANTENNA)
**INCLUDES SENSOR COMPENSATION VARIABLES (60 FOR BEAM, 360 FOR ANTENNA)

DISTRIBUTION OF VIBRATION CONTROL AND SENSOR COMPENSATION COMPUTATIONS

- A RANGE OF CHOICES BETWEEN THE TWO FOLLOWING EXTREMES WAS INVESTIGATED:
  - CENTRAL COMPUTATION OF BOTH CONTROL AND SENSOR COMPENSATION
  - CONTROL COMPUTATIONS DISTRIBUTED AMONG CENTRAL AND LOCAL PROCESSORS; LOCAL PROCESSORS ALSO PERFORM SENSOR COMPENSATION
    - PORTIONS OF THE CONTROL COMPUTATIONS CAN BE DISTRIBUTED BECAUSE THE ROWS OR COLUMNS OF THE MATRICES INVOLVED CORRESPOND TO INDIVIDUAL SENSORS OR ACTUATORS
      - DISTRIBUTION IS SUPPORTED BY THE FACT THAT THE MATRICES INVOLVED ARE EITHER CONSTANT OR INFREQUENTLY CHANGED

LSSC COMPUTATION DISTRIBUTED AMONG CENTRAL AND LOCAL PROCESSORS

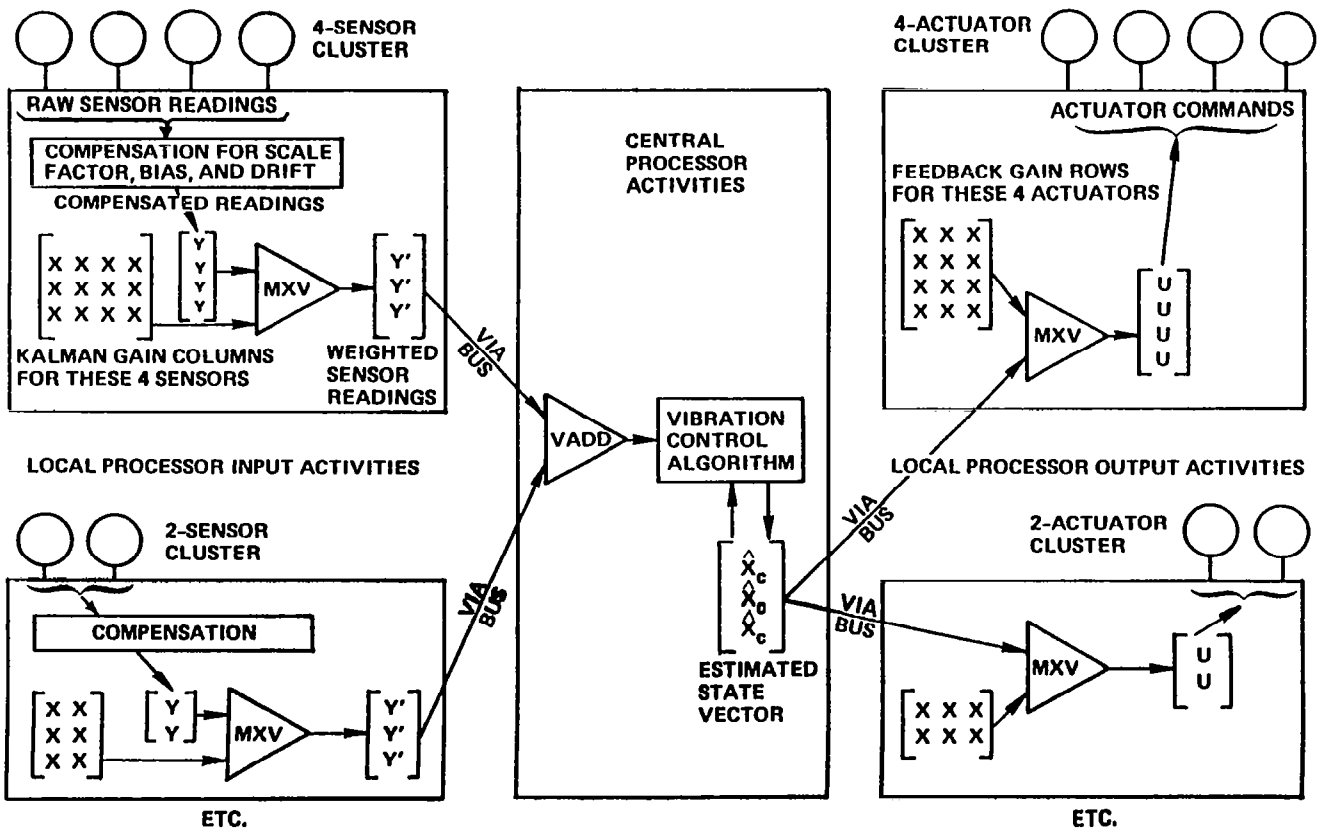

RECOMMENDATIONS FOR CENTRAL/LOCAL PROCESSOR PARTITIONING

- LQG COMPUTATIONS THAT SHOULD BE DISTRIBUTED TO LOCAL PROCESSORS, IN ORDER OF DECREASING PREFERENCE
  - COMPENSATING SENSOR READINGS FOR SCALE FACTOR, BIAS, AND DRIFT
  - APPLYING FEEDBACK GAIN TO ACTUATOR COMMANDS
  - APPLYING KALMAN GAIN TO COMPENSATED SENSOR READINGS
- HAC/LAC COMPUTATIONS THAT SHOULD BE DISTRIBUTED TO LOCAL PROCESSORS, IN ORDER OF DECREASING PREFERENCE
  - COMPENSATING SENSOR READINGS FOR SCALE FACTOR, BIAS, AND DRIFT
  - APPLYING LOW-AUTHORITY GAIN TO ACTUATOR COMMANDS
  - APPLYING HAC FEEDBACK & FILTER GAINS TO ACTUATOR COMMANDS
  - APPLYING KALMAN GAIN TO COMPENSATED SENSOR READINGS
- FREQUENCY SHAPING FILTER COMPUTATION (HAC/LAC) SHOULD STAY IN CENTRAL PROCESSOR

LQG ALGORITHM (n_c = 20) FOR BEAM

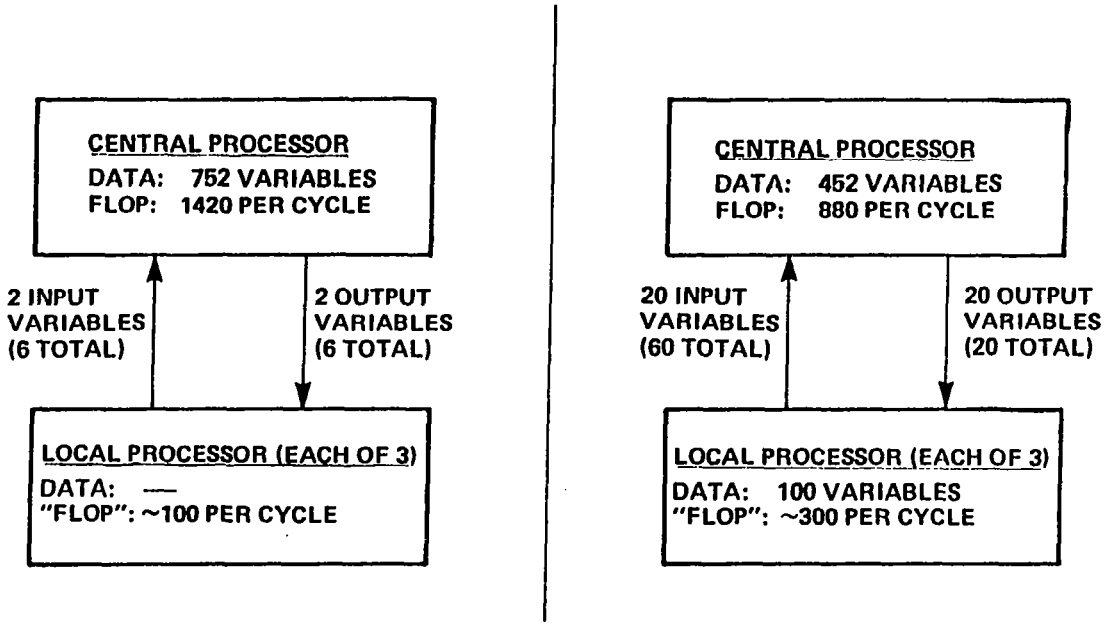

LOG ALGORITHM (n_c = 20) FOR ANTENNA

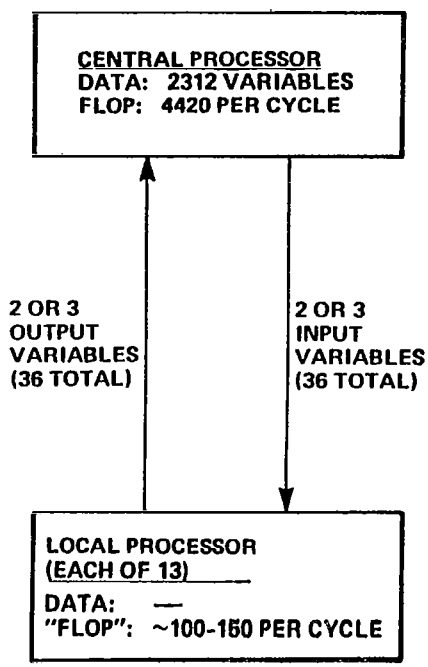

CENTRALIZED

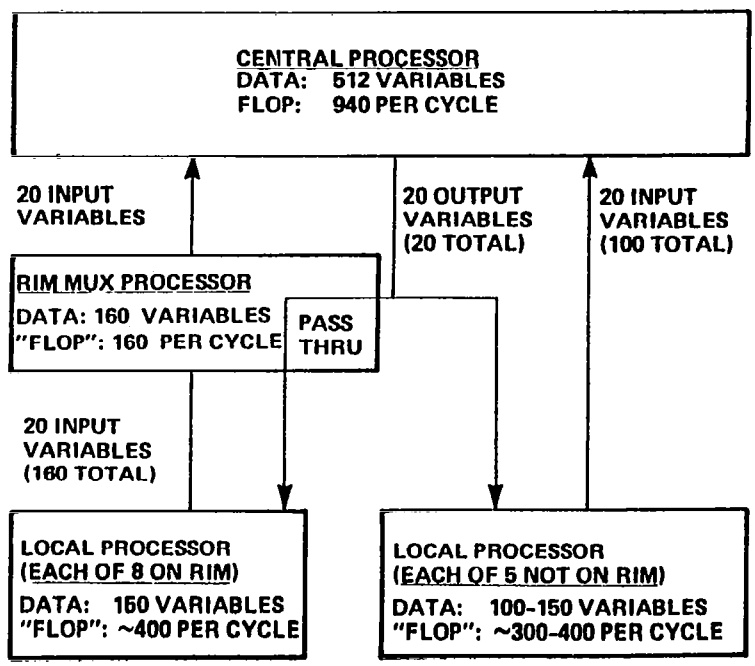

DISTRIBUTED

HAC/LAC ALGORITHM (n_c = 12) FOR BEAM

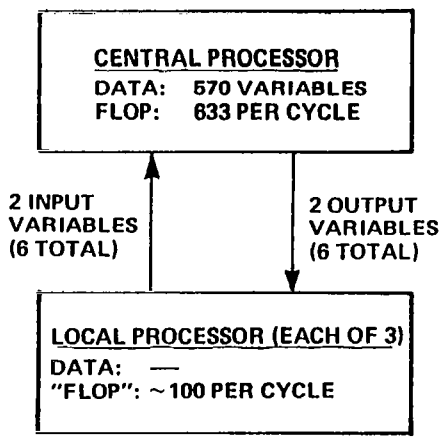

CENTRALIZED

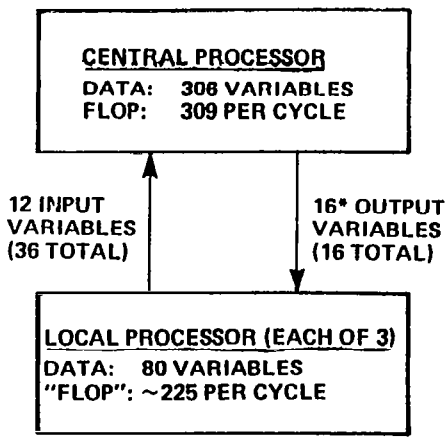

*THESE OUTPUTS ARE SENT ON EVERY OTHER CYCLE

DISTRIBUTED

HAC/LAC ALGORITHM (n_c = 12) FOR ANTENNA

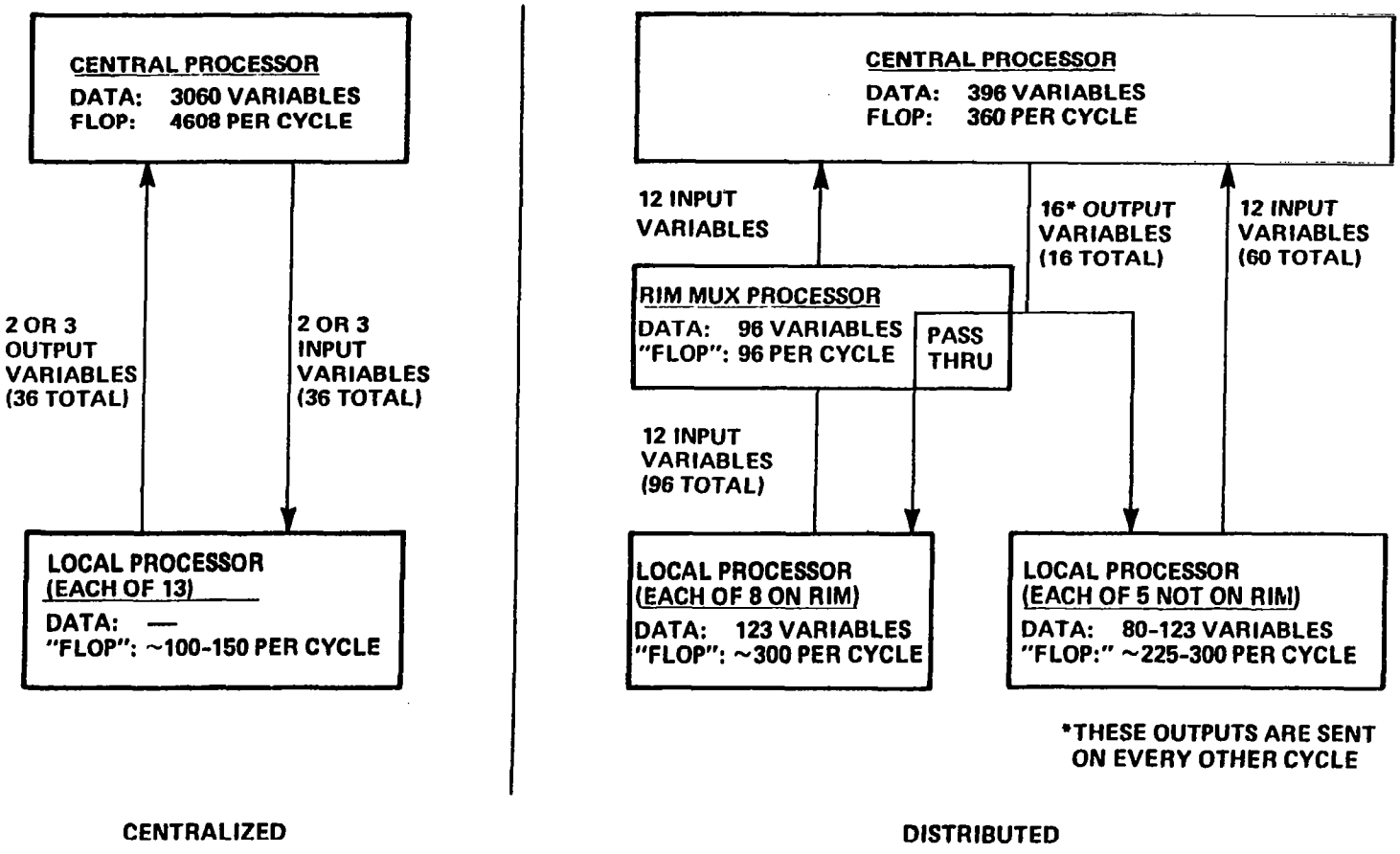

CONCLUSION

- VIBRATION CONTROL OF LARGE SPACE STRUCTURES IS COMPUTATIONALLY DEMANDING - DRIVEN BY
  - NUMBER OF VIBRATION MODES CONTROLLED
  - NUMBER OF SENSOR/ACTUATORS PAIRS
  - CONTROL BANDWIDTH

- DISTRIBUTION OF THE VIBRATION CONTROL COMPUTATIONS AMONG CENTRAL AND LOCAL PROCESSORS CAN SIGNIFICANTLY REDUCE THE THROUGHPUT REQUIRED FROM THE CENTRAL PROCESSOR AND MAY ALSO RESULT IN IMPROVED PERFORMANCE DUE TO REDUCED TRANSPORT LAG

SHUTTLE FLIGHT CONTROL AND STRUCTURE INTERACTION

Michael Paluszek
Charles Stark Draper Laboratory, Inc.
Cambridge, Massachusetts

- A brief overview of the DAP
- Results of the dynamic interaction study of the Orbiter with the General Dynamics Beam attached
- Preliminary results of the three degree of freedom payload parametric study

This is a diagram of the Orbiter Flight Control System (FCS). The functions relating only to the OMS have been eliminated for clarity. The vehicle can be maneuvered either manually or automatically. To perform an automatic maneuver the pilot specifies a new orientation for the Orbiter. This is processed by the steering processor, which sends a corresponding attitude error to the RCS processor. Jets are commanded to fire to reduce this error. The jet firings produce attitude changes that are measured by the IMU and sent to the state estimator at 6.25 Hz. The state estimator produces rate and acceleration estimates, filtering out high-frequency oscillations. The steering processor produces a new rate and attitude error from this data.

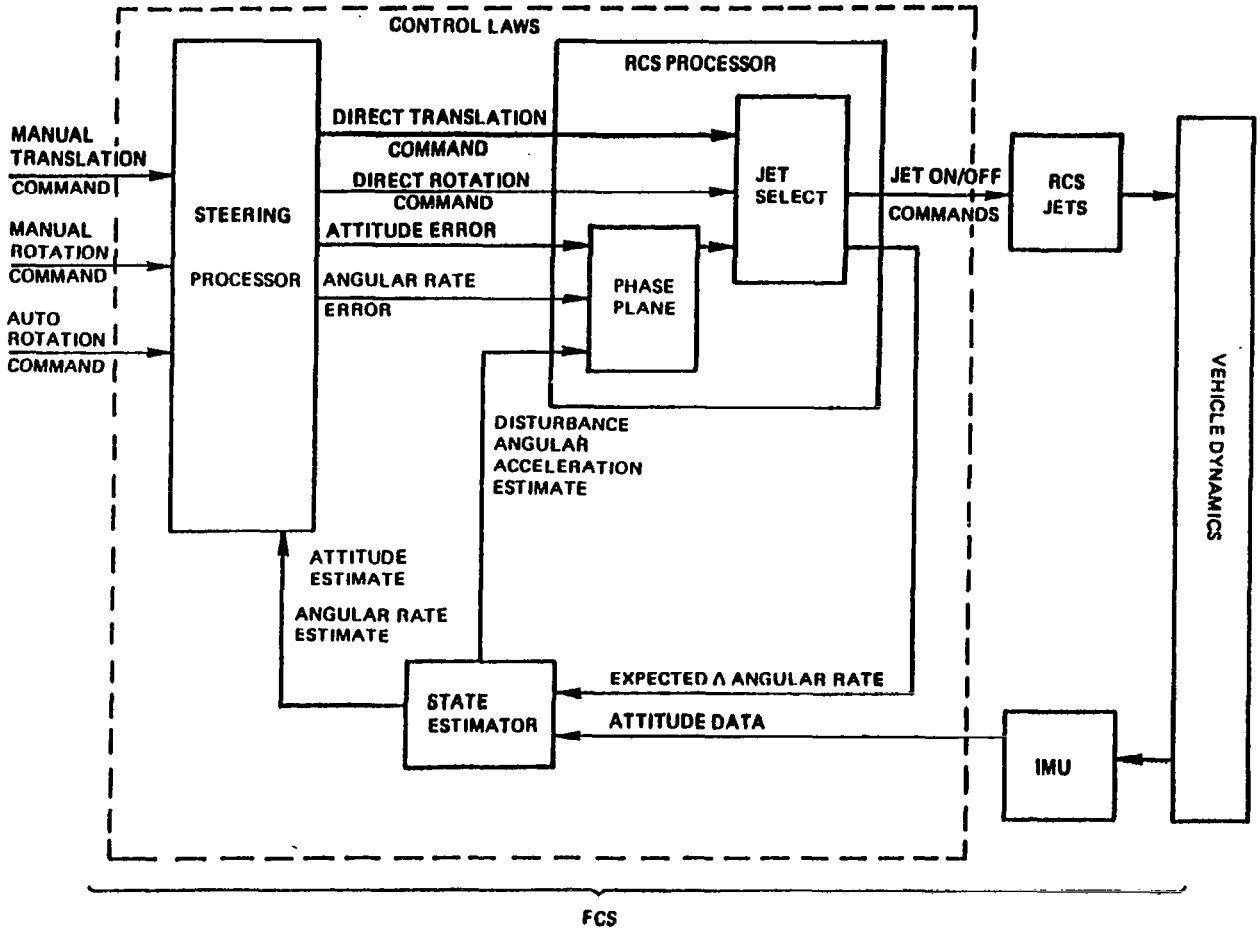

Characteristics of the Orbiter and DAP

Orbiter

- Low inertial cross coupling
- First bending frequency 0.431 Hz
- Large RCS jet coupling particularly roll to yaw
- I_{xx} = .883x10^6 slug-ft^2, 12.5% of I_{zz}
- Operational maneuver rate limit of 2 °/sec

DAP

- Phase Plane autopilot assuming decoupled axis
- State Estimator uses IMU data only
    - second order filter characteristic
    - 6 dB down at .06 Hz with vernier gains
- Designed assuming a rigid vehicle

This flow chart maps the interrelation of different criteria for the Orbiter flight envelope. The three parameters that are used to define an envelope are payload pointing accuracy, propellant budget and payload loads. While often considered independently, they affect one another as indicated in the block diagram.

Definition of the Orbiter Flight Envelope

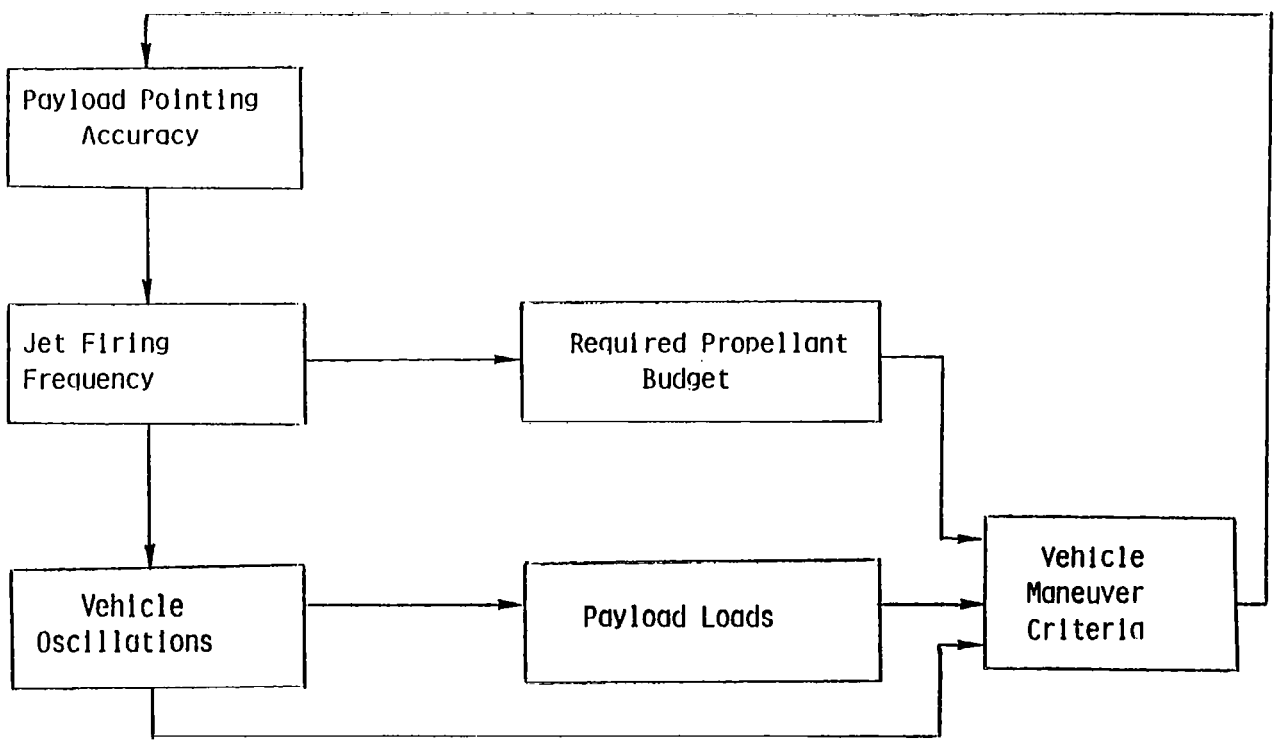

Classes of System Response for the Orbiter with a Flexible Payload

1. The Autopilot does not respond to the payload oscillations
   - vehicle oscillations small
   - payload oscillations may be large
2. The Autopilot responds to payload oscillations
   - vehicle rate or attitude errors exceed set limits
   - vehicle oscillations may diverge
   - attitude excursions may be small

This graph defines the regions of autopilot interaction for the Orbiter with a flexible payload. The x axis is the roll fundamental frequency and the y axis is the ratio of payload roll inertia to empty Orbiter roll inertia. Little or no interaction occurs in the region to the right of the solid line. In the region to the left some closed-loop response has been observed. The dotted line indicates the state estimator 6 dB point. The ruled region is the current area of interest for the parametric study of the DAP response.

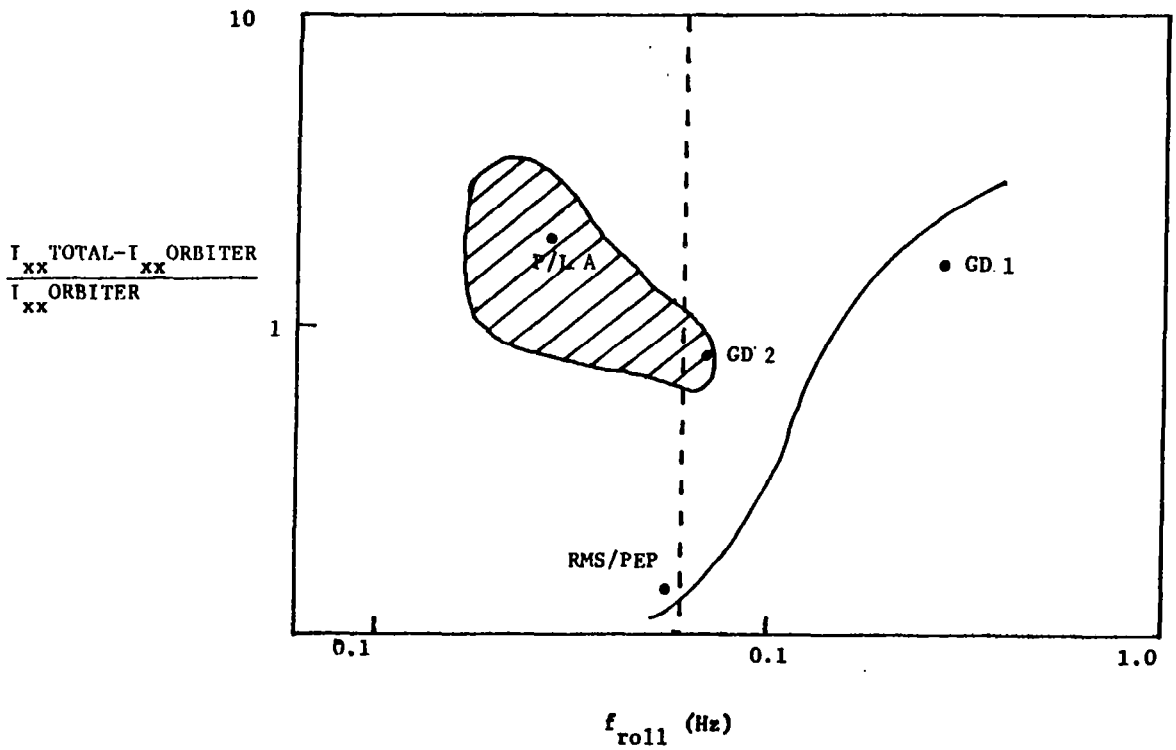

Summary of results of the dynamic interaction analysis of the General Dynamics beam

The Orbiter with the General Dynamics beam experiment is pictured here.

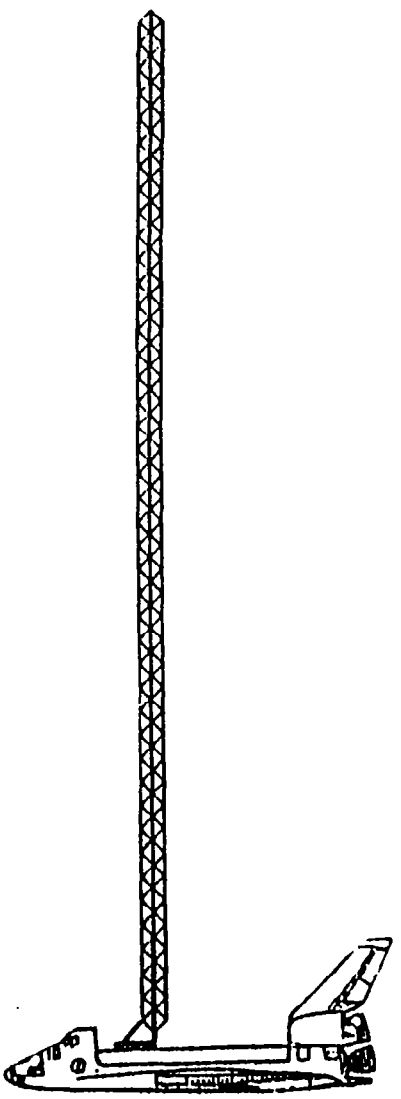

This table gives the results of the dynamic interaction analysis of the Orbiter/GS beam combination. The columns list the maneuver performed, the fuel expended, the type of Orbiter and payload oscillations, whether the DAP sent oscillatory firing commands to the jets, and comments.

Except for the 5° roll case with rate limit clampdown, the vehicle and payload remained stable. In cases 4 and 7 through 10 oscillatory commands were sent to the jets indicating vibration feedback. Note that 4 was the worst case. Case no. 8 is worse than case no. 1, but case no. 10 is not worse than no. 4, as might be expected.

DYNAMIC INTERACTION STUDY SUMMARY

[Fundamental frequency in pitch = 0.046 Hz]

	Maneuver	Fuel	Oscillations			comments
			Payload	Vehicle	ROT-JET-CMD	
1	5° Roll	6.1	stable	stable		
2	Pitch	4.2	stable	stable		
3	Yaw	6.3	stable	stable		
4	5° Roll with att. hold RL=.01, DB=.1	12.0	diverge	diverge	roll,pitch	results after clampdown
5	Astronaut Forced Osc.	-	stable	stable		results after autopilot on
6	Jet F3U Stuck on	-	stable	stable		
7	Jet R4U Stuck on	-	stable	stable	yaw	
8	3.2° Roll Rate =.2	6.1	stable	stable	roll up to 60 sec	.046 Hz pulse
9	5° Pitch with att. hold	7.5	stable	stable	pitch	
10	3.2° Roll with att. hold	10.5	stable	stable	roll until clampdown	

This figure and the next one are examples of the output from two SLS runs. Note that in both cases oscillatory commands are being sent to the jets, but only in the roll case are diverging oscillations seen.

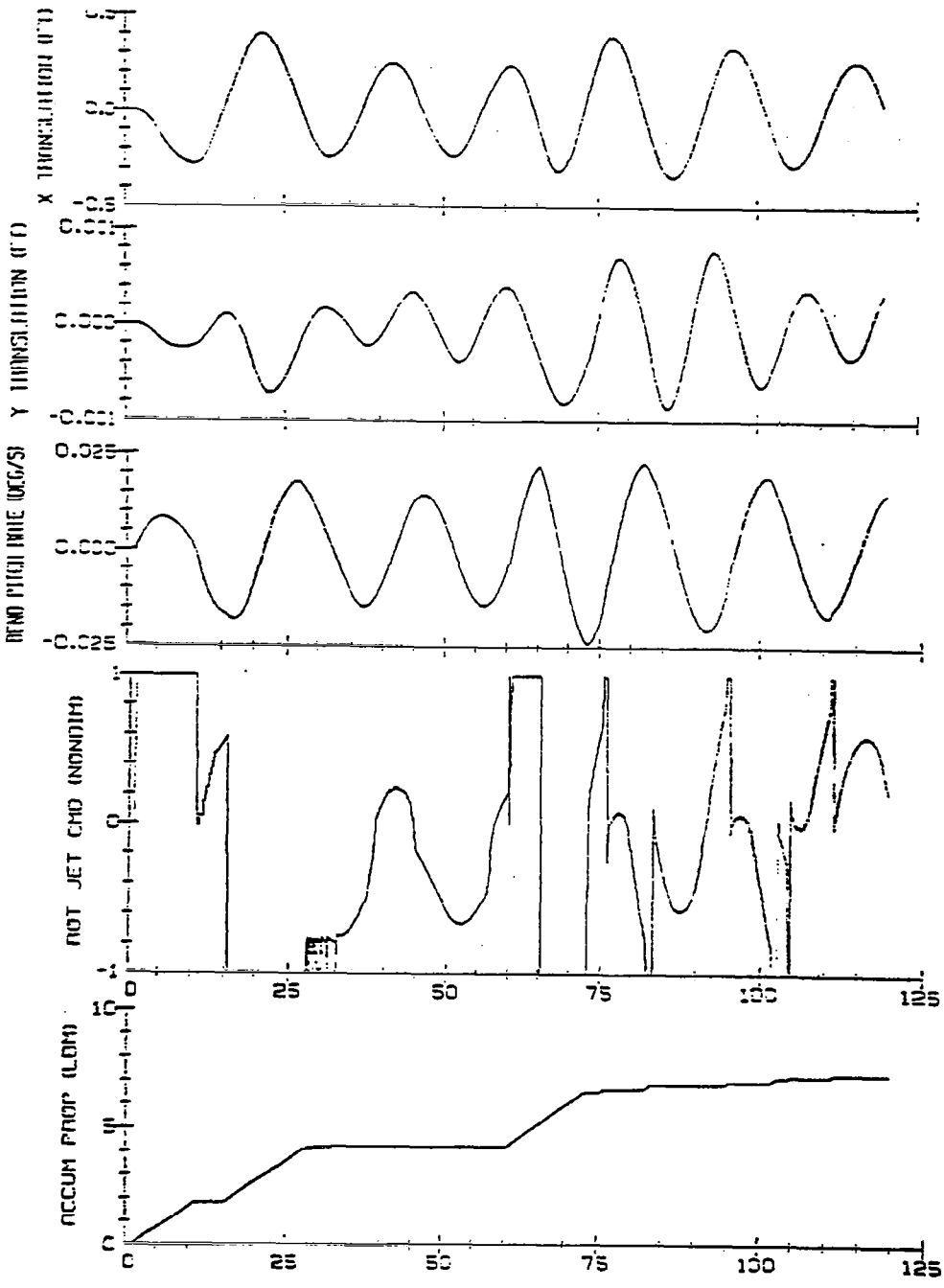

5 deg pitch with rl = .02 deg/sec, db = 1 deg with an attitude hold at 60 sec with rl = .01 deg/sec, db = 1 deg

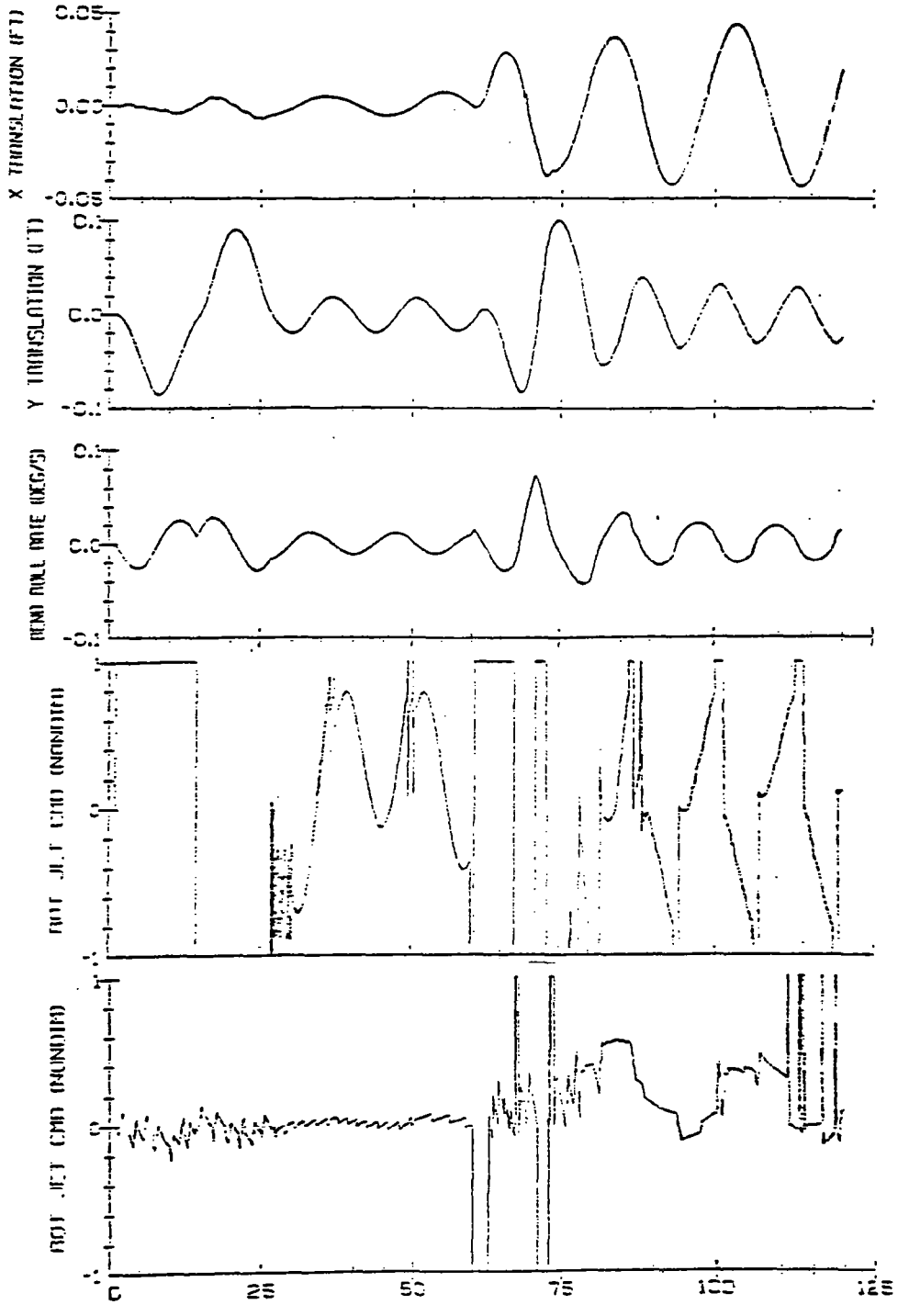

5 deg roll with r1 = .02 deg/sec, db = 1 deg with an attitude hold at 60 sec with r1 = .01 deg/sec, db = 1 deg

The Three Degree of Freedom Payload Simulation for Orbiter/Payload Parametric Studies

The General Dynamics Beam

- Base Properties
  - I_{xx} payload/I_{xx} vehicle = .698
  - f_{roll} .0642 Hz
    f_{pitch} .049 Hz
    f_{yaw} .667 Hz
- Results with base model
  - payload diverges in pitch
  - oscillatory jet firings after rate limit change
- Trends with parameter changes
  - vehicle oscillations are greatest at f_{roll} = .046 Hz
  - behavior insensitive to yaw frequency and I_{zz} payload changes
  - increasing rate limits and deadbands can limit small oscillations
  - vehicle oscillations increase as payload inertia increases

The last four figures give results from the parametric study. The first case is for a three-degree-of-freedom model of the GD beam. The second is for a payload with a roll bending frequency of 0.02 Hz and a larger inertia ratio. In the latter case a more severe oscillatory rotation command is seen and the vehicle maneuvering is more sluggish.

5° Roll Maneuver

rl = .02 °/sec , db = .5°

at 60 sec set

rl = .01 °/sec , db = .1°

With

General Dynamics Beam as the Payload

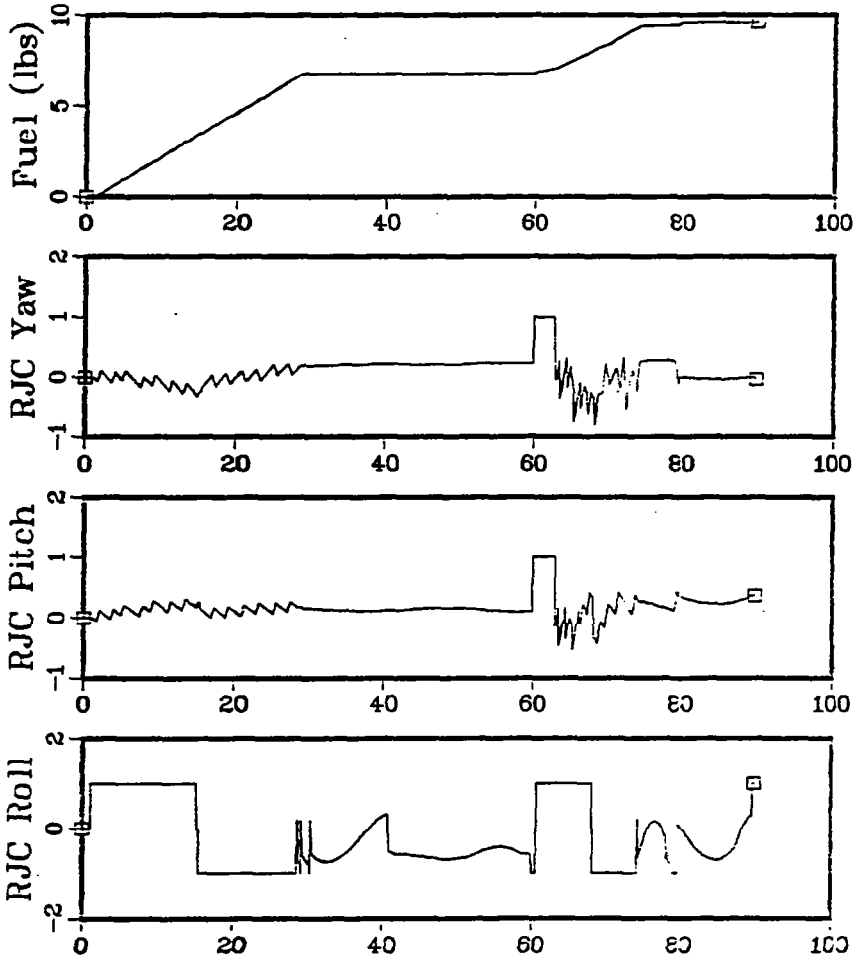

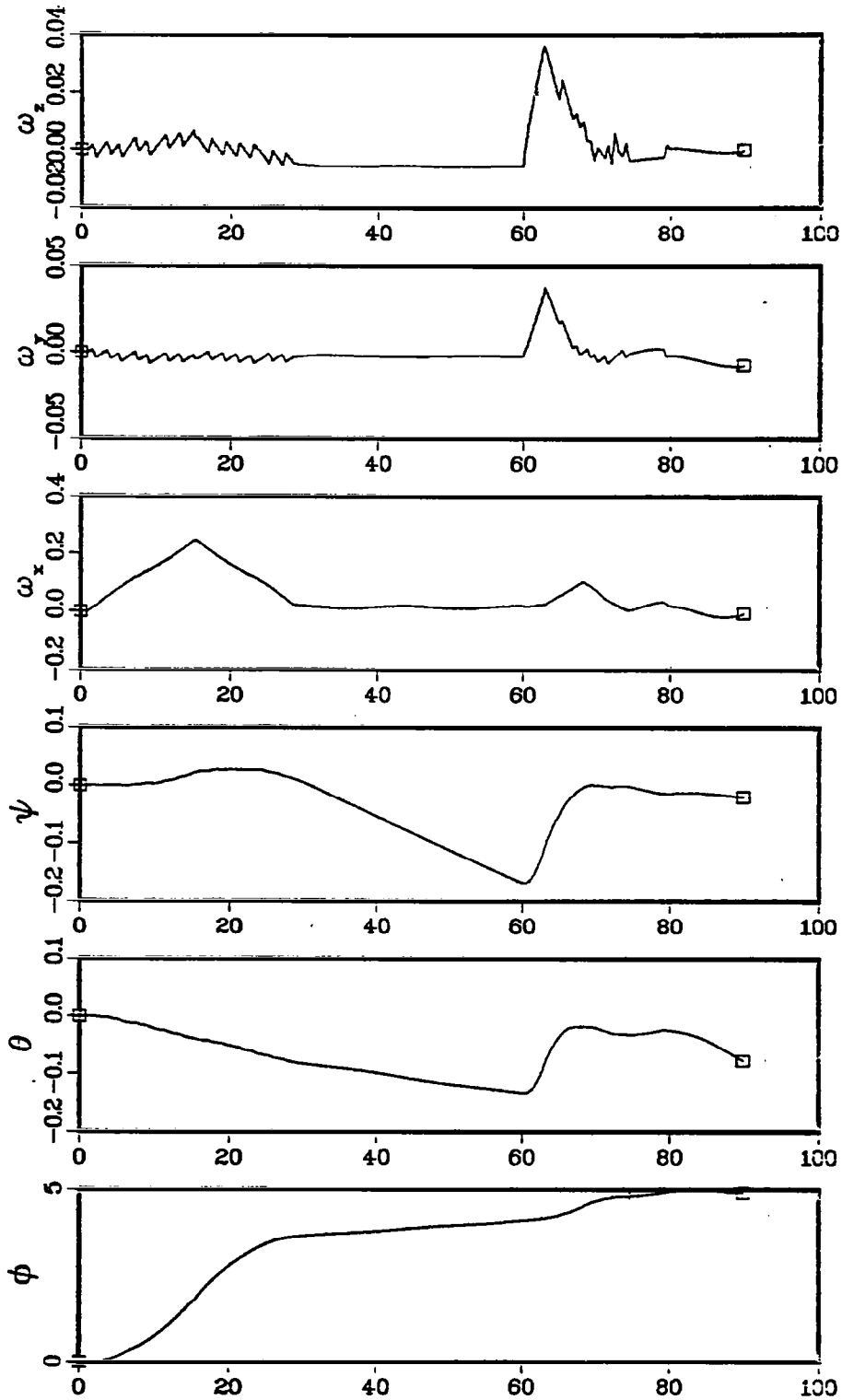
ω_z
0.04
0.02
0.00
−0.02
0
20
40
60
80
100
ω_y
0.05
0.00
−0.05
ω_x
0.4
0.2
0.0
−0.2
ψ
0.1
0.0
−0.1
−0.2
θ
ϕ
5
0

5° Roll Maneuver

rl = .02 °/sec , db = .5°

at 60 sec set

rl = .01 °/sec , db = .1°

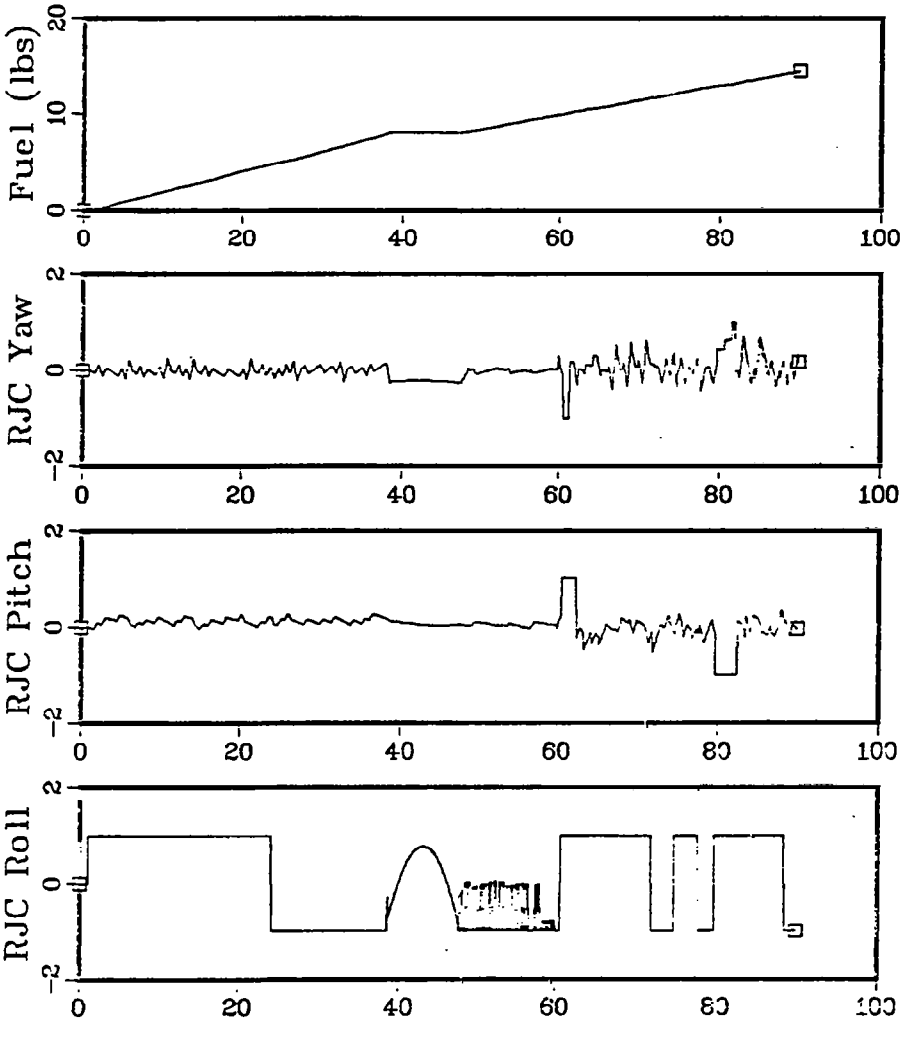

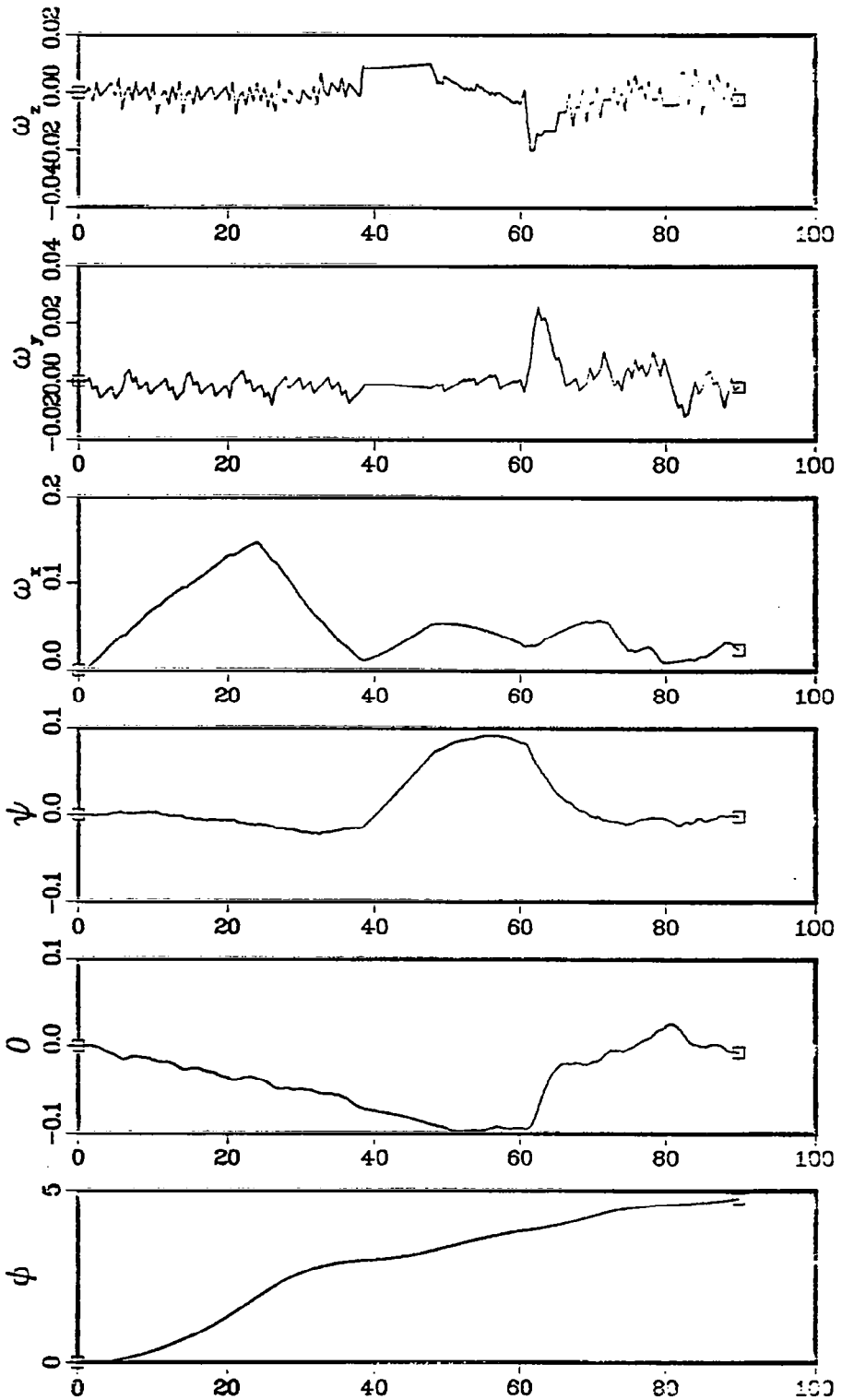
ω_z
0.02
0.00
−0.02
−0.04
0
20
40
60
80
100
ω_y
0.04
0.02
0.00
−0.02
ω_x
0.2
0.1
0.0
ψ
0.1
0.0
−0.1
θ
ϕ
5
0

LARGE SPACE STRUCTURES CONTROLS RESEARCH AND DEVELOPMENT AT MARSHALL SPACE FLIGHT CENTER - STATUS AND FUTURE PLANS

H. Buchanan
Marshall Space Flight Center
Systems Dynamics Laboratory
Huntsville, Alabama

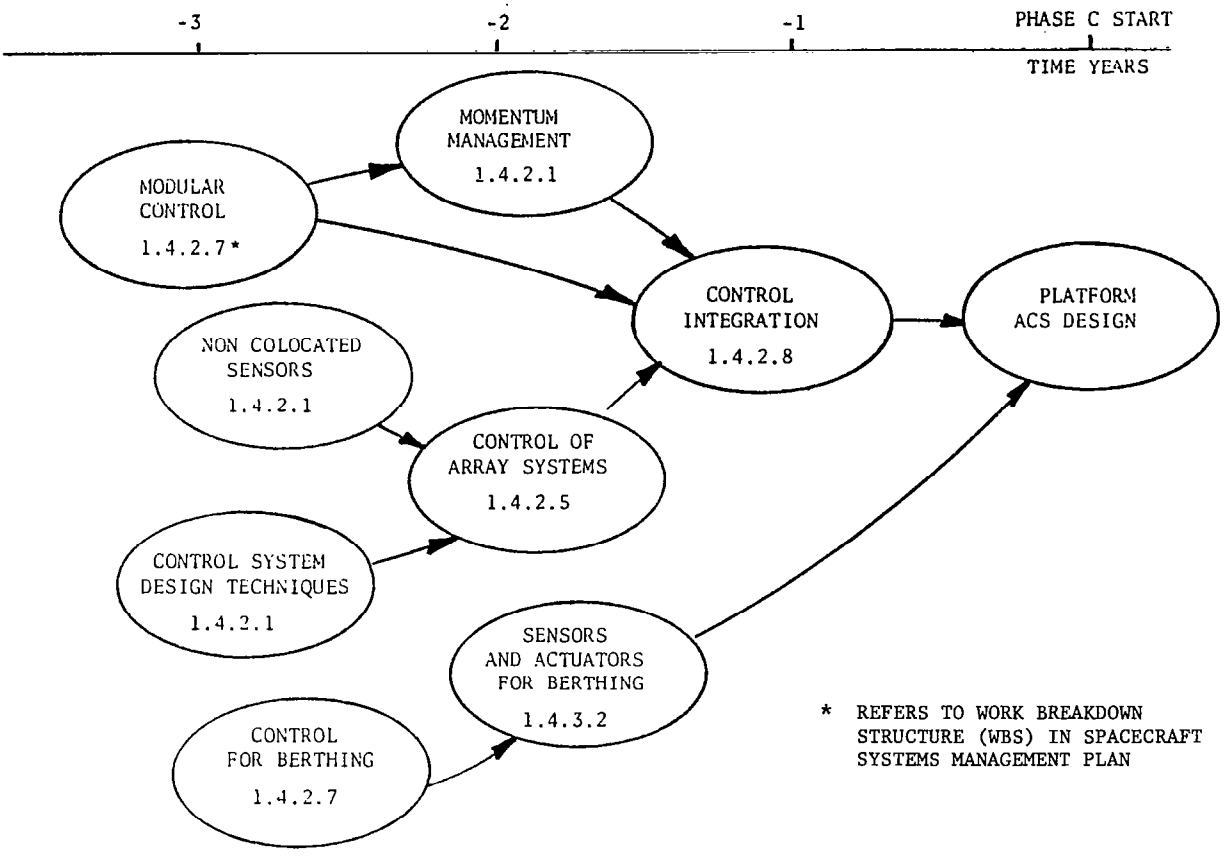

OBJECTIVE I: STABILITY AND MODAL CONTROL

DEMONSTRATE THAT THE FIRST NINE MODES (THREE RIGID + SIX FLEX) OF THE SEPS TEST ARTICLE CAN BE ACTIVELY CONTROLLED.

FEATURES:

- **LOW FREQUENCY (f < 1 Hz).**
- **ACTIVE MODAL DAMPING – EXPERIMENT GOAL OF 10%.**
- **CONTROL OF ASYMMETRIC STRUCTURE WITH COUPLED MODES.**
- **INVESTIGATE EFFECT OF CONTROLLER SATURATION ON DYNAMICS.**

SEPS SOLAR ARRAY FLIGHT TEST MODES

FREQUENCY Hz	DESCRIPTION
0	RIGID BODY
0	RIGID BODY
0	RIGID BODY
.032	OUT OF PLANE* BENDING
.035	IN PLANE BENDING + TORSION**
.059	IN PLANE BENDING + TORSION
.096	OUT OF PLANE BENDING
.117	IN PLANE BENDING + TORSION
.165	OUT OF PLANE BENDING

*PLANE OF SOLAR BLANKET
**TORSION OF MAST

OBJECTIVE: TO DEVELOP A MULTILEVEL CONTROL APPROACH WHICH SUPPORTS A MODULAR OR BUILDING BLOCK APPROACH TO THE BUILDUP OF SPACE PLATFORMS.

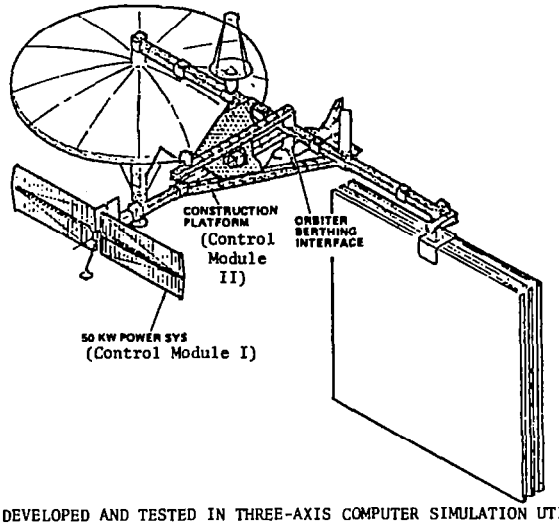

OUTLOOK: CONCEPT HAS BEEN DEVELOPED AND TESTED IN THREE-AXIS COMPUTER SIMULATION UTILIZING A FIVE-BODY MODEL OF A BASIC SPACE PLATFORM MODULE. ANALYTICAL EFFORTS HAVE CONTINUED TO FOCUS ON EXTENSION OF THE BASIC THEORY AND SUBSEQUENT APPLICATION.

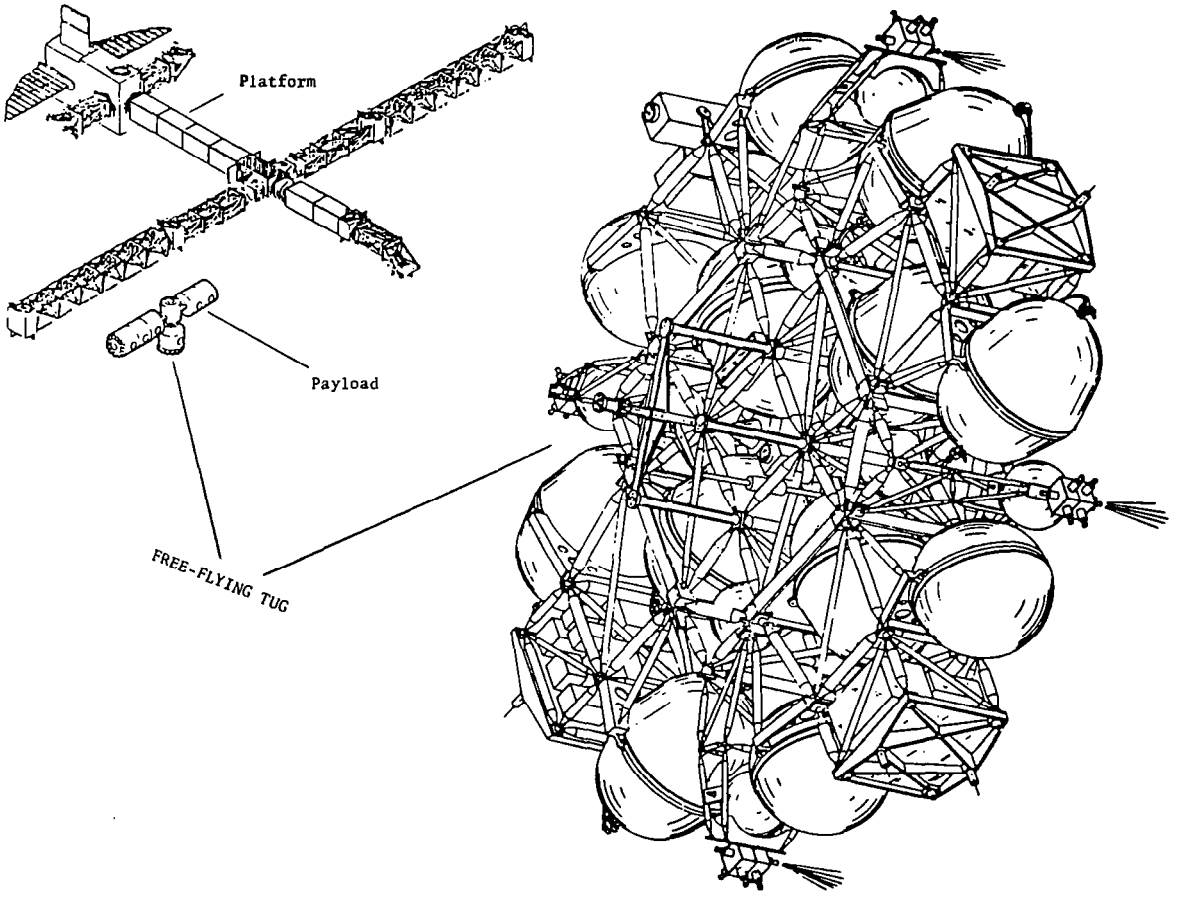

DEPLOYABLE ANTENNA SURFACE SHAPE CONTROL

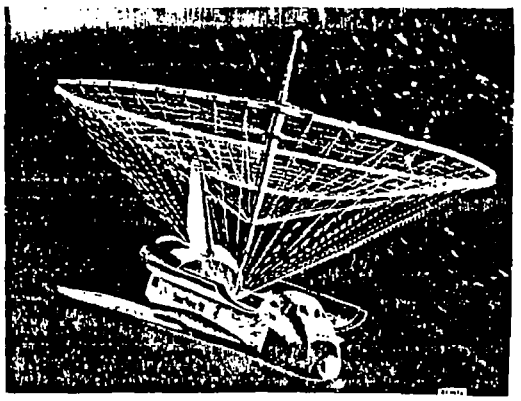

- OBJECTIVE - DEVELOP PRELIMINARY SPECIFICATIONS FOR A FLIGHT EXPERIMENT TO EVALUATE SEVERAL ALGORITHMS FOR CONTROLLING THE SHAPE OF LSS.

- STATEMENT OF WORK SUMMARY
  - DEMONSTRATE ANALYTICALLY THE FEASIBILITY FOR SUCH AN EXPERIMENT.
  - SPECIFY HARDWARE AND SOFTWARE REQUIREMENTS.
  - IDENTIFY REQUIREMENTS WHICH WOULD IMPACT CURRENT DESIGN.
  - DEFINE A FLIGHT TEST PLAN.

SAFE CONTROL EXPERIMENT

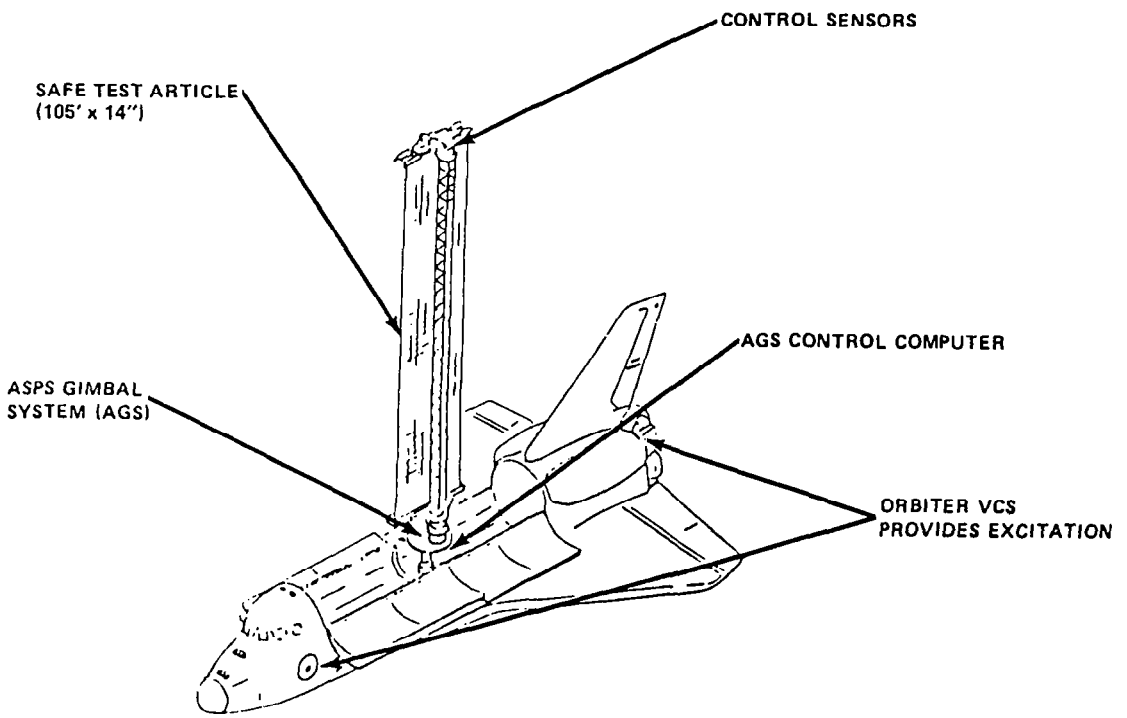

OBJECTIVE II: DISTURBANCE ISOLATION AND LOAD ALLEVIATION DURING MANEUVERS

DEMONSTRATE THAT DISTURBANCES ORIGINATING IN THE ORBITER (VCS FIRINGS AND CREW MOTION) CAN BE EFFECTIVELY ISOLATED FROM THE TEST ARTICLE BY MEANS OF SOFTWARE AND ACTIVE CONTROL. IN A SIMILAR MANNER LOADS IMPOSED ON THE STRUCTURE BY MANEUVERING WILL BE ALLEVIATED.

- 1×10^{-3} g DISTURBANCE LEVEL.
- 33 NM TORQUE ALLEVIATION.

OBJECTIVE III: POINTING

DEMONSTRATE CONTROLLER CAN POINT BASE OF APPENDAGE TO 1 $\widehat{\text{sec}}$ ACCURACY (EXPERIMENT GOAL). NO STAR TRACKER SUN SENSOR INPUT WILL BE USED AND PERIOD OF PERFORMANCE WILL BE SHORT TO MINIMIZE RATE GYRO DRIFT.

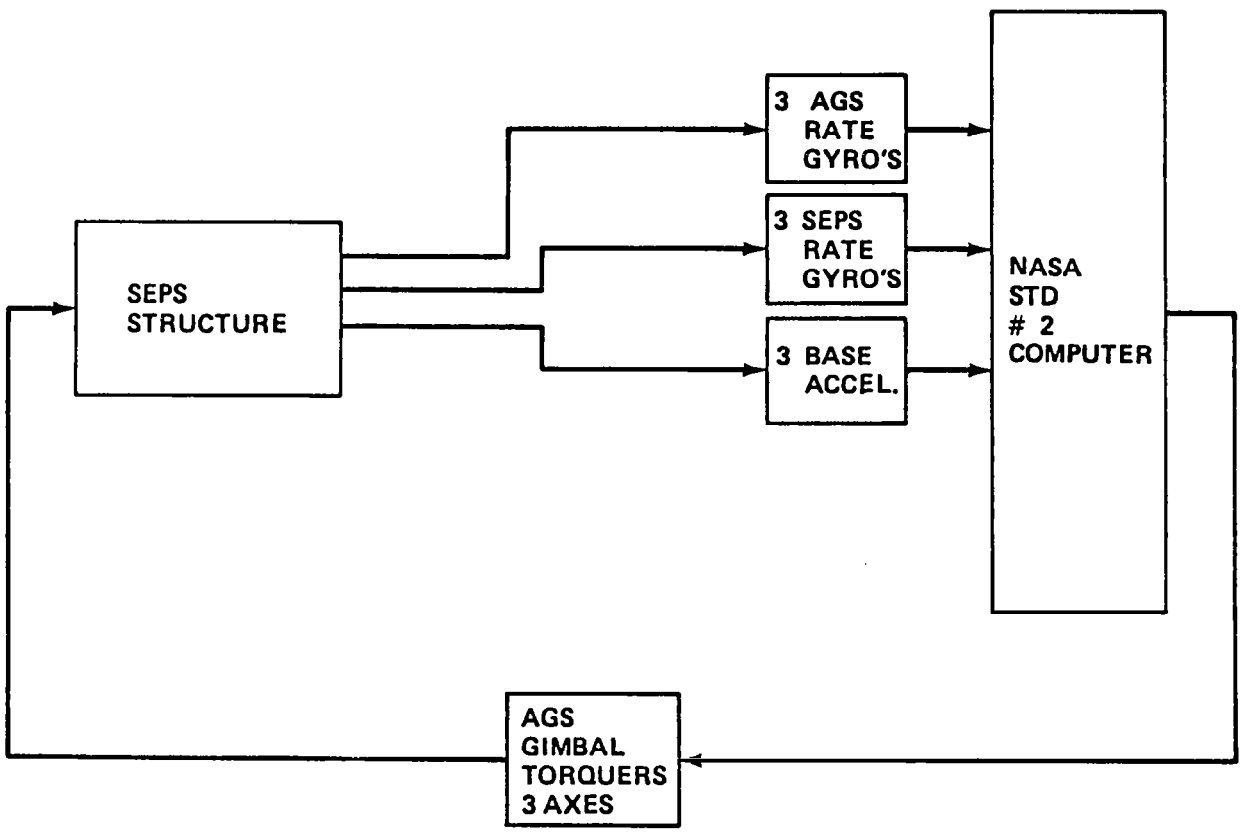

CONTROL GROUND TEST SCHEMATIC

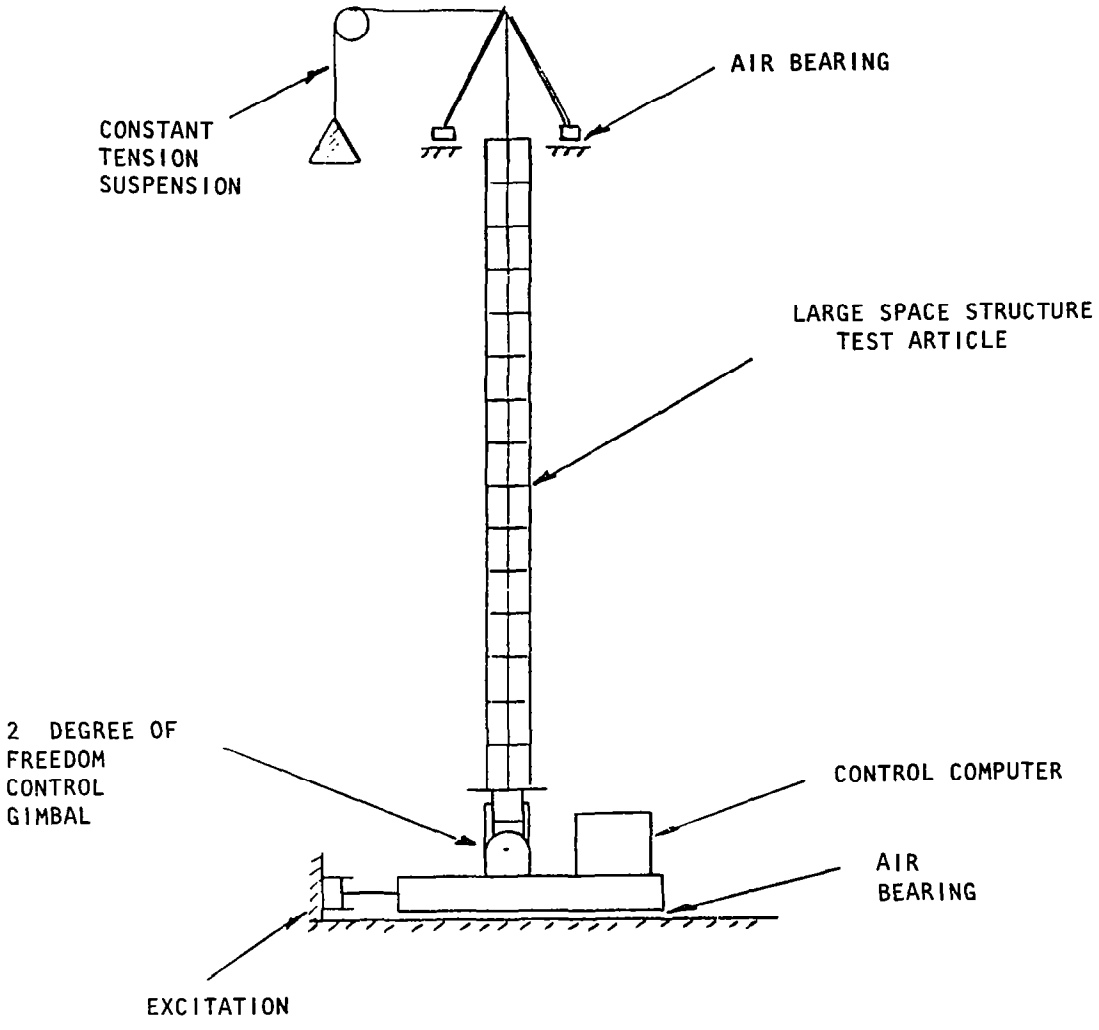

Research on the Control of Large Space Structures*

E. D. Denman
Department of Electrical Engineering
University of Houston
Houston, Texas

*Paper not presented at conference. This work was partially supported by NASA Langley Research Center under grant NSG-1603.

INTRODUCTION

The research effort on the control of large space structures at the University of Houston has concentrated on the mathematical theory of finite-element models; identification of the mass, damping, and stiffness matrix; assignment of damping to structures; and decoupling of structure dynamics. The objective of the work has been and will continue to be the development of efficient numerical algorithms for analysis, control, and identification of large space structures. The major consideration in the development of the algorithms has been the large number of equations that must be handled by the algorithm as well as sensitivity of the algorithms to numerical errors.

The finite-element model that has been used in the linear second-order matrix differential equation

$$\frac{Md^2x(t)}{dt^2} + \frac{\bar{C}dx(t)}{dt} + \bar{K}x(t) = f(t) \tag{1}$$

where $M \varepsilon R^{m \times m}$ is the mass matrix, $\bar{C} \varepsilon R^{m \times m}$ is the damping matrix, $\bar{K} \varepsilon R^{m \times m}$ is the stiffness matrix, $x(t) \varepsilon R^{m \times 1}$ is the node displacement vector, and $f(t) \varepsilon R^{m \times 1}$ is the forcing function vector.

The Laplace transform of equation (1) gives the matrix equation

$$[Ms^2 + \bar{C}s + \bar{K}]x(s) = B(s) \tag{2}$$

where $B(s)$ contains the initial condition information as well as the forcing function. If s is replaced in equation (2) by λ, equation (2) then takes the form of a lambda matrix:

$$\bar{A}(\lambda)X(\lambda) = B(\lambda) \tag{3}$$

If it is assumed that the initial conditions are zero and no forcing function is present, then

$$\bar{A}(\lambda)X(\lambda) = [M\lambda^2 + \bar{C}\lambda + \bar{K}]X(\lambda) \tag{4}$$

is the homogeneous equation that will be of interest. The latent roots λ_i of $A(\lambda)$ are given by

$$\det \bar{A}(\lambda) = \det[M\lambda^2+\bar{C}\lambda+\bar{K}] = 0 \tag{5}$$

and the latent vectors y_i are obtained from

$$\bar{A}(\lambda_i)y_i = [M\lambda_i^2+\bar{C}\lambda_i+\bar{K}]y_i = 0$$

provided that all latent roots are distinct, of multiplicity one.

Lancaster (ref. 1) and Dennis et al. (ref. 2), as well as others, have published material on lambda matrices. One of the tasks during the past research period has been to consider their work as well as extensions of the algebraic theory of lambda matrices for the control of structures.

ALGEBRAIC THEORY OF LAMBDA MATRICES

A comprehensive treatment of the algebraic theory of lambda matrices cannot be presented in this short paper. Only the essentials necessary to understand the damping assignment problem will be given.

Consider the lambda matrix

$$\bar{A}(\lambda) = Q[I\lambda^2+C\lambda+K]Q^T = QA(\lambda)Q^T \tag{6}$$

where Q is the Cholesky matrix of the decomposition of $M = QQ^T$. The normalization process in equation (6) will retain the symmetry of C and K. The lambda matrix $A(\lambda)$ will be considered in the following work and it will be assumed that the latent roots of $A(\lambda)$ appear in conjugate pairs as well as being distinct. This restriction is not necessary but is made to simplify the analysis.

It can be shown that the matrix

$$A_c = \begin{bmatrix} 0 & I \\ -K & -C \end{bmatrix} \tag{7}$$

has eigenvalues λ_i that are equal to the latent roots of $A(\lambda)$. The right and left eigenvectors of A_c contain the right and left latent vectors of $A(\lambda)$ with

$$y_{ci} = \begin{bmatrix} y_i \\ \lambda_i y_i \end{bmatrix} \tag{8}$$

and

$$z_{ci} = \begin{bmatrix} (\lambda_i I + C) z_i \\ z_i \end{bmatrix} \tag{9}$$

where y_{ci} and z_{ci} are the right and left eigenvectors, respectively. An eigenprojector, P_i, will be defined as the matrix

$$P_i = \frac{y_{ci} z_{ci}^T}{z_{ci}^T y_{ci}} \tag{10}$$

where the matrix A_{ci} defined by

$$A_{ci} = P_i A_c = A_c P_i \tag{11}$$

will have the same eigenvectors as A_c but all eigenvalues will be zero except for λ_i, which will be the same as in A_c. The eigenprojectors are the matrix residues of the partial fraction expansion of $[A_c(\lambda)]^{-1}$ with

$$[A_c(\lambda)]^{-1} = \sum_{i=1}^{2m} \frac{P_i}{\lambda - \lambda_i} \tag{12}$$

where

$$P_i = \lim_{\lambda \to \lambda_i} (\lambda - \lambda_i)[A_c(\lambda_i)]^{-1} \tag{13}$$

A latent projector will be defined as the matrix residues of the partial fraction expansion of $[A(\lambda)]^{-1}$ where

$$[A(\lambda)]^{-1} = \sum_{i=1}^{2m} \frac{\hat{P}_i}{(\lambda-\lambda_i)} \tag{14}$$

with

$$\hat{P}_i = \lim_{\lambda\to\lambda_i} (\lambda-\lambda_i)[A(\lambda)]^{-1} \tag{15}$$

The latent projectors are also given by

$$\hat{P}_i = \frac{y_i z_i^T}{z_i^T \frac{dA(\lambda_i)}{d\lambda} y_i} \tag{16}$$

where y_i and z_i are the latent vectors of $A(\lambda)$.

To complete the limited discussion of the algebraic theory, the relationship that exists between the eigenprojectors and latent projectors must be given. By inverting $A_c(\lambda)$ it can be shown that

$$P_i = \hat{P}_i \begin{bmatrix} \lambda_i I+C & I \\ -K & \lambda_i I \end{bmatrix} \tag{17}$$

with the past definitions holding.

ASSIGNMENT OF DAMPING

An algorithm to assign damping to a particular undamped mode has been developed, although the theory has not been fully explored at this time. Considerable work remains to be carried out to develop and test a comprehensive algorithm. Therefore the material in this section is only preliminary.

Consider the undamped structure with the associated lambda matrix

$$A(\lambda) = I\lambda^2+K \tag{18}$$

If it is assumed that K is symmetric and positive definite then all latent roots of $A(\lambda)$ lie along the $j\omega$ axis. Since K is positive definite all of its eigenvalues will be real with $\bar{\lambda}_i = \omega_{ni}^2$, and the eigenprojectors of K are given by

$$(\bar{\lambda}I-K)^{-1} = \sum_{i=1}^{m} \frac{\bar{P}_i}{(\bar{\lambda}-\bar{\lambda}_i)} \tag{19}$$

where it can be shown that P_i is given by

$$\bar{P}_i = \hat{P}_i \quad \lambda_i + \hat{P}_i^* \quad \lambda_i^* \tag{20}$$

which will be defined as the augmented latent projector. It is not difficult to show that the undamped A_c is

$$A_{cu} = \begin{bmatrix} \sum_{i=1}^{m} (\hat{P}_i\lambda_i^2+\hat{P}_i^*\lambda_i^{*2}) & \sum_{i=1}^{m} (\hat{P}_i\lambda_i+\hat{P}_i^*\lambda_i^*) \\ -\sum_{i=1}^{m} (\hat{P}_i\lambda_i+\hat{P}_i^*\lambda_i^*)K & \sum_{i=1}^{m} (\hat{P}_i\lambda_i^2+\hat{P}_i^*\lambda_i^{*2}) \end{bmatrix} \tag{21}$$

but since the undamped matrix is

$$A_{cu} = \begin{bmatrix} 0 & I \\ -K & 0 \end{bmatrix} \tag{22}$$

then

$$\sum_{i=1}^{m} (\hat{P}_i\lambda_i^2+\hat{P}_i^*\lambda_i^{*2}) = 0 \tag{23}$$

$$\sum_{i=1}^{m} (\hat{P}_i\lambda_i+\hat{P}_i^*\lambda_i^*) = I \tag{24}$$

The damped case has a similar form with the exception that the upper diagonal block is modified with

$$A_{cd} = \begin{bmatrix} \sum_{i=1}^{m} (\hat{P}_i\lambda_i^2+\hat{P}_i^*\lambda_i^{*2}+C\lambda_i+C\lambda_i^*) & \sum_{i=1}^{m} (\hat{P}_i\lambda_i+\hat{P}_i^*\lambda_i^*) \\ -\sum_{i=1}^{m} (\hat{P}_i\lambda_i+\hat{P}_i^*\lambda_i^*)K & \sum_{i=1}^{m} (\hat{P}_i\lambda_i^2+\hat{P}_i^*\lambda_i^{*2}) \end{bmatrix} \tag{25}$$

$$= \begin{bmatrix} 0 & I \\ -K & -C \end{bmatrix}$$

Suppose now that the undamped structure is to have damping added to the jth mode (i.e., λ_j and λ_j^*) and all other modes are to remain undamped. Using equations (21) and (22), A_c becomes

$$A_{cd} = \begin{bmatrix} \sum_{\substack{i=1 \\ i\neq j}}^{m} (\hat{P}_i\lambda_i^2+\hat{P}_i^*\lambda_i^{*2}) & \sum_{\substack{i=1 \\ i\neq j}}^{m} (\hat{P}_i\lambda_i+\hat{P}_i^*\lambda_i^*) \\ -\sum_{\substack{i=1 \\ i\neq j}}^{m} (\hat{P}_i\lambda_i+\hat{P}_i^*\lambda_i^*)K & \sum_{\substack{i=1 \\ i\neq j}}^{m} (\hat{P}_i\lambda_i^2+\hat{P}_i^*\lambda_i^{*2}) \end{bmatrix} +$$

$$\begin{bmatrix} (\hat{P}_j\lambda_j^2+\hat{P}_j^*\lambda_j^{*2}+C_j\lambda_j+C_j\lambda_j^*) & \hat{P}_j\lambda_j+\hat{P}_j^*\lambda_j^* \\ -(\hat{P}_j\lambda_j+\hat{P}_j^*\lambda_j^*)K & \hat{P}_j\lambda_j^2+\hat{P}_j^*\lambda_j^{*2} \end{bmatrix} \tag{26}$$

which can be rewritten as

$$A_{cd} = \begin{bmatrix} 0 & \sum_{\substack{i=1 \\ i\neq j}}^{m} \overline{P}_i \\ -\sum_{\substack{i=1 \\ i\neq j}}^{m} \overline{P}_i K & 0 \end{bmatrix} + \begin{bmatrix} 0 & \overline{P}_j \\ -\overline{P}_j K & -C_j \end{bmatrix} \tag{27}$$

and also in the form

$$A_{cd} = A_{cd} \sum_{\substack{i=1 \\ i\neq j}}^{2m} P_i + A_{cd}P_j = A^{+}+A_j \tag{28}$$

The matrix A^{+} denotes the matrix constructed from the summation and A_j is the complement to A^{+}.

The last step in the algorithm is to recognize that A^{+} is orthogonal to A_j; thus

$$\begin{bmatrix} 0 & \sum_{\substack{i=1 \\ i\neq j}}^{m} \bar{P}_i \\ -\sum_{\substack{i=1 \\ i\neq j}}^{m} \bar{P}_i K & 0 \end{bmatrix} \begin{bmatrix} 0 & \bar{P}_j \\ -\bar{P}_j K & -C_j \end{bmatrix} = \begin{bmatrix} 0 & 0 \\ 0 & 0 \end{bmatrix} \tag{29}$$

Finally, C_j is the matrix that is orthogonal to $\sum_{\substack{i=1 \\ i\neq j}}^{m} \bar{P}_i$. The eigenprojector $\bar{P}_j$ must be orthogonal to all $\bar{P}_i$ as the set of eigenprojectors have the orthogonal property

$$\bar{P}_i\bar{P}_j = 0 \qquad i \neq j \tag{30}$$

The C_j matrices are therefore nothing more than $\alpha_j\bar{P}_j$ where α_j is a scaling constant. The trace of C_j is

$$\text{trace } (C_j) = \sum_{i=1}^{m} c_{ii,j} = 2\sigma_j \tag{31}$$

where trace $(\bar{P}_j) = 1$. The scaling constants are then used to place the latent roots of $A(\lambda)$ with

$$\sigma_j = \frac{\alpha_j}{2} \tag{32}$$

$$\omega_j^2 = \omega_{nj}^2 - \sigma_j^2 \tag{33}$$

An example will now be given to illustrate the algorithm. Let $C = 0$ and select K as

$$K = \begin{bmatrix} 300 & -200 \\ -200 & 350 \end{bmatrix}$$

which has eigenvalues $\pm j11.1105$ and $\pm j22.9468$. The augmented projectors are

$$\bar{P}_1 = \begin{bmatrix} 0.562017 & 0.496139 \\ 0.496139 & 0.437983 \end{bmatrix}$$

and

$$\bar{P}_2 = \begin{bmatrix} 0.437983 & -0.496139 \\ -0.496139 & 0.562017 \end{bmatrix}$$

The matrices

$$C_1 = \begin{bmatrix} 1 & 0.8827824 \\ 0.8827824 & 0.7793048 \end{bmatrix}$$

and

$$C_2 = \begin{bmatrix} 1 & -1.1327785 \\ -1.1327785 & 1.283187 \end{bmatrix}$$

are orthogonal to $\bar{P}_1$ and $\bar{P}_2$. Note that the columns in C_1 and C_2 can be scaled by constants and remain orthogonal to $\bar{P}_1$ and $\bar{P}_2$.

The eigenvalues of

$$A_c = \begin{bmatrix} 0 & I \\ -K & -C_j \end{bmatrix}$$

are given in the computed results below.

A(I,J) MATRIX

$$\begin{bmatrix} 0 & 0 & 1 & 0 \\ 0 & 0 & 0 & 1 \\ -300 & 200 & 0 & 0 \\ 200 & -350 & 0 & 0 \end{bmatrix}$$

EIGENVALUES	REAL	IMAGINARY
1	0	22.9468
2	0	-22.9468
3	3.04403E-22	11.1105
4	3.04403E-22	-11.1105

No damping

A(I,J) MATRIX

$$\begin{bmatrix} 0 & 0 & 1 & 0 \\ 0 & 0 & 0 & 1 \\ -300 & 200 & -1 & -.882783 \\ 200 & -350 & -.882783 & -.779305 \end{bmatrix}$$

EIGENVALUES	REAL	IMAGINARY
1	3.99893E-08	22.9468
2	3.99893E-08	-22.9468
3	- .889652	11.0748
4	- .889652	-11.0748

Damping in lowest mode

A(I,J) MATRIX

$$\begin{bmatrix} 0 & 0 & 1 & 0 \\ 0 & 0 & 0 & 1 \\ -300 & 200 & -1 & 1.13278 \\ 200 & -350 & 1.13278 & -1.28319 \end{bmatrix}$$

EIGENVALUES	REAL	IMAGINARY
1	-1.14159	22.9184
2	-1.14159	-22.9184
3	2.84795E-08	11.1105
4	2.84795E-08	-11.1105

Damping in highest mode

A(I,J) MATRIX

$$\begin{bmatrix} 0 & 0 & 1 & 0 \\ 0 & 0 & 0 & 1 \\ -300 & 200 & -1 & .125 \\ 200 & -350 & .125 & -1.03125 \end{bmatrix}$$

EIGENVALUES	REAL	IMAGINARY
1	-.570798	22.9399
2	-.570798	-22.9399
3	-.444827	11.1019
4	-.444827	-11.1019

Damping in both modes

The undamped system matrix and its eigenvalues are given first. The lowest mode was then damped with the system matrix and its eigenvalue given. The third test was to include damping for the highest mode where $C = C_2$. The last test was to combine the damping for the two modes with

$$C = \frac{1}{2}(C_1+C_2) = \alpha_1\overline{P}_1+\alpha_2\overline{P}_2 = 0.889655\overline{P}_1 + 1.141595\overline{P}_2$$

The system matrix and its eigenvalues are then given. It should be noted that the new values of σ_j of the two modes are

$$\sigma_1 = \frac{0.889652}{2} = 0.444827$$

and

$$\sigma_2 = \frac{1.141595}{2} = .570797$$

The algorithm allows damping to be assigned to all modes and to the prediction of the location of the system eigenvalues.

The major problem that remains to be resolved is that of constructing the $\bar{C}$ matrix, which is symmetric and positive definite as well as realizable. It will be assumed that $\bar{C}$ and $\bar{K}$ are tridiagonal with the off-diagonal elements having a smaller magnitude than the diagonal elements. The off-diagonal elements must be negative with positive diagonal terms.

IDENTIFICATION OF M, C, AND K

The quadrature algorithm for identifying the mass, damping, and stiffness matrices of a structure is still under study. The algorithm performs well with simulated data, but attempts to utilized data from the beam experiment at NASA Langley Research Center have not produced useable results. It is believed that the conditions on the beam during the data collection may not have satisfied the requirements of the algorithm.

The quadrature identification, as well as other algorithms, will receive major attention in the future. One of the major problems in developing an efficient algorithm is the availability of test data, either by computer simulation or from a test bed. The Langley Research Center experimental beam is a suitable test bed, but planning and running test data are costly and time consuming. Plans for the future include construction of an electronic analog test bed that will be low cost and will provide flexibility in the types of structures that can be simulated. The test bed will be used primarily in the development of the identification algorithm, but it can also be used for developing control algorithms.

SIMULATION OF STRUCTURES

Some of the preliminary work on designing a structures test bed at the University of Houston has been completed. The type of simulator considered is an electronic analog that will be constructed from low-cost operational amplifiers, resistors, and capacitors. Data acquisition will be handled by a PDP 11/70 computer for signal processing. The PDP 11/70 is equipped with analog-to-digital and digital-to-analog converters and has adequate storage to perform on-line data collection and processing.

CONCLUSIONS

Some of the work that has been supported under grant from NASA Langley Research Center has been described in this report. Preliminary details on the assignment of damping are covered, as well as some information on identification and simulation.

The identification work has not been described since the algorithm is given in reference 3. The simulation facility is still in the planning stage and a decision to build such a test bed has not been made. Further descriptions of this research are given in references 4 and 5.

REFERENCES

1. Lancaster, P.: Lambda Matrices and Vibrating Systems. Pergamon Press, N.Y., 1966.

2. Dennis, J. E., Jr.; Traub, J. F.; and Weber, R. P.: The Algebraic Theory of Matrix Polynomials. SIAM J. Numer. Analy., vol. 13, no. 6, Dec. 1976, pp. 831-845.

3. AIAA Guidance and Control Conference. A Collection of Technical Papers. Albuquerque, N.M., August 19-21, 1981.

4. Denman, E. D.: Roots of Real Matrices. Linear Alg. & Appl., vol. 36, 1981, pp. 133-139.

5. Denman, E. D.; and Leyva-Ramos, J.: Spectral Decomposition of a Matrix Using the Generalized Sign Matrix. Appl. Math. & Comp., vol. 8, no. 4, June 1981, pp. 237-250.

ACTIVE CONTROL OF A FLEXIBLE BEAM

Jeffrey P. Williams
NASA Langley Research Center
Hampton, Virginia

ACTIVE CONTROL OF A FLEXIBLE BEAM

Because of inherent low damping and high flexibility, large space structures may require some form of active control of their dynamics. Because of the apparent inability to accurately model the dynamics of these structures, methods for parameter adaptive control are now being developed at Langley. The process currently being studied is shown in the block diagram below. This approach uses a digital computer to process discrete sensor data, identify modal parameters, calculate modal control gains, and then convert the modal forces to real forces. The last two blocks are the topic of this presentation. Some of the problems considered are: (1) the possibility that there may be many modes to control with limited amounts of hardware, and (2) the required accuracy of identified structural parameters.

BACKGROUND:

- NEED TO CONTROL FLEXIBLE MOTION OF LARGE SPACE STRUCTURES
- ABILITY TO ACCURATELY MODEL THE DYNAMICS OF THESE STRUCTURES IS UNCERTAIN
- THEORY NOW BEING DEVELOPED FOR PARAMETER ADAPTIVE CONTROL OF THESE STRUCTURES

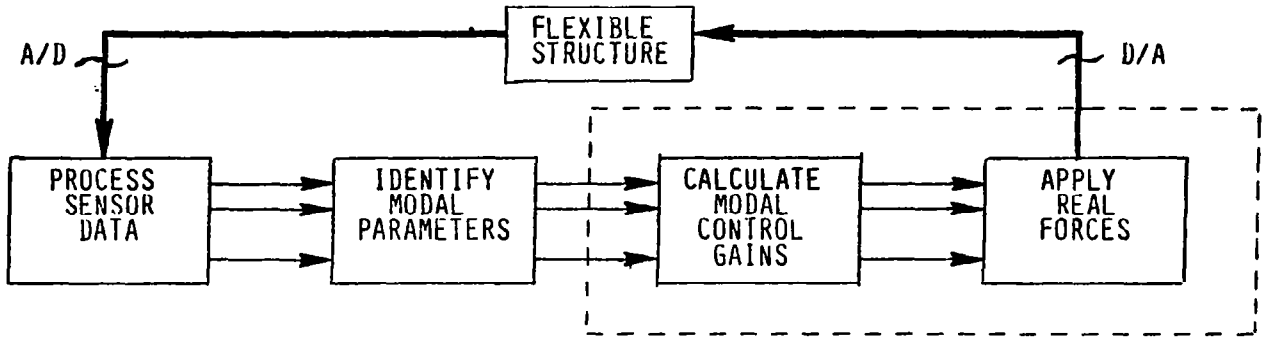

PROBLEMS:

- POSSIBLY MANY MODES TO CONTROL
- LIMITED HARDWARE (COMPUTATION, SENSORS, ACTUATORS)
- HOW WELL STRUCTURAL PARAMETERS MUST BE IDENTIFIED FOR CONTROL

RESEARCH TASK

The specific research task was to design a digital control scheme to suppress vibration of a homogeneous free-free beam. A digital computer simulation algorithm was then used to test (1) the effects of controlling more modes than available actuators, and (2) the sensitivity to identified structural parameters.

- DESIGN A DIGITAL CONTROL SCHEME TO SUPPRESS VIBRATION OF A HOMOGENEOUS FREE-FREE BEAM
- EXAMINE EFFECT ON STABILITY OF:
  - FEWER ACTUATORS THAN CONTROLLED MODES
  - ERRORS IN STRUCTURAL MODEL PARAMETERS
- TEST WITH AN EXISTING SIMULATION ALGORITHM

MATHEMATICAL MODEL

The continuous beam was modeled by using the SPAR finite element algorithm which generates mode shapes and frequencies. These were used to write a modal representation of the beam dynamics which was used to design the control gains.

- CONTINUOUS MODEL

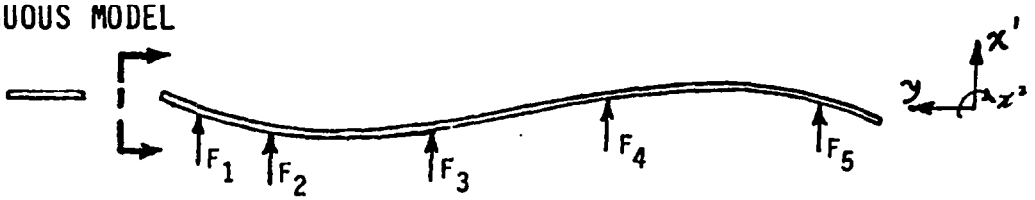

- FINITE ELEMENT MODEL OF BEAM
  - MODE SHAPES AND FREQUENCIES FOR 25 ELEMENT MODEL ARE GENERATED BY SPAR

$$[M]\ddot{\underline{x}} + [K]\underline{x} = \underline{F}$$

- MODAL REPRESENTATION

$$x = [E]\,q$$

$$\begin{bmatrix} \ddots & \\ & m_i \\ & & \ddots \end{bmatrix} \ddot{\underline{q}} + \begin{bmatrix} \ddots & \\ & k_i \\ & & \ddots \end{bmatrix} \underline{q} = \underline{u} \; ; \quad \underline{u} = [E]^T \underline{F}$$

  - SET OF 50 UNCOUPLED 2ND-ORDER SYSTEMS

- CONTROL SYSTEM DESIGNED USING THIS MODAL REPRESENTATION OF THE STRUCTURAL DYNAMICS

DISCRETE TIME MODEL

In order to simplify the digital simulation and prepare for eventual digital implementation, the modal equations of motion were discretized. This results in the scalar equation which shows the present modal amplitude to be a function of the past two amplitudes and the past two controls. There is a discrete time transformation analogous to the Laplace transform which results in a characteristic polynomial in z. The roots of this polynomial may be plotted in the complex plane with stability represented by magnitudes of less than 1. Analysis of the control system will be done primarily in this z-plane.

- NECESSARY FOR:
  - DESIGN OF DIGITAL SIMULATION
  - EVENTUAL DIGITAL IMPLEMENTATION
- DISCRETE EQUATION OF MOTION:

$$q_{(k)} = A_1 q_{(k-1)} + A_2 q_{(k-2)} + B_1 u_{(k-1)} + B_2 u_{(k-2)}$$

where $A = f(w, \tau)$, τ = sampling interval,

$B = f(w, \underline{e}, \tau)$, $\underline{e}$ = mode shapes.

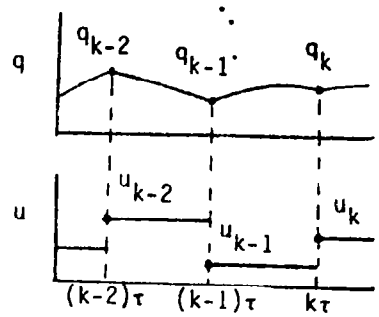

- DISCRETE TIME TRANSFORM (ANALOGOUS TO LAPLACE TRANS.) RESULTS IN A CHARACTERISTIC POLYNOMIAL IN Z:

$$0 = \sum_{i=1}^{n} c_i z^{i-1}$$

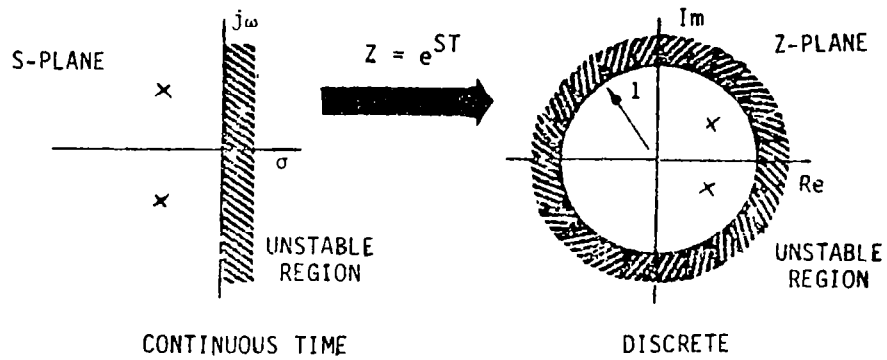

CONTROL DESIGN APPROACH

The modal control design approach is to choose desired closed-loop roots from which the modal controller gains can be calculated. The modal control forces may be calculated directly, and the actual control forces can be calculated using a pseudo-inverse.

- CHOOSE DESIRED CLOSED LOOP ROOTS FOR EACH MODE
- CALCULATE MODAL CONTROLLER GAINS
- CALCULATE MODAL CONTROL FORCES
- CONVERT MODAL FORCES TO ACTUATOR FORCES

DIGITAL CONTROL OF ONE MODE

The control of one mode is achieved by using the minimum order control law required for pole placement. This is of the same form as the modal equation of motion. The closed loop controller has a fourth-order characteristic equation as shown. The coefficients of this equation are determined from the desired closed-loop roots and are functions of the mode and control coefficients in the plant and control modal equations. The control objective is to achieve the desired roots defined by (a,b,c,d) by solving for the controller gains (C_1, C_2, D_1, D_2).

- MINIMUM ORDER CONTROL LAW FOR POLE PLACEMENT

$$u_{(k)} = C_1 q_{(k-1)} + C_2 q_{(k-2)} + D_1 u_{(k-1)} + D_2 u_{(k-2)}$$

  - NOTE SAME FORM AS PLANT MODEL

$$[q_{(k)} = A_1 q_{(k-1)} + A_2 q_{(k-2)} + B_1 u_{(k-1)} + B_2 u_{(k-2)}]$$

  - C'S & D'S ARE FOUR CONTROL GAINS

- CLOSED LOOP CONTROLLER

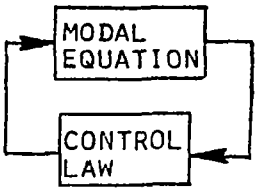

  - HAS DISCRETE TIME CHARACTERISTIC EQUATION

$$z^4 + a z^3 + b z^2 + c z + d = 0$$

where $\{a, b, c, d\} = f(A, B, C, D)$.

- CONTROL OBJECTIVE:

  - ACHIEVE DESIRED CLOSED LOOP ROOTS (AS DEFINED BY a,b,c,d) BY CALCULATING THE CONTROL GAINS.

CLOSED-LOOP CHARACTERISTICS

The control problem is shown in the block diagram below. The parameter uncertainties affect the calculation of the modal controller gains and a pseudo-inverse results in a least squares type error in the actual forces applied to the beam. A typical set of closed-loop roots is shown in each of the two complex plane plots. The design criterion is to place the roots of the controlled modes on a constant damping line in the s-plane. This line maps onto a constant-radius circle on the complex z-plane, with uncontrolled roots on the unit circle.

- CONTROL PROBLEM

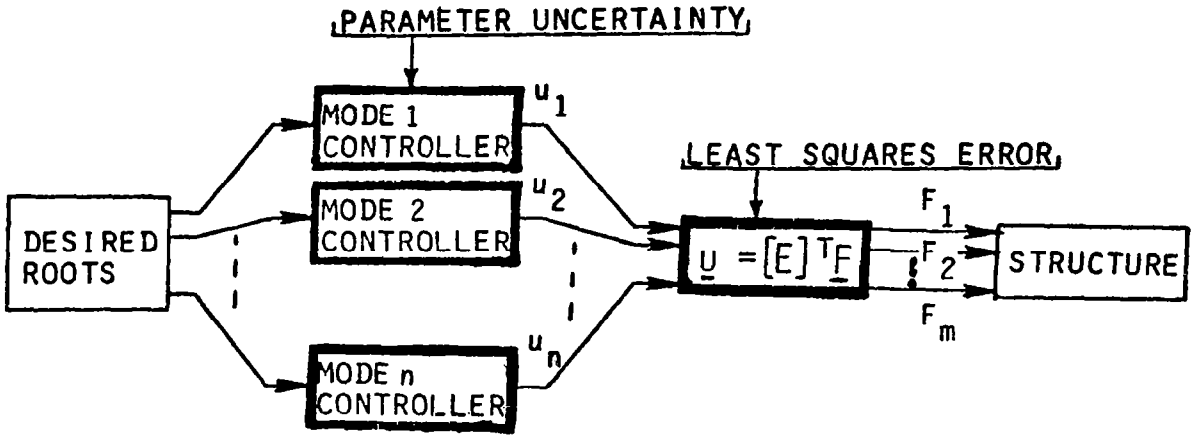

- REPRESENTATION OF CLOSED LOOP DYNAMICS

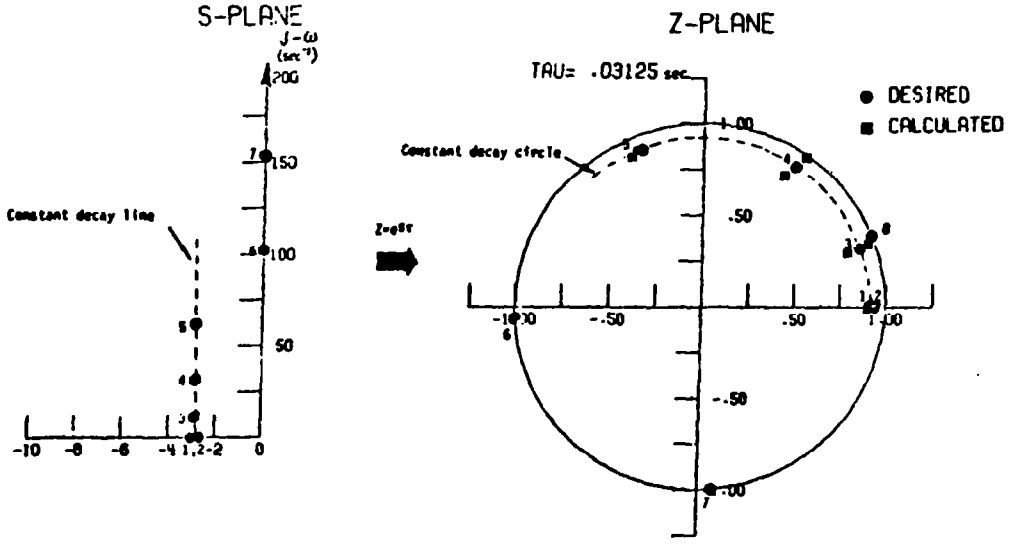

RESULTS - CASE 1

A baseline set of results is shown below. Exact parameters are used to calculate the control gains and five modes are controlled with five actuators. Note that all roots are calculated exactly so that all modal amplitudes have the same decay envelope. Also, mode six, which is not controlled, does show "minor" excitation and continues to "ring" after control to the other modes is stopped. This is not evident from the figure.

• CASE I: EQUAL NUMBER OF ACTUATORS AND CONTROLLED MODES

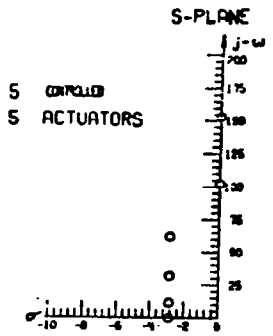

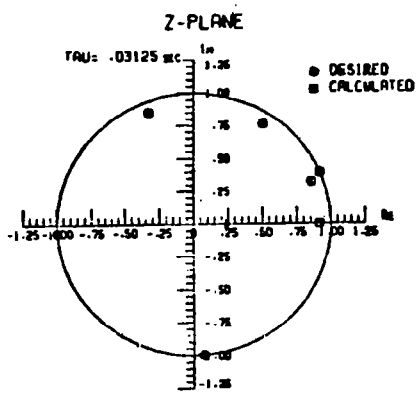

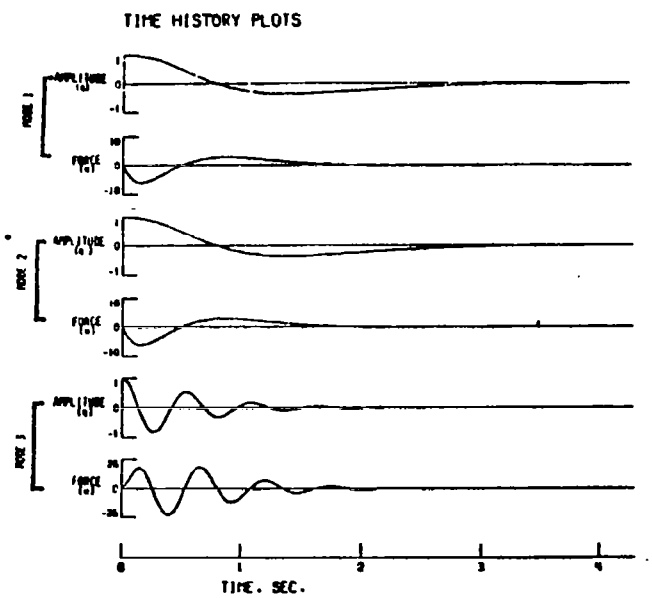

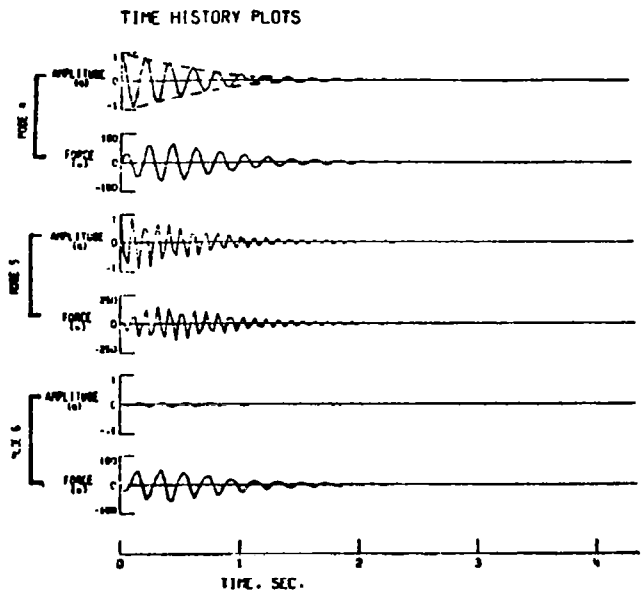

RESULTS - CASE II

This next case illustrates an attempt to control more modes than available actuators. Here it is no longer possible to solve exactly for the desired roots, and one root does become unstable, as shown by the increasing amplitude of the fourth mode.

- CASE II: FEWER ACTUATORS THAN CONTROLLED MODES - UNSTABLE

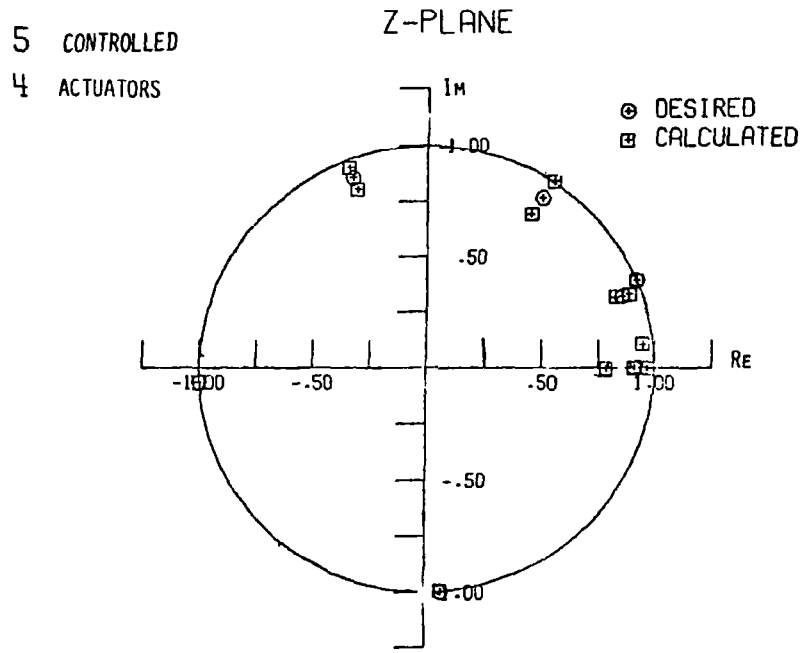

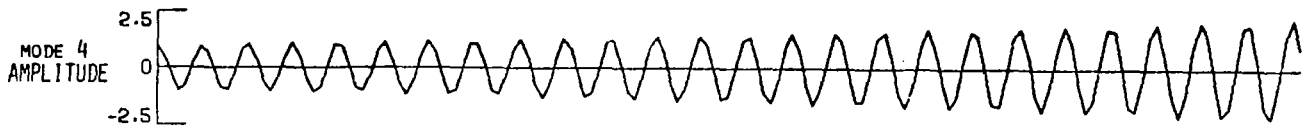

RESULTS - CASE III

In the third case it is shown that attempting to control more modes than available actuators does not necessarily mean the system will be unstable. Note here that the calculated roots are closer to the desired roots and that, while the fourth mode is near the unit circle, it now is slightly stable. This can be explained by considering that the additional actuator and mode provide one more data point for the least squares fit.

- CASE III: FEWER ACTUATORS THAN CONTROLLED MODES - STABLE

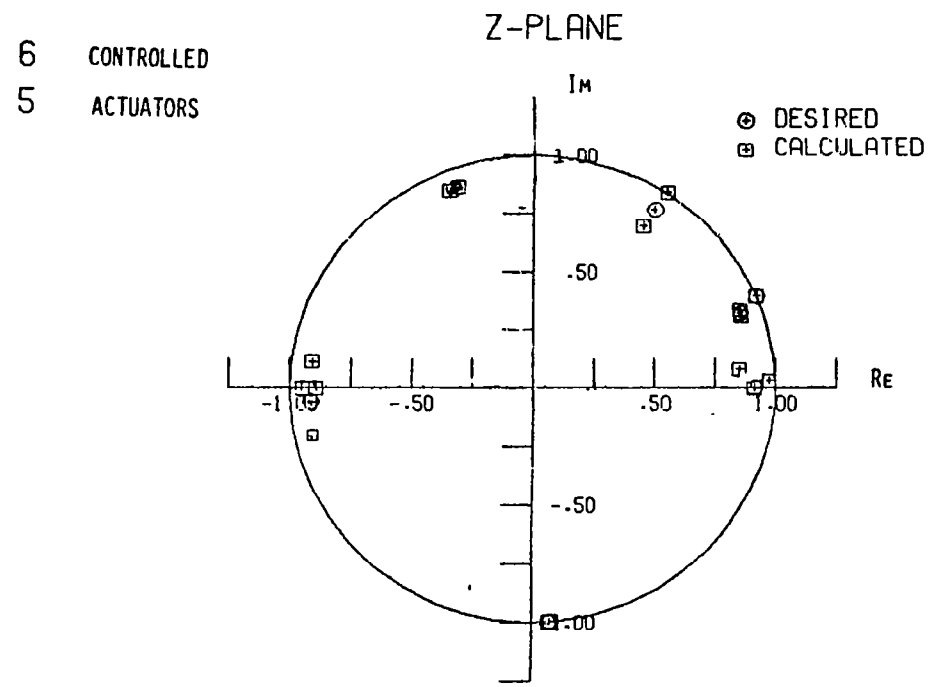

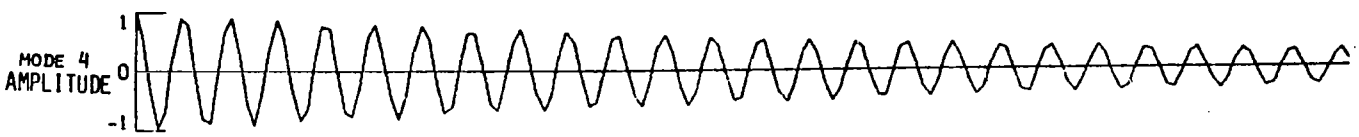

PARAMETER ERROR SENSITIVITY

The results of the parameter error sensitivity study are shown below. Error was placed on the modal frequency and damping parameters of the modes selected for control. Experimental results show that the parameter estimator may have errors on the order of ±5 percent. The locus of roots calculated using a parameter error range of ±20 percent is plotted below. The magnitude of the error at which the modes became unstable is summarized in the table. Note that as the mode number increases, the sensitivity decreases for the first three modes. The high sensitivity of mode six in case III is unexplained at this time.

- ERROR ON MODAL FREQUENCY AND DAMPING PARAMETERS ONLY

$$q^i_{(k)} = \underline{A^i_1}\, q_{(k-1)} + \underline{A^i_2}\, q_{(k-2)} + B^i_1\, u_{(k-1)} + B^i_2\, u_{(k-2)}$$

- NO ERROR ON RIGID BODY PARAMETERS
- BASED ON EXPERIMENTAL PARAMETER ESTIMATE ERRORS OF ± 5%

5 CONTROLLED
5 ACTUATORS

Z-PLANE

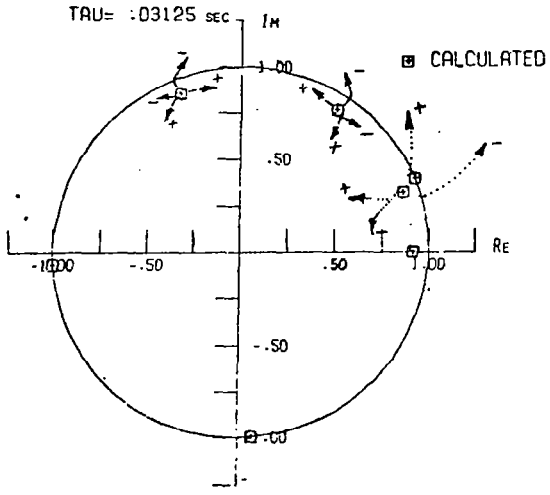

CASE	PARAMETER ERROR AT INSTABILITY			
	MODE 3	MODE 4	MODE 5	MODE 6
I 5 CONT.	-10 %	-12%	-14%	
5 ACT.	+8 %	—	—	
II 5 CONT.	-6 %	0.0 %	-14 %	
4 ACT.	+14%	—	—	
III 6 CONT.	-8 %	-12 %	-16%	-2 %
5 ACT.	+8 %	—	—	+2 %

CONCLUSIONS

1. LIMITED ACTUATORS:

   - THIS DESIGN PROCESS YIELDS UNDESIRABLE CLOSED LOOP DYNAMICS WHEN THE NUMBER OF CONTROLLED MODES EXCEEDS THE NUMBER OF AVAILABLE ACTUATORS.

2. PARAMETER ERROR:

   - ERRORS WITHIN THE RANGE OF EXPERIMENTAL RESULTS CAN CAUSE INSTABILITY.

   - CONTROL SYSTEM MUST BE MADE MORE TOLERANT OF PARAMETER ERROR.

OPTIMAL DAMPING FOR A TWO-DIMENSIONAL STRUCTURE

W. D. Pilkey and B. P. Wang
University of Virginia
Charlottesville, Virginia

SYNTHESIS OF THE DAMPING MATRIX

FOR SPECIFIED DAMPING RATIOS

$$[M]\{\ddot{x}\} + [k]\{x\} = \{F\} \qquad \{x\} \text{ is } n \times 1$$

CONTROL FORCES

$$\{F\} = [B]\{u\} \qquad \{u\} \text{ is } A \times 1$$

A = number of actuators

$$\{u\} = -[D]\{\dot{x}\} \qquad [D] \text{ is } A \times n$$

or

$$\{F\} = -[C]\{\dot{x}\}$$

where

$$[C] = [B][D]$$

PROBLEM

Find C_{ij} such that

$$J = \sum_{i,j} | C_{ij} |$$

is minimized subject to the constraints

$$\zeta_\ell > \zeta_{\ell p} \quad \text{for } \ell = 1 \text{ to } L$$

and

$$C_{ii} > 0 \quad , \quad C_{ij} = C_{ji}$$

$\zeta_{\ell p}$ = prescribed damping ratios for the ℓth mode

Eigenvalue Problem:

$$(s^2[M] + s\,[C] + [K])\{\rho\} = \{0\}$$

with roots

$$s_\ell = -\zeta_\ell \omega_{\ell n} + j\omega_{\ell n}\sqrt{1 - \zeta_\ell^2}$$

DAMPED EIGENVALUE PROBLEM:

$$\{\dot{z}\} = \begin{bmatrix} 0 & I \\ -M^{-1}K & -M^{-1}C \end{bmatrix}_{2n\times 2n} \{z\}$$

ALTERNATE EFFICIENT FORMULATION FOR CHARACTERISTIC EQUATION :

$$\det([I] + s[\hat{R}(s)][\hat{C}]) = 0$$

ASSUMING NO. OF DAMPERS << NO. OF D.O.F.

$[\hat{R}]$ = SUBMATRIX OF $[R]$

$$[R] = (s^2[M] + [K])^{-1}$$

SPECTRAL REPRESENTATION

$$R_{ik} = \sum_{l=1}^{n} \frac{\phi_{il}\,\phi_{kl}}{G_l(s^2+\omega_l^2)}$$

$$\simeq \sum_{l=1}^{L} \frac{\phi_{il}\,\phi_{kl}}{G_l(s^2+\omega_l^2)}$$

DERIVATION OF CHARACTERISTIC EQUATION :

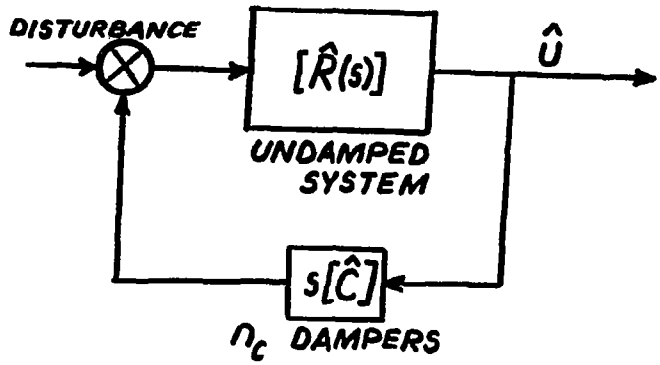

∴ CHARACTERISTIC EQ. IS :

$$det([I] + s[\hat{R}][\hat{C}]) = 0$$

SPECIAL CASE :

INTRODUCE SINGLE DAMPER AT D.O.F. J

CHARACTERISTIC EQUATION:

$$1 + sC R_{JJ} = 0$$

OR

$$\frac{1}{C} = -\sum_{l=1}^{n} \frac{s \phi_{Jl}^2}{G_l (s^2 + \omega_l^2)}$$

DEFINITION:

OPTIMAL DAMPER LOCATIONS FOR A PARTICULAR MODE ARE WHERE EITHER

MAXIMUM DAMPING CAN BE INTRODUCED

OR

ACHIEVE GIVEN DAMPING WITH MINIMUM DAMPING CONSTANTS

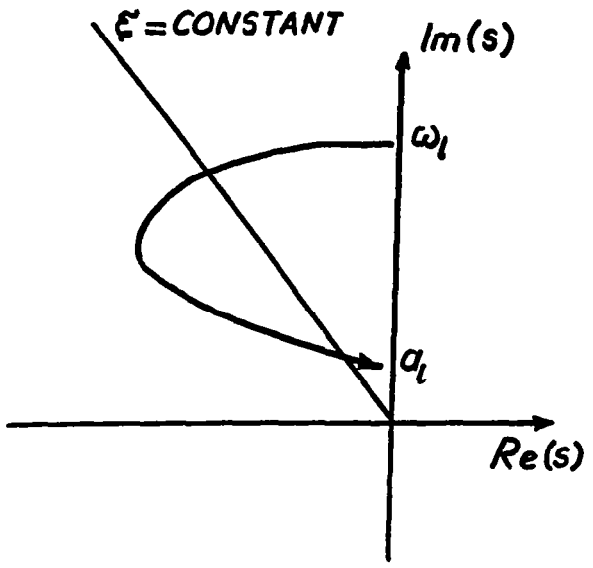

TYPICAL ROOT LOCUS PLOT

MINIMUM CONSTRAINED FREQUENCY CRITERION (MCFC)

THE OPTIMAL DAMPER LOCATION IS WHERE THE CONSTRAINED FREQUENCY IS A MINIMUM

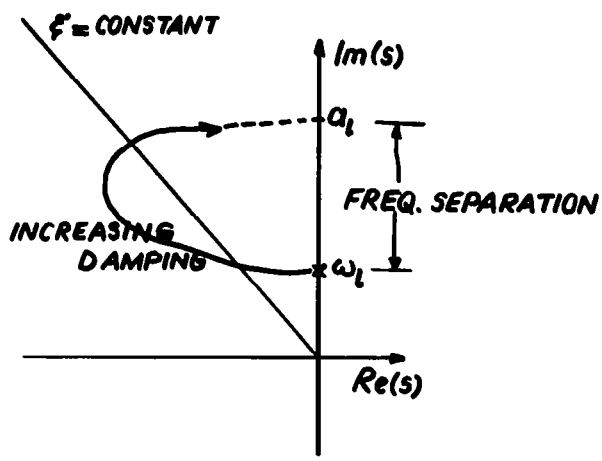

TYPICAL ROOT LOCUS FOR INTRODUCING MORE DAMPERS THAN NO. OF RIGID BODY MODES

MAXIMUM FREQUENCY SEPARATION CRITERION (MFSC)

THE OPTIMAL DAMPER LOCATION IS WHERE THE SEPARATION BETWEEN THE CONSTRAINED FREQUENCY AND THE NATURAL FREQUENCY IS MAXIMUM

SYNTHESIS OF SINGLE DAMPER

CHARACTERISTIC EQUATION IS

$$f(s) = 1 + s R_{JJ}(s)\, c$$

$$= 1 + c\,P(s) + jc\,Q(s) = 0$$

SPECIFY ξ (OR ω_{nl})

THEN

$$s_l = -\xi_l \omega_{nl} + j\sqrt{1-\xi_l^2}\,\omega_{nl}$$

SOLVE FOR ω_{nl} (OR ξ_l)

FROM $Q(s_l) = 0$

THE DESIRED DAMPING CONSTANT

$$c = -\frac{1}{P(s_l)}$$

$c > 0$ IF s_l IS REALIZABLE

SYNTHESIS OF MULTIPLE DAMPERS

CHARACTERISTIC EQUATION IS

$$f(s) = \det(I + s\hat{R}(s)\hat{c})$$
$$= P(s, \underline{c}) + jQ(s, \underline{c}) = 0$$

CASE 1

SPECIFY nc ξ's

THEN SOLVE FOR

$$\underline{c} = [c_1, c_2, \ldots, c_{nc}]^T$$

AND

$$\omega_{n_1}, \omega_{n_2}, \ldots, \omega_{n_{nc}}$$

FROM THE $2nc$ EQS

$$P(s_l, \underline{c}) = 0$$
$$Q(s_l, \underline{c}) = 0 \quad \text{FOR } l = 1 \text{ TO } nc$$

CASE 2

SPECIFY E ξ'S WITH $E < nc$

THEN $\underline{c}$ AND $\omega_{n_1}, \omega_{n_2}, \ldots, \omega_{n_E}$ CAN BE FOUND FROM

$$\text{MINIMIZE } J = \sum_{i=1}^{nc} c_i + \sum_{l=1}^{E} |f(s_l)|$$

WITH $c_i \geq 0$

$\omega_n \geq 0$

RANK OF SOME TWO DAMPER LOCATIONS ACCORDING TO MCFC

DAMPER LOCATIONS	CORRESPONDING LOWEST CONSTRAINED FREQUENCY	RANK
1, 88	4.58 RAD/SEC	1
1, 50	6.89	3
11, 58	7.50	4
34, 44	6.54	2

DAMPING CONSTANTS REQUIRED TO ACHIEVE $\xi_4 = 0.6$

DAMPER LOCATION		REQUIRED		
NO. 1	NO. 2	C_1	C_2	$C_1 + C_2$
1	88	0.296	0.136	0.432
1	50	0.262	1.024	1.286
11	58	0.311	1.130	1.441
34	44	0.498	0.565	1.064

THREE DAMPER EXAMPLE

DAMPER LOCATIONS	a_4	$\lvert\omega_4 - a_4\rvert$	a_5	$\lvert\omega_5 - a_5\rvert$
1, 50, 88	0.62	13.13	11.56	4.81
1, 44, 78	6.40	7.35	8.48	7.89

MAXIMUM DAMPING ACHIEVED IN FIRST TWO VIBRATORY MODES

(WITH SAME DAMPING CONSTANT AT ALL LOCATIONS)

DAMPER LOCATIONS	ξ_4	DAMPER VALUE	ξ_5	DAMPER VALUE
1, 50, 88	0.95	0.34	0.05	0.48
1, 44, 78	0.60	0.31	0.46	0.34

CONCLUSIONS

- CRITERIA FOR SELECTION OF OPTIMAL DAMPER LOCATIONS PRESENTED

- DAMPING SYNTHESIS PROBLEM FORMULATED AND APPLIED TO NASA GRILLAGE MODEL

DAMPING SYNTHESIS
EXAMPLE 1

DESIRED $\xi_4 = 0.6$
$\xi_5 = 0.5$

DAMPER LOCATIONS :
D.O.F. 1, 44, 78

RESULTS :

LOCATION	GAIN
1	0.272
44	0.514
78	0.269

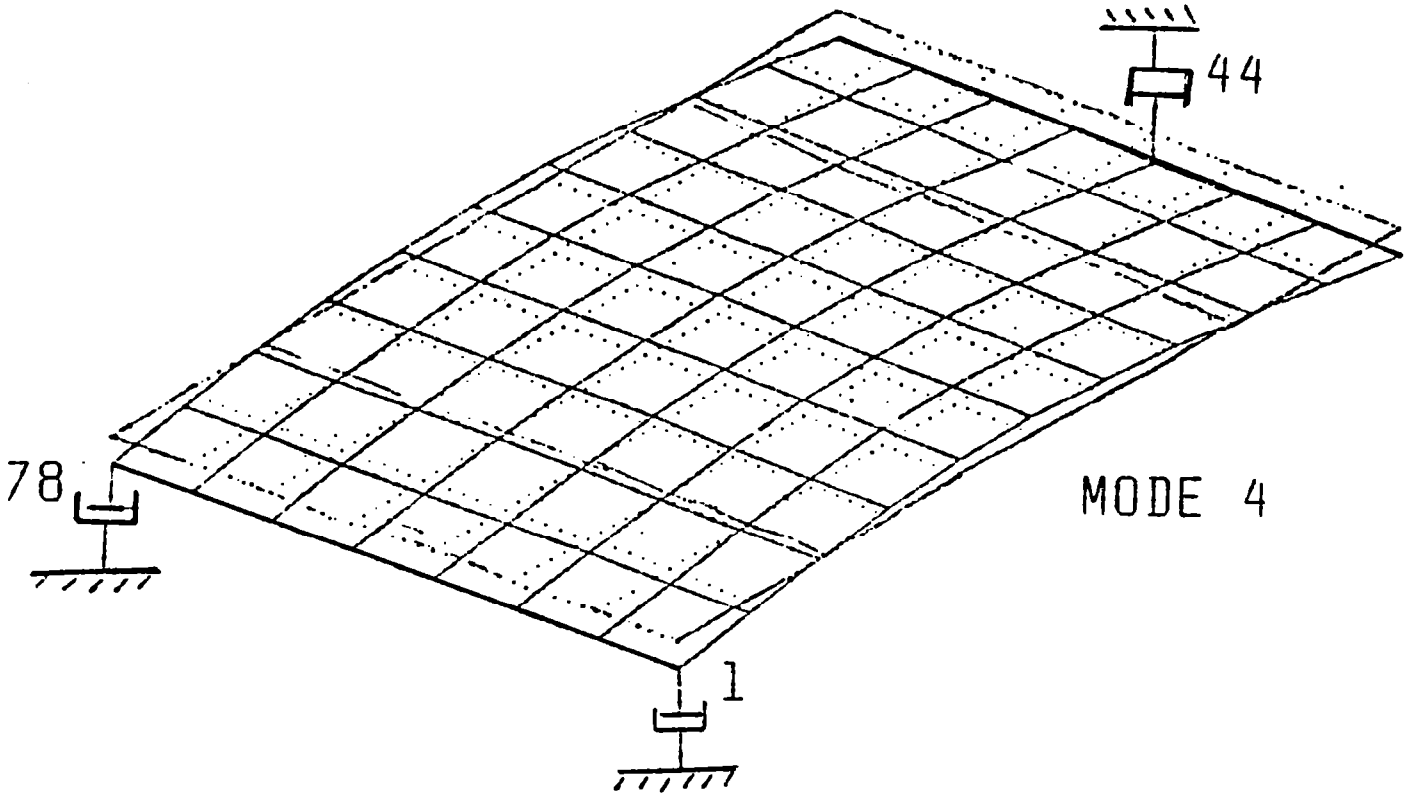
44
78
1
MODE 4

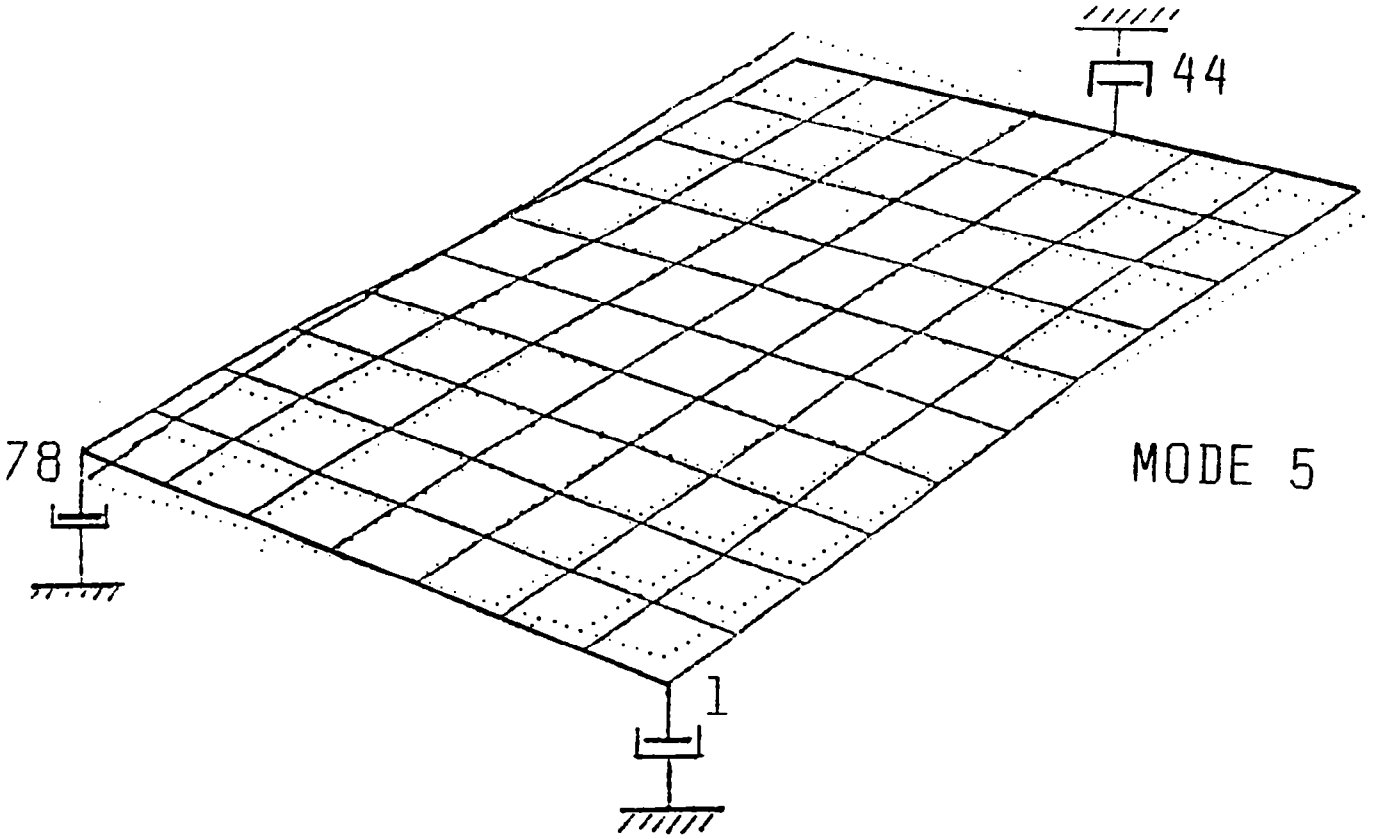
44
78
1
MODE 5

DAMPING SYNTHESIS EXAMPLE 2

DESIRED $\xi_4 = 0.7$

$\xi_5 = 0.6$

USE 6 DAMPERS AT D.O.F :

1, 11, 39, 50, 78, 88

RESULTS :

LOCATION i	c_i	c_i
1	0.21	0.240
11	0.25	0.240
39	0.20	0.131
50	0.20	0.131
78	0.20	0.247
88	0.21	0.245

ACHIEVED DAMPING

$\xi_4 = 0.71$ $\xi_4 =$

$\xi_5 = 0.59$ $\xi_5 =$

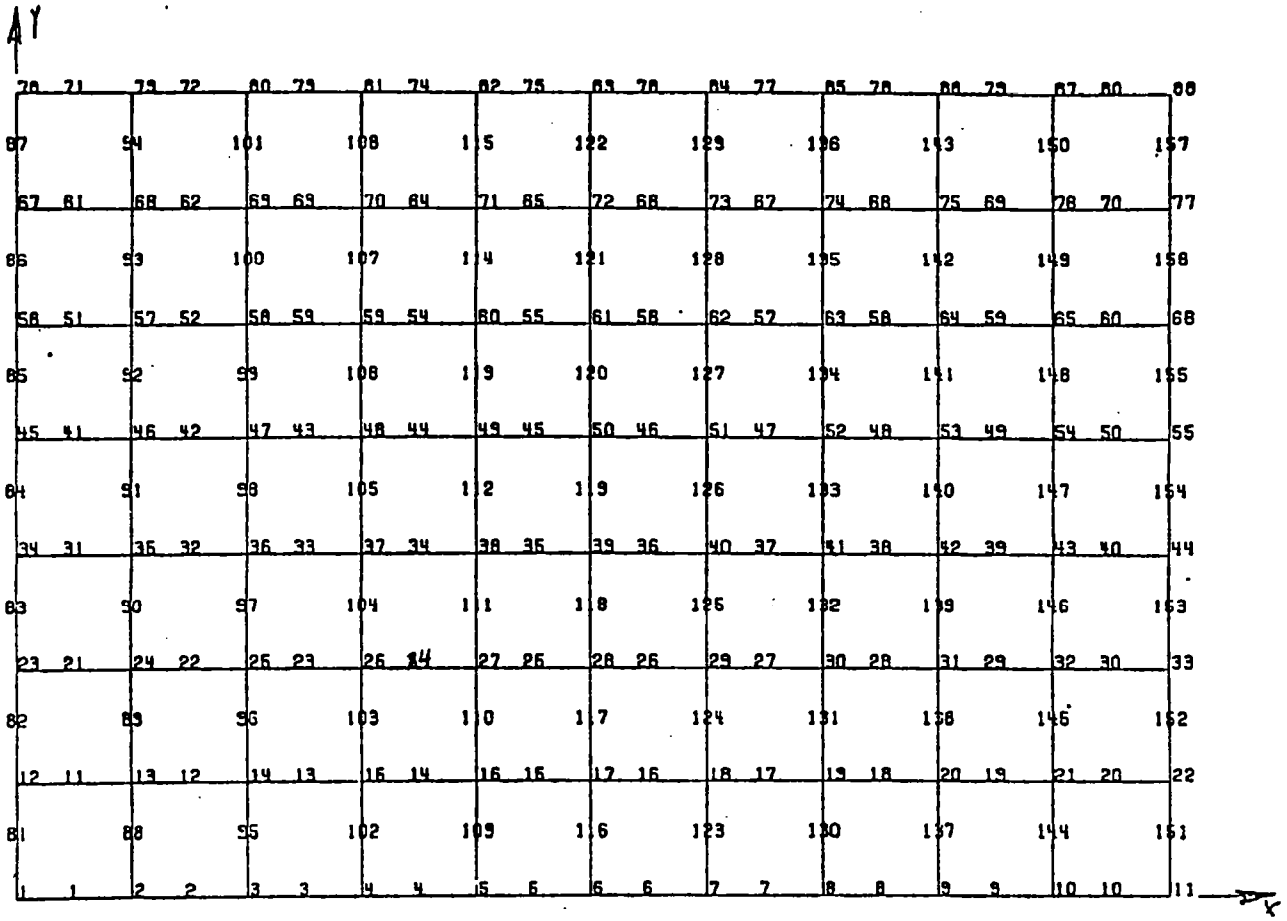

☆U.S. GOVERNMENT PRINTING OFFICE:1983 -639 -008/ 1 REGION NO. 4

1. Report No.	2. Government Accession No.	3. Recipient's Catalog No.
NASA CP-2266		

4. Title and Subtitle	5. Report Date
STRUCTURAL DYNAMICS AND CONTROL OF LARGE SPACE STRUCTURES - 1982	April 1983
	6. Performing Organization Code 506-57-13-03
7. Author(s)	8. Performing Organization Report No.
M. Larry Brumfield, Compiler	L-15579
	10. Work Unit No.
9. Performing Organization Name and Address	
NASA Langley Research Center Hampton, VA 23665	11. Contract or Grant No.
	13. Type of Report and Period Covered
12. Sponsoring Agency Name and Address	Conference Publication
National Aeronautics and Space Administration Washington, DC 20546	14. Sponsoring Agency Code

15. Supplementary Notes

16. Abstract

This publication contains the proceedings of a workshop held at NASA Langley Research Center, January 21-22, 1982. The workshop, which focused on technology for controlling large structures currently being conceived for space applications, was a follow-up to a workshop held at Langley in October 1980. (NASA CP-2187, Structural Dynamics and Control of Large Space Structures, 1981, contains the proceedings of that workshop.)

The workshop focused on progress in NASA Langley's basic research program in control of large space structures, and included reports on in-house efforts, university grants, and industry contracts, as well as on some efforts not directly supported by the NASA Langley Research Center program. This document contains copies of most of the visual material presented by each participant, together with as much descriptive material as was provided to the compiler.

17. Key Words (Suggested by Author(s))	18. Distribution Statement
Control systems Large space structures Structural dynamics	Unclassified - Unlimited Subject Category 15

19. Security Classif. (of this report)	20. Security Classif. (of this page)	21. No. of Pages	22. Price
Unclassified	Unclassified	267	A12

N-305

For sale by the National Technical Information Service, Springfield, Virginia 22161

National Aeronautics and Space Administration

Washington, D.C.
20546

Official Business
Penalty for Private Use, $300

SPECIAL FOURTH CLASS MAIL
BOOK

Postage and Fees Paid
National Aeronautics and
Space Administration
NASA-451

POSTMASTER: If Undeliverable (Section 158 Postal Manual) Do Not Return